Electro-polymerization of Organic Derivatives and their Electrochromic Effects

Thesis Submitted to Jadavpur University

For the Degree of

Doctor of Philosophy (Science)

by

Subhra Nad

School of Applied and Interdisciplinary Sciences

Indian Association for the Cultivation of Science

Jadavpur, Kolkata 700 032

India

February 2023

INDIAN ASSOCIATION FOR THE CULTIVATION OF SCIENCE
Prof. Sudip Malik
School of Applied and Interdisciplinary Sciences
Indian Association for the Cultivation of Science
Jadavpur-700032, West Bengal, India.
Telephone: 033-2473 4971 (Extension: 1564)
Fax: 033-24732805
Email:*psusm2@iacs.res.in*

CERTIFICATE FROM THE SUPERVISOR

This is to certify that the thesis entitled "**Electro-polymerization of Organic Derivatives and their Electrochromic Effects**" submitted by **Ms. Subhra Nad**, who got her name registered on **12thSeptember, 2018** for the award of Ph.D. (Science) degree of Jadavpur University, is absolutely based upon her own work under my supervision and that neither this thesis nor any part of it has been submitted for either any degree/diploma or any other academic award anywhere before.

Date: 24/02/2023

Dr. Sudip Malik
Professor and Chairman
School of Applied & Interdisciplinary Sciences (SAIS)
I.A.C.S, Jadavpur, Kolkata-700 032

Sudip Malik

(Signature of the supervisorwith official seal)

DECLARATION

I hereby declare that the research work presented in this thesis entitled "**Electro-polymerization of Organic Derivatives and their Electrochromic Effects**" is the results of the thesis carried out by me under the supervision of **Prof. Sudip Malik** at School of Applied & Interdisciplinary Sciences, Indian Association for the Cultivation of Science, Kolkata, and the same has not been submitted elsewhere for any degree or diploma.

Date: 24/02/2023

Subhra Nad

Subhra Nad

[Index No.: 162/18/chem./26]

To My Family Members

Acknowledgements

Completing this thesis, a product of several years' work, I feel deeply indebted to a great many people who have greatly inspired and supported me during my Ph.D at Indian Association for the Cultivation of Science and the writing of this thesis. First and foremost, I am deeply grateful for the invaluable guidance, continuous support, encouragement, patience, academic stimulus and generous help of my supervisor Prof. Sudip Malik, without his constant support this thesis would not have been completed. I will not forget those enjoyable and illuminating discussions with him which led me to the final completion of this thesis. Besides his scientific discussion, I never forget his kind mental support for me when my mother was ill. When I want leave for mother's treatment, he gave me permission without any hesitation.

I would like to express my special thanks to Professor Ayan Datta, School of Chemical Sciences, IACS for theoretical collaboration work. When I need any theoretical discussion, he always welcomes me.

My heartiest thanks to Prof. Arun Kumar Nandi, School of Material Sciences, for his continuous encouragement about my doctoral work. He not only encourages and supports me but also takes care of me fatherly. For me, he is the person next to my supervisor. I have never seen such down to earth person.

Also, I am thankful to all faculty members of SAIS, Prof. S. Ghosh, Prof. S. Acharya, Prof. S. Sinha, Prof. A. Das, Prof. K.D.M. Rao, Prof. S. Varghese, Prof. R. Paul for their valuable suggestion.

I would like to recognize my funding source DST-INSPIRE, Government of India for JRF and SRF fellowships. I am grateful to the almighty for being a research scholar in IACS for its excellent research infrastructure and friendly environment.

Many thanks to all SAIS stuff members, CSS instrument operators specially NMR, MALDI, IR, SEM, HRMS, AFM operators, canteen, workshop, cleaning, electrical security stuff members of IACS.

My special thanks to all past and present lab members, Dr. Chanchal, Dr. Utpal, Dr. Pradip, Dr. Sanjoy, Dr. Manas, Dr. Dines, Dr. Rajkumar, Dr. Saptarshi, Dr. Kaushik, Dr. Arkapal, Mrs. Shrabanti, Dr. Ketaki, Puspendu, Prasanta, Ayan, Gopal, Saily, Praduman, Lalmohan, Mustak, Runa, Bankim for their friendship and invaluable help during many difficult situations. I am grateful to my senior Dr. Dinesh for his valuable guidance and

training in my early stage of Ph.D. My special gratitude to Dr. Rajkumar for his theoretical collaboration work and fruitful scientific discussions. I would like to thanks my juniors Subhradeep, Mayank, Bhaskar, Bankim, Arijit, Shibu, Dwaipayan, Arindam

My special and sincere thanks to Dr. Sanjoy, Dr. Sujoy, Dr. Radha, Dr. Debashis, Dr. Arnab, Dr. Nabasmita, Mrs. Aditi, Ms. Mahuya, Dr. Somdeb, Dr. Tanmoy, Dr. Madhab, Dr. Palash, Mr. Anas, Dr. Subir, Dr. Sabuj, Dr Debobrata, Dr. Anurag, Dr. Raju, Dr. Ranjit, Mr. Akshoy, Mr. Aritra, Mr. Prabhat, Mr. Madubrata, Mr. Buddhadeb for their generous help in various situations.

I would like to thank my friends from my school days to Ph.D. The list is too big to write. However, a few of them are Anila, Kusum, Soumyajit, Shilpi, Isita, Puja, Dipayan, Biplab, Debobrata, Avik, Suman, Arnab, Arnab.

Most importantly, I am eternally grateful to my parents, brother, my uncles and aunts, my cousin brother for all the moral supports and for everything they have given me from my immemorial past. They all are the pillars of my life. No words are enough to express my gratitude to them for my success.

Finally, I would like to thank all who have made my stay at IACS, Kolkata so joyful and easy.

Subhra Nad

Synopsis

Electrochromic materials which reversibly modulate optical transmittance by applying potentials are the key components for energy saving and colour-tuning applications, especially in smart window technology which switch between dark state and a colourless state to control solar heat and increasing the energy efficiency of buildings sectors. Organic ECMs include conducting polymers and small organic molecules that have a large degree of conjugation have the advantages of good optical switching, fast response time, flexible device fabrication, large coloration efficiency, low driving voltage, and easy molecular design. The present thesis deals with electroactive and photoactive Triphenylamine based different donor acceptor donor based EC polymers which are synthesized by oxidative electrochemical deposition method on conducting surface. Triphenylamine based DAD type EC polymers exhibit strong colour change at low working potential. All works embodied in thesis have been performed in School of Applied and Interdisciplinary Sciences (SAIS) of Indian Association for the Cultivation of Science, Jadavpur, Kolkata-700032 under the supervision of Prof. Sudip Malik.

This thesis is divided into five chapters. **Chapter 1**, introduces a brief discussion about Electrochromism, different types of Electrochromic materials, literature on Triphenyl amine based EC materials, the important parameters which control the Electrochromism, Electrodeposited polymerization technique, the appearance of different colours with voltage change, the mechanism of colour change, Electrochromism with device fabrication.

Chapter 2, deals with the characterization technique after monomer formation like NMR, MALDI-TOF, HRMS, FTIR. FESEM and AFM technique for polymer film morphology characterization and photo physical UV-Vis spectroscopy for film absorbance characterization. Electrochemical technique like Cyclic Voltametry, Chronoampherometry and Spectro-electrochemical technique for checking EC performance.

Chapter 3 describes the influence of number of electropolymerizable group of the donor side on electrochromic behaviors, three donor-acceptor-donor type monomers containing isonaphthalene diimide as acceptor core and electro-polymerizable triphenyl amine (TPA) as the donor moiety have been designed and successfully synthesized via imidization of isonaphthalene anhydride with corresponding TPA derivatives. Three polymers show multi-electrochromic properties in a reversible manner with the colour change from colourless to brown to blue at low working potential. Spectro-electrochemistry studies of these films have revealed the high optical contrast (51.4%, 69.8 %, 84.5% respectively) of these polymers with the very fast bleaching (less than 1 s) and coloration (less than 2 s) time with very high coloration efficiencies. The electro switching stability has been performed up to 500 cycles and activity loses only 10% after 3000 s.

Chapter 4 presents the effect of different acceptor core like pyromellitic dianhydride, naphthalenetetracarboxylic dianhydride, perylenetetracarboxylic dianhydride and terminal triphenylamine based three DAD type monomers which are subsequently electropolymerized on conductive glass surface to have polymers which are explored by cyclic voltammetry studies. Density functional theory (DFT) studies disclose that HOMO is localized solely on triphenylamine unit which accounts for the electropolymerization process upon oxidation. Besides, TD-DFT calculations unveil the responsible electronic transitions for electrochromism in the polymers. Three polymers exhibit the reversible multiple colour changes of colourless to brown to deep blue in the anodic region by applying voltage 0 to 1 to 1.2 V and also colourless to deep pink in the cathodic region (voltage window of 0 to -2 V) with attractive response times, optical contrast, switching stabilities, and coloration efficiencies. These polymers can be switched upto 10,000 cycles with the colouration efficiency 800 cm^2/C in the anodic process and 600 cycles for the cathodic process in a three electrodes configuration.

In **Chapter 5**, Several triphenylamine end capped to substituted central naphthalene tetracarboxylic diimide based four donor - acceptor - donor type electroactive monomers have been designed and developed to explore the effect of substituent on the formation of electro-polymers and subsequent the chromic effect of prepared films on the conductive surface. Initially, with the help of density functional theory (DFT) studies, it has observed that HOMO is located over triphenylamine unit, responsible electropolymerization

process upon oxidation, LUMO is residing on the central naphthalene core, and all substituents are not coplanar with naphthalene moiety. Also, the band gap energy is gradually decreased with the effect of strong electron withdrawing substituents on NDI core. In three electrode configuration, reversible multiple colour changes of brown to deep blue by applying voltage 0 to 1.1 V and also brown to deep pink with the voltage change of 0 to -2 V are investigated with relatively good response times, optical contrast, switching stabilities, and coloration efficiencies.

Chapter 6 represents the overall work summary with future scope.

Table of Contents

Chapter 1

Chapter 2

Instrumentation

Chapter 3

Design, Synthesis, and Electrochromic Behaviours of Donor-Acceptor-Donor type Triphenylamine iso-Naphthalenediimide Derivatives

Chapter 4

ABBREVIATIONS

ACN acetonitrile

CE coloration efficiency

CP conjugated polymer

CV cyclic voltammetry

DA donor acceptor

TPA Triphenylamine

DAD donor-acceptor- donor

DCM dichloromethane

E_g band gap (eV)

EC electrochromic

EFC electrofluorochromic

ECD electrochromic device

EDOT ethylenedioxy thiophene

HOMO highest occupied molecular orbital

LUMO lowest unoccupied molecular orbital

NMR nuclear magnetic resonance

ITO indium tin oxide

Pt Platinum

LED light emitting diode

PANI poly-aniline

PC propylene carbonate

PPy polypyrrole

ProDOT propylenedioxy thiophene

ProDOP propylenedioxy pyrrole

PMMA poly(methyl methacrylate)

PT polythiophene

DMAc dimethylacetamide

DMF N, N- dimethylformamide

DMSO dimethyl sulfoxide

DPPF 1,10-bis(diphenylphosphino)ferrocene

NDI naphthalene diimide

NDA naphthalene dianhydride

OFET organic field effect transistor

OLED organic light emitting diode

OPV organic photovoltaic cells

THF tetrahydrofuran

TEA triethylamine

Δ%T percent transmittance change

TBAP tetra-butylammonium perchlorate

Chapter-1


INTRODUCTION

Saving energy in automobile industry and building sectors mainly focus on maintaining comfortable and healthy indoor environment. Reversible modulation of the indoor environment is one of the suitable approaches to adjust it according to our daily needs. Now-a-days, it is possible to a greater extent with the integration of so-called chromogenic technologies into daily used items like automobiles, glazing in buildings, planes and various electronic displays as they can change their optical properties in a response to different external stimuli namely temperature (thermochromism), light (photochromism), external potential (electrochromism) and polymer dispersed liquid crystals. Among various chromogenic technologies, electrochromism has been considered to be superior compared to other technologies as electrochromic technology allows user friendly control of switching which is not directly possible by means of thermochromism or photochromism.

1.0. INTRODUCTION

With the progress of modern display technologies, the electrochromic display which is a non-emissive display, has received considerable attention **[1-5].** The working principle of this display is based on a redox mechanism to produce colour and transmittance changes those present in displayed content **[6-18].** Commercialized displays namely liquid crystal, organic and inorganic (quantum-dot) light-emitting diode displays and some other non-emissive displays like electrophoretic and dielectrophoretic, electro-wetting and photonic crystal displays and recently used EC displays are still in the preliminary stage and practically non-viable **[19-27].** EC displays are the potential candidates for the long-awaited next-generation displays.

1.01. Electrochromism: discovery and applications

Discovery: The term "Electrochromism" was first coined by Platt in 1961 but the first change ofcolour by electrochemical means was observed by Kobosew and Nekrassowin 1930 due to electrochemical reduction of a bulk tungsten oxide. In 1969, Deb demonstrated the electrochromism with tungsten oxide films and it was really the true birth of electrochromic technology. In 1971, Blanc and Staebler produced an electrochromic effect which was superior to most of the previously published report. Nowadays, Deb's paper form 1973 is quoted as the work responsible for the true birth of electrochromic technology. In 1972, Beegle succeeded in developing a display with identical counter and working electrodes. In 1975, a significant progress was achieved by Faughan et al. in the field of the electrochromic display device. People interest towards electrochromic materials was gradually increasing in the mid 1980 when they apply power efficient EC smart windows in building blocks consisting two electrodes and electrolytes.

1.02. Applications

The phenomenon of electrochromism is associated with some reversible colour change by some redox reaction in presence of external voltage. Even this term includes the modulation of the electromagnetic spectrum **[28],** this will be restricted to the visible region. The electro active moiety is either reduced or oxidized by an external voltage. The redox forms exhibit different transitions between the ground state and excited states.

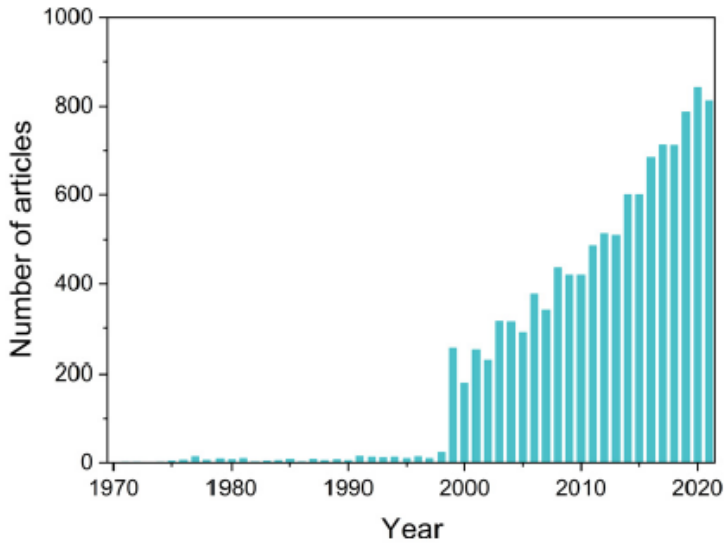

Fig.1.01. Number of published articles on EC fields from 1970 to 2021.

Therefore, the redox forms require certain energy for electronic transition, by absorbing photons from electromagnetic spectrum, a colour change occurs in the visible region **[29-32].** In the last few decades, EC materials have great interest as electronic paper and smart window for the automobiles and building sectors, optical information and storage device, rear viewed mirrors, helmet visors, protective eyewear, air craft canopies, climate adaptive building shell (CABS) **[33-37]. Fig.1.01.** represents the number of published articles on EC fields from 1970 to 2021.

1.03. Commercialization:

Smart windows have been produced by the renowned company, View Inc., Sage Electrochromics Inc. USA, but their practical applicability was limited for long-term

cycle switching process, nearly 100 000 cycles are needed for application purpose **[38, 39].** EC windows developed by Sage Glass are pass the test ASTM-E-2141-06.

Electrochromic antiglare mirrors (rear viewed) have reached the market successfully and widely commoditised by many branded vehicles. This requires very fast switching times which is less than 5s and the temperature requires in between +10 to +40ºC. Companies like Gentex and Donnelly have showed bluish coloured that requires continuous power supply for maintaining its coloration. Another EC systems like smart sunglasses and tint-visor helmets provide visual comfort for the driver **[40-42].**

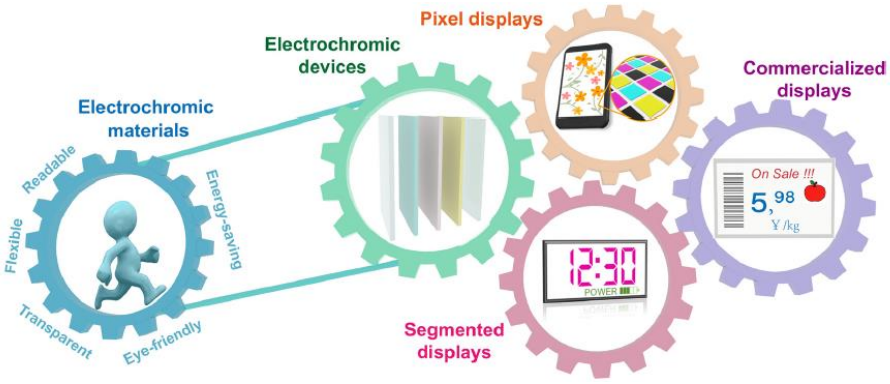

Fig.1.02. Advantages and values of electrochromic materials and corresponding developmental trajectory from electrochromic devices to mainstream display prototypes (segmented displays and pixel displays) and commercialized displays.

In informative display panels like in airports, shops, rail stations, city squares, EC displays have a great applicability due to their prominent view from any viewing angle having paper-like appearance. EC materials which offer colourless-to gray or black electrochromism, provide multicoloured behaviour for maintaining device architecture which remains a challenge till now **[43].**

Currently two display prototypes are existing, one is segmented display and another is pixel display shown in **Fig.1.02.** In According to different working strategy and information storage capacities, these two prototypes are divided. Compared to antiglare rear view mirrors, smart windows, an ideal electrochromic display has high performance requirements, as for examples, faster switching capability, faster

response times for fast information transferring and better cycle stability and also high durability to support their for lifetime, and high optical contrast for having an enjoyable reading moment. Admittedly, EC displays till have far away to reach for practical application due to its immature and imperfect presentation at this stage.

1.04. Advantages of Electrochromic display over others

The comparison of Electrochromic display with other displays is showing in **Table 1.1.** Some properties of ECD is comparable to the LCD with extra advantage that different colours form without adding external dyes, does not depending on viewing angle **[44].**

Table 1.1. A comparison of EC display with other displays

Serial no	property	ECDs	EP displays	FELC displays	DSLC displays	DS displays
1	Viewing angle	Wide	Wide	Narrow	Narrow	Narrow
2	Colour	Two or more	Two	dye	B/W	B/W
3	Operating mode	dc pulse	dc pulse	ac	ac	ac
4	Voltage (V)	0.25-20	30-80	2-10	10-30	2-30
5	Memory	Yes	Yes	No/Yes	No/Yes	No
6	Write time (ms)	100-1000	60	20	20	20
7	Erase time (ms)	100-500	30	1-500	100	30

ECDs = Electro chromic displays

EP = Electro phoretic displays

FELC = Field effect liquid crystal displays

DSLC = Dynamic scattering liquid crystal displays

DS = Dipole suspension displays

1.05. Main classes of EC material:

There are mainly three types of EC materials.

a. Inorganic based EC materials which includes transition metal oxides, prussian blue system,

b. Organic based EC material which includes viologen, conjugated conducting polymers,

c. Transition metal coordination complexes.

1.05.01. Transtion metal oxides

Many transition metal oxide films are electrochemically switched to a non-stoichiometric redox state which has an intense electronic absorption band due to optical intervalence charge transfer **[45, 46].** Among them transition metal oxides have been one of the most widely studied classes of EC materials. Depending on the metal oxide, either anodic or cathodic colouration is observed, Cr, Mn, Fe, Co, Ni, Rh, and Ir are anodically colouring, whereas Ti, Nb, Mo, Ta, and W are cathodically colouring. There are two principally different kinds of EC oxides: those referred to as 'cathodic' and colouring under ion insertion, and the 'anodic' ones that colour under ion extraction. For the electrochromism of WO_3 although there is still controversy about the detailed colouration mechanism, it is generally accepted that the injection and extraction of electrons and metal cations (Li^+, H^+) play a key role **[47-49]. Fig.1.03.** represents tungsten oxide film used in flight window.

$$WO_3 + x(Li^+ + e^-) \longrightarrow Li_xW^{vi}_{(1-x)}W_x^{V}O_3$$

At low x, the films show an intense blue colour because of photo effected inter-valence charge transfer between W^V and W^{Vi} sites. At higher x, insertion irreversibly forms a metallic bronze which is red or golden in colour.

Fig.1.03. Tungsten oxide film used in flight window.

Tungsten trioxide coatings have been produced by different deposition techniques like thermal evaporation in vacuo, electrochemical oxidation of tungsten metal, chemical vapour deposition (CVD), sol-gel methods and by RF-sputtering. When tungsten oxides mixed with other metal (like Ti, Li, C, N, V, Ni, Nb, Mo, Ru, Sn, Ta, polyoxometalates) have improved the EC properties that those of the pure oxide **[50-52].** The addition of Ti with tungsten leads to enhanced cyclic stability by stabilizing a highly disordered structure. Electrochromism of mixed W-Ti oxide has been reported for films made from W-Ti oxide core shell nanorods and on WO_3-TiO_2 nanocomposites and nanotube arrays. Investigators also have been reported on W oxide containing coinage metal nanoparticles of Ag, Pt, and Au that are capable of giving Plasmon induced optical absorption of visible light. Hybrid materials also have been developed such as WO_3-H_w where, H_w indicates PEDOT : PSS, chitosan (PEO),

PBZT, PANI or an electropolymerized deposit. Many other thin film transition metal oxides are electrochromic **[53-56],** for example oxides of molybdenum and vanadium,

$$MoO_3 + x\,(M^+ + e^-) \longrightarrow M_xMo^{vi}_{(1-x)}\,Mo^{V}_{x}\,O_3$$
(transparent) (blue)

$$V_2O_5 + x\,(M^+ + e^-) \longrightarrow M_xV_2\,O_5$$
(yellow) (pale blue)

Here, the intensely absorbing redox state is produced on reduction. In contrast, group 8 metal oxides become coloured on electrochemical oxidation, as in the case of hydrated iridium oxide (strictly iridium hydroxide). Mechanism for colouration is proton extraction and anion insertion routes being proposed in the following equation.

$$Ir(OH)_3 \longrightarrow IrO_2.H_2O + H^+ + e^-$$
(transparent) (blue black)

$$Ir(OH)_3 + OH^- \longrightarrow IrO_2.H_2O + H_2O + e^-$$
(transparent) (blue black)

Iridium oxide is too expensive for most applications, even if diluted with less costly Sn or Ta. However, Ni oxide is adjudged as a good alternative as discovered many years ago. Ni oxide based films are used in several of today's smart windows with EC properties. A major present aim is the development of 'smart windows' for control of thermal conditions within a building, thereby reducing winter heating and summer cooling requirements. Glass manufacturers have recognised this opportunity, with the Pilkington Technology Centre having produced a prototype electrochromic window (dimensions 0.7 X 1 m) which when coloured is capable of reducing light transmission by a factor of four. In the development of such variable transmission windows, glass companies favour the sputtering technique because it is already in place for the production of a range of coatings for architectural glazing **[57-60].**

1.05.02. Prussian blue

Prussian blue is a number of polynuclear transition metal hexacyanometallates that form an insoluble mixed-valence compound. PB thin films are generally formed by electrochemical reduction of solutions containing iron (iii) and hexacyanoferrate ions. Reduction of PB yields Prussian white (PW), also known as Everitt's salt, which appears transparent as a thin film. The intense blue colour in the $[Fe^{III}Fe^{II}(CN)_6]$ chromophore of PB is due to an intervalence charge-transfer (CT) absorption band centred at 690 nm. The aqueous solution of PB$[Fe^{III}Fe^{III}(CN)_6]$ is reduces, where by PB$[Fe^{III}Fe^{II}(CN)_6]$ is deposited in form of blue film and electro neutrality in solution is solely maintained by K^+ present in the electrolyte.

$$[Fe^{III}Fe^{II}(CN)_6]^0 + e^- \longrightarrow [Fe^{III}Fe^{II}(CN)_6]^-$$

Partial electrochemical oxidation of PB produces Prussian green, known as Berlin green. Generally, Prussian green has a fixed composition with anion, for thin films there is a continuous composition range between PB and Prussian brown, which becomes a golden yellow in the fully oxidised form. The latter is also obtained by electrochemical oxidation of a particularly pure form of PB in the following equation.

$$[Fe^{III}Fe^{II}(CN)_6]^- \longrightarrow [Fe^{III}Fe^{II}(CN)_6]^0 + e^-$$

Prussian blue Prussian brown

Reduction of PB yields Prussian white, also known as Everitt's salt, which appears transparent as a thin film according to the following equation,

$$[Fe^{III}Fe^{II}(CN)_6]^- + e^- \longrightarrow [Fe^{II}Fe^{II}(CN)_6]^{2-}$$

(Prussian blue) (Prussian white)

Replacing the coordinate iron in the PB framework with other transition metals results in a distinct Prussian blue analogue (PBA) showing a different colour and is used as in modified electrode studies. As majority are expected to be electrochromic, absorption spectra as a function of redox state have rarely been reported and only ruthenium purple [iron (III) hexacyanoruthenate (II)] and osmium purple [iron (III) hexacyanoosmate (II)] are used in ECDs. Moreover, Ruthenium hexacyanoferrate (Ru-PBA) changes its colour from transparent to purple. Co-PBA produces pale green to reddish brown, Cu-PBA reveals pale yellow to red and Ni-PBA created transparent to yellow electrochromism **[61].** With increasing voltage to +0.50 V, the original PB peak shifts to higher wavelengths continuously with decreasing absorption, but 425 nm peak increases, due to the increasing $[Fe^{III}Fe^{II}(CN)_6]$ absorption.

1.05.03. Organic EC materials

1.05.03.01. Viologen systems

4,4 ' bipyridylium salts is known as 'Viologens'. The compound is named as 1,l ' -disubstituent-4,4' -bipyridylium if two substitution on nitrogen are same, and 1-substituent- 1' substituent- 4,4 ' -bipyridylium they should differ. The prototype, 1,l ' -dimethyl-4,4 ' -bipyridylium, is known as methyl viologen (MV). Among three redox states, the dication form is the most stable and colourless **(scheme 1.1).** Electron transfer by reduction to viologen forms coloured radical cations. Due to the delocalisation of the radical electron, through the Π framework of the bipyridyl nucleus, the dication form is stable.

Electrochromism for viologens is due to the viologen dications, the radical has a positive charge which is delocalised. Colouration is arising from intra-molecular charge transfer. Alkyl groups promote a violet colour where as aryl groups impart a green colour to the radical cation. The colour intensity have exhibited by double reduction of viologen is less, since no optical transfer occurs in the visible wavelengths. For display purpose, the write and erase efficiency of any ECDs using small alkyl chain viologens such as MV in aq. electrolytes should be low due to that both dicationic and mono radical cation are highly soluble. Improvements can be made in MV ECDs by reducing the rate, at which the radical will perform electron

transfer diffusion away from electrode and also in the solution either by taking the dication on the surface of an electrode, another way is by immobilising the viologen within a semi-solid electrolyte like Nafion.

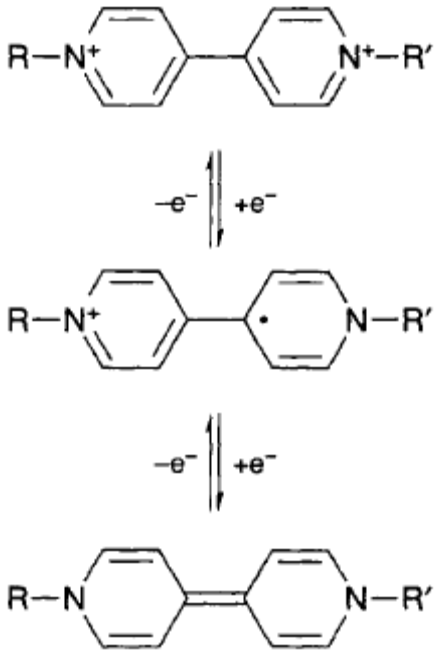

Scheme 1.1. Three common redox states of viologen.

High response times are not essential in EC car rear viewed mirrors and in 'smart windows'. Gentex's commercialised auto-dimming 'Night Vision Safety' mirror functions by solution electrochromism. A cationic viologen provides cathodic colouring EC material, with a –ve ly charged phenylene diamine acting as anodically colouring EC material. Gentex Corporation is marketing rear view mirrors to 16 main vehicle manufacturers. NVS mirrors are available on 95 modelled vehicles. This company also have produced wing mirrors, from 1987 to the end of 1996, 10 million EC mirrors have been sold. Now a day, commercial application such as railway termini, long term data displays are now use a nano structured EC organic/inorganic dual system, where EC groups like phophonated viologens and phenothiazine molecules attach to a very high surface area porous film **[62, 63].** Here two metal oxides have been used, one at –ve glass electrode and another is at +ve electrode.

Negative electrode is coated with TiO_2 which is coated with layer of viologen molecules. The +ve electrode is added with another crystalline film which is making from antimony doped tin dioxide. This film has phosphonated phenothiazine molecules layer. Normally, these molecules show a light yellow colour, but on oxidation, they turn red. The EC cell is sealed with an electrolyte. ECD switched from colourless to deeply coloured state by applying voltage 1.2 V. This is due to the viologen reduction, turning blue and on oxidation the phenothiazine turns red. Overall result is blue-red colour, when the potential is reversed the colour will remove. This cycle repeated for several times without no significant degradation. The colour exists for greater than 600 s although removal of the voltage **[64].**

The disadvantage of viologen electrochrome is that once the dual EC colouration process has started, the electrochromes will diffuse away and mixed with the intervening solution. Therefore, ECD requires a small amount of current flow for the removal of the colour, electro active systems lost by mutual redox reaction. Bleaching occurs when the circuit is open by homogeneous electron transfer to the bulk solution. A photosensitive detector is kept to monitor dazzling incident. However, this will be triggered in daylight, causes unwanted darkening. To avoid this problem, a second looking detector is employed, which operated when daylight is programmed it cancels the operation of controlling sensor.

1.05.03.02. Conducting polymers

Conducting polymers have been known since 1862, when electrochemical synthesis of polyaniline yields a black coloured powdered. After discovery of metallic like conductivity of polyacetylene by Hideki Shirakawa, Alan Heeger and Alan MacDiarmid in 1977 that led to Nobel prize in Chemistry in 2000 **[65, 66].** The three pioneers explained lucidly that conjugated polymers became conductive if C-atoms were linked through alternative single and double bonds and e^- s were removed or introduced by redox processes. Heeger et.al demonstrated that the conductivity of trans poly acetylene increased seven orders in magnitude upon iodine doping.

Electrochemical oxidation of aromatic molecules like thiophene, pyrrole, furan, aniline, azulene, carbazole, indole forms novel conducting polymers. On oxidation,

conducting polymers 'doped' with balancing counter anions and it possess a delocalised band structure, the band gap between valence band and conduction band determines the optical properties. Oxidation introduces polarons those are major charge carriers. On reduction, the neutral 'undoped' electrically insulator forms.

Theory of conjugated conducting polymers

Band Theory

Depending on conductivity, materials can be divided into 3 categories, conductors, semiconductors, insulators. Band theory explains the conductivity of a polymeric material. According to the band theory, when two half filled orbitals are overlapped, new orbital is produced, one is at lower energy and another is at higher energy. The energy difference is calculated by how much extend of orbital overlapping occurs.

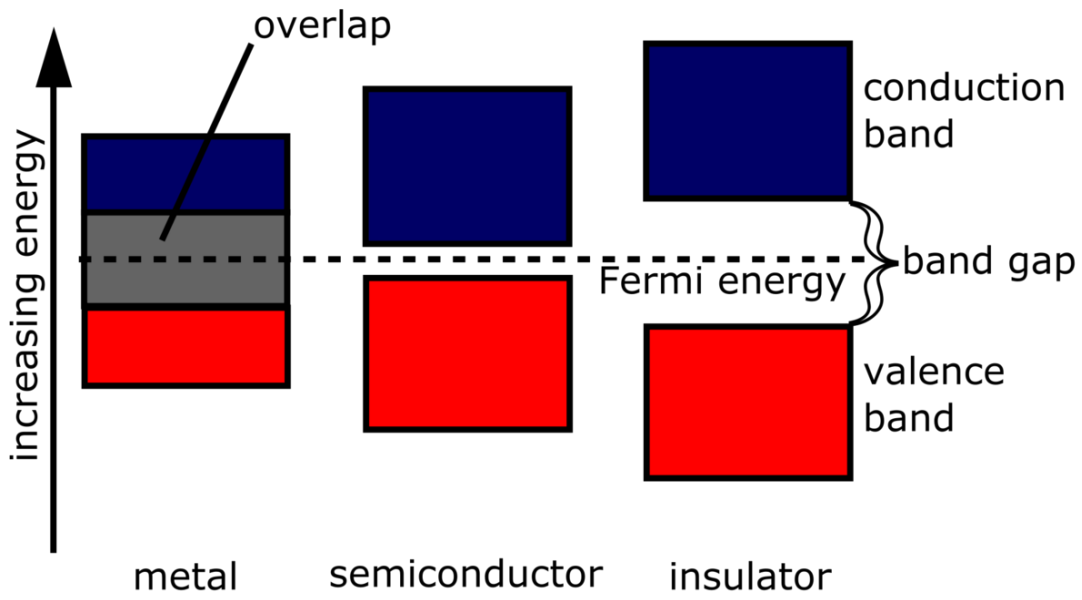

Fig.1.04. Band structure schematic diagram.

Two electrons move to lower energy orbital which is the bonding orbital and the higher energy orbital is an anti-bonding orbital. The energy gap between HOMO and LUMO is known as band gap (E_g). It is also the difference in energy between the valence band (VB) and the conduction bands (CB) **(Fig.1.04).** For metal, valence

band and conduction band are overlapped. For insulator, band gap is very high (E_g > 3.0 eV). When the band gap neither high nor near to zero (E_g = 1.30 eV), this type of material is called semiconductor. For this situation, electron may be thermally excited and create an empty hole in the upper band **[67-70].**

Mechanism of conduction

Charge Carriers

The conduction behaviour of the conjugated conducting polymers can be defined by the concept of solitons, polarons and bipolarons **[71].** During doping in CPs, Solitons, Polarons and Bipolaron named conjugated defect has been formed. Solitons can be divided into 3 categories.

a. Neutral soliton, S=1/2
b. Positive soliton, S=0
c. Negative soliton, S=0

Charged Solitons are spinless but neutral ones have spin but no charge. By oxidation, an e^- is removed from its localized state and positively charged Soliton forms and similarly when an electron is inserted by reduction, negatively charged Soliton is produced. Conductivity of CPs increases by the formation of Polarons. A radical cation is known as Polaron that is partially delocalized over some polymer segment. After removal, e^- from the top of the VB of a CP, a vacancy is created, when an electron is removed that does not delocalize completely. When an e^- is removed from an oxidized polymer containing the polaron, 2 things may happen, firstly, this e^- will create another independent polaron or from the first polaron level to create special dication which is called a bipolaron. Generally, a low doping level of polymers generate polarons, but bipolarons is produced by higher dopping levels. The bipolaron is structurally deformed. The bipolaron containing two +ve charges are depended pair. Polarons and bipolarons are mobile and can enter to the polymer network by resonance in presence of an electric field. If much more bipolarons are produced

which create narrow bipolaron bands in the band gap and easy to conduct the electron throughout the system.

1.05.03.02.a. Polypyrrole(s)

The electrochromic properties of polypyrrole are investigated using thin-film polypyrrole prepared by electrochemical polymerisation of pyrrole from acetonitrile solution. The oxidative electropolymerisation process is initiated by monomer oxidation to yield a radical-cation species **[72] (Scheme 1.2).** Polypyrrole generate in its oxidised conducting form, follows a mechanism that is believed to involve either radical-cation/radical-cation coupling or attack of radical-cation on neutral monomer. Polypyrrole thickness is controlled through the charge passed, further film growth occurring at the polypyrrole-solution interface. Doped (oxidised) polypyrrole is blue-violet, on electrochemical reduction yielding the yellow-green. Removal of all dopant anions from polypyrrole yields a pale yellow film, however, complete de-doping is only achieved if films are extremely thin. This means that polypyrrole of thickness commensurate with device construction (> 1 pm) has a low contrast ratio **[73].** The electrochromism of polypyrrole is unlikely to be exploited, mainly due to the degradation of the film on repetitive colour switching. Conducting polymers with improved electrochromic properties are however formed on electrochemical polymerisation of 3,4-disubstituted pyrroles. PPy show lower oxidation than thiophene analogues. The addition of oxygen at the 3, 4 position lowers the band gap of the resulting polymer. For Poly(3,4 ethylenedioxy)pyrrole, insertion of charge compensating anions exhibit a bright red colour in its neutral state and a light blue transmissive state upon oxidation and has a band gap of 2.05, 0.65 eV lower than the pyrrole **[74, 75].** Substitution at nitrogen of pyrrole has adverse effect due to the breaking of conjugation. The increase band gap of polymer results in the absorbance of the transition blue shifted and the intra gap polaron and bipolaron transitions occurring in the visible region.

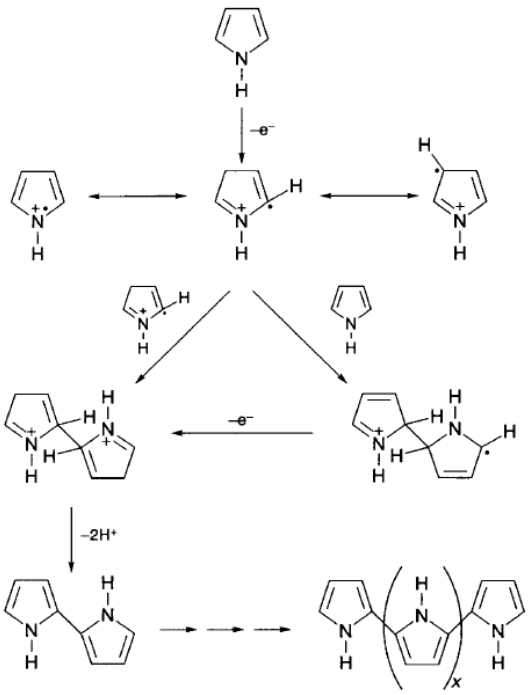

Scheme 1.2. Mechanism of polymer formation from pyrrole.

1.05.03.02.b. Polythiophene(s)

As for polypyrrole, polythiophene thin films may be prepared by the electrochemical oxidation of solution monomer. Tuning of colour states is possible by suitable choice of thiophene monomer. For example, the electrochromic properties of polymer films prepared from 3-methylthiophene-based oligomers are strongly dependent on the relative positions of methyl groups on the polymer backbone. In research directed to using the same electrochromic material for both the working and counter electrodes, a series of conducting polymer films based on 3-(p-X-phenyl)thiophene monomers (R = -H, $-C_8H_{17}$, $-C_{14}H_{29}$) have been investigated **[76].** The presence of electronwithdrawing groups on the phenyl ring serves to assist the stabilisation of the n-doped state and these materials can be both reversibly reduced and oxidized (n- and p-doped).

Table 1.2. Monomers and their colours in different states

Monomer	Polymer λ_{max}/nm and colour	
	Oxidised	Reduced
Thiophene	730 Blue	470 Red
3-Methylthiophene	750 Deep blue	480 Red
3,4-Dimethylthiophene	750 Dark blue	620 Pale brown
2,2′-Bithiophene	680 Blue–grey	460 Red–orange

A large number of substituted thiophenes have been synthesized such as poly(3 substituted thiophenes) and poly(3,4 disubstituted thiophenes). Thin polymeric films in the doped state are blue and red in the undopped state. However, 3 methylthiophene has lower oxidation potential than the parent thiophene. Poly (3 methylthiophene) is purple **(Table 1.2)** when an absorption maximum at 530 nm (2.34 eV) and turns pale blue on oxidation. Investigation on structural modifications of the PTh, for colour and properties tuning has been carried out. For regioregular P3MT and P3HT, both exhibit red in their neutral states.

P3MT reveals a dark blue on oxidation, P3HT exhibits a light blue colour. On the contrary, both PEDOT and PProDOT switch between dark blue and a highly P3MT reveals a dark blue on oxidation, P3HT exhibits a light blue colour. On the contrary, both PEDOT and PProDOT switch between dark blue and a highly transmissive and near colourless state. Fig. shows the spectroelectrochemical series for an alkylenedioxy substituted thiophene polymer, poly (3,4 (ethylenedioxy) thiophene). The undopped polymer's shows strong absorption at 2.0 eV due to Π- Π* interband transition **[77-79].**

After doping, the interband transition decreases and two new optical transitions appear at lower energy, corresponding to the formation of polaron. Further oxidation leads to formation of bipolaron and lower energies absorption appears **(Fig. 1.05).** Facile tuning of the steric effects and effective conjugation we can tune band gaps of the poly thiophene. For instance, utilization of shorter side chains facilitates the relaxation of steric distortions, resulting in a red shift of the absorption and colour transition from orange to red **[80].** A large number of polymers displaying vibrant hues of orange, red, magenta and purple **(Table 1.3)** within the intermediate range of the visible spectrum were thus generated.

Table 1.3. Monomers and their colours in different states

Monomer (figure does not represent the molecule's stereochemistry)	Polymer colour	
	Oxidised	Reduced
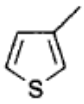	Pale blue	Purple
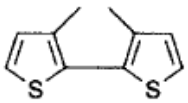	Violet	Yellow
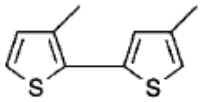	Blue	Red
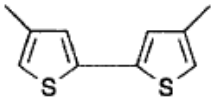	Blue	Orange
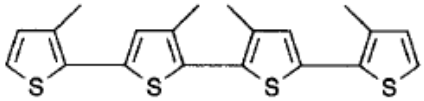	Blue	Yellow
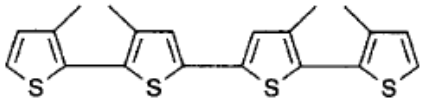	Violet	Yellow
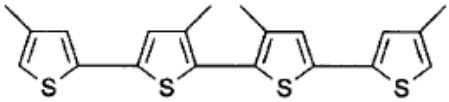	Blue–violet	Yellow
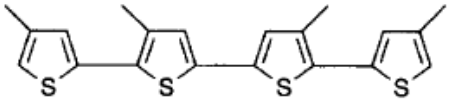	Blue	Yellow–orange

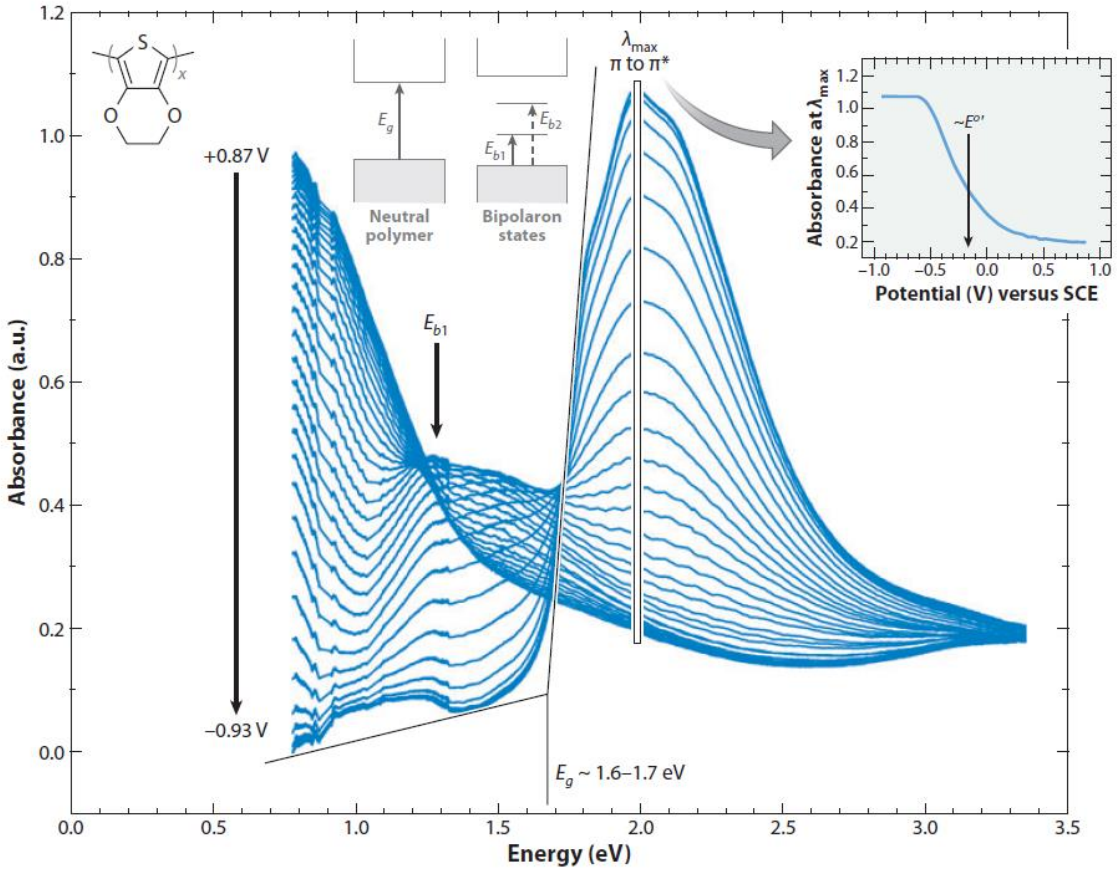

Fig.1.05. Spectroelectrochemistry for a poly[3,4-(ethylenedioxy)thiophene] (PEDOT) film on tin-doped indium oxide (ITO)/glass.

PEDOT or its copolymers are unique example as they have relatively lower band gap than PTh itself owing the presence of two oxygen atoms adjacent to thiophene units **[81].** Scheme 2 represents some ProDOT based derivatives.

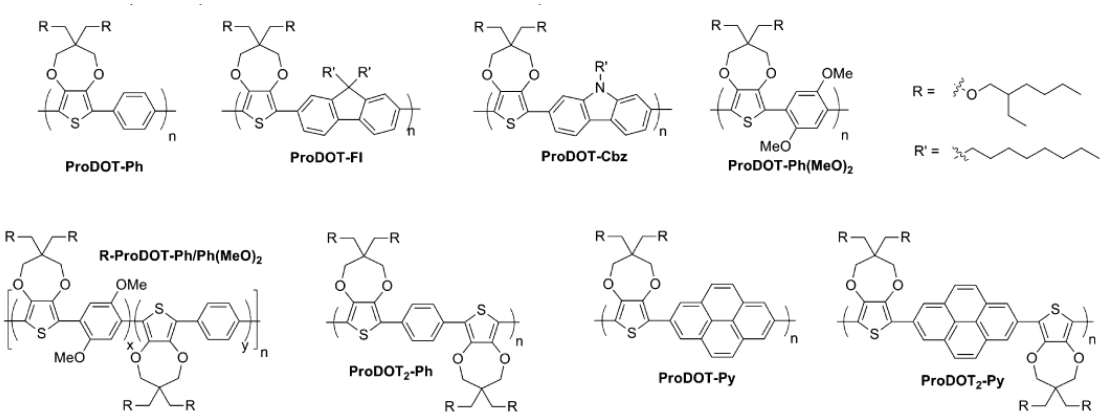

Scheme 1.2. ProDOT based derivatives.

Compared to other substituted PThs, these materials exhibit excellent stability in the doped state, which is associated with high conductivity. Tuning of colour can be obtained by careful selection of the heterocyclic moieties forming the backbone. Fine tuning is highly accomplished by the proper choice of electron donating or electron withdrawing units at the β positions and the steric chains for control of steric interactions and distortions.

1.05.03.02.c. Polyaniline(s)

The electrical and electrochromic properties of polyaniline not only depend on its oxidation state, but also on its protonation state, and hence the pH of the electrolyte used. The electrochemistry of polyaniline thin films has been extensively investigated in aqueous acid solutions and in organic media, and several redox mechanisms involving protonation- deprotonation and/or anion ingress/egress have been proposed. Polyaniline films are polyelectrochromic (transparent yellow to green to dark blue to black), the yellow-green transition being durable to repetitive colour switching. The two low-wavelength spectral bands observed in the polyanilines are assigned to an aromatic n-n* transition (330 nm) related to the extent of conjugation between the adjacent rings in the polymer chain, and to radical cations formed in the polymer matrix (440 nm). With increase in applied potential the 330 nm band absorbance decreases. Beyond +0.30 V the conducting region is entered; the 440 nm band decreases as a broad free carrier electron band and a 800 nm is introduced. Polyaniline has been combined with PB in complementary ECDs that exhibit deep blue, green electrochromism.' Electrochromic compatibility is obtained by combining the coloured oxidised state of the polymer with the blue PB and the bleached reduced state of the polymer with PG. Whilst electropolymerisation is a suitable method for the preparation of relatively low surface area electrochromic conducting polymer films, it may not be suitable for fabricating large-area coatings. Significant effort therefore goes into the synthesis of soluble conducting polymers such as poly (O-methoxy aniline) which can then be deposited as thin films by casting from solution. In a novel approach large-area electrochromic coatings have been prepared by incorporating polyaniline into polyacrylate-silica hybrid sol-gel networks using

suspended particles or solutions and then spray or brush coating onto ITO surfaces **[82, 83].** Silane functional groups on the polyacrylate chain act as coupling and cross-linking agents to improve surface adhesion and mechanical properties of the resulting composite coatings.

1.05.03.02.d. Metallopolymers

Transition metal coordination complexes are potentially useful electrochromic materials because of their intense colouration and redox reactivity. Chromophoric properties typically arise from low-energy metal-to-ligand charge transfer (MLCT), intervalence CT, intra ligand excitation, and related visible region electronic transitions. Because these transitions involve valence electrons, chromophoric characteristics are altered or eliminated upon oxidation or reduction of the complex. While these spectroscopic and redox properties alone would be sufficient for direct use of transition metal complexes in solution-phase ECDs, polymeric systems have

Table 1.4. Comparison between inorganic and polymeric EC materials.

Property	Inorganic materials	Organic polymers
Method of preparation	Needs sophisticated techniques like vacuum evaporation, spray pyrolysis, sputtering etc.	The material can be easily prepared by simple chemical, electrochemical polymerization and the films can be obtained by simple techniques such as dip coating, spin coating etc.
Processibility of the materials	The materials are poor in processability.	The materials can be processed very easily.
Cost for making the final product	High as compared to the polymer based devices.	Low cost as compared to the inorganic materials.
Colours obtained	Limited number of colours	Colours depends on the

	are available from a given material.	doping percentage, choice os the monomer, operating potential therefore large number of colours are available for polymeric material.
Contrast	Contrast is moderate.	Very high contrast can be obtained.
Switching time (ms)	10-750	10-120
Lifetime	10^3-10^5	10^4-10^6 cycles

also been investigated **[84].** Many schemes have been described for the preparation of thin-film 'metallopolymers', the reductive electropolymerisation of suitable polypyridyl complexes being a particularly versatile technique. Vinyl-substituted pyridyl ligands are generally employed, although metallopolymers have also been formed from chloro-substituted pyridyl ligands, electrochemically initiated carbon-halide bond cleavage. In either case, electrochemical reduction of their metal complexes generated radicals leading to carbon-carbon bond formation and oligomerisation. Oligomers above a critical size are insoluble and thus thin films of the electroactive metallopolymer are produced on the electrode surface. Repetitive cyclic voltammograms (CVs) for a typical electropolymerisation process, the film thickness increases with CV scan number owing to the electrocatalytic reduction of the fresh solution metal complex monomer by the growing electroactive polymer. The steady increase in current is attributable to the combined electroactivity of the orange polymeric film and the inward-diffusing metal complex monomer. The electroactivity of the resulting modified electrode is stable on transfer to pure supporting electrolyte solution, transparent electrochromicity being observed. The colour of such metallopolymer films may be selected by suitable choice of the metal (e.g. M = Fe, red; M = Ru, orange; M = Os, green). Electrochromicity results from loss of the MLCT absorption band on switching between the M(I) and the M(II) redox states. Interestingly, the chromophoric properties of the coloured state of such

supramolecular metallopolymers are modified on binding of Group I/II metal cations by the crown ether groups. In a recent development, spatial electrochromism has been demonstrated in metallopolymeric films. Contact lithography can be used to spatially control the photosubstitution process to form laterally resolved bicomponent films with image resolution below 10 pm. Dramatic changes occur in the colours and redox potentials of such ruthenium complexes upon substitution of chloride for the pyridine ligands. Striped patterns of variable colours are observed on addressing such films with a sequence of potentials. **Table 1.4.** represents the Comparison between inorganic and polymeric EC materials.

1.06. Important parameters for EC display:

1.06.01. Electrochromic Contrast

Optical contrast is the percent of transmittance change at a particular wavelength **(Fig. 1.06 and Fig.1.07).** The EC contrast is one of the important parameter for overall performance of an electro-chrome. Transmittance are recorded by applying square-wave voltage to the polymer film kept in spectrophotometer. Spectro-electrochemistry that monitors the origination of polarons, bipolarons by applying voltage, can be utilized to measure the transmittance change. As

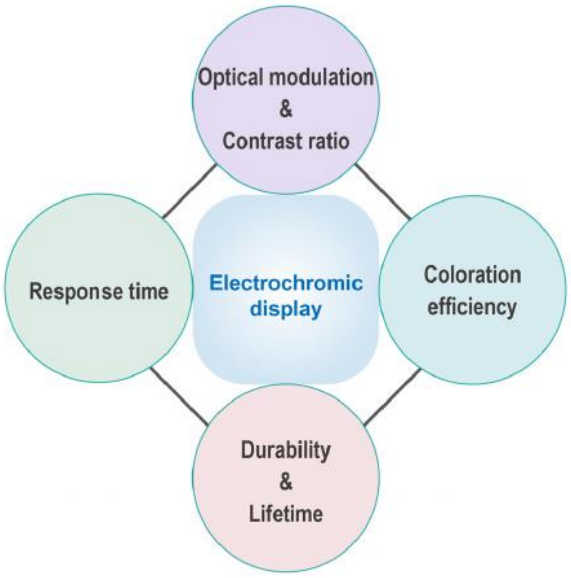

Fig.1.06. Performance indexes for EC display including optical modulation and contrast ratio, response time, coloration efficiency, and durability and lifetime.

optical transition in long wavelength is associated with some charge-carrier production, EC contrast has been evaluated in NIR region.

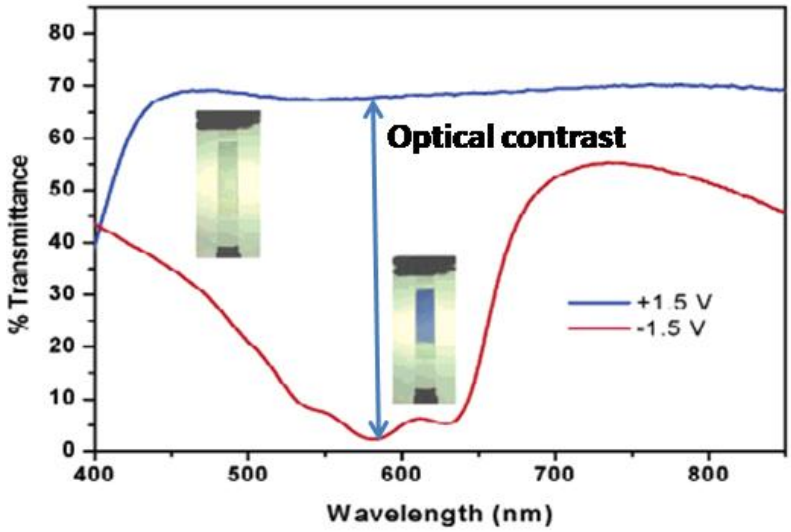

Fig.1.07. Representation of Optical Contrast.

1.06.02. Coloration Efficiency (CE)

Coloration efficiency is one of the crucial parameter for detecting the performance of an electrochromic material. CE value is used for the comparison of the performances of different EC materials. The proportionality of the absorbance change to the ejected charge density at a particular wavelength for an electrochrome, is known as coloration efficiency **[85, 86].** CE value is an inherent property of an electrochromic material, the quantitative measurement of the EC contrast and CE is estimated through the following equations:

$$\Delta OD = \left[\frac{T_b(\lambda)}{T_c(\lambda)}\right]$$

$$CE = \frac{\Delta OD\ (\lambda)}{Q_d}$$

Where, Q_d is in C cm^{-2}, CE is in cm^2 C^{-1}, and T_b and T_c are the bleached and coloured state transmittance values respectively.

Higher CE value suggests that a little amount of charge need to make a large amount of transmittance change of an EC material, that is related to the injected charge and the contrast ratio. Most of the EC contrast is calculated from the first 90% of the overall optical change such that smaller charge density windows can be used for more representative CE values. The measurement of the injected/ejected charge is calculated from the chronoamperometry technique while square-wave potential-steps between bleached state and coloured state are applied.

1.06.03. Switching Times

Switching time means the time taken for an electrochromic material to switch in between two different redox states **(Fig. 1.08).** The time requires to reach in coloured state is known as colouration time (t_c) and to reach its bleached state is known as bleaching time (t_b). Switching time depends on some parameters, like the capability of an electrolyte to conduct electrons and ions and the diffusion of the ionic species around the EC layer. Along with device architecture, cell configuration and the extent of the bias applied, thickness and morphology of the EC layer also affect optical change. Rapid EC switching in sub-second order desires for display applications. EC shutters for optoelectronic communication and other applications like switchable window technology is less demanding **[87].**

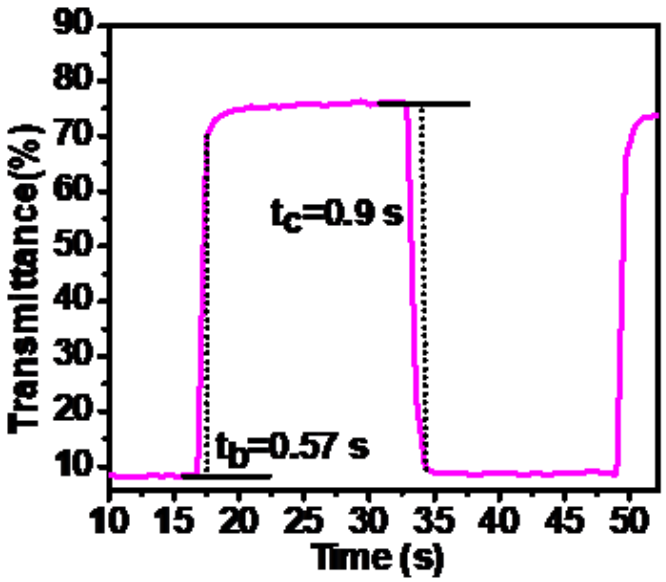

Fig.1.08. Representation of Switching times.

1.06.04. Cycle Stability

An ECM must undergo stable redox cycling for its repeating switching steps **(Fig. 1.09).** A rapid loss of EC contrast may occur due to the degradation of any redox components which affect the full performance. Degradation occurred due to water and oxygen interaction, high potentials etc. Also, degradation of the electrode material and evaporation of electrolyte reduces cycle stability. Redox cycling may be improved by thin-film depositions with homogeneity, smoothness, and thickness. Long-term cycle stability are measured in a three electrode cell via repeated cycling of potential. ECDs must be sealed to minimize solvent evaporation and areal oxidations. Charge compensation around the device extends its lifetime.

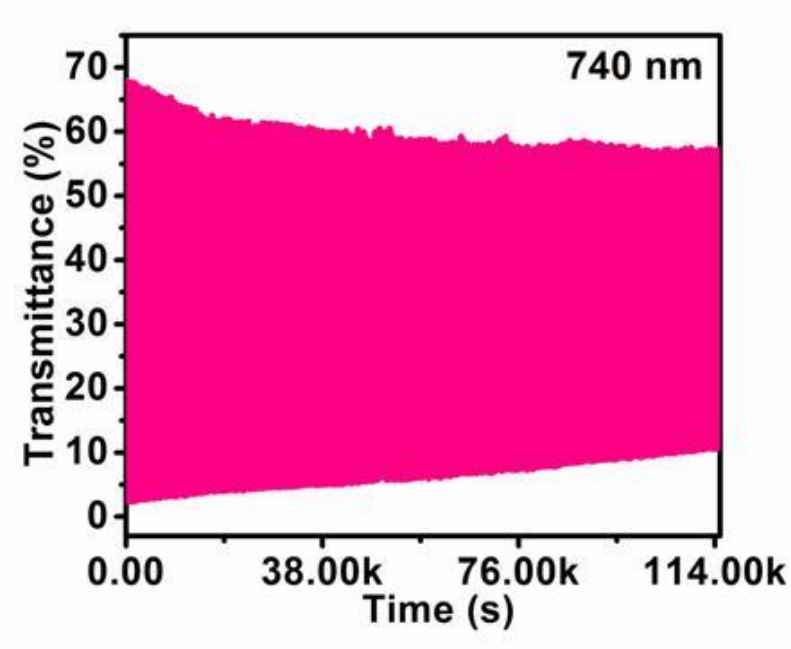

Fig.1.09. Representation of Cycle stability.

1.06.05. Optical Memory

Optical memory means the propensity of an EC system to retain its coloured state although the external bias is removed, also known as open-circuit memory. In absence of applied voltage, electrochromes will freely diffuse by self-erasing mechanism thats why Solution based ECDs exhibit their coloured state to bleach state rapidly. On the

other hand, conjugated polymers are good adhered into the electrode surface which minimizes self-erasing effect.

1.06.06. Durability and Lifetime:

Durability refers to the ability of a material to withstand an unfavorable external environment. For example, the requirements of the international equipment durability standard, American Society for Testing and Materials (ASTM) E2141-14 for ECDs should be satisfied. An eligible EC display should be able to work under certain extreme conditions including temperature (from −40 to 80 °C), humidity (reaching 80%), and even some degree of external force. At the same time, organic materials generally have imperfect photostabilities, especially to ultraviolet (UV) rays and oxygen, which is an inherent disadvantage that needs to be addressed urgently. Moreover, the lifetimes are also critical parameters. On one hand, the electro-optical switching capacity of an ECD should be maintained after coloring-bleaching cycles. To meet the demand of high-intensity information switching in future practical applications, the ideal reversibility (cyclic life) of EC displays should reach at least 10^4–10^6 cycles without significant optical degradation.

1.06.07.Quantification of colour

Another important parameter is the development of coloration during redox process. A colour description is difficult due to its subjective nature. The objective colour absorption do not suggest a clear intuition into the human eye. Colorimetry measures human eye's sensitivity towards light. A colour is predicted and quantified by using three attributes, a) the hue which is the wavelength associated with some colour, b) the saturation which is the relative levels of black and white and c) luminance which is the brightness of colour **[88].**

For CIE (Commission Internationale de l'Eclairage) calculation has established several colour spaces expressed in terms of XYZ tristimulus concept, based on the three-component theory of colour vision (blue, green and red). CIE 1976 colour space represents the relation between green (- *a**) and red (+ *a**), and between blue (- *b**) and yellow (+ *b**), while *L** value indicates the lightness **[Fig. 1.10].** The values of *a** and *b** increase with the saturation of colour, whereas the 0, 0 value corresponds to an

ideal achromatic sample (i.e., neutral colours such as gray or black). Although colour is a three-dimensional phenomenon, colour spaces are usually represented graphically separated into two attributes, chromaticity and luminance, in such a way that can be more easily visualized in a two dimensional space **[89].** Thus, chromaticity which represents the hue and saturation are represented in a two-dimensional space, while the luminance which describes the brightness of the colour is set at a fixed value (e.g., xy chromaticity diagrams).

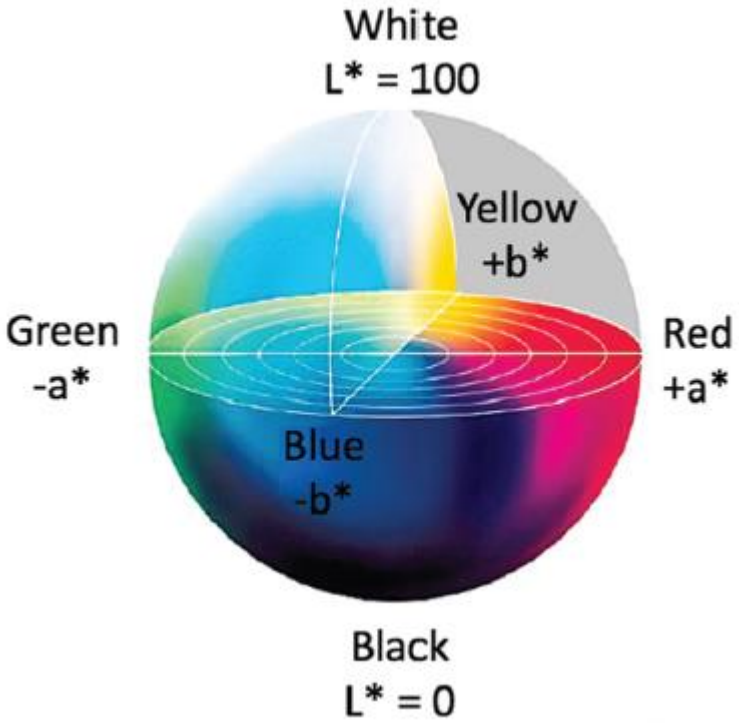

Fig. 1.10. 1976 CIE L*a*b* colour space used for colorimetric analysis.

1.07. Electrochromic device fabrication

Electrochromic displays have been constructed by a transparent electrode coated with a layer of EC materials, transparent semi solid gel electrolytes and an EC material for counter electrode. Electrochromic devices consist of one transparent electrode with a cathode material and anode material and ion conducting electrolyte. When one electrode is oxidised then the other is reduced by applying electric potential, which leads a device switch in between a neutral colour and the oxidized colour. The

conductive electrolyte provides separation between cathode and anode as well as it is a source of ions to balance the oxidation and reduction process. 0.512 g lithium perchlorate and 2.8 g poly methyl methacrylate is dissolved in 6.65 ml propylene carbonate and 28 ml dry acetonitrile is pipetted and let it to dry under room temperature for 15 minutes. By sandwiching two substrates, one is with polymer film and gel electrolyte, the device is fabricated. The device was covered using parafilm spacer. The schematic diagram of fabricated device in **Fig.1.11.**

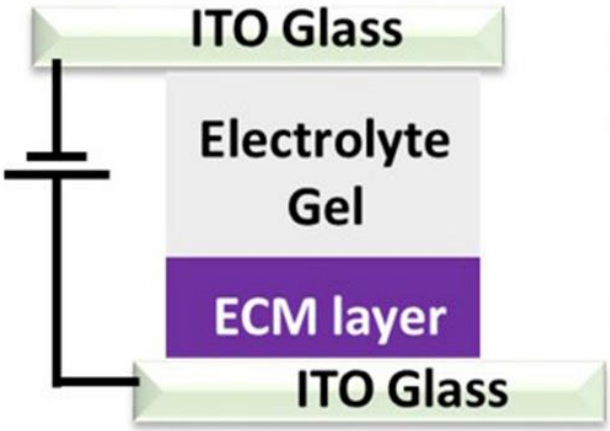

Fig.1.11. Schematic diagram of an ECD.

With increasing the demand of wearable and stretchable displays, EC e-skins, and highly foldable EC films, technologies have targeted in soft EC devices **(Fig.1.12 and Fig.1.13)** ITO or FTO coated glass cannot be used in these innovative ECDs because of the brittle and rigid nature of the conducting glasses. An innovative concepts, foldable, flexible, and stretchable conductors with high conductivity and transparency are very crucial. ITO-coated poly (ethylene terephthalate) (PET), a flexible substrate, can do excellent EC performance **[90].** Various flexible and transparent electrodes have been invented substituting ITO and FTO like carbon nanotubes **[91],** graphene **[92, 93]** conducting polymers **[94]** metal nano wires **[95, 96]** and metal grids **[97, 98]** etc.

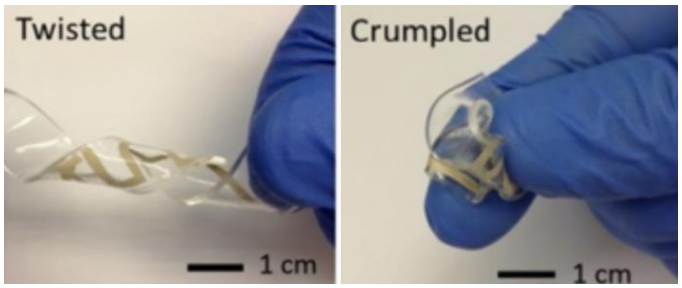

Fig.1.12. Stretchable devices being twisted and crumpled, showing excellent mechanical robustness.

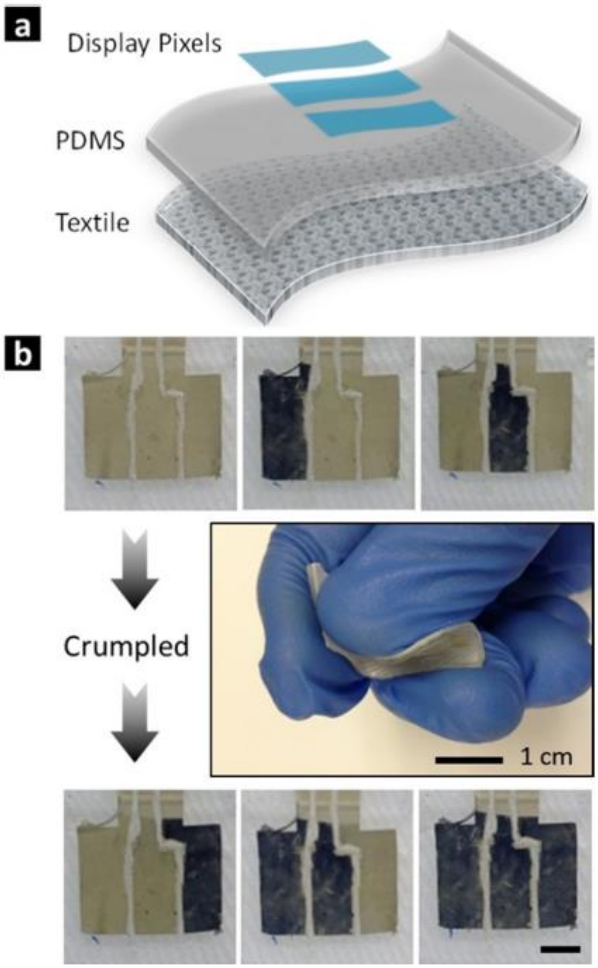

Fig.1.13. (a) Schematic of the electrochromic electrode implanted onto wearable textiles. (b) Example images showing the ability to control the coloration/bleaching of individual display pixels and their mechanical stabilities against deformations such as crumpling. Scale bars for display pixels: 2 mm.

1.08. Electrochemical Polymerisation:

Advance electronic devices like sensors, OLED, organic solar cells are increasing the interest about electrosynthetic conjugated conducting polymers. Electrochemical

polymerization is a less time consuming technique by which polymerization of a monomer solution occurs electrochemical oxidation method within a potential window without using any catalyst or polymerisation agents. The potential is generally applied by Cyclic Voltametry. The polymer is formed on working electrode. The growth of the polymer film is simply tuned by the number of CV scans. An easy to use method for electro-synthesis conducting polymer preparation **[99-108, 109].** Electro-chemically polymerized materials show the unique morphology, physical, electrochemical properties that are making the films amenable to different applications **[110].** Because of this oxidation is current-induced, EP is a green methodology **[111-115].** As no toxic oxidant is used, the technique produces real-time controlled conducting polymer film with high purity **[116].** The polymer film exhibits excellent electronic, optical, magnetic and rheological properties **[117].**

1.08.01. General Principle of Electrochemical Polymerization:

Electropolymerization occurs by a general accepted mechanism by forming radical cation by monomer oxidation on a electrode surface **(Scheme 1.3).** The EP method can be divided into 2 groups, one is anodic EP and another is cathodic EP. Anodic EP is one of the best method for oxidizing monomer to make conducting polymers. This method starts by forming of radical cation from a monomer **[118, 119].**

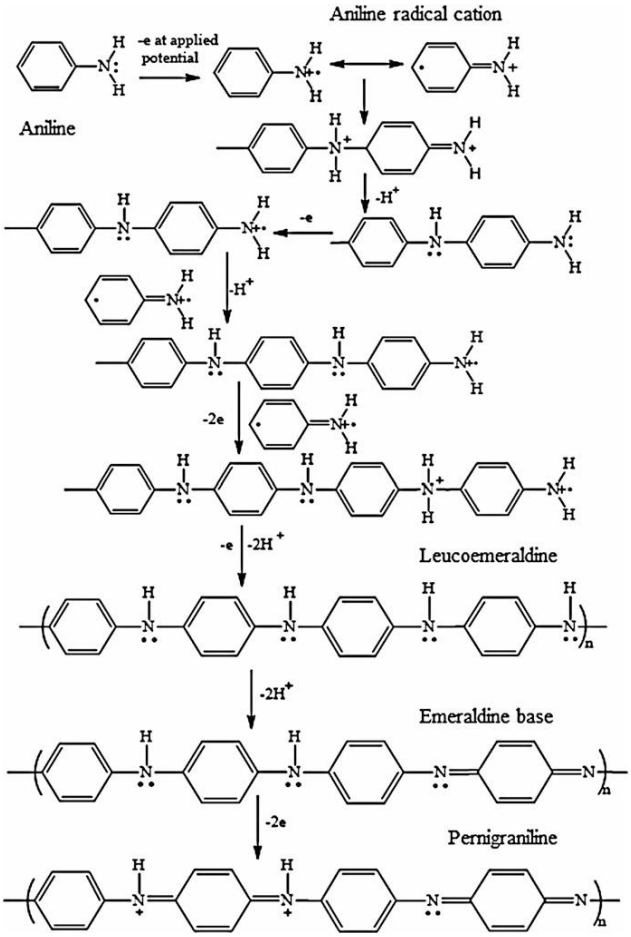

Scheme 1.3 Mechanism for the anodic electrochemical polymerization of polyaniline.

The growth involves coupling between radical cations. The radical cation reacts either with neighbouring cations or with neutral monomer. The cathodic electropolymerization is used rarely for synthesising CP. Although, this process involves reductive electrosynthetic processes which lead to polymer formation with low yield. Only Poly (p-phenylene vinylenes) (PPVs), used for OLED **[120, 124],** are produced by the cathodic electropolymerization method.

1.08.02. Electrodes Materials:

A conventional 3 electrode electro-chemical cell is taken. Working electrode (WE) on which the desired reaction happens, be an inert metal like Au, Pt, Ti **(Fig. 1.14) [125-131],** a C- material like glassy carbon, Pyrolytic graphite and boron-doped diamond **[132-138],** a conducting glass like indium tin oxide (ITO) **[139-141].** WE surface

nature influences the oxidation of the monomer, polymerization rate, and the polymer film formation. The alloys used is limited for WE due to the high potential requires for monomer oxidation. The reference electrode (RE) measures working electrode potential. It is prepared from a silver wire immersed in 3 M Ag/AgCl solution, when aqueous electrolyte is used. Silver wire wire is used as pseudo reference electrodes when the EP medium is organic. The

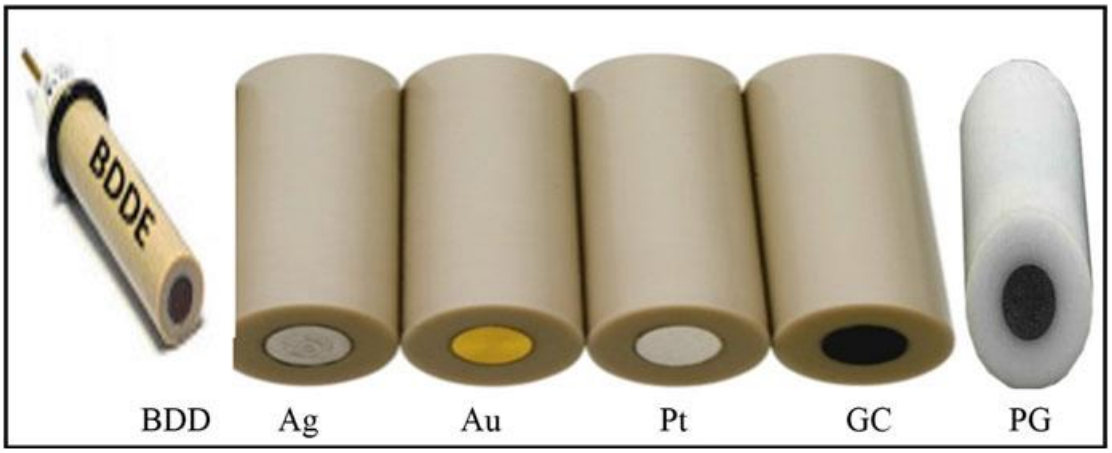

Fig.1.14. Examples of working electrodes used for the electropolymerization of conducting polymers.

counter electrode should be an inert material, like Pt wire. To close the circuit in an EC cell, counter electrode is used.

1.08.03. Supporting Electrolyte Solution:

EP is an useful technique for synthesizing electro-active polymers. The growth of the polymer films, morphology, properties are influenced by supporting electrolyte. It is also an important parameter and optimized when designing the electrochemical polymerization protocol. Supporting electrolytes used for aqueous and organic solvents for different monomers are listed in **Table 1.5.** Addition with aqueous and organic medium, microemulsion medium is also a new approach for EP. Some studies identified aqueous medium is ideal for the electrosynthesis of CP because of low

pollution and applicability for large-scale applications. But, some limitations are there including low solubility in water of many organic molecules. Micro-emulsion is suggested as supporting electrolyte for EP, in order to solve the solubility problem in aqueous media.

Table 1.5. Relationship between solvent and polymerization

Medium	Electrolyte	Polymer
Organic solution	Tetrabutyl ammonium perchlorate/ACN or DCM, tetramethylammonium trifluoromethane-sulfonate/ACN, tetrabutylammonium hexafluoro phosphate/acetonitrile or DCM.	Poly TPA and poly carbazole
	ACN, DCM, nitrobenzene, and propylene carbonate	Polypyrrole, polyindole
Aqueous solution	H_2SO_4, HCl, HNO_3, copper (II) nitrate, sodium sulfate, sodium sulfate/sodium perchlorate, lithium perchlorate, sodium benzoate, propylene carbonate/lithium perchlorate, phosphoric acid and trifluoroacetic acid	PANI

1.08.04. Solvent:

The cell contains solvent in addition to supporting electrolyte, in which the monomer is dissolved. Electrochemical reaction rate is affected by the solvent where the monomer is dissolved **[142].** Depending on the nucleophilicity and polarity of solvents, the solvent is chosen **[143].** The above two things determine the interaction of the solvent with radical cation intermediates. Solvent is chosen according to the solubility of the monomer, which must be highly pure and O_2 free to avoid areal reaction with the radical which forms hydroxides.

1.08.05. Reactivity of the Monomer:

The monomers used for EP are aromatic in nature **(Table 1.6).** The coupling reaction involves here is aromatic electrophilic substitution reaction. If the nucleophilic character of the solvent **(scheme 1.4) Table 1.6.** The electrophilic reactivity sites of some monomers and their idealized polymer structures obtained on the material surface.

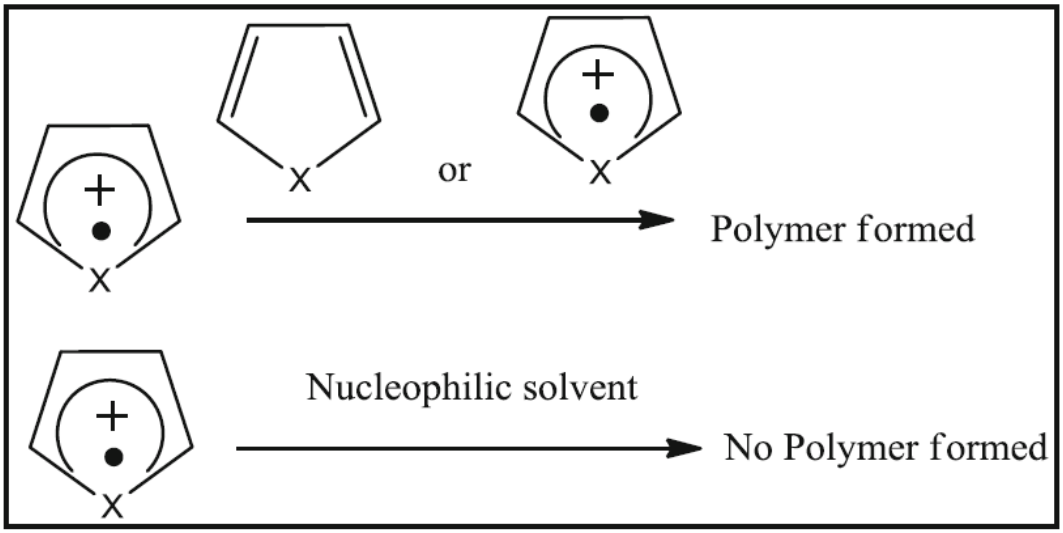

Scheme 1.4. Reactivity of the monomer depending on the solvent.

Table 1.6: Reactivity of the monomer depending on the solvent

Monomer	Electrophilic reactive site(s)	Ideal polymer structure
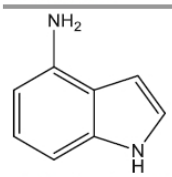 4-Aminoindole	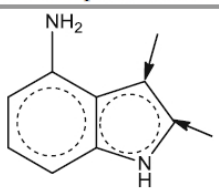	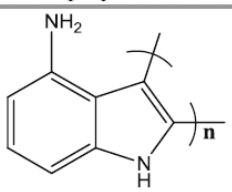
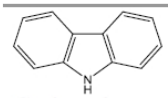 Carbazole	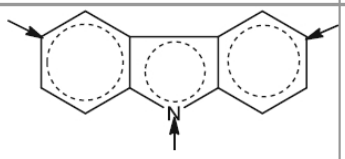	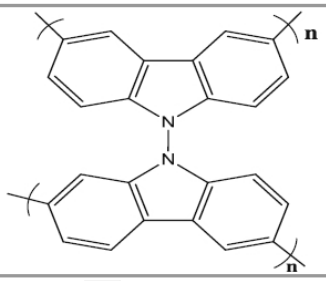
 Thiophene	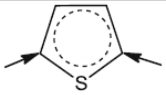	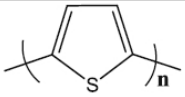
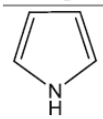 Pyrrole	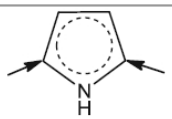	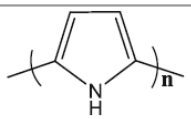
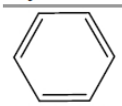 Benzene	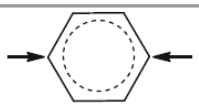	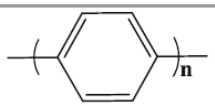
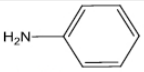 Aniline	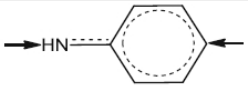	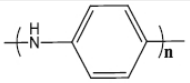
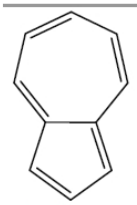 Azulene	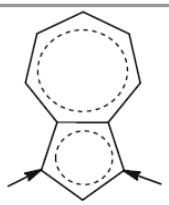	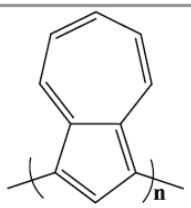
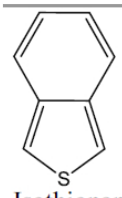 Isothionaphthalene	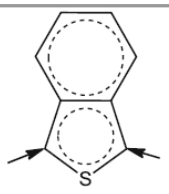	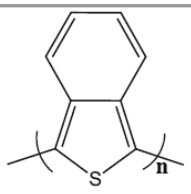
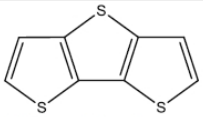 Ithienothiophene	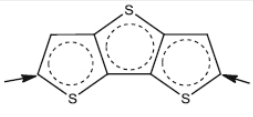	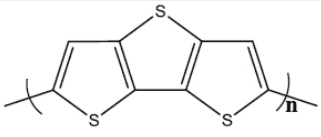
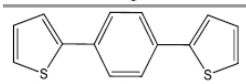 Dithienylbenzene	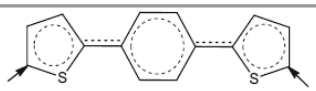	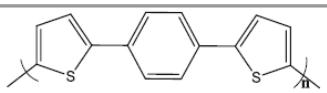

Monomer	Electrophilic reactive site(s)	Ideal polymer structure
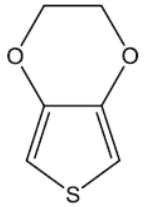 Ethylenedioxythiophene	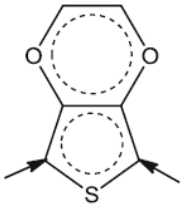	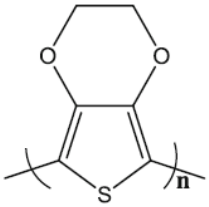
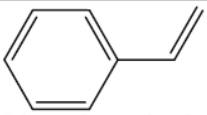 Phenylenevinylene	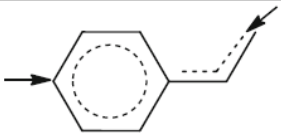	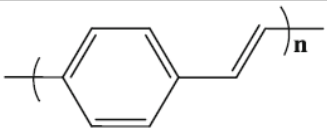
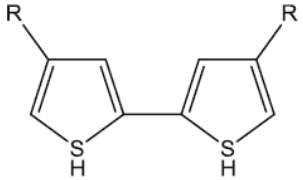 Bithiophene	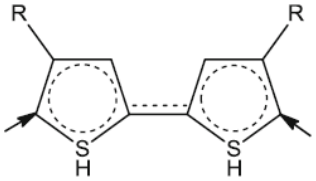	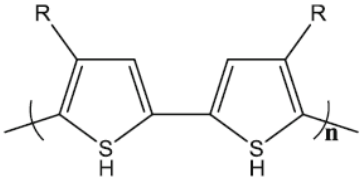
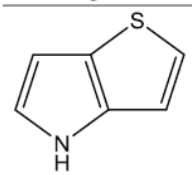 Thieno[3,2-b]pyrrole	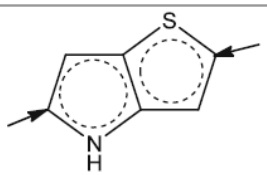	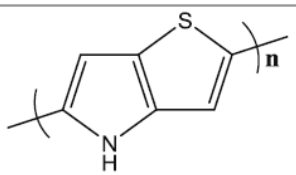
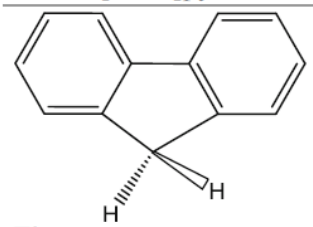 Fluorene	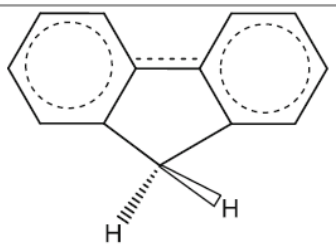	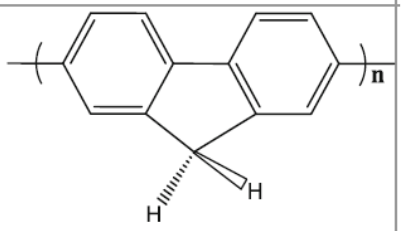

1.08.06. Choice of monomer

For electrochemical polymerisation, monomers having relatively lower anodic oxidation potential (less than 2 V) are picked up and are susceptible to electrophilic substitution reaction that lead to produce conjugated polymers. **Table 1.7** shows that the electrochemically polymerizable reported so far have peak potential below 2.1 V. The advantage of low peak potential is that low peak potential avoids complications in the polymerisation arising from the oxidative decomposition of the solvent and the

electrolyte. Another factor is all the monomer being aromatic in nature undergoes electrophilic substitution reaction by maintaining the aromaticity.

Table 1.7. Electrochemical data for some heterocyclic and aromatic monomers

Monomer	**Oxidation potential (V) vs SCE**
Pyrrole	1.20
Bipyrrole	0.55
Thiophene	2.07
Azulene	0.91
Pyrene	1.30
Carbazole	1.82
Fluorene	1.62
Fluoranthene	1.83
Aniline	0.71
Triphenylamine	0.98

1.08.07. Techniques for Electrochemical Polymerization

Electrochemical polymerization is an important method for the synthesis of electroactive polymer films, the properties of the film depend on the choice of technique. Generally, galvano-static, potentio-static, or potentio-dynamic techniques are employed for electrochemical polymerization.

1.08.07. a. Galvanostatic Polymerization Technique

At a constant current, Galvanostatic polymerization is performed and it results the formation of a doped polymer **[144].** The advantage of this technique is that it is

simple, suitable for practical application, and the thickness of the polymer film can be controlled by specifying the polymerization time. The current density should be chosen properly to avoid an increase the resistance at the electrode surface which may affect the intermediate reactions **[145].**

1.08.07. b. Potentiostatic Polymerization Technique:

Potentiostatic technique involves polymerization reaction takes place at a constant potential. The applied potential should be such that it oxidizes the monomer, as the polymerization process is initiated by the monomer oxidation. Also, the potential should be such that it avoids secondary reactions **[146].** Linear sweep voltammetry (LSV) is used to oxidize the monomer. The potential window within which electro-polymerization occurs without the over oxidation of the monomer which may impede the polymerization process or cause undesired reactions to take place. Some monomers are easily oxidized. Over oxidation may lead to the formation of polymers with reduced electro activity and conductivity. In addition, over oxidation may lead to the formation of hydroxyl and oxo derivatives as well as dimer and trimer products rather than the desired polymer.

1.08.07. c. Potentiodynamic Technique:

Potentiodynamic technique involves by using cyclic Voltammetry (CV). A cyclic change is occurring of the monomer exposed on the electrode by the applied voltage within a potential window by switching between oxidative and reductive scans. Thickness of the deposited film depends on the number of CV cycles operated. Depending on the reaction mechanism, Potentio-dynamic polymerization results in the formation of Cyclic Voltammograms with some characterization peaks.

1.08.08. Monomer Concentration:

Monomer concentration is also an important parameter for the electropolymerization process and the polymer films formed is conductive **[147].** The current density increases with increasing the monomer concentration that is because of the faster dimerization, which can be expressed by the following equations:

$$i_a = i_0 e \frac{(1-\alpha)nF(E-E_{OCV})}{RT}$$

$$i_0 = nFAC_R^{bulk\ (1-\alpha)} C_0^{bulk\ (\alpha)} k_a$$

where i_a is the oxidation current, i_0 is the exchange current, k_a is the rate of oxidation, R is the ideal gas constant, T is the temperature, C_R and C_0 are concentration of the reduced and oxidized monomer, respectively, A is area, F is the Faraday constant, n is the number of electrons exchanged, α is charge transfer coefficient, E is the oxidation potential, and EOCV is the open circuit voltage.

However, for some conducting polymers, increase in monomer concentration results in a decrease in the oxidation potential. In addition, pH is used to control the critical potential beyond which the degradation of the polymer can occur during polymerization **[148].** Indeed, when polymerization takes place at low pH, the potential exceeds the critical value. The potential subsequently decreases with time to a constant potential value, which is low enough to prevent the degradation of the polymer chain. On the other hand, at high pH, the opposite behaviour is observed, where the increased deposition of insulating polymer species reduces the conductivity of the working electrode. This increases the polymerization potential, resulting in the degradation of the already deposited polymer film, due to the formation of hetero junctions or other unusual chemical bonds **[149].** Other parameters, like the rate of the polymerization reaction and the cathodic charge determine the mechanisms of polymer growth.

1.08.09. Doping effect on electrochemical polymerization:

Doping involves the introduction of a species called dopant or counter ions into a polymer structure. This occurs usually stoichiometrically in order to compensate the positive charge of the polymeric species to attain electro-neutrality. The insertion of dopants into a polymer is one way of improving its properties, such as morphology,

conductivity, electrochemical activity, and the rate of polymerization **[150].** The dopant should be both chemically and electrochemically stable within the potential range for the polymerization process. Beside the enhancement of the conductivity and the electro-activity of a polymer, counter ion dopants have significant effect on the polymer growth rate and its redox characteristics. The doping of a conductive polymer is classified as either chemical or electrochemical doping. Chemical doping is more frequently achieved by exposing the polymer to an oxidant (such as iodine or bromine), and less frequently by using a reductant (typically an alkali metal). In electrochemical doping, on the other hand, a polymer film deposited on a working electrode is suspended in an electrolyte solution (in which the polymer is insoluble) along with separate counter and reference electrodes. An electric potential difference is created which charges the polymer and causes appropriate counter ions from the electrolyte to enter the polymer. This charge transfer process creates a localized negative (n-doping) or positive (p-doping) charge on the polymer. This often leads to the distortion of the bonding structure of the polymer backbone and the formation of polarons and bipolarons which can delocalize along the polymer chain or in an electric field. Electrochemical n-doping is far more common because of the ease of excluding oxygen from a solvent in a sealed flask. The interaction between the polymer and the p-type dopant usually leads to the partial oxidation of the organic polymer π-backbone. The transfer of electrons from the valence band of the polymer to the acceptor dopant leads to the delocalization of holes within the polymer backbone and the enhancement of the conductivity of the polymer system **[151].** The illustration of the concept of n- and p-doping is as shown in **Fig. 1.15.** Many dopants such as anthracene sulfonic acid, benzene sulfonic acid, chloride ion, dibenzene sulfonic acid, hydrochloric acid, methane sulfonic acid, naphthalene sulfonic acid, perchloric acid, poly (acrylic acid), poly (aniline sulfonic acid), poly (4-styrene sulfonic acid) (PSSA), poly (vinyl sulfonic acid), p-toluene sulfonic acid and sulfuric acid) have been used in the electrochemical doping of polymers **[152-155].**

1.08.10. Mode of Initial Scan:

When monomer is electropolymerized onto an electrode surface, different coloured polymer films are obtained. The colour of the polymer depends on the initial scan direction. When the scan is cathodically carried out, p-doped polymer film is formed, while when the scan is anodically carried out, the polymer formed is neutral. Both formed p-doped and neutral polymer

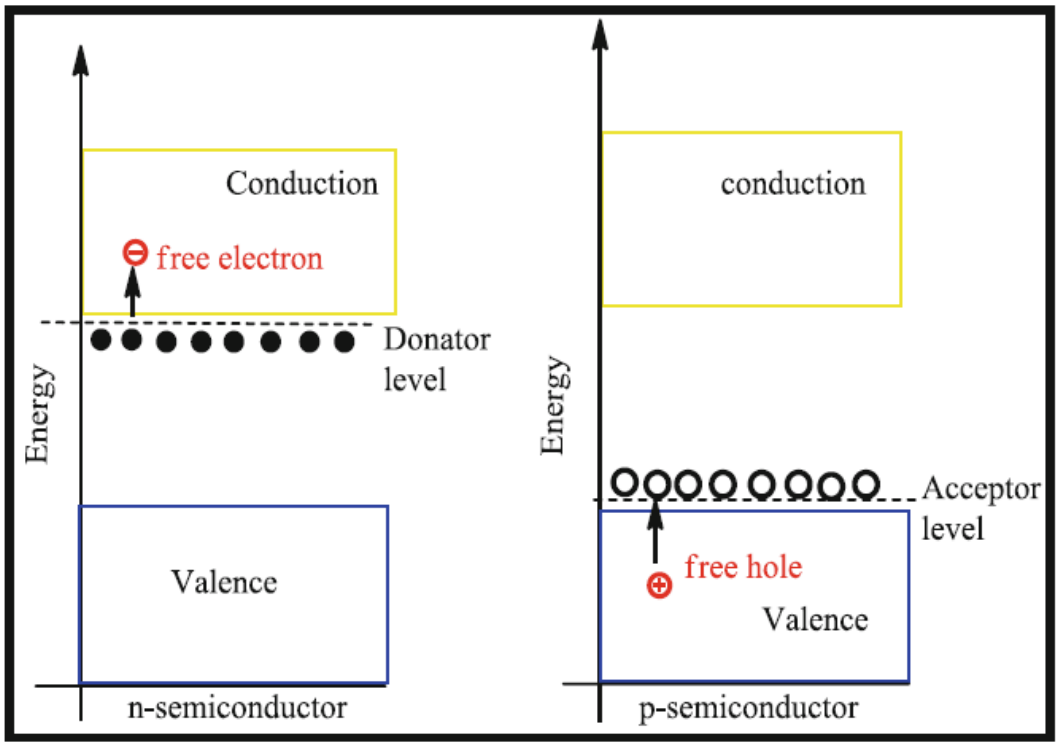

Fig.15. Schematic representation of the n- and p-doping processes.

vary in solubility, electrochemical properties, and conductivity. Other factors influence EP reactions include temperature and the nature of substituents of the monomer. Temperature affects the kinetics of the polymerization reaction process and also determine the extent of the undesired side reactions. For example, the oxygen species in the reaction medium are sensitive to high temperature, they can easily react with free radicals formed from anodic processes, thus decreasing the polymerization efficiency **[156].** On the other hand, the rate of polymerization increases with

temperature due to improved conductivity and electro-activity of the monomer at high temperatures.

1.08.11. Advantages of EP process:

In the electrochemical process, the synthesis as well as modification is done in one step. Electrochemical oxidation of a monomer produces free radical which is adsorbed on the electrode surface. The film thickness can be controlled, and a multilayer film is also obtained within few minutes by using a tiny amount of monomer on the surface of electrode. The polymer films can easily be characterized. For chemically synthesise, further purification and characterization is required to confirm the product formation. Another advantage is that the polymer film formed exhibits some physical properties those are inherent to metals or semiconductors **[157].**

1.08.12. Disadvantages:

The disadvantage of EP is that the polymer film is formed with very low yield and insoluble in most of the organic solvents. Also for large scale and large area polymer film production, this method is not suitable.

Another widely employed polymerisation technique is chemical polymerisation. Other techniques are also used to synthesize conjugated polymers including photochemical polymerisation, metathesis polymerisation, plasma, pyrolysis and solid state polymerisation.

1.09. Chemical polymerisation:

To obtain solution processable EC polymers, such as the Suzuki-Miyaura cross coupling reaction, 2+2 cyclo-dimerization and the oxidative coupling reaction were employed. For synthesis of conduction polymer by chemical polymerisation method one has to use stoichiometric amount of oxidising reagent. Oxidative chemical polymerisation is the low cost, simple and normally used in the synthesis of EC polymers. Heterocyclic monomers are usually polymerised with $FeCl_3$ as the chemical oxidant although other oxidants can also be employed. Although chemically prepared

polymers are more laborious to synthesize, there are significant advantages presented by this method. Chemically prepared polymers allow for more complete characterisation, including elucidating the molecular weight, thermal characteristics like crystallization, thermal stability, T_g, and analysis of the polymer end groups **[Table 1.8].** Furthermore, solution processability of chemically prepared polymers facilitates practical large scale film preparation. Some drawback of chemically synthesized polymers are products are generally in power form ultimately decreasing the intrinsic propertied of the materials obtained such as having very low conductivity and also an abundance of side reactions occurring during chemical oxidation polymerisation of hetero-cycles including formation of coupling defects along the backbone.

Table 1.8. Comparison between Electrochemical and chemical polymerisation

Electrochemical polymerisation	**Chemical polymerisation**
Time taking for polymerisation is very less. It will occur in few minutes.	More time is required for chemical polymerisation.
No catalyst is required, polymerisation occurs by using a little amount of monomer.	Catalyst is required, polymerisation requires a certain amount of monomer.
The synthesis and modification can be done in one step.	**3.** The synthesis and modification can not be done in a single step.
No further product purification and characterization is required to confirm the product formation.	4. Polymer purification and characterization is required to confirm the product formation.
Yield of polymer formed is very less and the product is insoluble in most of the organic solvent.	5. Yield of polymer formed is high.
For large area polymer film coating, this method is not suitable.	6. Polymer film may be coated in large area by vacuum deposition, spray coating, ink jet printing method.

1.10. The Optimization and Innovation of Manufacturing Technologies

Other manufacturing technologies for EC materials include vacuum evaporation, magnetron sputtering, solution processing, sol−gel method and so on. Different processes will affect the performance and manufacturing cost to varying degrees. Therefore, the optimization and innovation in manufacturing technologies are also important for enhancing the commercial potential of future EC displays.

To date, there are two prototypes, one is a) segmented displays and another is b) pixel displays for future EC displays, which serve as carriers of emerging EC materials and devices. EC segmented display is a relatively simple display mode, it is used to display some fixed graphics, numbers or letters. This display can also achieve dynamic switching of some contents through simple control of inputted electrical signals. A classic example is the segmented alphanumeric display. Currently, EC segmented displays have attracted widespread attention due to their remarkable application potential in the aesthetic design of intelligent displays with vivid colour and fantastic patterns, although information capacity is not as good as that of pixelated displays. The key point in fabricating EC segmented displays is to prepare EC patterns. According to the working principle of ECDs, several necessary processes must be met, (i) electron transfer on electrodes and at electrode/active material interfaces, (ii) electrochemically driven redox processes of active materials, and (iii) ion transfer inside the device.

1.10.1. Electrode Patterning

Segmented displays can be realized with the electrode patterning strategy by limiting the interfacial electron transfer between EC materials and electrodes, as shown in **Fig. 1.16.** Electrode patterning is a simple and convenient process to quickly obtain the anticipated EC patterned (segmented) displays **(Fig.1.16).** This strategy avoids the complicated synthesis or modification in patterning active materials and does not depend on the structures and properties of related materials. Therefore, it exhibits

attractive application potential in simple EC devices/ displays. There are many approaches for fabricating patterned electrodes, such as laser etching, inkjet printing, and template-assisted coating/printing methods. As a good verification of the above approaches, Pooi S. Lee's group have fabricated patterned Ag NW electrodes and further have demonstrated the first stretchable and wearable patterned WO_3 ECDs. Sean X. A. Zhang, Yu-Mo Zhang, and coauthors demonstrated various EC segmented displays (e.g., electronic billboards, eye glasses, e-readers, and shelf labels) based on patterned ITO electrodes prepared by laser/chemical etching. In 2020, Masayoshi Higuchi and coauthors have reported an interesting EC "flower" display based on [Fe(II)/Os(II)] supramolecular polymers as EC materials and patterned ITO electrodes. Three patterns have been realized through point-to-point control of different circuits. It is commendable that this display could completely implement the reversible change in different colors under different applied voltages **(Fig. 1.17).**

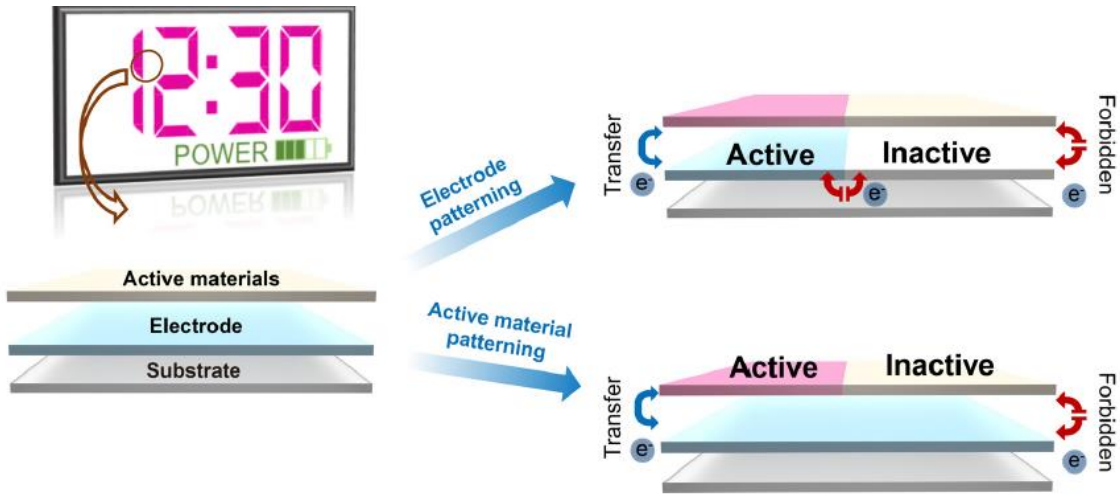

Fig.1.16. Schematic of EC segmented displays and related fabrication strategies including electrode patterning and active material patterning.

On the other hand, its disadvantage is that the resistance of the patterned electrode after etching will increases, especially when the size of the etched patterns is very small.

1.10.2. Active Material Patterning

In the fabrication of EC segmented displays, even pixel displays, the active material patterning strategy is widely used. To achieve this strategy, many advanced processing technologies (e.g., printing and coating, photolithography, etc.) have been reported and applied. Because the size of the required single patterns/ pixels varies depending on the application scenario, there is no uniform size standard that can be used as the judging criterion in this field. For instance, the required size of an EC pattern/pixel is on the order of micrometers when the display is used as an electronic screen for mobile phones or monitors, but is on the order of millimeters (even centimeters) when used as a large area electronic billboard.

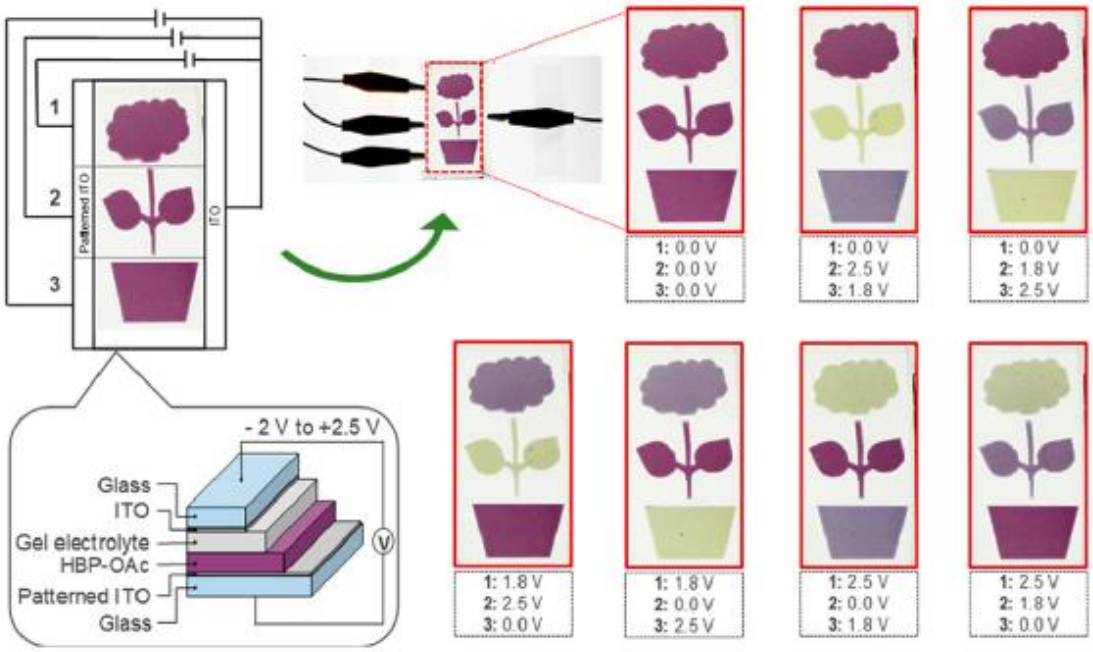

Fig.1.17. Copyright 2019 Springer Nature. The structure and images of EC segmented display with different colour information at different voltages.

1.10.3. Printing and Coating

As typical solution-processing strategies, conventional printing and coating techniques have wide applications in the fabrication of ECDs and in other fields. With these techniques, the strict production environment and expensive equipment required

for traditional processing (for example, vacuum evaporation and magnetron sputtering) can be efficiently avoided. Based on the differences in manufacturing processes, printing and coating techniques can be divided into two types: (i) coating techniques and (ii) digital printing techniques. The first type mainly includes blade coating, slot-die coating, spin coating, spray coating, etc. Coating techniques play an important role in roll-to-roll or simple solution-processing for ECDs. Furthermore, some representative EC patterned/segmented display prototypes were fabricated with these techniques. The realization of fine EC patterns is inseparable from additional patterning processes (e.g., printing templates). Unlike the aforementioned coating techniques, digital printing techniques (such as inkjet printing, dispensing printing, and 3D printing) have the advantage of simple and efficient direct-patterning. These techniques have shown incredible applications in the solution-processing of active materials for EC segmented displays.

Inkjet printing has achieved remarkable progress in the fabrication of printed circuit boards (PCBs), electronic components, solar cells, and other functional materials. With this technology, quantitative droplets of functional inks are ejected out from digital-circuit-controlled nozzle(s) and dropped on substrates to form the desired patterns. In this process, the compatibility of EC inks, printing equipment, and substrates is the key factor. In addition, the relevant material (ink) should maintain the appropriate physical and chemical properties before/during/after printing. The properties described herein include solubility, viscosity, corrosion resistance, electrical resistivity, and compatibility of different components. To date, the inkjet printing technique has shown outstanding application potential in the processing of commonly used EC materials (including small organic molecules, CPs, and even inorganic materials) and related auxiliary materials (such as electrolytes, ion storage materials, elasticizers/flow promoters, and suspending/dispersing agents).

Next I will discuess about triphenyl amine and TPA based EC systems as my thesis work contains TPA based EC polymers.

1.11. TPA based EC polymers:

The three dimensional, propeller-shaped triphenylamine (TPA) is a promising optoelectronic molecule **[Fig.1.18]** for its good thermal and morphological stability **[158-160].** Being a good electron donating properties, TPA derivatives are used in semiconducting industry **[161-167].** Unsubstituted TPA is readily oxidized to form radical cation on application of potential **[168-175].** This radical cation resonates and dimerizes to form tetraphenyl benzidine (TPB) **(Scheme 1.5) [176, 177].** Two consecutive oxidation of TPB radical cation occur to form a spinless dication in the second step. The TPB is easily oxidized rather than TPA and undergoes further oxidations give $TPB^{+\cdot}$ and TPB^{+2}.

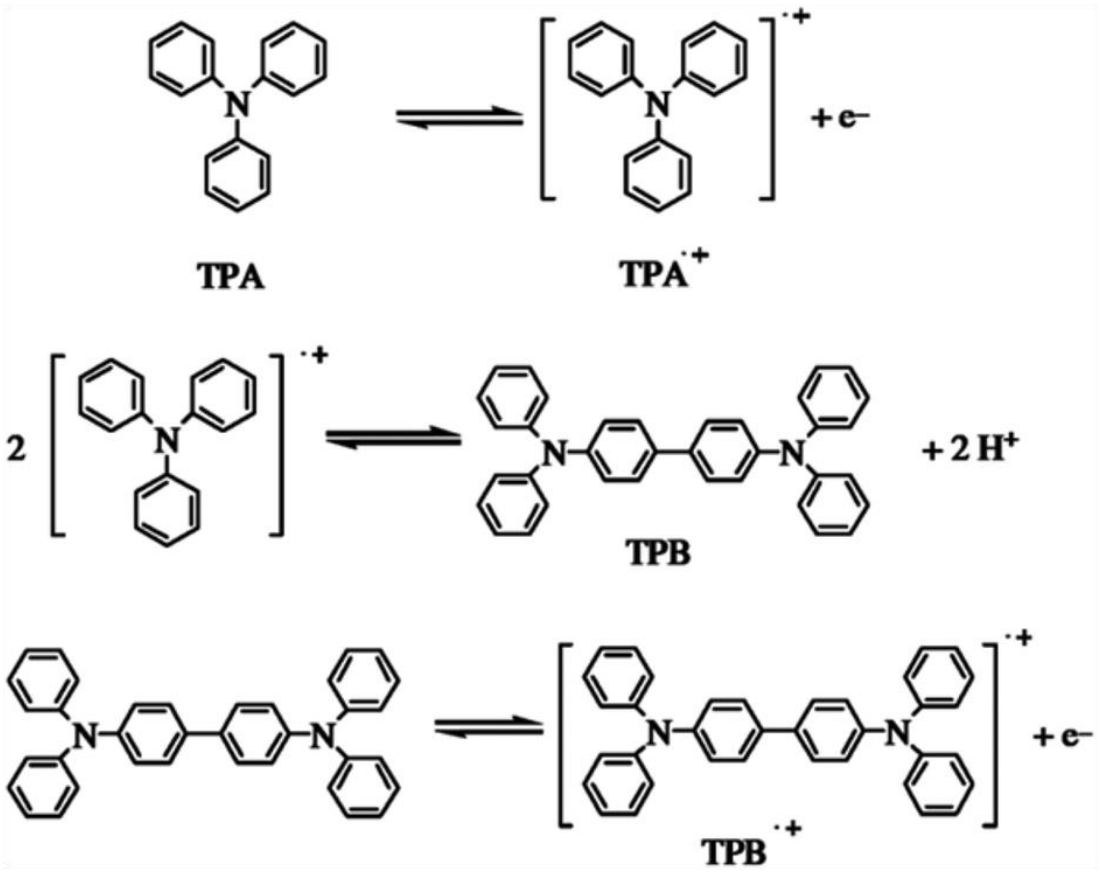

Scheme 1.5. Mechanism of TPB formation.

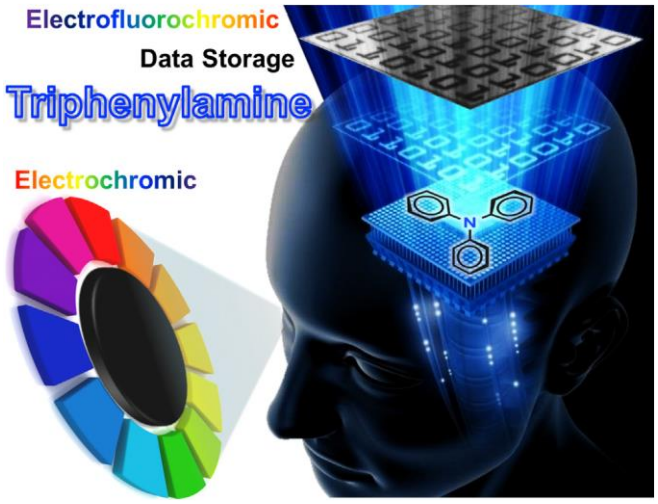

Fig.1.18. TPA and electrochromism.

Radical cation of TPA explains the electrical transport properties. A hole injection from the electrode results a temporal transformation of a neutal molecule to a radical cation. This charge carrier hopping between molecules is considered as an internal redox reactions. Semiconductor properties of TPA derivatives are evidenced from quantum chemical calculations that show a better planarity of TPA than sp^3 hybridization **[178-180],** which indicates a significant contribution of sp^2 hybridization by n-π conjugation, which increases the semiconducting properties. Among all cathodically and anodically TPA containing polymers, TPA is far extensively studied ECM for smart window application as an anodically colouring material due to its low material cost, high EC efficiency, cycle stability and reversibility large dynamic range. There are so many techniques are available to prepare TPA containing EC thin films. Majority of method is categorized into physical, chemical and electrochemical thin films. Most noticeable properties of electro-active polymers based on TPA are either electrochromic or electrofluorochromic in nature. The detailed survey of TPA based EC systems like aromatic polyimides and/or polyamides, epoxy resins, various conjugated polymers, different metal complexes, poly-siloxane gels as well as various small molecules have been discussed in the following section.

1.11.1. Triphenylamine based polyimides

Aromatic poly-imides are considered as a pivotal class of materials as it can be appraised as a possible substitute to glass and metals in mainly in the semiconductor and electric packaging industry **[181-193].** The formation of charge transfer (CT) complex is due to the strong intra and intermolecular interactions between electron-accepting dianhydrideand electron-donating diamine moieties. In 1991, Vasilenko first prepared TPA-based Poly-imides, followed by Nishikata **[194, 195]** from 4,4′-diaminoTPA and different tetracarboxylic dianhydrides **[Scheme 1.6].** TPA containing materials are generally colourless unless they undergo some form of charge transfer interaction with an electron deficient acceptor species. By contrast, electron rich TPAs are easily oxidized to form stable radical cations and the oxidation process is always associated with a noticeable colour change. In 2002, Liou et al. reported first article to describe the EC property of the polymers containing TPA derivatives **[196].**

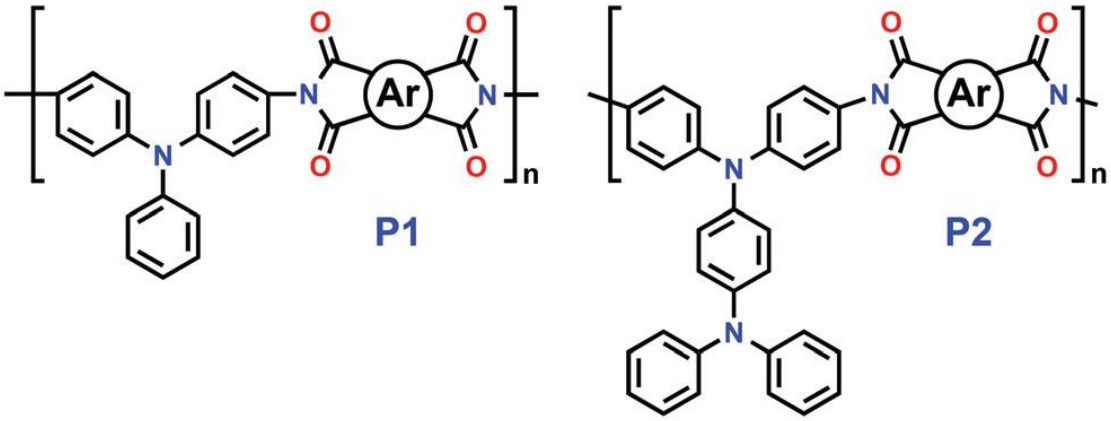

Scheme 1.6. Different polyimides.

These polyimides (PIs) are mostly thermally stable and soluble in polar solvents with very high glass-transition temperatures (Tg). Almost all of the thermally stable PIs are organo soluble and they can easily be solution cast into tough as well as flexible films. The PI films exhibit two reversible redox couples with the change of colour from pale yellowish to green and blue. They also show excellent EC stability **[197-202].** Liou

and Hsiao synthesized some TPA and/or triarylamine containing high-performance Poly-imides **[Scheme 1.7].**

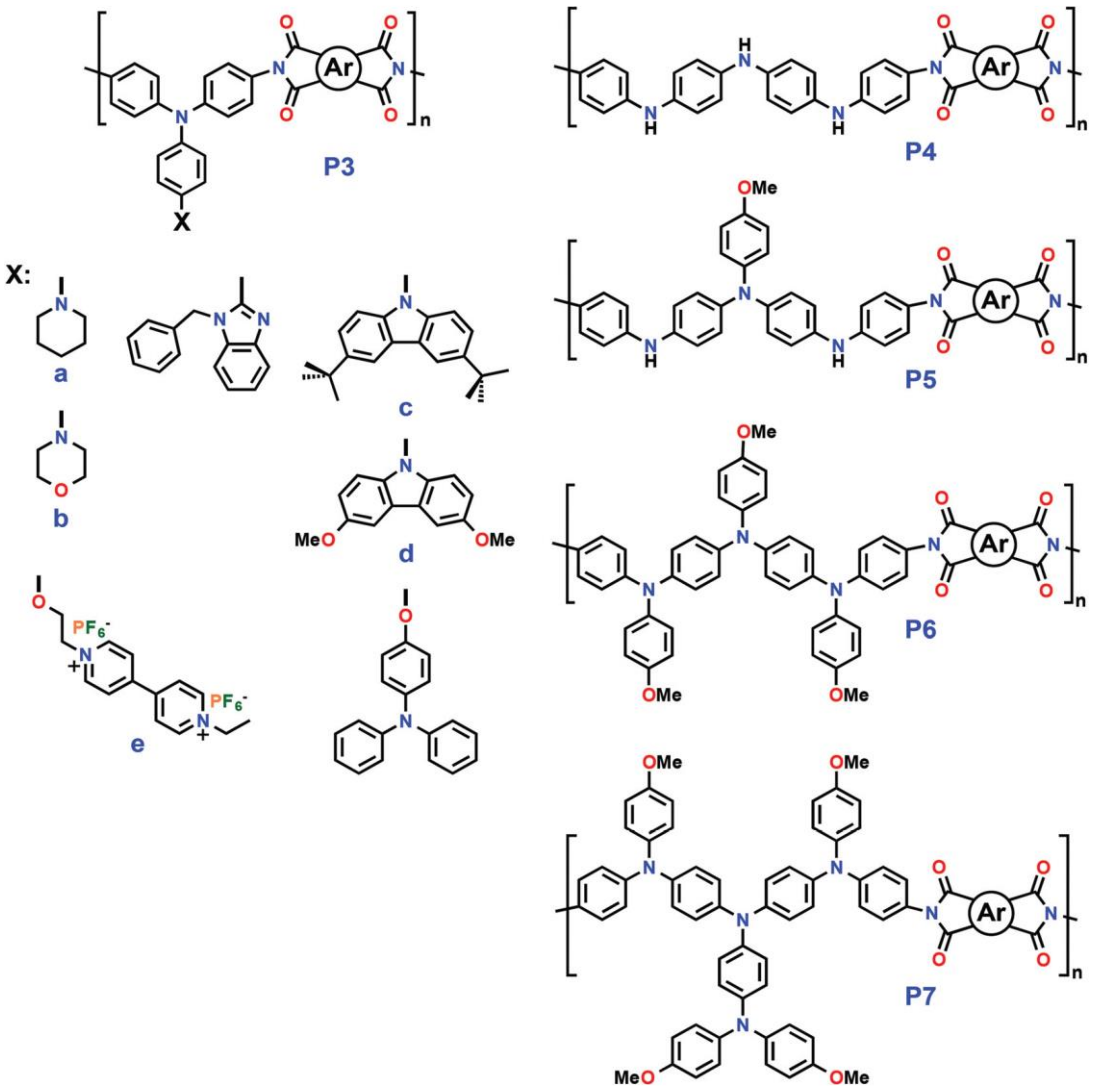

Scheme 1.7. Different polyimides.

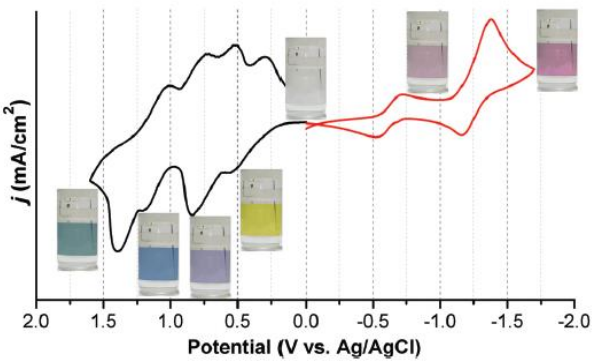

Fig.1.19. Cyclic voltammetric diagrams of P7 and its EC behaviours at various applied potentials.

Lower oxidation potentials with improved electrochemical stability have been observed for two types of PIs namely piperidine (P3-a) and morpholine (P3-b) substituted TPA. In addition, bulky tert-butyl (P3-c) or electron-donating methoxy (P3-d) substituents incorporated at the electrochemically active C-3 and C-6 sites of the carbazole unit also could prevent the coupling reactions of carbazoles, resulting in greatly improved redox and EC stability of the obtained PIs **[203-207].** Three novel solution-processable PIs P3e containing TPA and pendant viologen moieties have been prepared from the newly synthesized diamine and three commercially available dianhydrides. The obtained multi-coloured films have revealed ambipolar electrochemical behaviour with coloration changes from a transmissive neutral state to the cyan/magenta/yellow redox states, implying great potential for application in smart windows and displays **[208-215].** The stabilization of oxidized cationic radical is less feasible in DPA-based Poly-imides compared to TPA-based ones as DPA-based PIs lack an extra phenyl ring for resonance. Furthermore, due to the presence unrecoverable protons at the amino groups, DPA-based PIs exhibit lower electrochemical stability compared to TPA-based ones in the non-acidic electrolyte solution **[216-220].** The organo soluble PIs namely P7films have demonstrated high thermal stability and glass-transition temperatures. Reversible electrochemical oxidation and electrochromism have displayed by the P7 films both in the visible **(Fig. 1.19)** as well as near-infrared (NIR) regions with a considerably high coloration efficiency, contrast ratio along with low switching time, and extraordinary stability which is an essential requirement for long-term EC operation. These merits of P7 films make them a potential candidate for practically viable electronics applications **[221-224].**

1.11.2. Electropolymerized poly (triphenylamine)s

Nelson and Adams et al. have pioneered the work on unsubstituted TPA. Liou and Hsiao have demonstrated that introducing electron-donating substituent to triarylamine moieties can efficiently prevent the well-known formation of TPB **[225, 226]** from the unstable radical cation radical from TPA. The concept of radical coupling can be exploited to design and develop electropolymerizable monomers by

linking two or more unsubstituted TPA units with an electron-withdrawing core. Moreover, TPA core can easily be combined with thiophene, ethylene dioxy thiophene, dithienyl pyrrole, and chalcogenophene (Se, Te) derivatives through simple electrochemical processes as shown in **Schemes 1.8 and 1.9 [227–236].** Carbazole is another type of arylamine. Ambrose and Nelson have first systematically investigated the effect of substitution on carbazole and its N-substituted derivatives in 1968 **[237].** The oxidative dimerization reaction has been extensively used to fabricate electro-active polymer films on the electrode surface. This fabrication technique is advantageous for the electroploymerization of unprotected TPA and N-phenylcarbazole.

Hsiao's group have first reported a series of TPA and N-phenyl carbazole compounds with amide, imide, and ester units to achieve the EC polymer films via this facile electropolymerization **[Scheme 1.10] [238].**

Oxidative electrochemical polymerisation is also affected by the orientation of amide linkage and the structure of terminal TPA unit **[239].** The electro-deposited film exhibited reversible electrochemical oxidation and strong colour changes having high colouration. Besides amide and imide functional group can act as a linkage between TPA carbazole and triptycene group **[Scheme 1.11].** Electrosynthesis and electrochromic properties of 1,4 bis (3,4 dicarboxyphenoxy) triptycene units as a interior core and TPA as a Electroactive site are deposited onto the working electrode during polymerization and showing anodically colouring by applying low external voltage.

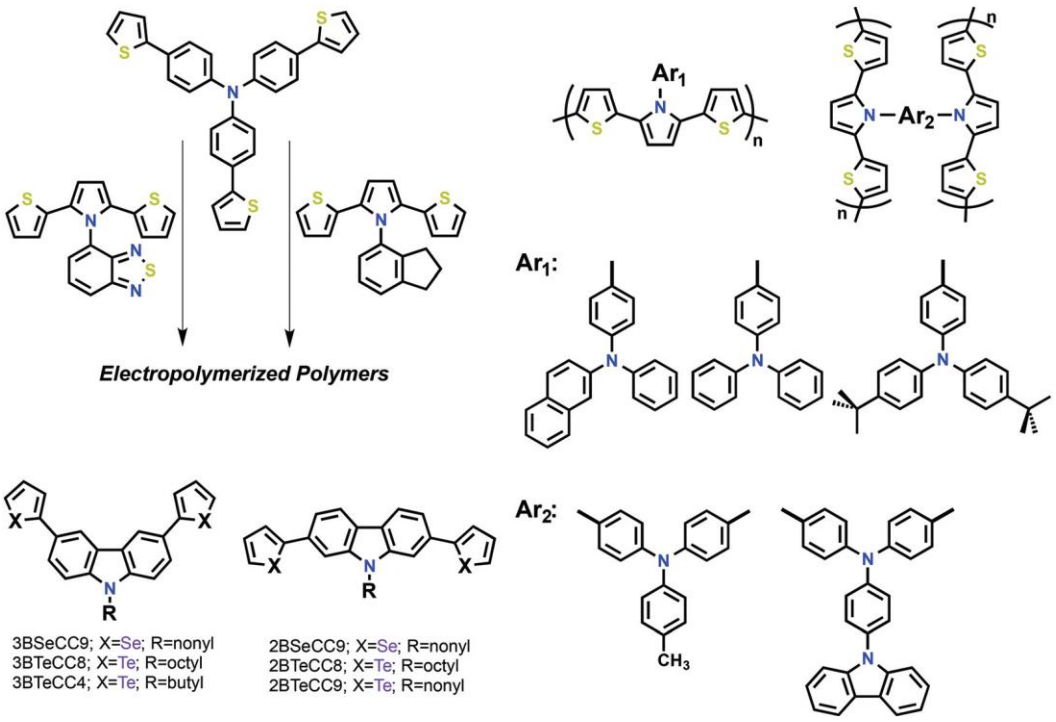

Scheme 1.8. Electropolymerisable TPA.

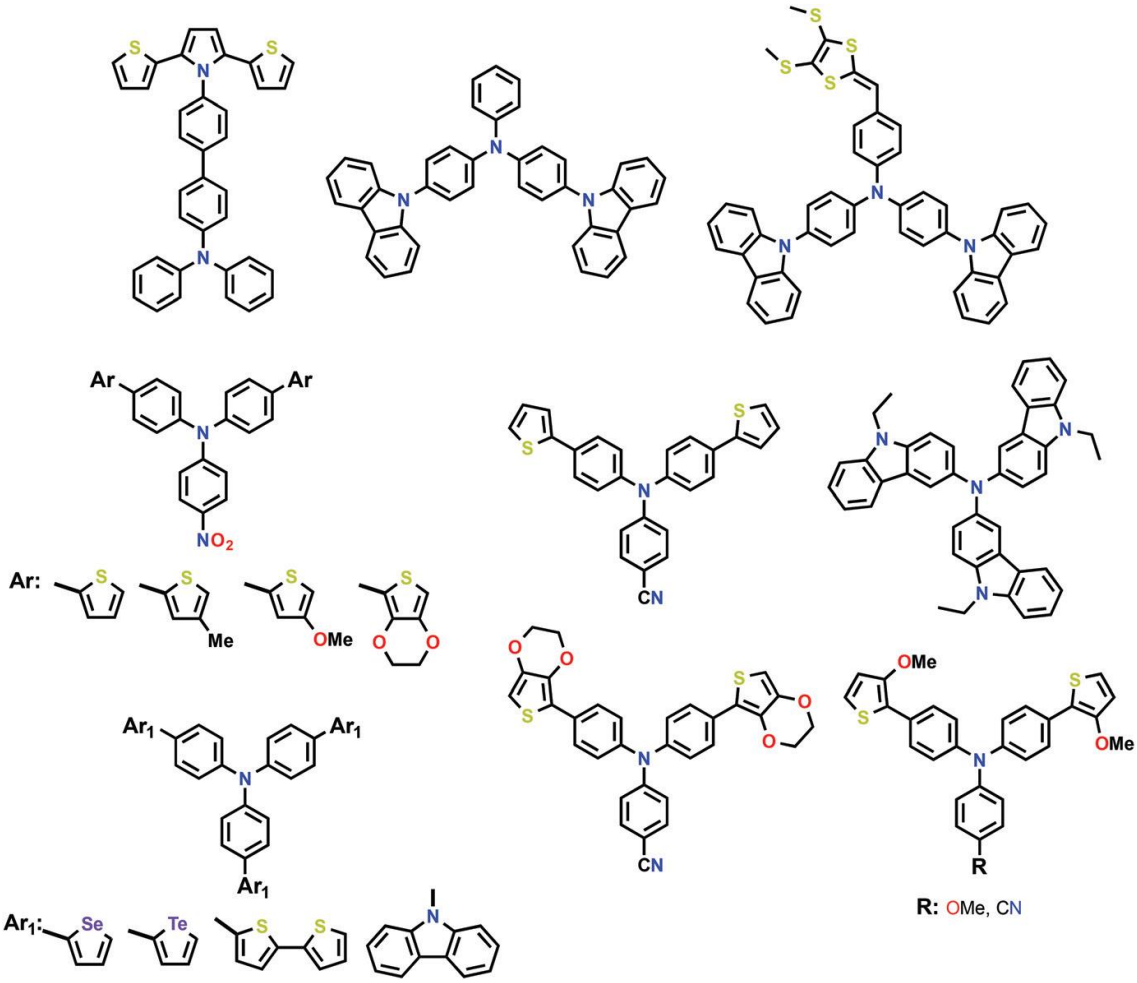

Scheme 1.9. Electropolymerisable TPA derivatives.

Oxidative electrochemical polymerisation is also affected by the orientation of amide linkage and the structure of terminal TPA unit **[240-246].** The electro-deposited film have exhibited reversible electrochemical oxidation and strong colour changes having high colouration. Besides amide and imide functional group can act as a linkage between TPA carbazole and triptycene group. Electrosynthesis and electrochromic properties of 1,4 bis (3,4 dicarboxyphenoxy) triptycene units as a interior core and TPA **(scheme 1.11)** as a electroactive site are deposited onto the working electrode during polymerization and showing anodically colouring by applying low external voltage **[247-266].**

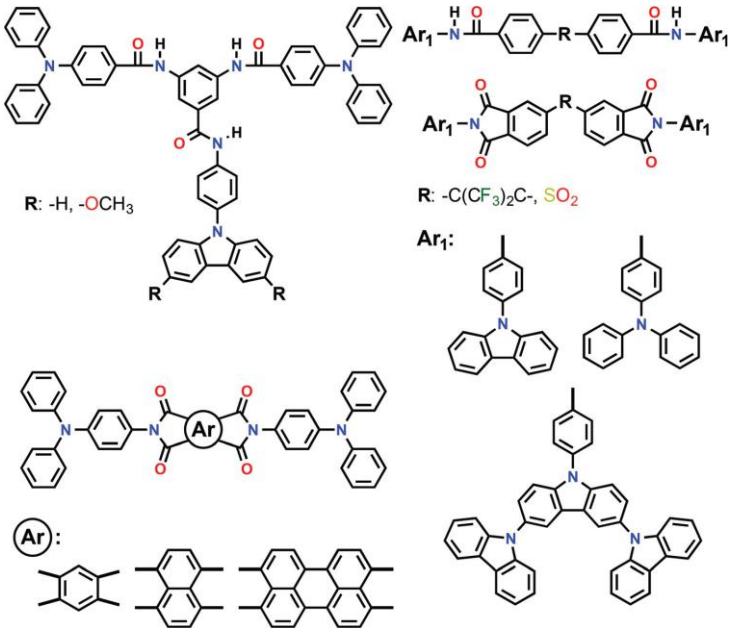

Scheme 1.10. TPA derivatives with different acceptor cores.

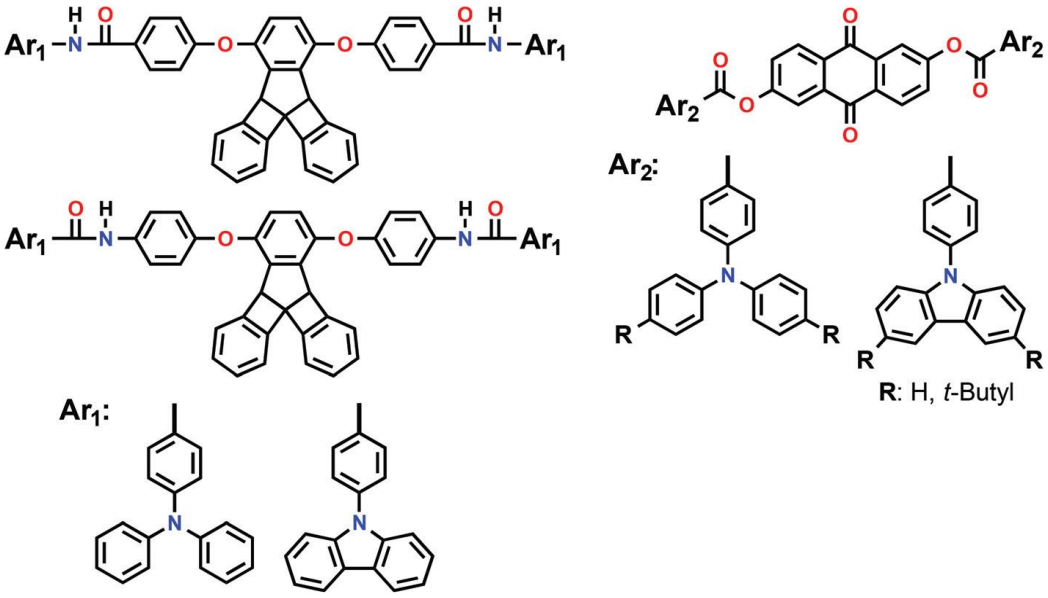

Scheme 1.11. Different terminal sides.

1.11.3. Triphenylamine-based metal complexes

Smart molecules which exhibit multiple redox reaction with distinguishable redox states at low driving voltages have received great attention recently **[267–270].** Till now finding and understanding of four or more redox states have been challenging. To obtain molecules displaying multiple redox processes at relatively low potentials, solution-based measurements should be conducted by surface-confined technologies for practical applications. Polypyridyl ruthenium complexes with a Ru–C bond, denoted as cyclometalated ruthenium complexes, are particularly capable of achieving multistate redox processes in molecular switches **[271, 272]**. The presence of the Ru–C bond in cyclometalated ruthenium complexes could greatly lower the Ru(III/II) potential and give rise to diruthenium or ruthenium-amine **[273–275]** complexes with three redox states. These complexes with strong absorptions in the visible and NIR regions are promising as EC materials for fiber-optic communications. Recently, Zhong et al. have successfully prepared a star shaped tris-cyclometalated ruthenium complex M1 with a redox-active triaryl amine core, which showed four redox states in a low potential region **(Scheme 1.12).**

The complex M1 and the electropolymerized films of the vinyl-functionalized complex M2 both display four consecutive one-electron anodic redox couples at low potentials, functioning as a molecular redox switch with up to five well-separated states. Leung and Su have reported a convenient and effective method to access conjugated polymers containing electron donating accepting pairs from a TPA-based ruthenium complex M3. The diphenyl amino group in M3 is beneficial for electropolymerization to give donor–acceptor polymers, and the resulting polymerized-M3 also have demonstrated interesting EC and photo responsive behaviour.

Zhong have synthesized six metallic terpyridine-based complexes M4 with two TPA end groups could produce four terminal active sites for the purpose of following electrochemical polymerization. The EC memory ability depends on both the rigidity

and length of these TPA-based moieties. Meanwhile, the TPA-based moieties with more rigid and conjugated linkages effectively increase intra-molecular CT from the TPA group (D) to the metallic terpyridine (A) that is beneficial for stabilizing the oxidized states (i.e., Ru^{3+}, Fe^{3+}) of metallic terpyridine and thus enhance the memory ability of the EC films.

In addition, cyclometalated ruthenium complex M5 with a redox-active arylamine substituent and three carboxylic acid groups have demonstrated feasibility as a self-assembling monolayer on ITO electrode surfaces for fabricating NIR EC three state switching. The obtained monolayer film has exhibited intense NIR absorption with long optical retention time at each oxidation state. Thus, this approach can provide an excellent molecular platform for the construction of a surface-confined flip-flop system with high ON/OFF ratios, which is attractive for the preparation of NIR EC and memory devices at the molecular scale.

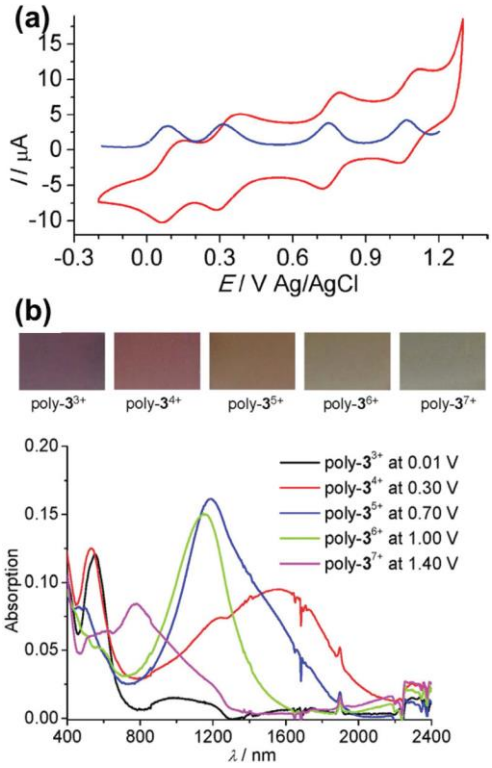

Fig. 1.20. CV and UV plot at different voltages.

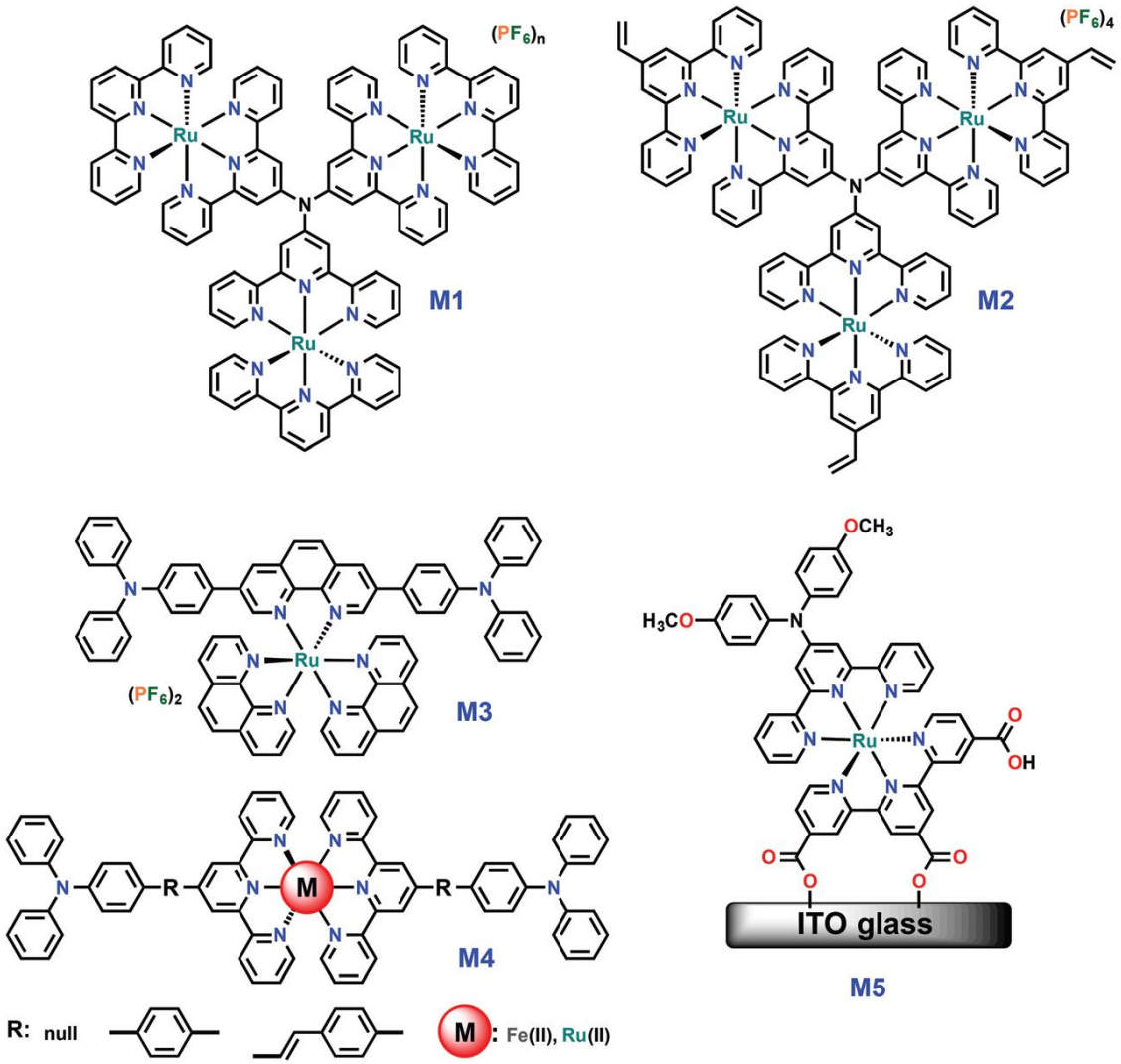

Scheme 1.12. Metal coordinating systems.

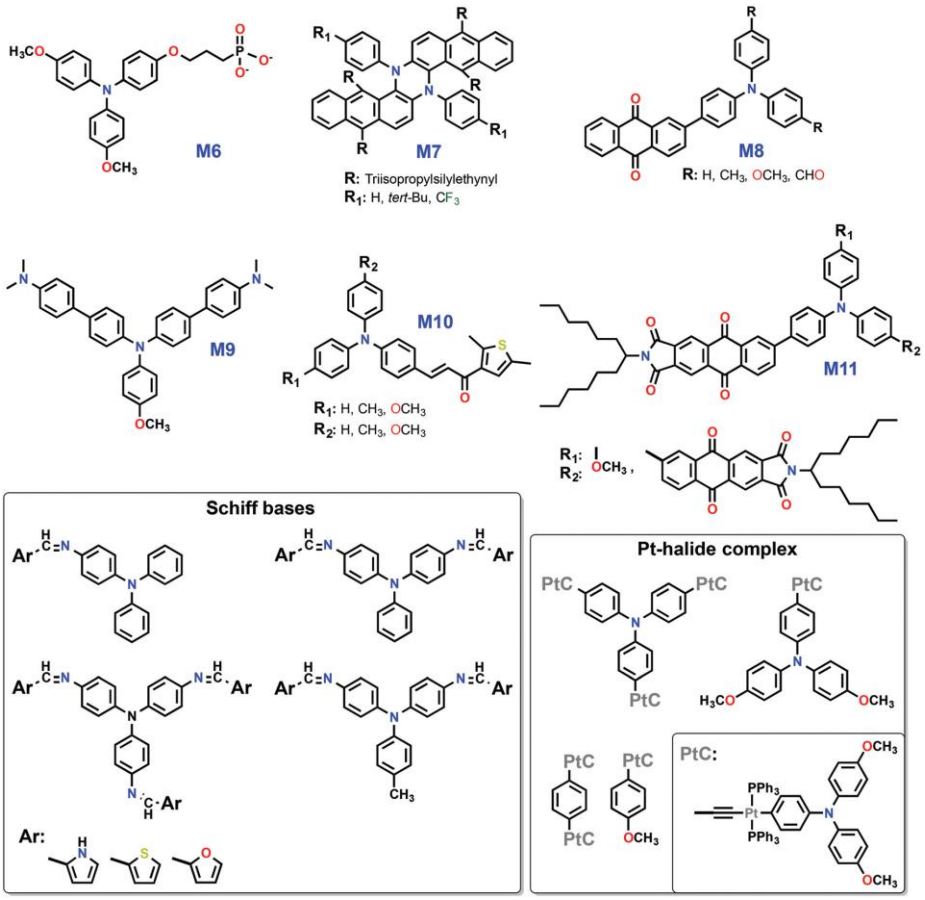

Scheme 1.13. TPA based Schiff bases.

1.11.4. Triphenylamine-based molecules

Molecules reveal physical responses under stimuli have been widely investigated as promising functional switching and memory devices **[276, 277].** Redox-active materials have received great attention due to the prospects as electronic devices **[278–284].**

M6 is rapidly oxidized in aqueousI_3 solution to generate the coloured form, $M6^{\bullet+}$ radical cation and it reduces back to the original colourless M6 by aqueous I^- solution. Aqueous I_3^- or I^- electrochemically generated in an external two-compartment cell could be pumped through the window cavity to form the redox-flow EC window between coloured and colourless states **(Fig. 1.20).**

Hiroto and Shinokubo have reported the synthesis of π-extended N, N′-diaryl dihydrophenazines M7, which exhibited dramatic conformational and three-state NIR absorption changes by both chemical and electrochemical stimuli **[285].** Upon chemical oxidation, the change of optical absorption has been confirmed in a two-step procedure, and the NMR analysis has demonstrated a conformational change upon oxidation, which is also supported by theoretical calculations. Such molecules with interesting NIR EC behaviour and dramatic conformational changes caused by an electrochemical stimulus are promising for applying in low-energy molecular memory and molecular actuator devices.

A series of dyes M8 with intra-molecular CT between AQ and TPA units have been synthesized by the Suzuki reaction, which are ideal candidates as probes for the detection of less polar solvents **[286].** Cyclic Voltammetry and DFT calculation simply that these dyes could be potentially applied in the wide field of optoelectronics.

In order to obtain several redox and protonation states, three amino groups were incorporated into M9 as well as two biphenyl linkages, which allow an extended electron delocalization and a better stabilization of its redox states. M9 has found to exhibit three redox states with EC of colourless, yellow, green, and blue, and three protonated states. In addition, the fluorescence switches at different oxidation and protonation states have been also investigated. The molecular orbital energy levels and excitation energies have been calculated and the fluorescence intensity decreases with the formation of the CT state. The spectro-electrochemical results have indicated that M10 reveals good EC stability with colour changes from yellow to blue.

Wan et al. have reported three D–A molecules M11 with different AQ imide arms connected to the TPA core **[287].** These compounds showed high solubility in common organic solvents due to the propeller-like structures. CV results have revealed that all these compounds exhibit three redox peaks, two in the cathodic regime owing to the formation of AQ imide radical anions and dianions, respectively,

and one in the positive regime corresponding to the TPA radical cations. Spectroelectrochemical measurements have demonstrated that the intra-molecular CT absorption is tuned electrochemically. In addition, the multiple EC colour and intensive NIR absorptions can be achieved in one single ambipolar molecule due to the formation of radical cations and radical anions in the oxidation and reduction process, respectively.

TPA based Schiff bases containing pyrrole, thiophene, or furan moieties have been synthesized and have revealed interesting EC behaviours with an obvious colour change from pale yellow **(scheme 1.13)** at neutral form to red at oxidative form. In addition, all the obtained compounds display multiple colour changes at different pH values and the results show a perfect linear relationship between the absorption and proton concentration. Thus, these new Schiff bases can be used as proton detection and EC materials due to their sensitive acido-chromic properties **[288–290].**
In addition, the Pt-ethynyl complexes containing up to four redox-active TPA cores have been prepared by oxidative addition followed by the CuI-catalyzed dehydro halogenation reaction. The complexes undergo a single electrochemical process for each chemically distinct type of TPA in the molecular backbone. The perfect reversibility of the larger systems indicates that they can be used as charge storage materials and are capable of releasing up to four electrons.

1.12. Current status, challenges, and proposed solutions

The field of electrochromic materials have a few scientific and technological challenges that need to be addressed by both materials optimization/exploration and device engineering methods, to further improve the optical performance and stability of the ECDs in order to meet the demands of large-scale, cost-effective and commercialised applications.

1.12.1. Ion-trapping

The electron for oxidation/reduction processes of both the polymer and the transition metal oxide based electrochromic films are accompanied by counter-ion de-

/intercalations to maintain charge-neutrality. Upon repeated cycling, transition metal oxides and polymer based electrochromic layers indicate a decrease of the optical contrast along with a decrease in charge density. For metal-oxide, counter-ions being bound to trap-sites, are affected by both the intrinsic properties of the materials. Applying sufficient over potential for long time have driven out ions in ‘‘shallow’’ traps, reviving the performance to a certain extent **[291]** In organic conjugated polymers, cations and anions are trapped and absorbed on polymers to form compact and dense microstructures, which prevent further intercalation of counter ions, resulting in less electro-active sites. Cycling performance can be improved by forming a more porous morphology **[292],** reducing the interaction time between polymers and counter ions by using a lower concentration of electrolyte, applying a smaller voltage, or reducing the anodic or cathodic polarisation time. Decreasing interaction between polymers and counter ions also decrease the optical contrast. Up to now, the strategies investigated for both inorganic and organic materials do not provide a permanent solution. Further investigations are warranted for the study of the ion-trapping phenomena and the design of EC materials with minimum trap sites.

1.12.2. Optical memory

The optical memory means the tendency of an electrochromic materials to maintain its coloured or bleached states after removing the external bias **[293].** Self-bleaching are commonly observed in small molecule based ECDs which can easily diffuse into electrolyte and undergo electron transfer **[294].** For conjugated electrochromic materials, self-bleaching and self-colouring **[295, 296]** phenomena have been observed due to spontaneous electron transfer from the ECPs to the transparent conductive substrates. In order to maintain the optical state of the ECDs, refreshing potential pulses can be applied, which increases the power consumption of the devices. While side-chain modifications of the electrochromic polymers could effectively tune the HOMO levels of the electrochromic materials to address the self-bleaching issue, chemical modifications inevitably change their colour and electrochemical properties **[297].** Alternatively, a general protocol with the combination of cathodic polarisation and surface modification of the conductive

substrate has been proposed to minimise the self-bleaching of ECPs, as cathodic polarisation closes up the opening conformation of ECPs after electrochemical conditioning. Partial surface modifications impede the spontaneous charge transfer between the ECPs and the conductive substrates **[298].**

1.12.3. Residual colour and black-to-transmissive switching

This is difficult for high band gap polymers, as high potentials may be required for complete bleaching. The higher potentials may decrease device life time. For anodically colouring materials, which are already transmissive in the neutral state with oxidation leading to colouration. However, the presence of the intermediate colours makes it not suitable for most applications, and similar issues related to the cathodically colouring polymers may be encountered. Although colour tuning for a specifically coloured polymer can be achieved based on the understanding of polymer compositions and structures, obtaining a polymer that can be switched between black and transmissive state can be nontrivial, as it requires high absorption over the visible region in the neutral state, and suppression of the absorbance in the bleached state. The reversible and controlled tuning of such broad absorption has been demonstrated using triarylamine based polymers, donor–acceptor based conjugated polymers, **[299].** However, challenges in controlling the optical contrast, switching time, and uniformity of colour transition for the black-to-transmissive switching ECPs may arise when using these approaches.

1.12.4. Environmental stability

Electrochromic windows can be integrated to buildings for energy saving purposes. However, the high production cost has become one of the biggest barriers to market penetration **[300].** One way to compensate the high cost is to extend their lifespan and save energy in the long run. In general, lifetimes greater than 20 years are targeted for energy saving applications. To achieve long-term stable performances, the thermal and photo- stabilities of the ECDs need to be considered. Unfortunately, investigations on the thermal stability of the ECDs are scarce and not many conclusions and clues from the instability of materials at high temperature have been

drawn **[301].** One factor that plays an important role in multiple layered ECDs is the thermal expansion coefficients. Different components integrated within a single electrochromic device can have very different thermal coefficients, which causes problems in mechanical and physical stabilities upon heating and cooling cycles. Photostability of the electrochromic materials is another key factor that determines the lifetime of the ECDs used in outdoor conditions. The photochemical breakdown of the conjugation in the polymers is known as a combinatory effect of oxygen, moisture and light, which induces oxidation of the alkyl side chains, leading to chain scission and/or loss of conjugation in the backbone **[302].** ECPs with relatively lower lying HOMO levels typically have better photochemical stability, although the position of the HOMO level is not necessarily correlated with the photochemical stability **[303-305]**. To address the issues of the photochemical degradation of electrochromic materials, the encapsulation of devices in an inert atmosphere is required for the fabrication and assembly of the ECDs, which further increase the cost of the device.

Aims and perspective:

Electrochromic materials which reversibly modulate optical transmittance by applying potentials are the key components for energy saving and colour-tuning applications, especially in smart window technology which switch between dark state and a colourless state to control solar heat and increasing the energy efficiency of buildings sectors. Organic ECMs include conducting polymers and small organic molecules that have a large degree of conjugation have the advantages of good optical switching, fast response time, flexible device fabrication, large coloration efficiency, low driving voltage, and easy molecular design. The present thesis deals with electroactive and photoactive Triphenylamine based different donor acceptor donor based EC polymers which are synthesized by oxidative electrochemical deposition method on conducting surface. Triphenylamine based DAD type EC polymers exhibit strong colour change at low working potential.

This thesis is divided into six chapters. **Chapter 1**, introduces a brief discussion about Electrochromism, different types of Electrochromic materials, literature on Triphenyl amine based EC materials, the important parameters which control the Electrochromism, Electrodeposited polymerization technique, the appearance of

different colours with voltage change, the mechanism of colour change, Electrochromism with device fabrication.

Chapter 2, deals with the characterization technique after monomer formation like NMR, MALDI-TOF, FTIR. FESEM and AFM technique for polymer film morphology characterization and photo physical UV-Vis spectroscopy for film absorbance characterization. Electrochemical technique like Cyclic Voltametry, Chronoampherometry and Spectro-electrochemical technique for checking EC performance.

Chapter 3 describes the influence of number of electropolymerizable group of the donor side on electrochromic behaviors, three donor-acceptor-donor type monomers containing isonaphthalene diimide as acceptor core and electro-polymerizable triphenyl amine (TPA) as the donor moiety have been designed and successfully synthesized via imidization of isonaphthalene anhydride with corresponding TPA derivatives. Three polymers show multi-electrochromic properties in a reversible manner with the colour change from colourless to brown to blue at low working potential. Spectro-electrochemistry studies of these films have revealed the high optical contrast (51.4%, 69.8 %, 84.5% respectively) of these polymers with the very fast bleaching (less than 1 s) and coloration (less than 2 s) time with very high coloration efficiencies. The electro switching stability has been performed up to 500 cycles and activity loses only 10% after 3000 s.

Chapter 4 presents the effect of different acceptor core like pyromellitic dianhydride, naphthalenetetracarboxylic dianhydride, perylenetetracarboxylic dianhydride and terminal triphenylamine based three DAD type monomers which are subsequently electropolymerized on conductive glass surface to have polymers which are explored by cyclic voltammetry studies. Density functional theory (DFT) studies disclose that HOMO is localized solely on triphenylamine unit which accounts for the electropolymerization process upon oxidation. Besides, TD-DFT calculations unveil the responsible electronic transitions for electrochromism in the polymers. Three polymers exhibit the reversible multiple colour changes of colourless to brown to

deep blue in the anodic region by applying voltage 0 to 1 to 1.2 V and also colourless to deep pink in the cathodic region (voltage window of 0 to -2 V) with attractive response times, optical contrast, switching stabilities, and coloration efficiencies. These polymers can be switched upto 10,000 cycles with the colouration efficiency 800 cm^2/C in the anodic process and 600 cycles for the cathodic process in a three electrodes configuration.

In **Chapter 5**, Several triphenylamine end capped to substituted central naphthalene tetracarboxylic diimide based four donor - acceptor - donor type electroactive monomers have been designed and developed to explore the effect of substituent on the formation of electro-polymers and subsequent the chromic effect of prepared films on the conductive surface. Initially, with the help of density functional theory (DFT) studies, it has observed that HOMO is located over triphenylamine unit, responsible electropolymerization process upon oxidation, LUMO is residing on the central naphthalene core, and all substituents are not coplanar with naphthalene moiety. Also, the band gap energy is gradually decreased with the effect of strong electron withdrawing substituents on NDI core. In three electrode configuration, reversible multiple colour changes of brown to deep blue by applying voltage 0 to 1.1 V and also brown to deep pink with the voltage change of 0 to -2 V are investigated with relatively good response times, optical contrast, switching stabilities, and coloration efficiencies.

Chapter 6 represents the overall work summary with future scope.

1.13. REFERENCES:

[1] X. Shi, Nature 591 (2021) 240−245.

[2] J. Park, Nat. Photonics 15 (2021) 449−455.

[3] X. Yu, Nature 575 (2019) 473−479.

[4] J. Park, J. Kim, S. Y. Kim, W. H. Cheong, J. Jang, Y. G. Park, K. Na, Y. T. Kim, J. H. Heo, C. Y. Lee, J. H. Lee, F. Bien, J. U. Park, Sci. Adv. 4 (2018) 9841.

[5] J. Kim, H. J. Shim, J. Yang, M. K. Choi, D. C. Kim, J. Kim, T. Hyeon, D. H. Kim, Adv. Mater. 29 (2017) 1700217.

[6] N. Verplanck, E. Galopin, J. C. Camart, V. Thomy, Y. Coffinier, R. Boukherroub, Nano Lett. 7 (2007) 813−817.

[7] M. Miles, E. Larson, C. Chui, M. Kothari, B. Gally, J. Batey, J. Soc. Inf. Display 11 (2003) 209− 215.

[8] L. Nucara, F. Greco, V. Mattoli, J. Mater. Chem. C 3 (2015) 8449−8467.

[9] P. M. Beaujuge, J. R. Reynolds, Chem. Rev. 110 (2010) 268−320.

[10] R. J. Mortimer, Annu. Rev. Mater. Res. 41 (2011) 241−268.

[11] Z. Wang, X. Wang, S. Cong, F. Geng, Z. Zhao, Mater. Sci. Eng. 140 (2020) 100524.

[12] M. J. Han, D. Y. Khang, Adv. Mater. 27 (2015) 4969−4974.

[13] Y. Huang, S. Y. Liao, J. Ren, B. Khalid, H. L. Peng, H. Wu, Nano Res. 9 (2016) 917−924.

[14] S. Kwon, Adv. Mater. 32 (2020) 1903488.

[15] C. Wang, X. Jiang, P. Cui, M. Sheng, X. Gong, L. Zhang, S. Fu, ACS Appl. Mater. Interfaces 13 (2021) 12313−12321.

[16] H. Park, D. S. Kim, S. Y. Hong, C. Kim, J. Y. Yun, S. Y. Oh, S. W. Jin, Y. R. Jeong, G. T. Kim, J. S. Ha, Nanoscale 9 (2017) 7631−7640.

[17] D. Kim, M. Kim, G. Sung, J. Y. Sun, Nano Convergence 6 (2019) 21.

[18] S. S. Malagón, D. R. Colín, H. Azizkhani, M. A. Pellitero, G. Guirado, F. J. Del. Campo, Biosens. Bioelectron. 175 (2021) 112879.

[19] Y. Kim, E. Kim, G. Clavier, P. Audebert, Chem. Commun. (2006) 3612−3614.

[20] P. Audebert, F. Miomandre, Chem. Sci. 4 (2013) 575−584.

[21] J. H. Wu, G. S. Liou, Adv. Funct. Mater. 24 (2014) 6422− 6429.

[22] J. Sun, Y. Chen, Z. Liang, Adv. Funct. Mater. 26 (2016) 2783−2799.

[23] G. A. Corrente, A. Beneduci, Adv. Optical Mater. 8 (2020) 2000887.

[24] R. J. Mortimer, A. L. Dyer, J. R. Reynolds, Displays 27 (2006) 2−18.

[25] S. H. Choi, A. J. Duzik, H. J. Kim, Y. Park, J. Kim, H. U. Ko, H. C. Kim, S. Yun, K. U. Kyung, Smart Mater. Struct. 26 (2017) 093001.

[26] J. R. Platt, J. Chem. Phys. 34 (1961) 862.

[27] S. K. Deb, Appl. Opt. 8 (1969) 192−195.

[28] J. H. Karfunkel, Phys. Chem. 97 (1993) 1466-1472.

[29] H. Kurokawa, M. Shibayama, T. Ishimaru, S. Nomura, W. l. Wu, Polymer 33 (1992) 2182-2188;

[30] H. L. Lin, Y. F. Liu, T. L. Yu, W. H. Liu, S. P. R. Wei, Polymer 46 *(*2005) 5541-5549;

[31] E. T. Wise, S. G. Weber, Macromolecules 28 (1995) 8321-8327.

[32] R. F. Nickerson, J. Appl. Polym. Sci. 15 (1971) 111-116;

[33] E. Z. Casassa, A. M. Sarquis, C. H. Van Dyke, J. Chem. Educ. 63 (1986) 57.

[34] M. V. Duin, J. A. Peters, A. P. G. Kieboom, H. Van Bekkum, Tetrahedron 41 (1985) 3411-3421.

[35] K. W. McLaughlin, N. K. Wyffels, A. B. Jentz, M. V. Keenan, J. Chem. Educ. 74 *(*1997) 97.

[36] R. K. Schultz, R. R. Myers, Macromolecules 2 (1969) 281-285.

[37] G. G. Stroebel, J. A. Whitesell, R. M. Kriegel, J. Chem. Educ. 70 (1993) 893.

[38] A. L. Dyer, E. J. Thompson, J. R. Reynolds, ACS Appl. Mater. Interfaces 3 (2011) 1787-1795;

[39] R. H. Bulloch, J. A. Kerszulis, A. L. Dyer, J. R. Reynolds, ACS Appl. Mater. Interfaces 7 (2015) 1406-1412.

[40] I. F. Chang, B. L. Gilbert, T. I. Sun, J. Electrochem. Soc. 122 (1975) 955-962.

[41] P. Monk, R. Mortimer, D. Rosseinsky., Electrochromism and Electrochromic Devices, Cambridge University Press, (2007).

[42] C. G. Granqvist, in Handbook of Inorganic Electrochromic Materials, Elsevier Science

B.V., Amsterdam, (1995).

[43] P. M. S. Monk, R. J. Mortimer, D. R. Rosseinsky, in Electrochromism, Wiley-VCH

Verlag GmbH, (2007) 59-92.

[44] P. R. Somani, S. Radhakrishnan, Materials Chemistry and Physics 77 (2002) 117–133.

[45] V. K. Thakur, G. Ding, J. Ma, P. S. Lee, X. Lu, Adv. Mater. 24 (2012) 4071−4096.

[46] C. A. Nguyen, A. A. Argun, P. T. Hammond, X. Lu, P. S. Lee, Chem. Mater. 23 (2011) 2142−2149.

[47] M. Q. Cui, W. S. Ng, X. Wang, P. Darmawan, P. S. Lee, Adv. Funct. Mater. 25 (2015) 401−408.

[48] M. Q. Cui, P. S. Lee, Chem. Mater. 28 (2016) 2934−2940.

[49] J. M. Wang, L. Zhang, L. Yu, Z. H. Jiao, H. Q. Xie, X. W. Lou, X. W. Sun, Nat. Commun. 5 (2014) 4921.

[50] P. H. Yang, P. Sun, Z. S. Chai, L. H. Huang, X. Cai, S. Z. Tan, J. H. Song, W. J. Mai, Angew. Chem., Int. Ed. 53 (2014) 11935−11939.

[51] D. Zhou, F. Shi, D. Xie, D. H. Wang, X. H. Xia, X. L. Wang, C. D. Gu, J. P. Tu, J. Colloid Interface Sci. 465 (2016) 112−120.

[52] G. F. Cai, X. Wang, M. Q. Cui, P. Darmawan, J. X. Wang, A. L. S. Eh, P. S. Lee, Nano Energy 12 (2015) 258−267.

[53] G. F. Cai, X. L. Wang, D. Zhou, J. H. Zhang, Q. Q. Xiong, C. D. Gu, J. P. Tu, RSC Adv. 3 (2013) 6896−6905.

[54] A. Sumboja, U. M. Tefashe, G. Wittstock, P. S. Lee, Adv. Mater. Interfaces 2 (2015) 1400154.

[55] C. G. Granqvist, in Handbook of Inorganic Electrochromic Materials, Elsevier Science B. V., Amsterdam (1995) Vii-viii.

[56] P. M. S Monk, R. J. Mortimer, D. R. Rosseinsky, Electrochromism. Fundamentals, applications (1996).

[57] M. A. Arvizu, G. A. Niklasson, C. G. Granqvist, Chemistry of Materials 29 (2017) 2246-2253.

[58] R. S. Patil, M. D. Uplane, P. S. Patil, International Journal of Electrochemical Science, 3 (2008) 259-265.

[59] C. G. Granqvist, A. Azens, A. Hjelm, L. Kullman, G. A. Niklasson, D. Ronnow, M. Stromme Mattsson, M. Veszelei and G. Vaivars, Solar Energy 63 (1998) 199-216l.

[60] M. Gratzel, Nature 409 (2001) 575-576.

[61] D. Cummins, G. Boschloo, M. Ryan, D. Corr, S. N. Rao, D. Fitzmaurice, The Journal of Physical Chemistry B 104 (2000) 11449-11459.

[62] D. R. Rosseinsky, R. J. Mortimer, Advanced Materials 13 (2001) 783-793.

[63] C. K. Chiang, C. R. Fincher, Y. W. Park, A. J. Heeger, H. Shirakawa, E. J. Louis, S. C. Gau, A. G. MacDiarmid, Physical Review Letters 39 (1977) 1098-1101.

[64] A. G. Macdiarmid, M. Akhtar, C. K. Chiang, M. J. Cohen, J. Kleppinger, A. J. Heeger, E. J. Louis, J. Milliken, M. J. Moran, D. L. Peebles, H. Shirakawa, Journal of Electrochemical Society (1977) 304-308.

[65] M. G. Kanatzidis, Chemical and Engineering News Archive 68 (1990) 36-50.

[66] P. Schottland, K. Zong C. L. Gaupp, B. C. Thompson, C. A. Thomas, Macromolecules 33 (2000) 7051–61.

[67] C. L. Gaupp, K. Zong, P. Schottland, B. C. Thompson, C. A. Thomas, J. R. Reynolds, Macromolecules 33 (2000) 1132–33.

[68] E. Unur, J. H. Jung, R. J. Mortimer, J. R. Reynolds, Chem. Mater. 20 (2008) 2328–34.

[69] G. Sonmez, I. Schwendeman, P. Schottland, K. Zong J. R. Reynolds, Macromolecules 36 (2003) 639–47

[70] L. Groenendaal, G. Zotti, P. H. Aubert, S. M. Waybright, J. R. Reynolds, Adv. Mater. 15 (2003) 855–79.

[71] C. A. Thomas, PhD thesis. Univ. Florida. (2001) 226.

[72] S. A. Sapp, G. A. Sotzing, J. R. Reynolds, Chem. Mater. 10 (1998) 2101–8.

[73] A. Kumar, D. M. Welsh, M. C. Morvant, F. Piroux, K. A. Abboud, J. R. Reynolds, Chem. Mater.10 (1998) 896–902.

[74] D. M. Welsh, A. K. Meijer, E. W. Reynolds, Adv. Mater. 11 (1999) 1379–82.

[75] C. L. Gaupp, D. M. Welsh, J. R. Reynolds, Macromol. Rapid Commun. 23 (2002) 885-89.

[76] B. Sankaran, J. R. Reynolds, Macromolecules 30 (1997) 2582–88.

[77] A. Kumar, J. R. Reynolds, Macromolecules 29 (1996) 7629–30.

[78] D. M. Welsh, L. J. Kloeppner, L. Madrigal, M. R. Pinto, B. C. Thompson, Macromolecules 35 (2002) 6517–25.

[79] A. Cirpan, A. A. Argun, C. R. G. Grenier, B. D. Reeves, J. R. Reynolds, J. Mater. Chem. 13 (2003) 2422–28.

[80] B. D. Reeves, C. R. G. Grenier, A. A. Argun, A. Cirpan, T. D. McCarley, J. R. Reynolds, Macromolecules 37 (2004) 7559–69.

[81] R. J. Mortimer, K. R. Graham, C. R. G. Grenier, J. R. Reynolds, ACS Appl. Mater. Interfaces 1 (2009) 2269–76.

[82] S. Gottesfeld, A. Redondo, S.W. Feldberg, J. Electrochem. Soc. 1 (1987) 271.

[83] M. C. Bernard, A. H. L. Goff, W. Zeng, Electrochem. Acta 44 (1998) 781.

[84] M. Higuchi, Metallo-Supramolecular Polymers: Design, Function, and Device Application. In Intelligent Nanosystems for Energy, Information and Biological Technologies; Sone, J. i., Tsuji, S., Eds.; Springer: Japan Tokyo (2016) 217−248.

[85] M. Li, A. Patra, Y. Sheynin, M. Bendikov, Advanced Materials 21 (2009) 1707-1711.

[86] R. Greef, R. Peat, L. M. Peter, D. Pletcher, Robinson, Instrumental Methods in Electrochemistry, Chapter 10, Spectroelectrochemistry, Ellis Horwood, Chichester (1990) DOI: 978-1-899563-80-8 317-355.

[87] V. K. Thakur, G. Ding, J. Ma, P. S. Lee, X. Lu, Advanced Materials, 24 (2012) 4071-4096.

[88] P. M. S. Monk, R. J. Mortimer, D. R. Rosseinsky, Electrochromism and Electrochromic Devices: Optical effects and quantification of colour, Cambridge University Press, United States of America (2007).

[89] S. A. Agnihotry, P. Pradeep, S. S. Sekhon, Electrochim. Acta 44 (1999) 3121-3126.

[90] Y. Zhang, L. Y. Zhang, C. W. Zhou, Acc. Chem. Res. 46 (2013) 2329−2339.

[91] S. Shin, M. Yang, L. J. Guo, H. Youn, Small 9 (2013) 4036−4044.

[92] J. X. Wang, C. Y. Yan, W. B. Kang, P. S. Lee, Nanoscale 6 (2014) 10734−10739.

[93] S. R. Ye, I. E. Stewart, Z. F. Chen, B. Li, A. R. Rathmell, Wiley, B. J. Acc. Chem. Res. 49 (2016) 442−451.

[94] J. Jensen, F. C. Krebs, Adv. Mater. 26 (2014) 7231−7234.

[95] G. F. Cai, P. Darmawan, M. Q. Cui, J. X. Wang, J. W. Chen, S. Magdassi, P. S. Lee, Adv. Energy Mater. 6 (2016) 1501882.

[96] B. Deng, P. C. Hsu, G. C. Chen, B. N. Chandrashekar, L. Liao, Z. Ayitimuda, J. X. Wu, Y. F. Guo, L. Lin, Y. Zhou, M. Aisijiang, Q. Xie, Y. Cui, Z. F. Liu, H. L. Peng, Nano Lett. 15 (2015) 4206−4213.

[97] W. B. Kang, C. Y. Yan, C. Y. Foo, P. S. Lee, Adv. Funct. Mater. 25 (2015) 4203−4210.

[98] C. Y. Yan, W. B. Kang, J. X. Wang, M. Q. Cui, X. Wang, C. Y. Foo, K. J. Chee, P. Lee, ACS Nano 8 (2014) 316−322.

[99] M. A. De Paoli, W. A. Gazotti, J. Braz. Chem. Soc. 13 (2002) 410–424.

[100] A. A. Syed, M. K. Dinesan, Talanta 38 (1991) 815–837.

[101] P. Monk, R. Mortimer, D. Rosseinsky, Conjugated conducting polymers, in Electrochromism and Electrochromic Devices (Cambridge University Press, New York, (2007) 312.

[102] R. de Surville, M. Jozefowicz, L. T. Yu, J. Perichon, R. Buvet, Electrochim. Acta 13 (1968) 1451–1458.

[103] A. A. Syed, M. K. Dinesan, E. M. Genies, Bull. Electrochem. 4 (1988) 737–742.

[104] A. F. Diaz, J. A. Logan, J. Electroanal. Chem. 111 (1980) 111–114.

[105] N. Mermilliod, J. Tanguy, M. Hoclet, A. A. Syed, Synth. Met. 18 (1987) 359–364.

[106] A. G. MacDiarmid, J. C. Chiang, M. Halpern, W. S. Huang, S. L. Mu, N. L. D. Somasiri, W. Wu, S. I. Yaniger, Mol. Cryst. Liq. Cryst. 121 (1985) 173–180.

[107] G. Mengoli, M. T. Munari, C. Folonari, J. Electroanal. Chem. 124 (1981) 237–246.

[108] S. Cosnier, Biosens. Bioelectron. 14 (1999) 443–456.

[109] H. T. Santoso, Electrochemical processing of polythiophene films with enhanced structural order, Thesis, Georgia Institute of Technology, Atlanta (2011) 117.

[110] S. Yong, W. Kazuya, H. Kazuhito, J. Biosci. Bioeng. 112 (2011) 63–66.

[111] R. Gupta, M. Singhal, S. K. Nataraj, D. N. Srivastava, RSC Adv. 6 (2016)110416–110421.

[112] M. J. Bleda-Martínez, C. Peng, S. Zhang, G. Z. Chen, E. Morallón, D. Cazorla-Amorós, J. Electrochem. Soc. 155 (2008) 672–678.

[113] J. Heinze, B. A. Frontana-Uribe, S. Ludwigs, Chem. Rev. 110 (2010) 4724–4771.

[114] W. Schuhmann, C. Kranz, H. Wohlschliiger, J. Strohmeier, Biosens. Bioelectron. 12 (1997) 1157–1167.

[115] H. Okamoto, T. Kotaka, Polymer 39 (1998) 4349–4358.

[116] K. Imanishi, M. Satoh, Y. Yasuda, R. Tsushima, S. Aoki, J. Electroanal. Chem. 242 (1988) 203–208.

[117] L. J. Duic, Z. Mandic, F. Kovacicek, J. Polym. Sci. Part A 32 (1994) 105–111.

[118] G. Inzelt, Conducting Polymers-A New Area in Electrochemistry Springer, Berlin, (2008) 123–135.

[119] G. G. Wallace, P. R. Teasdale, G. M. Spinks, L. A. P. Kane-Maguire, Conductive Electroactive Polymers, 3rd edn. Taylor & Francis Group, Boca Raton (2009).

[120] A. M. Kumar, Z. M. Gasem, Prog. Org. Coat. 78 (2015) 387–394.

[121] G. Fomo, T. T. Waryo, P. G. Baker, E. I. Iwuoha, Int. J. Electrochem. Sci. 11 (2016)
10347–10361.

[122] A. M. P. Hussain, A. Kumar, Bull. Mater. Sci. 26 (2003) 329–334.

[123] A. Kraft, A. C. Grimsdale, A. B. Holmes, Angew. Chem. Int. Ed. 37 (1998) 402–428.

[124] G. Fomo, T. T. Waryo, C. E. Sunday, A. A. Baleg, P. G. Baker, E. I. Iwuoha, Sensors 15 (2015) 22547–22560.

[125] B. B. Berkes, G. Inzelt, E. Vass, Electrochim. Acta 96 (2013) 51–60.

[126] M. Hosseini, M. M. Momeni, M. Faraji, J. Mater. Sci. 45 (2010) 2365–2371.

[127] Y. Li, M. Liu, C. Xiang, Q. Xie, S. Yao, Thin Solid Films 497 (2006) 270–278.

[128] G. Fomo, Thesis, University of the Western Cape (2015) 344.

[129] B. N. Grgur, A. Žeradjanin, M. M. Gvozdenović, M. D. Maksimović, T. L. Trišović, B. Z. Jugović, J. Power Sources 217 (2012) 193–198.

[130] D. Bhattacharjya, I. Mukhopadhyay, Langmuir 28 (2012) 5893–5899.

[131] M. M. Gvozdenović, B. Z. Jugović, J. S. Stevanović, T. L. J. Trišović, B. N. Grgur, Electrochemical Polymerization of Aniline, Electropolzmeriyation, ed. by E. Schab-Balcerzak, In Tech, Rijeka (2011).

[132] M. M. Gvozdenović, B. Z. Jugović, J. S. Stevanović, B. N. Grgur, B. N. Hemijis, Electrochemical synthesis of electro-conducting polymers. Hem. Ind. 68 (2014) 673–684.

[133] A. Adenier, M. M. Chehimi, I. Gallardo, J. Pinson, N. Vila, Langmuir 20 (2004) 8243–8253.

[134] R. Zhang, G. D. Jin, D. Chen, X. Y. Hu, Sensors Actuators B Chem. 138 (2009) 174–181.

[135] X. Huang, Y. Li, Y. Chen, L. Wang, Sensors Actuators B Chem. 234 (2008) 780–786.

[136] J. H. Park, J. M. Ko, O. O. Park, D. W. Kim, J. Power Sources 105 (2002) 20–25.

[137] C. C. Hu, C. H. Chu, J. Electroanal. Chem. 503 (2001) 105–116.

[138] B. Jugović, M. Gvozdenović, J. Stevanović, T. Trišović, B. Grgur, Mater. Chem. Phys. 114 (2009) 939–942.

[139] T. Hatano, A. H. Bae, M. Takeuchi, N. Fujita, K. Kaneko, H. Ihara, M. Takafuji, S. Shinkai, Angew. Chem. 116 (2004) 471–475.

[140] L. H. Mascaro, A. N. Berton, L. Micaroni, Int. J. Electrochem. (2011) 1–8.

[141] M. Magnuson, J. H. Guo, S. M. Butorin, A. Agui, C. Såthe, J. Nordgren, A. P. Monkman, J. Chem. Phys. 111 (1999) 4756–4761.

[142] K. Matyjaszewski, T. Davys, Handbook of Radical Polymerization, Wiley, Hoboken, (2002) 1–177.

[143] K. Karon, M. Lapkowski, Carbazole electrochemistry: A short review. J. Solid State Electrochem.19 (2015) 2601–2610.

[144] R. Lazzaroni, J. Riga, J. J. Verbist, L. Christiaens, M. Renson, J. Chem. Soc. Chem. Commun. (1985) 999–1000.

[145] V. Gupta, N. Miura, Electrochem. Commun. 7 (2005) 995–999.

[146] G. Odian, Y. Atassi, M. Tally, Chapter 3: Radical chain polymerization, in Principles of Polymerization, 4th edn., Wiley, Hoboken, (2004).

[147] W. S. Huang, B. D. Humphrey, A. G. MacDiarmid, J. Chem. Soc. Faraday Trans. 82 (1986) 2385–2400.

[148] D. Seeger, W. Kowalchyk, C. Korzeniewski, Langmuir 6 (1990) 1527–1534.

[149] H. Okamoto, T. Kotaka, Polymer 40 (1998) 407–417.

[150] M. S. Lee, S. B. Lee, J. Y. Lee, H. S. Kang, H. S. Kang, S. Hyun, J. Joo, A. J. Epstein, Mol. Cryst. Liq. Cryst. 405 (2003) 171–178.

[151] M. Immaculate, Synthesis, electrodynamics and biosensor applications of novel sulphonated polyaniline nanocomposites, PhD Thesis, University of the Western Cape, (2007) 223.

[152] W. Yanyan, L. Kalle, Macromol. Symp. 317 (2012) 240–247.

[153] T. Lindfors, A. Ivaska, J. Electroanal. Chem. 535 (2002) 65–74.

[154] M. H. Pournaghi-Azar, B. Habibi, Electrochim. Acta 52 (2007) 4222–4230.

[155] M. Saraji, A. Bagheri, Synth. Met. 98 (1998) 57–63.

[156] M. K. L. Coelho, J. D. F. Giarola, A. T. M. Da Silva, C. R. T. Tarley, K. B. Borges, A. C. Pereira, Chemosensors 4 (2016) 1–15.

[157] C. Lambert, G. Noll, Synth. Met. 139 (2003) 57–62.

[158] Z. Fang, V. Chellappan, R. D. Webster, L. Ke, T. Zhang, B. Liu, Y. H. Lai, J. Mater. Chem., 22 (2012) 15397–15404.

[159] M. Y. Chou, M. K. Leung, Y. O. Su, C. L. Chiang, C. C. Lin, J. H. Liu, C. K. Kuo, C. Y. Mou, Chem. Mater. 16 (2004) 654–661.

[160] K. Y. Chiu, T. X. Su, J. H. Li, T. H. Lin, G. S. Liou, S. H. Cheng, J. Electroanal. Chem. 575 (2005) 95–101.

[161] J. Natera, L. Otero, L. Sereno, F. Fungo, N. S. Wang, Y. M. Tsai, T. Y. Hwu, K. T. Wong, Macromolecules 40 (2007) 4456–4463.

[162] S. H. Hsiao, H. M. Wang, S. H. Liao, Polym. Chem. 5 (2014) 2473.

[163] C. Quinton, V. Alain-Rizzo, C. Dumas-Verdes, F. Miomandre, G. Clavier, P. Audebert, RSC Adv. 4 (2014) 34332–34342.

[164] D. Sek, B. Jarzabek, E. Grabiec, B. Kaczmarczyk, H. Janeczek, A. Sikora, A. Hreniak, M. Palewicz, M. Lapkowski, K. Karon, A. Iwan, Synth. Met. 160 (2010) 2065–2076.

[165] Y. Oishi, H. Takado, M. Yoneyama, M. A. Kakimoto, Y. Imai, J. Polym. Sci., Part A: Polym. Chem. 28 (1990) 1763–1769.

[166] G. S. Liou, S. H. Hsiao, M. Ishida, M. Kakimoto, Y. Imai, J. Polym. Sci., Part A: Polym. Chem. 40 (2002) 3815–3822.

[167] M. K. Leung, M. Y. Chou, Y. O. Su, C. L. Chiang, H. L. Chen, C. F. Yang, C. C. Yang, C. C. Lin, H. T. Chen, Org. Lett. 5 (2003) 839–842.

[168] P. Monk, R. Mortimer and D. Rosseinsky, in Electrochromism and Electrochromic Devices, ed. D. Rosseinsky, P. Monk and R. Mortimer, Cambridge University Press, Cambridge (2007) 1–24.

[169] H. J. Yen, G. S. Liou, Polym. Chem. 3 (2012) 255–264.

[170] V. L. Bell, B. L. Stump, H. Gager, J. Polym. Sci. Polym. Chem. Ed. 14 (1976) 2275–2291.

[171] P. E. Cassidy, Thermally Stable Polymers: Synthesis and Properties, Marcel Dekker, New York (1980).

[172] T. L. S. Clair, D. A. Yamaki, U. S. Pat. (1983) 4398021.

[173] T. L. S. Clair, D. A. Yamaki, U. S. Pat. (1984) 4489027.

[174] P. M. Hergenrother, Angew. Makromol. Chem. 145 (1986) 323–341.

[175] D. Wilson, H. D. Stenzenberger, P. M. Hergenrother, Polyimides, Springer Netherlands, New York (1990).

[176] H. Yang, Kevlar aramid fiber, John Wiley & Sons, New York (1993).

[177] M. K. Ghosh, K. L. Mittal, Polyimides: Fundamentals and Applications, Marcel Dekker, New York (1996).

[178] J. de Abajo, J. G. de la Campa, in Progress in Polyimide Chemistry I, ed. H. R. Kricheldorf, Springer Berlin Heidelberg 140 (1999) 23–59.

[179] K. L. Mittal, Polyimides: Synthesis, Characterization, and Applications, Plenum, New York (1984).

[180] H. H. Yang, Aromatic High-Strength Fibers, John Wiley & Sons, Inc., New York (1989).

[181] M. J. M. Abadie, B. Mittal, Polyimides and Other High Temperature Polymers, Elsevier, Amsterdam (1991).

[182] P. E. Cassidy, Thermally Stable Polymers, Marcel Dekker, New York (1980).

[183] Y. Oishi, M. Ishida, M. A. Kakimoto, Y. Imai, T. Kurosaki, J. Polym. Sci., Part A: Polym. Chem. 30 (1992) 1027–1035.

[184] K. I. Okamoto, K. Tanaka, H. Kita, M. Ishida, M. Kakimoto, Y. Imai, Polym. J. 24 (1992) 451–457.

[185] N. A. Vasilenko, Y. I. Akhmet'eva, Y. B. Sviridov, V. I. Berendyayev, Y. D. Rogozhkina, O. F. Alkayeva, K. K. Koshelev, A. L. Izyumnikov, B. V. Kotov, Polym. Sci. USSR 33 (1991) 1439–1450.

[186] S. H. Cheng, S. H. Hsiao, T. H. Su, G. S. Liou, Macromolecules 38 (2005) 307–316.

[187] S. H. Hsiao, Y. H. Hsiao, High Perform. Polym. 29 (2017) 431–440.

[188] S. H. Hsiao, Y. H. Hsiao, Y. R. Kung, J. Electroanal. Chem. 764 (2016) 31–37.

[189] H. M. Wang, S. H. Hsiao, J. Polym. Sci., Part A: Polym. Chem. 52 (2014) 1172–1184.

[190] H. J. Yen, C. L. Tsai, S. H. Chen, G. S. Liou, Macromol. Rapid Commun. 38 (2017), 1600715.

[191] L. T. Huang, H. J. Yen, G. S. Liou, Macromolecules 44 (2011) 9595–9610.

[192] H. J. Yen, C. J. Chen, G. S. Liou, Adv. Funct. Mater. 23 (2013) 5307–5316.

[193] C. J. Chen, H. J. Yen, Y. C. Hu, G. S. Liou, J. Mater. Chem. C 1 (2013) 7623.

[194] Y. Oishi, H. Takado, M. Yoneyama, M. A. Kakimoto, Y. Imai, J. Polym. Sci., Part A: Polym. Chem. 28 (1990) 1763–1769.

[195] S. H. Hsiao, Y. M. Chang, H. W. Chen, G. S. Liou, J. Polym. Sci., Part A: Polym. Chem. 44 (2006) 4579–4592.

[196] G. S. Liou, H. W. Chen, H. J. Yen, J. Polym. Sci. Part A: Polym. Chem. 44 (2002) 4108–4121.

[197] C. W. Chang, G. S. Liou, S. H. Hsiao, J. Mater. Chem. 17 (2007) 1007–1015.

[198] S. H. Hsiao, G. S. Liou, Y. C. Kung, H. J. Yen, Macromolecules 41 (2008) 2800–2808.

[199] S. H. Hsiao, G. S. Liou, Y. C. Kung, H. Y. Pan, C. H. Kuo, Eur. Polym. J. 45 (2009) 2234–2248.

[200] Y. C. Kung, G. S. Liou, S. H. Hsiao, J. Polym. Sci., Part A: Polym. Chem. 47 (2009), 1740–1755.

[201] S. H. Hsiao, G. S. Liou, Y. C. Kung, T. J. Hsiung, J. Polym. Sci., Part A: Polym. Chem. 48 (2010) 3392–3401.

[202] H. J. Yen, S. M. Guo, G. S. Liou, J. Polym. Sci., Part A: Polym. Chem. 48 (2010) 5271–5281.

[203] H. J. Yen, G. S. Liou, J. Mater. Chem. 20 (2010) 9886.

[204] L. T. Huang, H. J. Yen, J. H. Wu, G. S. Liou, Org. Electron. 13 (2012) 840–849.

[205] H. J. Yen, K. Y. Lin, G. S. Liou, J. Polym. Sci., Part A: Polym. Chem. 50 (2012) 61–69.

[206] H. J. Yen, G. S. Liou, Chem. Commun. 49 (2013) 9797–9799.

[207] S. H. Hsiao, Y. T. Chou, Macromol. Chem. Phys. 215 (2014) 958–970.

[208] S. H. Hsiao, J. W. Lin, Polym. Chem. 5 (2014) 6770– 6778.

[209] H. M. Wang, S. H. Hsiao, J. Polym. Sci., Part A: Polym. Chem. 52 (2014) 272–286.

[210] S. H. Hsiao, S. L. Cheng, J. Polym. Sci., Part A: Polym. Chem. 53 (2015) 496–510.

[211] S. H. Hsiao, Y. H. Hsiao, Y. R. Kung, J. Polym. Sci., Part A: Polym. Chem. 54 (2016) 1289–1298.

[212] S. H. Hsiao, Y. H. Hsiao, Y. R. Kung, C. M. Leu, T. M. Lee, React. Funct. Polym. 108 (2016) 54–62.

[213] S. H. Hsiao, K. H. Lin, J. Fluorine Chem. 188 (2016) 33–42.

[214] S. H. Hsiao, C. N. Wu, J. Electroanal. Chem. 776 (2016) 139–147.

[215] S. H. Hsiao, J. S. Han, J. Polym. Sci., Part A: Polym. Chem. 55 (2017) 1409–1421.

[216] S. H. Hsiao, C. N. Wu, Polym. Int. 66 (2017) 916–924.

[217] N. Sun, F. Feng, D. Wang, Z. Zhou, Y. Guan, G. Dang, H. Zhou, C. Chen, X. Zhao, RSC Adv. 5 (2015) 88181– 88190.

[218] M. J. Lee, Y. J. Kwak, W. C. Seok, S. W. Lee, Polym. Bull. 73 (2016) 2427–2438.

[219] N. Sun, S. Meng, D. Chao, Z. Zhou, Y. Du, D. Wang, X. Zhao, H. Zhou, C. Chen, Polym. Chem. 7 (2016) 6055–6063.

[220] N. Sun, S. Meng, Z. Zhou, J. Yao, Y. Du, D. Wang, X. Zhao, H. Zhou and C. Chen, RSC Adv. 6 (2016) 66288–66296.

[221] N. Sun, Z. Zhou, D. Chao, X. Chu, Y. Du, X. Zhao, D. Wang and C. Chen, J. Polym. Sci., Part A: Polym. Chem. 55 (2017) 213–222.

[222] N. Sun, Z. Zhou, S. Meng, D. Chao, X. Chu, X. Zhao, D. Wang, H. Zhou and C. Chen, Dyes Pigm. 141 (2017) 356–362.

[223] S. Wang, X. Wu, X. Zhang, H. Niu, C. Wang, Y. Zhang, X. Bai, W. Wang and Y. Hou, Eur. Polym. J. 93 (2017) 368–381.

[224] R. R. Nelson, R. N. Adams, J. Am. Chem. Soc. 90 (1968) 3925–3930.

[225] E. T. Seo, R. F. Nelson, J. M. Fritsch, L. S. Marcoux, D. W. Leedy, R. N. Adams, J. Am. Chem. Soc. 88 (1966) 3498–3503.

[226] S. Cai, H. Wen, S. Wang, H. Niu, C. Wang, X. Jiang, X. Bai, W. Wang, Electrochim. Acta 228 (2017) 332–342.

[227] K. Karon, M. Lapkowski, A. Dabuliene, A. Tomkeviciene, N. Kostiv, J. V. Grazulevicius, Electrochim. Acta 154 (2015) 119–127.

[228] X. Lv, S. Yan, Y. Dai, M. Ouyang, Y. Yang, P. Yu, C. Zhang, Electrochim. Acta 186 (2015) 85–94.

[229] P. Zhou, Z. Wan, Y. Liu, C. Jia, X. Weng, J. Xie, L. Deng, Electrochim. Acta 190 (2016) 1015–1024.

[230] Y. Hou, L. Kong, X. Ju, X. Liu, J. Zhao, Q. Niu, Materials 9 (2016) 779.

[231] J. C. Lai, X. R. Lu, B. T. Qu, F. Liu, C. H. Li, X. Z. You, Org. Electron. 15 (2014) 3735–3745.

[232] S. Li, G. Liu, X. Ju, Y. Zhang, J. Zhao, Polymer 9 (2017) 173.

[233] T. Y. Wu, H. H. Chung, Polymer 8 (2016) 206.

[234] X. Yang, M. Wang, J. Zhao, C. Cui, S. Wang, J. Liu, J. Electroanal. Chem. 714 (2014) 1–10.

[235] P. Pander, R. Motyka, P. Zassowski, M. Lapkowski, A. Swist, P. Data, J. Phys. Chem. C 121 (2017) 11027–11036.

[236] J. F. Ambrose, R. F. Nelson, J. Electrochem. Soc. 115 (1968) 1159–1164.

[237] S. H. Hsiao, Y. Z. Chen, Dyes Pigm. 144 (2017) 173–183.

[238] S. H. Hsiao, Y. Z. Chen, J. Electroanal. Chem. 799 (2017) 417–423.

[239] S. H. Hsiao, S. W. Lin, J. Mater. Chem. C 4 (2016) 1271–1280.

[240] S. H. Hsiao, H. M. Wang, J. Polym. Sci., Part A: Polym. Chem. 54 (2016) 2476–2485.

[241] S. H. Hsiao, J. W. Lin, Macromol. Chem. Phys. 215 (2014) 1525–1532.

[242] S. H. Hsiao, H. M. Wang, RSC Adv. 6 (2016) 43470–43479.

[243] S. H. Hsiao, J. Y. Lin, J. Polym. Sci., Part A: Polym. Chem. 54 (2016) 644–655.

[244] S. H. Hsiao, Y. T. Chiu, RSC Adv. 5 (2015) 90941–90951.

[245] P. Shi, C. M. Amb, E. P. Knott, E. J. Thompson, D. Y. Liu, J. Mei, A. L. Dyer, J. R. Reynolds, Adv. Mater. 22 (2010) 4949–4953.

[246] S. Ming, S. Zhen, K. Lin, L. Zhao, J. Xu, B. Lu, ACS Appl. Mater. Interfaces 7 (2015) 11089–11098.

[247] L. You, J. He, J. Mei, Polym. Chem. 9 (2018) 5262–5267.

[248] A. Durmus, G. E. Gunbas, L. Toppare, Chem. Mater. 19 (2007) 6247–6251.

[249] P. Camurlu, RSC Adv. 4 (2014) 55832–55845.

[250] D. T. Christiansen, D. L. Wheeler, A. L. Tomlinson, J. R. Reynolds, Polym. Chem. 9 (2018) 3055–3066.

[251] M. Sezgin, O. Ozay, S. Koyuncu, H. Ozay, F. B. Koyuncu, Chem. Eng. J. 274 (2015) 282–289.

[252] Y. Li, T. Michinobu, J. Polym. Sci., Part A: Polym. Chem. 50 (2012) 2111–2120.

[253] H. Yen, C. Chen, G. Liou, Adv. Funct. Mater. 23 (2013) 5307–5316.

[254] S. Hsiao, G. Liou, H. Wang, J. Polym. Sci., Part A: Polym. Chem. 47 (2009) 2330–2343.

[255] C. W. Chang, C. H. Chung, G. S. Liou, Macromolecules 41 (2008) 8441–8451.

[256] G. S. Liou, H. Y. Lin, Macromolecules 42 (2008) 125–134.

[257] R. L. Elsenbaumer, K. Y. Jen, R. Oboodi, Synth. Met. 15 (1986) 169–174.

[258] W. Kaim, G. K. Lahiri, Angew. Chem. Int. Ed. 46 (2007) 1778–1796.

[259] M. Berggren, D. Nilsson, N. D. Robinson, Nat. Mater. 6 (2007) 3.

[260] G. S. Collier, I. Pelse, A. M. O. sterholm, J. R. Reynolds, Chem. Mater. 30 (2018) 5161–5168.

[261] P. M. Beaujuge, C. M. Amb, J. R. Reynolds, Adv. Mater. 22 (2010) 5383–5387.

[262] E. E. Havinga, L. W. van Horssen,W. ten Hoeve, H.Wynberg, E. W. Meijer, Polym. Bull. 18 (1987) 277–281.

[263] A. O. Patil, Y. Ikenoue, F. Wudl, A. J. Heeger, J. Am. Chem. Soc. 109 (1987) 1858–1859.

[264] N. S. Sundaresan, S. Basak, M. Pomerantz, J. R. Reynolds, J. Chem. Soc., Chem. Commun. (1987) 621–622.

[265] J. F. Ponder, A. M. O sterholm, J. R. Reynolds, Chem. Mater. 29 (2017) 4385–4392.

[266] L. R. Savagian, A. M. O. sterholm, J. F. Ponder, K. J. Barth, J. Rivnay, J. R. Reynolds, Adv. Mater. 30 (2018) 1–6.

[267] J. H. Tang, C. J. Yao, B. B. Cui, Y. W. Zhong, Chem. Rec. 16 (2016) 754–767.

[268] P. Mondal, M. Chatterjee, A. Paretzki, K. Beyer, W. Kaim, G. K. Lahiri, Inorg. Chem. 55 (2016) 3105–3116.

[269] G. de Ruiter, L. Motiei, J. Choudhury, N. Oded, M. E. van der Boom, Angew. Chem. 122 (2010) 4890–4893.

[270] C. Simão, M. Mas-Torrent, J. Casado-Montenegro, F. Otón, J. Veciana, C. Rovira, J. Am. Chem. Soc. 133 (2011) 13256–13259.

[271] G. de Ruiter, M. E. van der Boom, Acc. Chem. Res. 44 (2011) 563–573.

[272] M. Mas-Torrent, C. Rovira, J. Veciana, Adv. Mater. 25 (2013) 462–468.

[273] A. Winter, S. Hoeppener, G. R. Newkome, U. S. Schubert, Adv. Mater. 23 (2011) 3484–3498.

[274] J. Poppenberg, S. Richter, C. H. H. Traulsen, E. Darlatt, B. Baytekin, T. Heinrich, P. M. Deutinger, K. Huth, W. E. S. Unger, C. A. Schalley, Chem. Sci. 4 (2013) 3131–3139.

[275] T. Nagashima, H. Ozawa, T. Suzuki, T. Nakabayashi, K. Kanaizuka, M. A. Haga, Chem. Eur. J. 22 (2016) 1658–1667.

[276] C. J. Yao, Y. W. Zhong, H. J. Nie, H. D. Abruña, J. Yao, J. Am. Chem. Soc. 133 (2011) 20720–20723.

[277] Y. W. Zhong, Z. L. Gong, J.-Y. Shao, J. Yao, Coord. Chem. Rev. 312 (2016) 22–40.

[278] W. Polit, T. Exner, E. Wuttke, F. Winter Rainer, BioInorg. React. Mech. 8 (2012) 85–105.

[279] J. J. Shen, Y. W. Zhong, Sci. Rep. 5 (2015) 13835.

[280] G. Grelaud, M. P. Cifuentes, T. Schwich, G. Argouarch, S. Petrie, R. Stranger, F. Paul, M. G. Humphrey, Eur. J. Inorg. Chem. (2012) 65–75.

[281] R. J. Mortimer, D. R. Rosseinsky, P. M. S. Monk, Electrochromic Materials and Devices, Wiley (2015).

[282] V. Croué, S. Goeb, G. Szalóki, M. Allain, M. Sallé, Angew. Chem., Int. Ed. 55 (2016) 1746–1750.

[283] J. Winsberg, T. Hagemann, T. Janoschka, M. D. Hager, U. S. Schubert, Angew. Chem. Int. Ed. 56 (2017) 686–711.

[284] K. Yazaki, S. Noda, Y. Tanaka, Y. Sei, M. Akita, M. Yoshizawa, Angew. Chem. Int. Ed. 55 (2016) 15031–15034.

[285] C. R. Benson, E. M. Fatila, S. Lee, M. G. Marzo, M. Pink, M. B. Mills, K. E. Preuss, A. H. Flood, J. Am. Chem. Soc. 138 (2016) 15057–15065.

[286] Q. Chen, J. Sun, P. Li, I. Hod, P. Z. Moghadam, Z. S. Kean, R. Q. Snurr, J. T. Hupp, O. K. Farha, J. F. Stoddart, J. Am. Chem. Soc. 138 (2016) 14242–14245.

[287] J. Schäfer, M. Holzapfel, B. Mladenova, D. Kattnig, I. Krummenacher, H. Braunschweig, G. Grampp, C. Lambert, J. Am. Chem. Soc. 139 (2017) 6200–6209.

[288] J. R. Jennings, W. Y. Lim, S. M. Zakeeruddin, M. Gratzel, Q. Wang, ACS Appl. Mater. Interfaces 7 (2015) 2827–2832.

[289] J. Nagasaki, S. Hiroto, H. Shinokubo, Chem. – Asian J. 12 (2017) 2311–2317.

[290] Y. Li, T. Tan, S. Wang, Y. Xiao, X. Li, Dyes Pigm. 144 (2017) 262–270.

[291] C. Quinton, V. Alain-Rizzo, C. Dumas-Verdes, F. Miomandre, G. Clavier, P. Audebert, Chem. Eur. J. 21 (2015) 2230–2240.

[292] H. Y. Jin, X. G. Li, T. F. Tan, S. R. Wang, Y. Xiao, J. H. Tian, Dyes Pigm. 106 (2014) 154–160.

[293] F. Chen, X. Fu, J. Zhang, X. Wan, Electrochim. Acta 99 (2013) 211–218.

[294] X. T. Wu, W. Wang, B. Li, Y. J. Hou, H. J. Niu, Y. H. Zhang, S. H. Wang, X. D. Bai, Spectrochim. Acta, Part A 140 (2015) 398–406.

[295] H. L. Wen, H. J. Niu, B. Li, X. C. Ma, X. D. Bai, Y. H. Zhang, W. Wang, Synth. Met. 202 (2015) 89–97.

[296] Y. Li, Y. H. Zhang, H. J. Niu, C. Wang, C. L. Qin, X. D. Bai, W. Wang, New J. Chem. 40 (2016) 5245–5254.

[297] K. B. Vincent, M. Parthey, D. S. Yufit, M. Kaupp, P. J. Low, Polyhedron 86 (2015), 31–42.

[298] P. Andersson, R. Forchheimer, P. Tehrani, M. Berggren, Adv. Funct. Mater. 17 (2007) 3074−3082.

[299] P. A. Ersman, M. Zabihipour, D. Tu, R. Lassnig, J. Strandberg, J. Ahlin, M. Nilsson, D. Westerberg, G. Gustafsson, M. Berggren, R. Forchheimer, S. Fabiano, Flex. Print. Electron. 5 (2020) 024001.

[300] B. Bao, B. Rivkin, F. Akbar, D. D. Karnaushenko, V. K. Bandari, L. Teuerle, C. Becker, S. Baunack, D. Karnaushenko, O. G. Schmidt, Adv. Mater. 33 (2021) 2101272.

[301] H. Hu, Z. Wang, Q. Ye, J. He, X. Nie, G. He, C. Song, W. Shang, J. Wu, P. Tao, T. Deng, ACS Appl. Mater. Interfaces 8 (2016) 20483−20490.

[302] S. Coskun, E. S. Ates, H. E. Unalan, Nanotechnology 24 (2013) 125202.

[303] T. Tokuno, M. Nogi, M. Karakawa, J. T. Jiu, T. T. Nge, Y. Aso, K. Suganuma, Nano Res. 4 (2011) 1215−1222.

[304] Y. Fang, Y. Li, X. Wang, Z. Zhou, K. Zhang, J. Zhou, B. Hu, Small 16 (2020) 2000450.

[305] Y. Yang, ACS Nano 12 (2018) 2027−2034.

Chapter-2

Instrumentation

After synthesizing the monomers, different characterization techniques like NMR, FTIR and MALDI-TOF were employed. The electrochemical techniques like Cyclic Voltammetry, Chronoampherometry and Spectroelectrochemistry (combination CV and UV-Vis spectroscopy) were carried out to measure the electrochromic parameters. The morphology of the polymer film was checked by FESEM and AFM. All the techniques have discussed briefly in this chapter.

2.01. Nuclear magnetic resonance (NMR)

Nuclear magnetic resonance (NMR) spectroscopy is an analytical technique used to detect structure of a molecule. It was first demonstrated by Isidor I. Rabi in 1938. In early days, NMR spectroscopy progressed concurrently with advances in many other fields, such as mathematics, physics and informatics. NMR spectroscopy is based on the interaction of an externally applied radiofrequency radiation with internal frequency of atomic nuclei. During this interaction there is an exchange of energy which leads to a change in an intrinsic property of the atomic nuclei called nuclear spin. The nuclear spin can be defined by a quantum number (I), which varies depending on the isotope. The nuclei with $I \neq 0$ are detectable by NMR spectroscopy (NMR-active nuclei, such as ^{1}H, ^{2}H, ^{13}C and ^{15}N). These NMR-active nuclei behave like a tiny magnet with magnetic dipoles, capable of aligning with external magnetic fields by a process called magnetization. The force of those tiny magnets is defined by a constant known as the magnetogyric ratio (γ), whose value depends on the isotope.

Nuclear spins of some NMR-active nuclei are able to adopt two different orientations when they align to an external magnetic field (B_0). One orientation corresponds to the lowest energy level of the nucleus (parallel to the external magnetic field), and the other one is associated to the highest energy level of the nucleus (anti parallel to the external magnetic field). The difference between energy levels (ΔE) depends on the magnetic field and the magnetogyric ratio and affects the sensitivity of the technique. Magnetic resonance is achieved when nuclei are irradiated with radiofrequency. This causes transitions between energy levels, which involves changes in the orientation of nuclear spins.

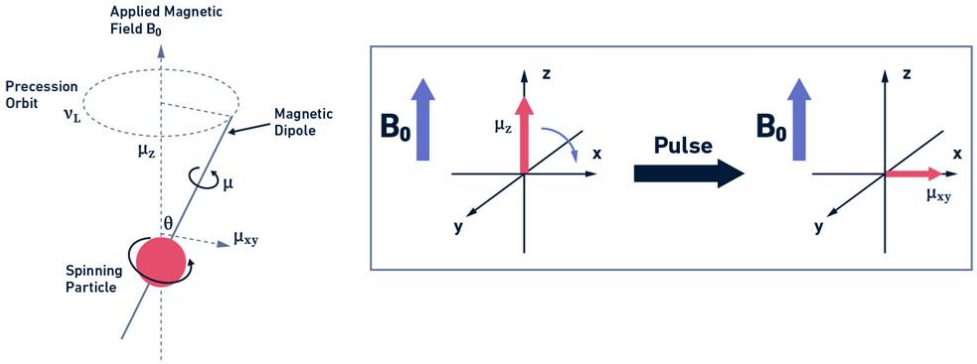

Fig.2.01. Nuclear spin behavior under the influence of an external magnetic field (left panel). Scheme of a basic NMR experiment in which the magnetization is transferred to the xy plane upon the application of a magnetic pulse (right panel).

When atomic nuclei are under the effect of a magnetic field, nuclear magnetic dipoles are not statically aligned with the magnetic field B_0, but rather move like a spinning top (precession movement) around an axis parallel to the direction of the field. The frequency of this precession movement, called Larmor frequency (ν_L), is defined by the magnetogyric ratio and the magnetic field. As a consequence of this precession movement, the magnetic vector (μ) associated with the nuclear magnetic dipoles possesses a component parallel to the magnetic field (μ_z) and another component perpendicular to the magnetic field (μ_{xy}), with this last one having a net value of zero in the absence of external perturbations. In an NMR experiment, it is not possible to measure the signal in the z direction, as the magnetic field is too intense in that direction. Therefore, it is necessary to transfer the magnetization of the z component to the xy plane.

For this purpose, a magnetic pulse containing frequencies close to the Larmor frequency is applied perpendicular to B_0 to reach the resonance of nuclear spins, which generates a non-zero μ_{xy} component. After this pulse, a relaxation process takes place and the μ_{xy} component gradually recovers its net value of zero **[Fig.2.01, right panel].** As a consequence of this relaxation, energy is emitted as radiofrequency, producing a characteristic signal called free induction decay (FID) which is registered by the detector. This FID is subsequently transformed into a plot of intensities versus frequencies known as an NMR spectrum. The position of resonance peaks on the

scale of frequency or magnetic field depend on the local magnetic fields that were result of the nature and location of the atomic groups in the vicinity of the protons. The shifting in the resonance is known as chemical shifts. Chemical shifts were measured in parts per million in frequencies on a scale labelled. The chemical shift is measured with respect to the internal standard tetramethyl silane (TMS) **[Fig.2.02].** The relation between chemical shift and radiofrequency is,

δ = [(frequency of signal – frequency of standard) / spectrometer frequency]*10^6.

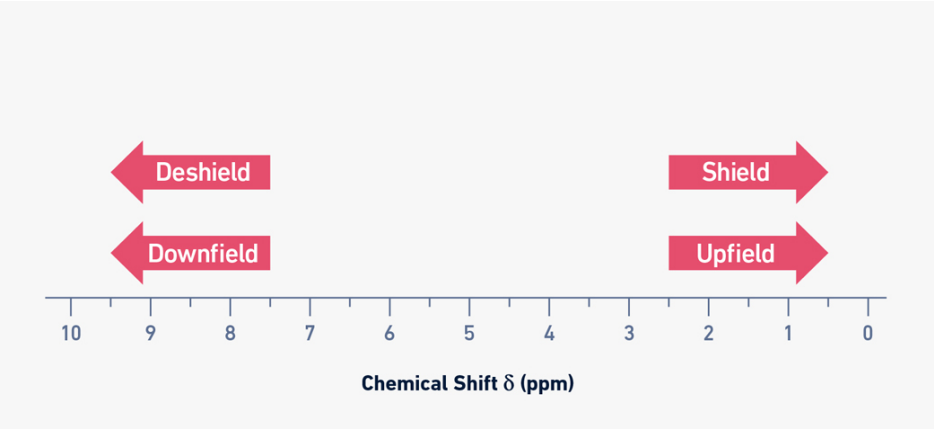

Fig. 2.02. NMR scale represents upfield and downfield

NMR spectrometers consist of three main components: a superconducting magnet, a probe and a complex electronic system (console) controlled by a workstation **[Fig. 2.03].** The magnet is responsible for the generation of a strong magnetic field that aligns the nuclear spins of the atoms present in the sample. Nowadays, the magnets used in NMR spectroscopy are based on superconducting materials, and thus, they require very low temperatures to work (around 4 K). For this reason, NMR spectrometers contain a cooling system composed of an inner jacket filled with liquid helium which is refrigerated by an additional jacket filled with liquid nitrogen, and many layers of thermal isolating materials.

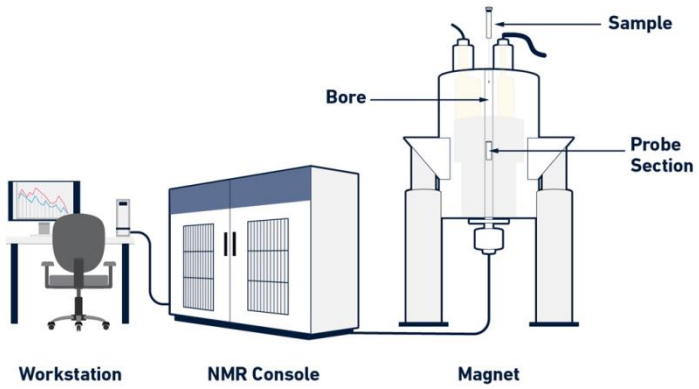

Fig. 2.03. General design of an NMR spectrometer with its principal components.

The superconducting magnet surrounds a cylindrical chamber known as the "probe", which is a crucial component of the instrument. The sample is introduced into the probe and thus placed under the influence of the magnetic field. Additionally, the probe contains a series of magnetic coils that are also located around the sample.

These coils have multiple purposes. On one hand, they are used to irradiate the radiofrequency pulses and to detect and collect the NMR signal emitted by the sample. On the other hand, they also enable control of the magnetic field homogeneity and the application of pulse gradients that are used in some NMR experiments.

In this thesis, ^{1}H and ^{13}C spectra were recorded by 300 MHz, 400 MHz, 500 MHz, 600 MHz Bruker instrument.

2.02. Matrix-assisted laser desorption/ionization (MALDI)

Mass spectrometry is an analytical technique in which samples are ionized into charged molecules and ratio of their mass-to-charge (m/z) can be measured. In MALDI-TOF mass spectrometry, the ion source is matrix-assisted laser desorption/ionization (MALDI), and the mass analyzer is time-of-flight (TOF) analyzer. MALDI is a soft ionization that involves a laser striking a matrix of small

molecules to make the analyte molecules into the gas phase without fragmenting or decomposing them. Some biomolecules are too large and can decompose when heated, and traditional techniques will fragment or destroy macromolecules. MALDI is appropriate to analyze biomolecules like peptides, lipids, saccharides, or other organic molecules.

The principle of MALDI

The analyte is embedded in a very large excess of a matrix compound deposited on a solid surface called a target, usually made of a conducting metal and having spots for several different samples to be applied **[Fig.2.04].** After a very brief laser pulse, the irradiated spot is rapidly heated and becomes vibrationally excited. The matrix molecules energetically ablated from the surface of the sample, absorb the laser energy and carry the analyte molecules into the gas phase as well. During the ablation process, the analyte molecules are usually ionized by being protonated or deprotonated with the nearby matrix molecules. The most common MALDI ionization format is for analyte molecules to carry a single positive charge.

Types of laser commonly used in MALDI

Lasers of both ultraviolet (UV) and infrared (IR) wavelengths are in use, but UV lasers are by far the most important light sources in analytical MALDI. Among these, nitrogen lasers and frequency-tripled or quadrupled Nd: Yag lasers often serve for the majority of applications.

Commonly used MALDI matrix substance

It is believed that the first function of the matrix essentially is to dilute and isolate analyte molecules from each other. This occurs during solvent evaporation and concomitant formation of a solid solution. Then, upon laser irradiation, it functions as a mediator for energy absorption. The choice of the right matrix is key to the success in MALDI. In general, highly polar analytes work better with highly polar matrices, and nonpolar analytes are preferably combined with nonpolar matrices. The most

commonly used matrixes are α-cyano-4-hydroxycinnamic acid, 2,5-dihydroxybenzoic acid, 3,5-dimethoxy-4-hydroxycinnamic acid, and 2,6-dihydroxyacetophenone, diathranol.

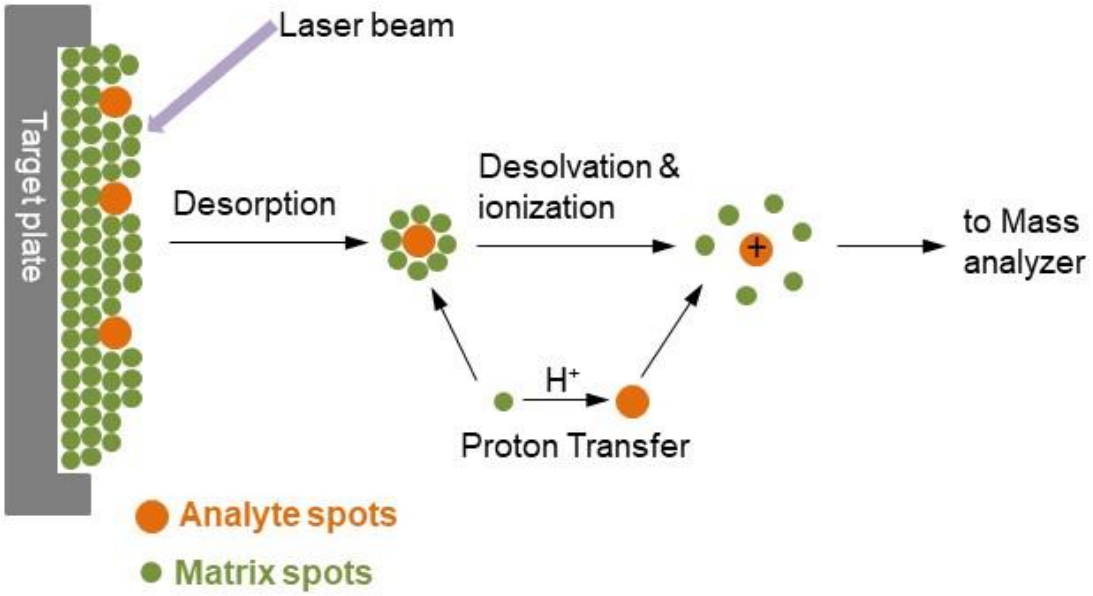

Fig.2.04. Schematic representation of MALDI TOF spectroscopy.

The analyte should be soluble to at least about 0.1 mg/ml in some solvent. And the matrix is dissolved to yield either a saturated solution or a concentration of about 10 mg/ml. The solution of the analyte is then admixed to that of the matrix. For optimized MALDI spectra, the molar matrix-to-analyte ratio is normally adjusted as to fall into the range from 1000: 1 to 100,000: 1. And then the mixture is then spotted onto a metal target plate for analysis. After drying, the mixture of the sample and matrix co-crystallizes and forms a solid deposit of sample embedded into the matrix. The plate is subsequently loaded into the MALDI-TOF instrument and analyzed by software associated with the respective system. The MALDI leads to the sublimation and ionization of both the sample and matrix. These generated ions are separated depending on m/z through a TOF analyzer, and a spectral representation of these ions is generated and analyzed by the MS software, generating an MS profile. The ion

masses (mass to charge ratio) were determined by measuring their TOF, which is longer for larger molecules than for smaller ones for the identical initial energies.

In my thesis, the mass of the derivatives were measured by Bruker Ultraflex Treme MALDI instrument and the matrix was used is diathranol.

2.03. Fourier transform infrared (FTIR) spectroscopy:

FTIR spectroscopy has been used to determine the functional groups present in a molecule. The FTIR instrument consists of one infrared (IR) light source, one beam splitter, one fixed mirror and one movable mirror **[Fig.05].** Those bonds in a molecule are IR active which can changes the dipole moment of the molecules under the irradiation of the electromagnetic radiation. When the molecules are excited by infrared radiation, then it becomes move lower to higher vibration level, consequently we get the infrared absorption spectra. The vibrational level is associated with number of rotational level. The term wavelength or wave number can be used to express the absorption of the infrared radiation and the intensity of the band observed in the FTIR spectrum is expressed in terms of transmittance (T) or absorbance (A). In this thesis, Perkin Elmer FTIR C120947 was operated; very dilute sample solution was used of the frequency range 400-4000 cm^{-1}.

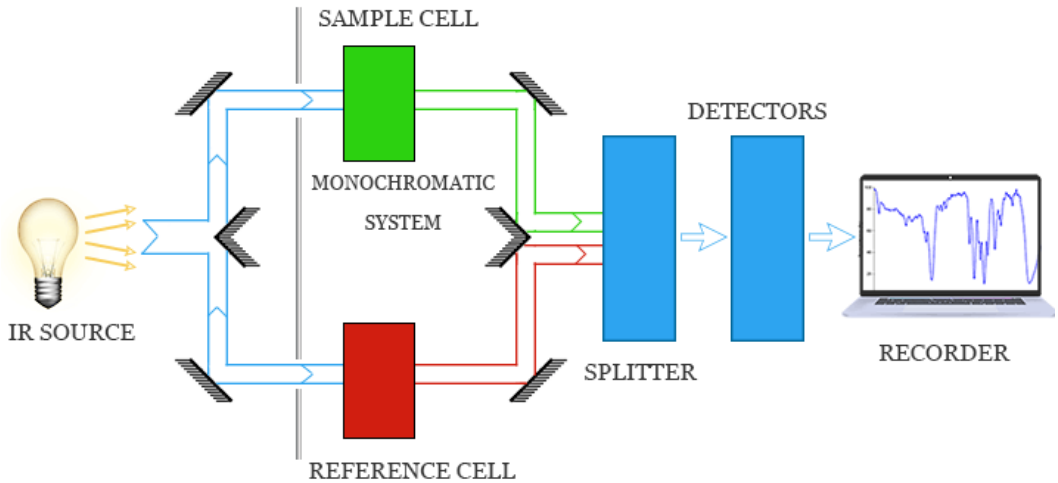

Fig.2.05. Schematic diagram of IR instrumentation.

2.04. Field Emission Scanning Electron Microscope (FESEM):

The SEM is a high vacuum instrument (less than 10^{-7} Pa in the gun zone). The vacuum allows electron movement along the column without scattering and helps prevent discharges inside the gun zone. The function of the electron gun is to provide a large and stable current in a small beam. There are two classes of emission source, a) Thermionic emitter and b) Field emitter. Depending upon the emitter the instrument are categories into scanning electron microscope (SEM) where thermionic emitter is working and field emission scanning electron microscope (FESEM) where field emitter is working. Thermionic emitters use electrical current to heat up a filament (most common filaments are Tungsten and Lanthanum hexaboride). Thermionic sources have relative low brightness, evaporation of cathode material and thermal drift during operation. Field emission is one way of generating electrons that avoids these problems. A field emission gun (FEG) also generating electrons which is cold cathode field emitter. FESEM uses field emission gun producing a cleaner image, less electrostatic distortions and spatial resolution less than 2 nm **[Fig.2.06].** Nanotechnology has strongly driven the development of recent electron microscopy with demands, not only for increasing resolution but also for more information from the sample. In electron microscopes use a beam of highly energetic electrons to probe objects on a very fine scale. In standard electron microscopes, electrons are mostly generated by heating a tungsten filament. But in a field emission electron microscope, cold source is employed. Field emission is the emission of electrons from the surface of a conductor caused by a strong electric field. An extremely thin and sharp tungsten needle works as a cathode. The FE source reasonably combines with scanning electron microscope whose development has been supported by advances in secondary electron detector technology. The acceleration voltage between cathode and anode is commonly in the order of magnitude of 0.5 to 30 kV and the apparatus requires an extreme vacuum in the column of the microscope. Therefore, the FE scanning electron microscope is very useful tool for high resolution surface.

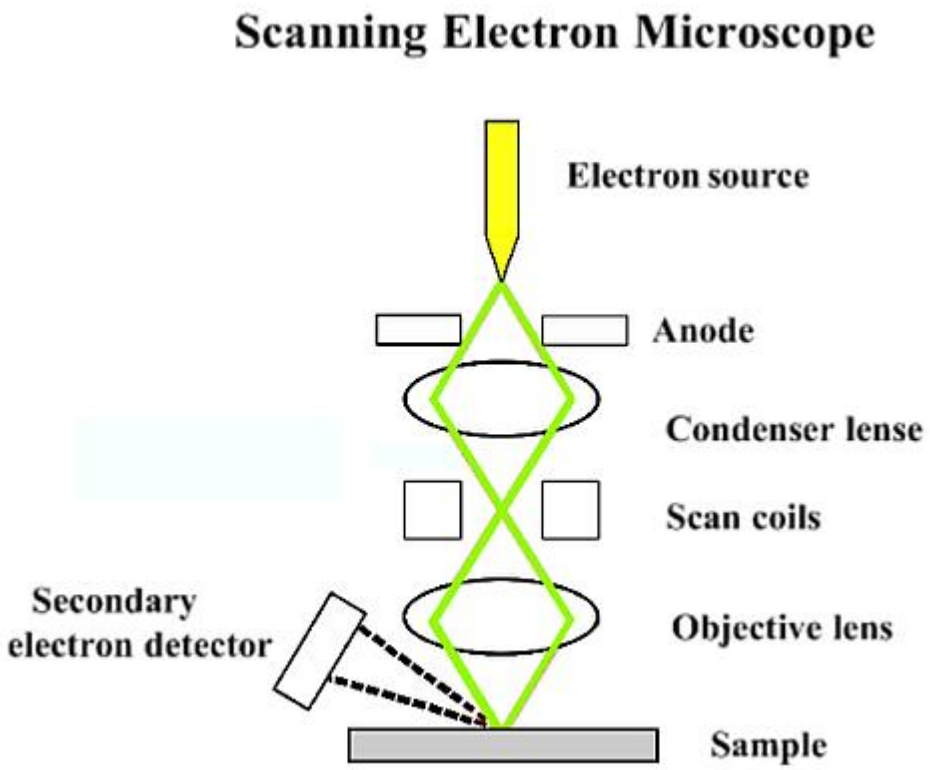

Fig.2.06. Schematic representation of SEM

In my thesis, surface morphology of the polymer sample was carried out by JEOL JSM 6700F FESEM instrument operating at 5 kV in secondary electron mode. The sample was prepared on ITO coated glass by electropolymerization at very slow scan (0.020 mV/s) for 8 cycles. The sample was dried in vacuum oven for overnight.

2.05. Atomic force microscopy (AFM):

Atomic force microscopy (AFM) is a very high resolution type of scanning probe microscopy technique. The topology of the dried sample were studied using atomic force microscope (Veeco, model AP0100). AFM provide 3D profile morphology of materials. The AFM instrument was conducted in the non contact mode at a resonance frequency of the tip end of 250 KHz **[Fig.2.07].** Before going to instrument the dilute

analyte samples solution was electropolymerized on ITO surface. Then the samples were dried over night at room temperature and finally in vacuum.

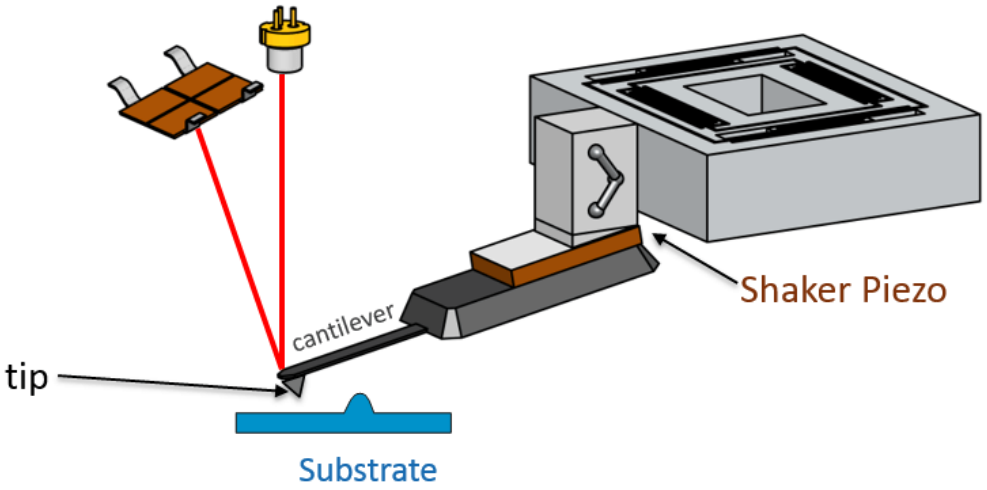

Fig.2.07. Schematic diagram of AFM.

2.06. UV-VIS Spectroscopy:

Ultraviolet-visible spectroscopy refers to absorption spectroscopy or reflectance spectroscopy in the ultraviolet-visible spectral region. Ultraviolet-visible (UV-VIS) spectroscopy is an analytical method that can measure the analyte quantity depending on the amount of light received by the analyte. UV visible spectroscopy is more important because of its versatility, speed, accuracy and cost effectiveness. When UV visible light passes through the sample solution some of the light is absorbed by the sample and rest part of the light transmit through the solution **[Fig.2.08].**

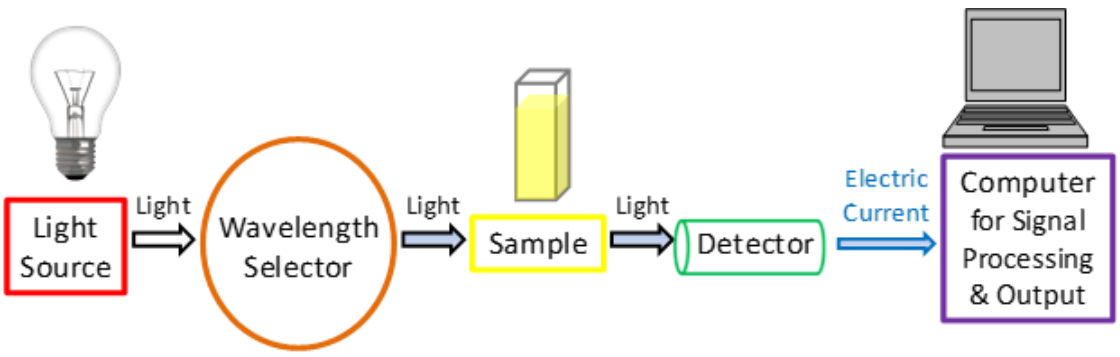

Fig.2.08. Schematic representation of UV Visible spectroscopy.

In UV Visible spectroscopy, Lambert Beer's law is used to measure the absorbance of the light absorbing sample solution. In my thesis, all UV measurement of all monomers and polymers was done in Agilent 8453 and the UV for spectroelectrochemistry was done by ocean optics in our lab.

2.07. Cyclic Voltammetry:

In the cyclic voltametry technique, three electrodes are employed, working electrode, reference electrode and counter or auxiliary electrode. Cyclic voltametry is a type of electrochemical measurement, where the working electrode potential is ramped linearly versus time. In CV experiment, the current flows between two electrodes (the working and counter electrodes) is plotted on the x axis. The resulting plot (X axis vs Y axis) is called a cyclic voltammogram, which is sometimes described as an electrochemical spectrum **[Fig.2.09].** The current which flows, particularly at the current peaks, is often directly proportional to the analyte solution concentration.

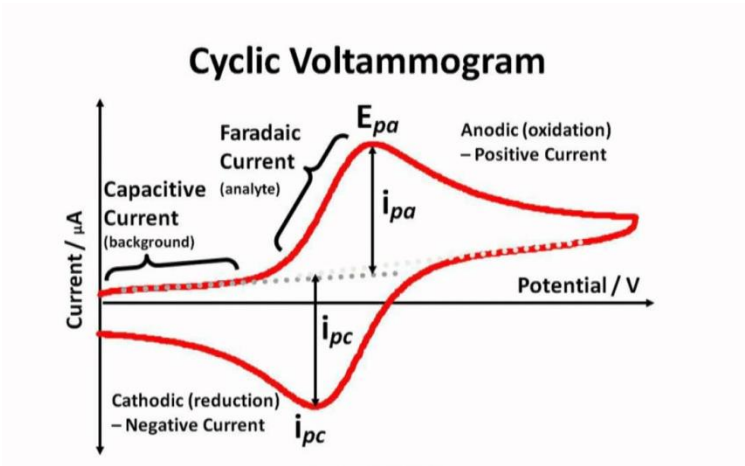

Fig.2.09. Cyclic Voltammogram.

The CV technique is widely used for acquiring qualitative information about electrochemical reactions. The cyclic voltametry provide considerable information on the thermodynamics of redox processes and the kinetics of heterogeneous electron transfer reactions. Electrochemical oxidation occurs during application of increasingly

positive voltage whereas the reverse process corresponds to electrochemical reduction. Critical information on the Electroactive polymers that can be obtained from CV measurements includes the oxidation and reduction onsets for the compulsion of HOMO and LUMO energy levels respectively, indicating the accessibility of the monomers or polymer towards oxidation or reduction. A shallower HOMO and deeper LUMO level facilitates oxidation and reduction respectively. Approximation of the oxidation and reduction onsets involves the determination of intersection point of the tangent lines between the baseline and the current signals. For a highly reversible redox reaction, the ration of anodic and cathodic current is close to one.

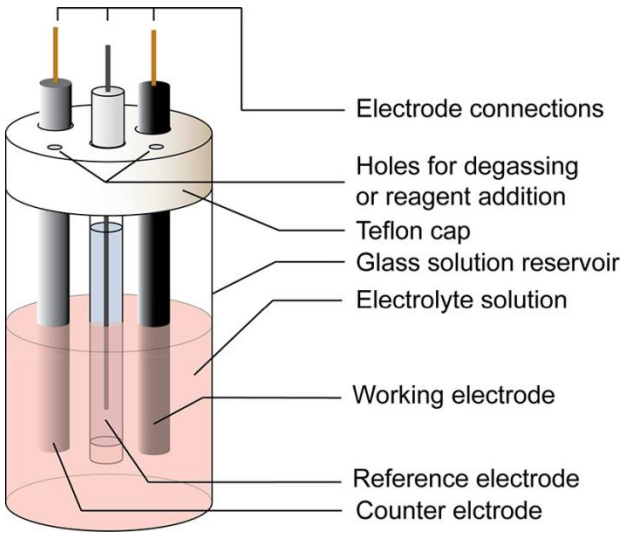

Fig.2.10. CV cell containing three electrodes.

The energy of HOMO can be determined from cyclic voltammetry. The equation for HOMO and LUMO energy levels computation based on the oxidation and reduction onsets were

$$HOMO = - (E_{onset\ ox} \text{ vs ferrocene}) - 4.8\ eV$$

$$LUMO = - (E_{onset\ red} \text{ vs ferrocene}) - 4.8\ eV$$

The value 4.8 is used in the equation as the reversible ferrocene/ferrocenium redox couple is taken to occur at -4.8 eV relative to the vacuum level. In most cases reduction peaks were not clearly observed for conjugated polymers, the LUMO of the polymer is approximated from the optical band gap using equation,

$$\text{Band gap} = \text{HOMO} - \text{LUMO}$$

CV was performed with a three electrode cell configuration in **CHI6087E** under inert atm, to negate any effects arising from the presence of oxygen and moisture. A carbon coated platinum disk or ITO coated glass, pt wire, silver wire were employed as the working, counter and reference electrode **[Fig.2.10].** Polymer films on working electrode were prepared from monomer solution ($5*10^{-4}$M) monomers in 0.1 M Bu_4NClO_4/DCM solutions via cyclic voltammetry repetitive cyclic at a scan rate of 50 mV/s for ten or twenty cycles. The polymer was deposited onto the surface of the working electrode, the deposited polymer film was rinsed with plenty of acetone, DCM and MeOH for the removal of unreacted monomer, inorganic salts and other organic impurities. Fresh polymer films were employed for oxidation and reduction CV scans in 0.1 M TBAP/ACN. Calibration of the reference electrode was carried out before CV measurement. This was done by dissolving ferrocene into the 0.1 M TBAP/ACN electrolyte solvent couple to form an approx 5 mM solution. A CV scan was carried out between the potentials to measure the oxidation potential of ferrocene-ferrocenium couple. All measurements were recorded at a scan rate of 50 mV/s.

2.08. Spectroelectrochemistry:

Spectroelectrochemistry refers to a technique that is used to trace the optical and electronic changes in the polymer upon electrochemical doing/dedoping. The spectroelectrochemical graphs provide key information on the electronic states of the conducting polymer such as the intrinsic band gap and intra band electronic transitions by tracking the formation of polarons and bipolarons bands upon oxidation/reduction, as well as the operation potentials for the electrochromic devices.

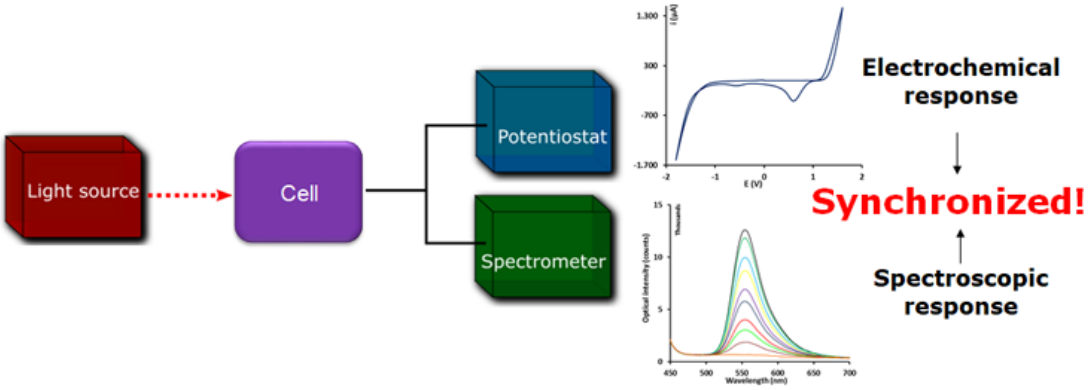

Fig. 2.11. Spectroelectrochemical schematic diagram.

Spectro electrochemical studies were generally performed using a UV-Vis spectrophotometer as well as a potentiostat **[Fig.2.11 and Fig.2.12].** Experimentally baseline is first recorded with blank devices or electrode placed at both the reference and sample cell compartments and held by double sided

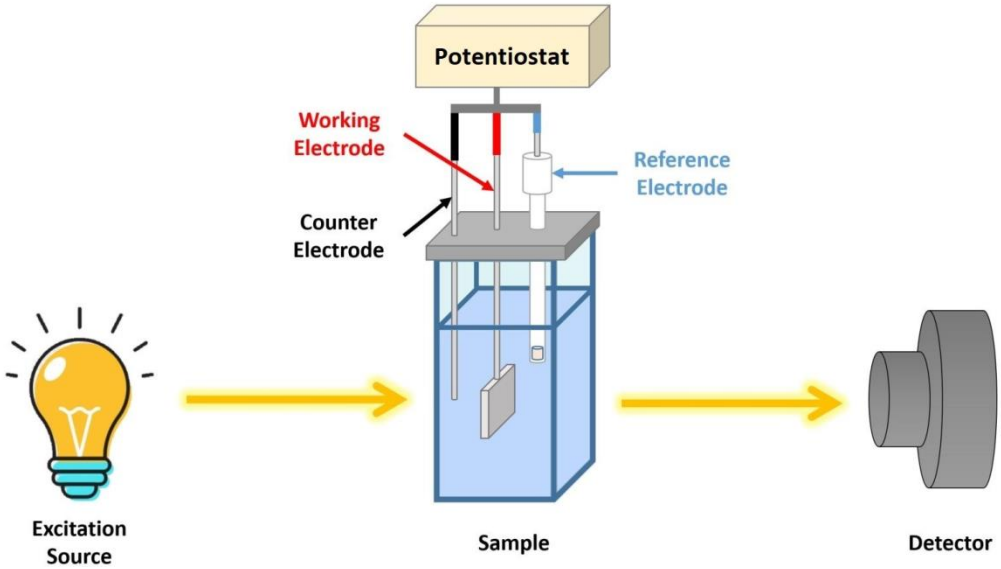

Fig.2.12. Spectroelectrochemical set up.

tapes. Subsequently, the device at the sample cell compartment was replaced by the fabricated polymeric ECD or polymer coated ITO electrode with counter and reference electrodes were connected. In-situ measurements of the UV-Vis spectra of the polymers were controlled by potentiostat. Measurements of the spectra were started after a time lapse of 10s.

2.09. Chronoampherometry:

In Chronoampherometry, the potential applied to the working electrode was stepped and the resulting current and charge occurring at the electrode was monitored as a function of time **[Fig.2.13].** The total charge consumed within a time range was computed from the integration of the current time. The charge density can be calculated from chronoampherometry curve which is needed for colouration efficiency measurement. The current response to the applied potentials generally exists as a spike followed by an exponential decay form as the electrochemical reaction occurred rapidly at the electrode surface followed by time dependent diffusion of charges across the bulk of the polymer film.

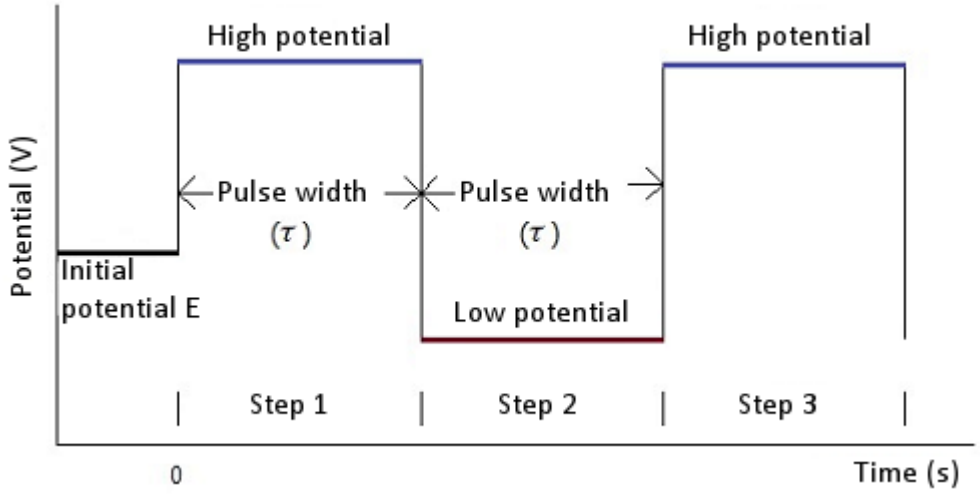

Fig.2.13. Chronoampherometry plot.

In my thesis work, all chronoampherometry measurements on the ECDs were coupled with the recording of the transmittance time profiles using the spectrophotometer. A two electrode cell configuration was utilized with the counter and reference electrodes shorted. The polymer coated ITO substrate acted as the working electrode whereas the second ITO substrate acts as the counter reference electrode.

Chapter-3

Design, Synthesis, and Electrochromic Behaviours of Donor-Acceptor-Donor type Triphenylamine iso-Naphthalenediimide Derivatives

The work reported in current chapter was published in *ChemElectroChem* **2020**, *7*, 4144–4152.

3.1. Indoduction

Upon applying voltage, optical properties such as transmittance/reflectance of some materials are changed in a persistent and reversible manner, this phenomenon is known as electrochromism and the materials responsible for this process are known as electrochromic materials. Change of optical property comes with the electrochemical oxidation or reduction process **[1, 2].** As this phenomenon is associated with some colour change, so it can be a potentially good candidate in display technology, optical switching device, sensors, protective eye wear, smart windows, memory elements **[3-10].** Different type of inorganic metal oxides especially transition metal oxides such as tungsten oxide (WO_3), nickel oxide (NiO or Ni_2O_3), V_2O_5, NbO_5, $Ir(OH)_3$ **[11, 12],** mixed valance metal complexes, organic small molecules and conjugated polymers are commercialized **[13–16].** In the recent decade, small molecular organic derivatives having electropolymerizable groups have shown tremendous interest as an electrochromic material and they are enjoying such as the ease of processing, the different colour shade owing to the chemical modification, relatively good value of coloration efficiency, comparable optical contrasts, improved switching speeds **[17-19].** The propeller-shaped triphenylamine (TPA) has become a promising optoelectronic molecule for emerging electronic applications owing to the prerequisites of its good thermal and morphological stability **[20–27].** Incorporation of bulky, packing disruptive and three- dimensional TPA moieties in polymer backbone helps to solubilise all polymers in organic solvents, and exhibits excellent thin-film-forming capability. Electron-rich TPA derivatives are easily oxidized to form stable polarons and bipolaron, and the oxidation process is always associated with a noticeable colour change in the visible region **[28].** They have a broad range of material systems, including high-performance polymers (aromatic polyimides or polyamides), conjugated polymers, epoxy resins, polysiloxane gels, metal complexes, and small molecules and nearly all these EC materials reveal specific and interesting EC properties. In the present chapter, three donor-acceptor-donor based monomers **(Fig. 3.1)** were designed and the central iso-napthalene diimide was taken as acceptor moiety and electro polymerizable TPA was taken as donor unit with the expectation to achieve the enhanced the coloration efficiency, optical contrast, cyclic stability

with increasing either with number of TPA units sequentially or the conjugation length of the donor part from **TPA$_2$ISO** to **TPA$_6$ISO**. By applying voltage, the TPA units should be oxidized and form radical cation which underwent dimerization to produce tetraphenylbenzidine (TPB) **[29–34].** For the propagation of the polymerization process, it was recently experienced that two factors were crucial, a) the stability of the TPB radical cation and b) non-conjugation of TPA radical with the central acceptor moiety **[35].** The electrochromism of the electro deposited polymers of **TPA$_2$ISO**, **TPA$_4$ISO**, **TPA$_6$ISO** possibly came from the combination effect of the TPA unit and iso-naphthalene unit. The reason for choosing iso-naphthalene unit was that it was neutral and absorbed ultra-violet light at a potential in which TPA is oxidized, as a consequence, it did not contribute any absorption in the bleached state. All the synthesized monomers were subjected to oxidative electro-polymerization process by applying potential through cyclic voltammetry (CV) and multi-colour electrochromism with very less response time and with high coloration efficiencies were explored.

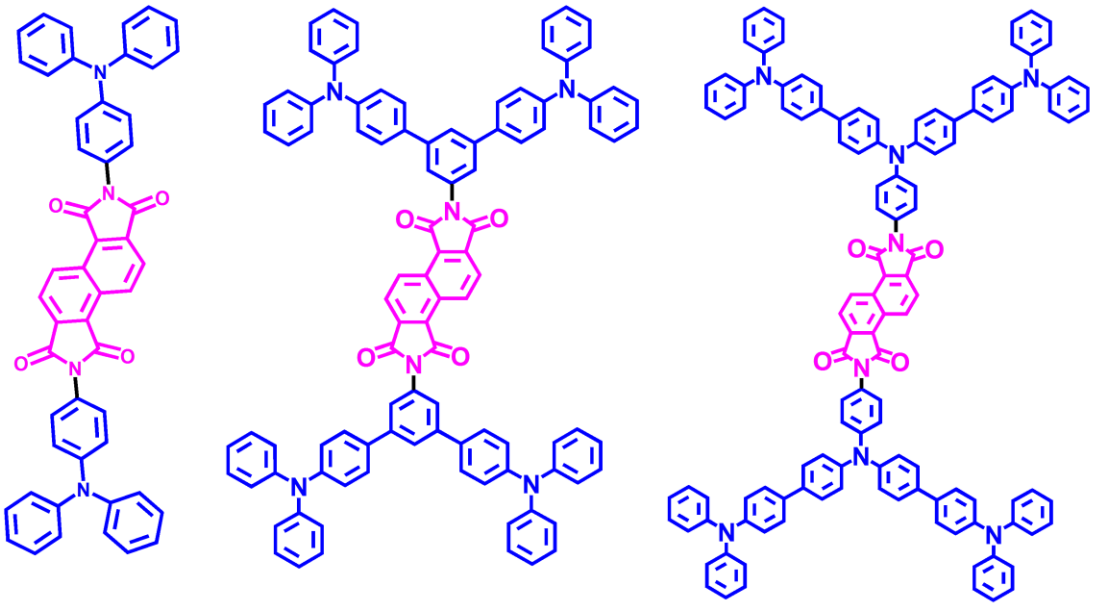

Fig. 3.01. Chemical structure of **TPA$_2$ISO**, **TPA$_4$ISO**, **TPA$_6$ISO.**

To the best of our knowledge, there was no report on the electrochromic behaviours of TPA based iso-naphthalenediimide derivatives and subsequent eletropolymerization. Hence, the investigation of electrochromic behaviours utilizing polymers made of these derivatives might lead to the development of the novel class of electrochromic material.

3.2. Results and discussion

3.2.1. Synthesis of Monomers

Three monomers **TPA$_2$ISO**, **TPA$_4$ISO**, **TPA$_6$ISO** were synthesized by the condensation of iso-naphthalene dianhydride with **D1**, **D2** and **D3** in dry DMF with relatively good yield according to the following scheme shown in **Fig. 3.02a.** Iso-naphthalene dianhydride was prepared from the starting material 2,6 dimethyl naphthalene whose formation was confirmed by the appearance of the peak at 268.75 **(Fig. 3.12)** in the mass spectra. **D1** was synthesized from the precursor diphenyl amine which showed the characteristic peaks of triphenyl amine as well as the peak corresponding to the free amine unit at 5.264 ppm in the ^{1}H NMR spectra **(Fig. 3.15).** **D2** and **D3** were synthesized by the Suzuki coupling from the borolane derivative of TPA **(Fig. 3.14).** The formation of the product **D2** and **D3** was confirmed by the appearance of the signal at 5.58 and 5.16 ppm which was due to the free -NH_2 unit of **D2** and **D3** respectively and disappearance of the proton signals at 1.29 ppm (12 protons) of the TPA-borolane unit in the ^{1}H NMR spectra **(Fig.3.16–Fig.3.17).** Also all the synthesized molecules were well characterized by NMR and MALDI-TOF mass spectra. Details of the procedure and characterization data were provided in the experimental section of **Fig. 3.02b** and **Fig. 3.18–Fig. 3.20.**

3.2.2. Optical Properties of Monomers

UV-Visible spectra of the three monomers were measured in DCM (5×10^{-4}M) solution. Firstly, we performed the UV spectra of the only three donor units (**D1**, **D2**, **D3**) with absorption maxima at 300 nm, 310 and 338 nm, 310 and 342 nm respectively. From the absorption spectra of **TPA$_2$ISO**, **TPA$_4$ISO**, **TPA$_6$ISO**, it was observed that there were two absorption peaks **(Fig. 3.03a)** at 305 nm, 332 nm and

310 nm, 342 nm and 310 nm, 343 nm for the monomer **TPA$_2$ISO**, **TPA$_4$ISO**, **TPA$_6$ISO** respectively, among those at 305 and 310 nm absorption band is characteristic of TPA itself and 332, 342 and 343 nm is due to the absorption of the π-π* transition **[36].**

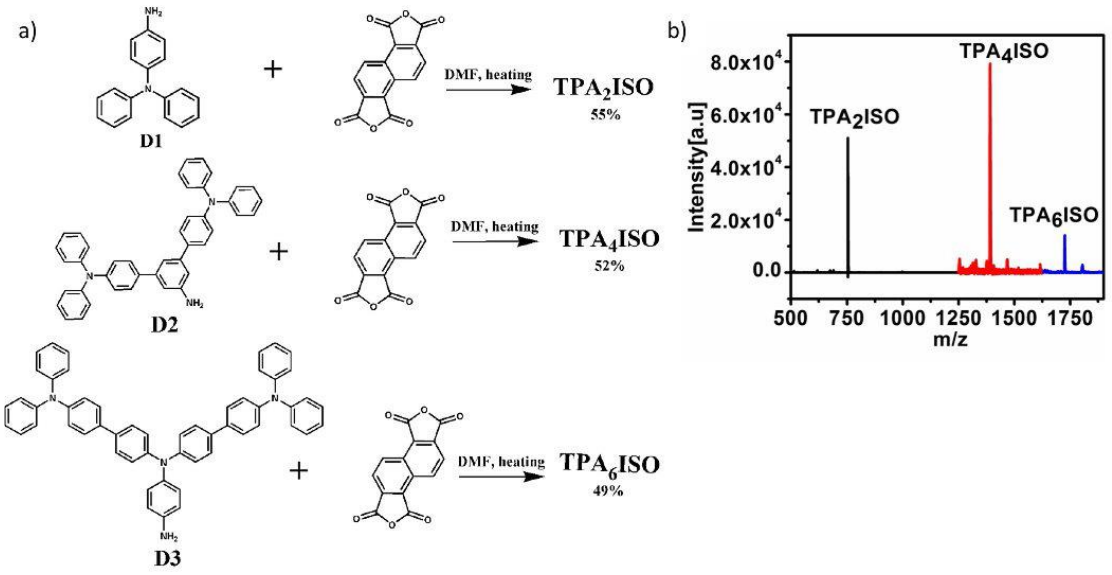

Fig. 3.02. a) Synthesis scheme and b) representative MALDI-TOF spectra of **TPA$_2$ISO**, **TPA$_4$ISO**, **TPA$_6$ISO**.

3.2.3. Electrodeposition of the Polymeric Films and Cyclic Voltammetry Studies

Electro-polymerizations of the monomers were carried out in a three-electrode system having ITO coated glass slides as working electrode, Ag/AgCl, as reference electrode and Pt wire as counter electrode using monomer solution (5×10^{-4} mol) in electrolytic solution of TBAP. The solution was purged with nitrogen gas for 20 min prior to the start of electro-polymerization. With the increasing number of CV scans, peak currents were increased and polymer film was deposited on the surface of working electrode (ITO). For all monomers, similar trend of increasing peak current densities with the increasing the number of scan was observed and it indicated the formation of polymers for all cases **(Fig. 3.03b).** The film thickness was easily tuned by controlling the number of the CV scans. During the electropolymerization process of the three

monomers, an oxidation peak was observed at 1.18 V in the first positive scan and it was the one electron oxidation of triphenyl amine unit. For the negative potential scan of the first cycle, two peaks appeared at 0.88 V, 0.80 V for **TPA$_2$ISO**, 0.93 V and 0.8 V for the **TPA$_4$ISO** and 0.93 V, 0.70 V for the **TPA$_6$ISO** **(Fig. 3.06)** and those were due to the subsequent oxidation of tetraphenyl benzidine (TPB) unit formed by the rapid oxidative coupling between TPA units **(Fig. 3.04).** TPB unit was produced by

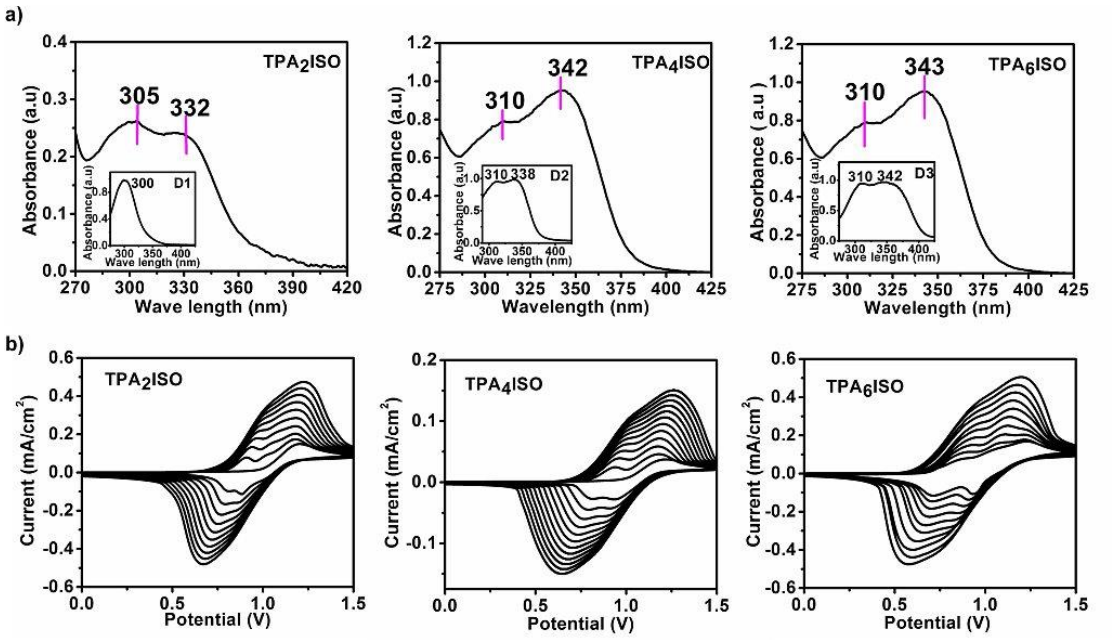

Fig. 3.03. a) Absorption spectra of all the three monomers in DCM solution (5×10^{-4} M), (Inset: absorption spectra of **D1**, **D2** and **D3**). b) CV recorded for 20 scan cycles using ITO as the working electrode, TBAP as supporting electrolytes at scan rate of 50 mV/s for the monomers **TPA$_2$ISO**, **TPA$_4$ISO**, **TPA$_6$ISO** respectively.

the oxidation of TPA, exhibited lower oxidation potential than the original TPA unit because of its more extended π-conjugation **[37].**

3.2.4. Energy-Minimized Structure

From the energy minimized structures and the HOMO and LUMO molecular orbitals, it was predicted that the LUMO was centralized on the isonaphthalene unit and the HOMO was localized on the terminal triphenylamine unit **(Fig. 3.05)** for all of the three monomers which facilitated the electropolymerization process. The energy of

the HOMO, LUMO and band gap obtained from DFT calculation was shown in **Table 3.1.**

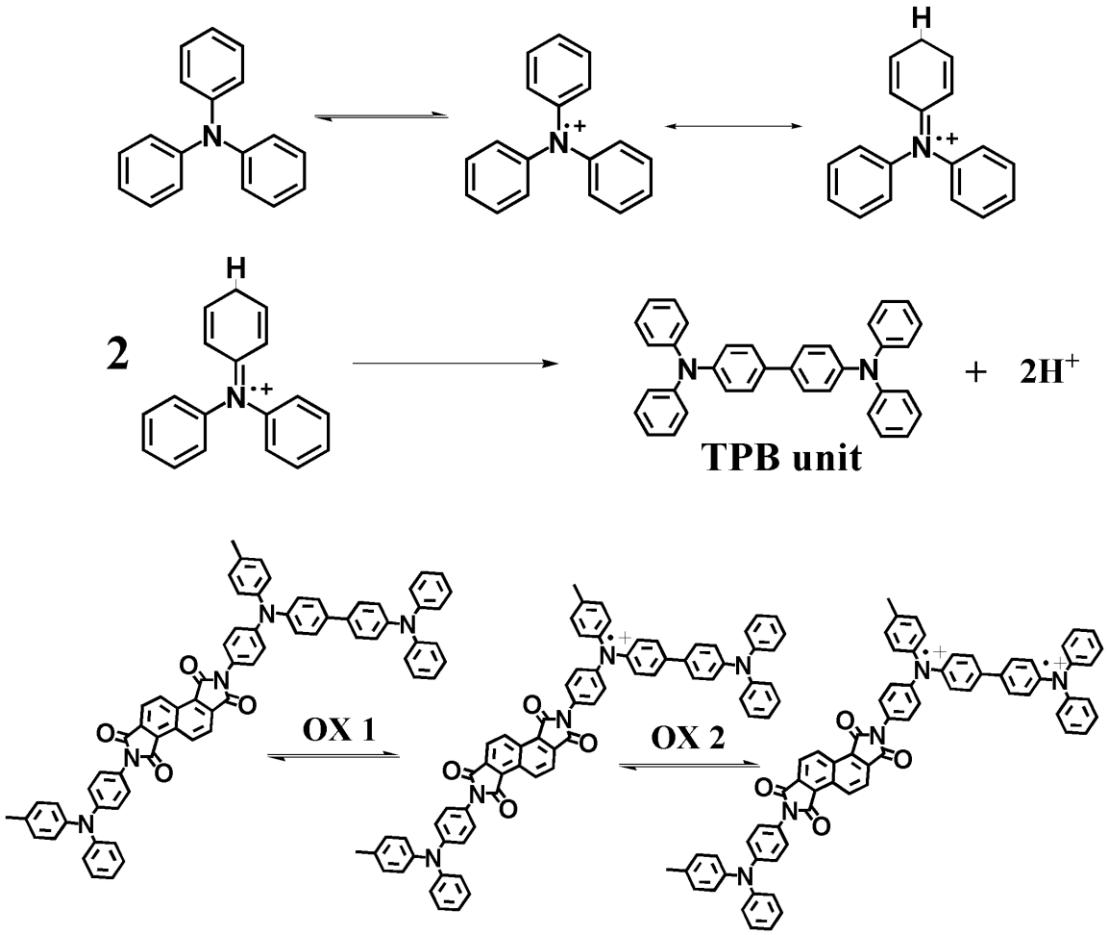

Fig. 3.04. Possible mechanism of electro-polymerization process involved for **TPAnISO** derivatives (n= 2, 4 and 6).

The experimental band gap of the monomers were also estimated from the UV-Vis spectroscopy and the energy level of the HOMO (experimental) was calculated from the cyclic voltammetry using Ferrocene/Ferrocenium ion as external standard. The absorption edges are at 367, 382 and 400 nm respectively for **TPA$_2$ISO**, **TPA$_4$ISO**, **TPA$_6$ISO**. The band gaps calculated from absorption edges were 3.37, 3.24 and 3.10 eV respectively. The experimentally obtained results were more or less closer to the theoretical values. It has also observed that with increasing the number of TPA units in donor part from **TPA$_2$ISO** to **TPA$_6$ISO** the band gap was also decreased. The

calculated HOMO energy levels of **TPA_2ISO**, **TPA_4ISO**, **TPA_6ISO** were -5.56, -5.57 and -5.58 eV and LUMO energy levels were -2.19, -2.33 and -2.48 eV respectively.

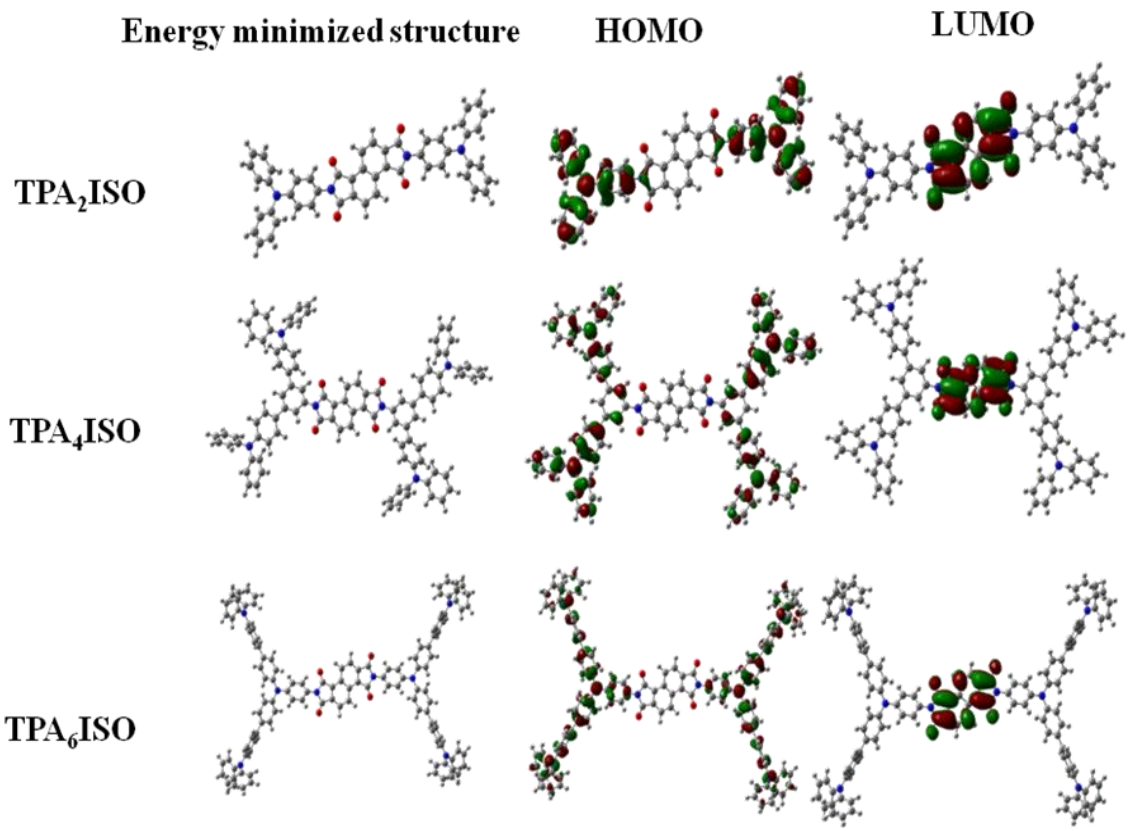

Fig. 3.05. Optimized structures and HOMO-LUMO levels derived by DFT calculations of all TPA_nISO derivatives (n = 2, 4 and 6).

3.2.5. Optical and Electrochemistry of the Polymer Films

Polymer films deposited on ITO surface from the electropolymerization process were subsequently washed with DCM, ethanol and acetone to remove the unreacted monomer and oligomers. Optical behaviours of the polymer films were investigated by UV-Vis spectroscopy. Electrochemical behaviours of the deposited films from the three monomers were investigated by CV measurements in 0.1M TBAP in ACN solution. Absorption peaks obtained from **p-TPA_2ISO**, **p- TPA_4ISO**, **p-TPA_6ISO** were appeared at 362, 369 and 370 nm respectively and those were attributed due to the π-π* transition of TPA backbone. Absorption edges of the three polymeric films

were exhibited at 423, 424 and 435 nm **(Fig. 3.06a)** from which the calculated band gaps were 2.93, 2.92, 2.85 eV **(Table 3.1)**.

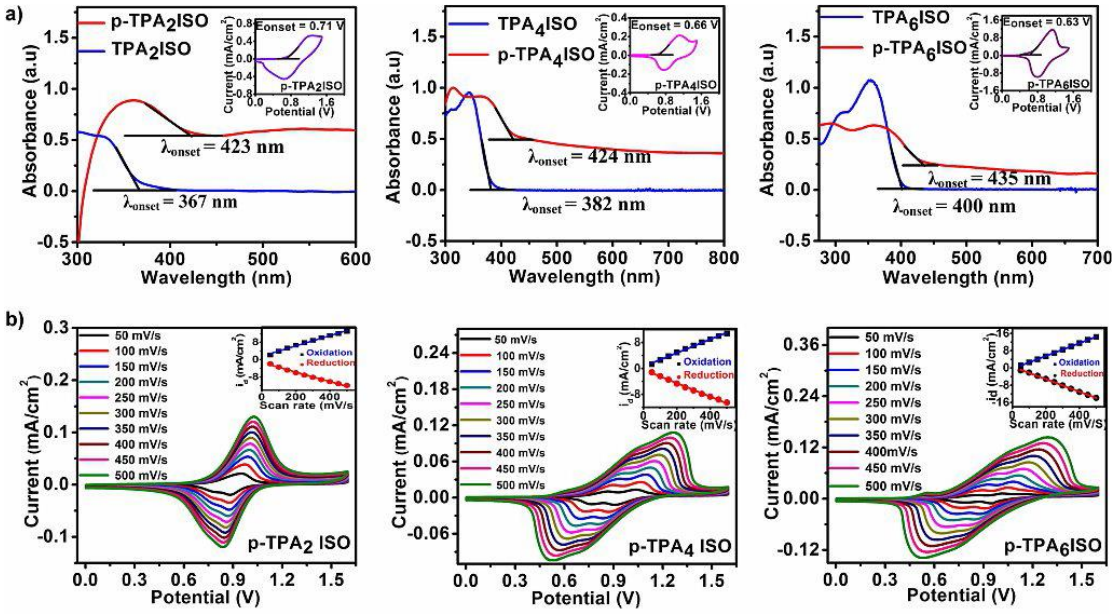

Fig. 3.06. a) Absorption spectra of the monomer and polymer of **TPA$_2$ISO**, **TPA$_4$ISO**, **TPA$_6$ISO** at 0 V (Inset: cyclic voltammetry of the cast film of individual polymer in 0.1 M TBAP/ACN solution (WE : Pt, CE: Pt wire, RE : Ag wire) at a scan rate 100 mVs^{-1}. b) CV plot of polymers on Pt working electrode in 0.1 M TBAP/ACN at different scan rate ranging from 50 mV/s to 500 mV/s (inset: plot of peak current Vs scan rate).

3.2.6. Scan Rate-Dependent Studies

CV studies of **p-TPA$_2$ISO**, **p-TPA$_4$ISO**, **p-TPA$_6$ISO** were performed by varying scan rate from 50–500 mV/s on Pt working electrode, Pt wire and Ag/AgCl were used as counter and reference electrode in 0.1 M TBAP/ACN solution. The scan rate dependent plot **Fig. 3.06b** vividly demonstrated that with increasing scan rate, peak current was increasing. A linear plot was obtained upon plotting cathodic or anodic peak current vs scan rate (inset of **Fig. 3.06b**, absolute value of linear correlation coefficient in each plot was ~0.993:0.003) and it suggested the reversible nature of the redox process occurring in the chains of those polymers without any diffusion limits **[38].**

Band gap calculation

Table 3.1. Estimation of HOMO and LUMO levels and band gap

Compounds	UV-vis wavelength (nm)		Oxidation potential (v)			Band gap (DFT/ Exp) (ev)	HOMO (DFT/ Exp) (ev)	LUMO (DFT/ Exp) (ev)
	Λ_{max}	Λ_{onset}	E_{onset}	$E_{1/2ox1}$	$E_{1/2ox2}$			
TPA_2ISO	330	367	1.00	1.17	-	1.93/3.37	-5.03/ -5.56	-3.10/ -2.19
p-TPA_2ISO	362	423	0.71	1.15	-	- / 2.93	-/ -5.54	- / -2.61
TPA_4ISO	343	382	1.01	1.18	-	1.80/3.24	-4.93/ -5.57	-3.13 / -2.33
p-TPA_4ISO	369	424	0.66	1.13	-	- / 2.92	-/ -5.52	- / -2.60
TPA_6ISO	355	400	1.04	1.19	-	1.60/3.10	-4.71/ -5.58	-3.10 / -2.48
p-TPA_6ISO	370	435	0.63	1.12	-	- / 2.85	-/ -5.51	- / -2.66

UV-vis absorption maximum and onset wavelengths for the monomers and polymer films. Read from the first CV scans, in acetonitrile at a scan rate of 50 mV/s (versus Ag/AgCl). Optical band gap was calculated from absorption edge. Eg = 1240/λonset . The HOMO and LUMO energy levels were calculated from Eox values of CV diagrams and were referenced to ferrocene (4.8 ev relative to vacuum energy level, Eonset = 0.37 V, $E_{1/2Fc}$ = 0.41 V in acetonitrile. E_{HOMO} = -[(E1/2ox1 – 0.41)+4.8] (ev); E_{LUMO} = (E_{HOMO} + Band gap energy) (ev).

3.2.7. Spectroelectrochemistry of Polymer Films

Spectroelectrochemistry studies with the help of integrated system of UV with CV system, were performed to understand the change of electronic structure as well as optical behavior of the electro generated polymeric film on ITO surface during electrochemical oxidation process with varying voltage using three electrode configuration in 0.1M TBAP/ACN electrolytic solution. As long as, no voltage was applied, single peak was appeared at 360, 359 and 376 nm **(Fig. 3.07)** for **p-TPA$_2$ISO**, **p- TPA$_4$ISO** and **p-TPA$_6$ISO**, respectively and those were the π-π* transition peak of the TPA unit present in the respective polymer backbone. Once, the voltage was gradually increased, intensity of that absorption band of polymer is gradually decreased. At 1.0 V, a new peak appeared at 489, 491 and 493 nm for **p-TPA$_2$ISO**, **p-TPA$_4$ISO** and **p-TPA$_6$ISO** respectively, signature of TBP radical cation. The colour of the polymer film was concurrently changed to brown for all the cases.

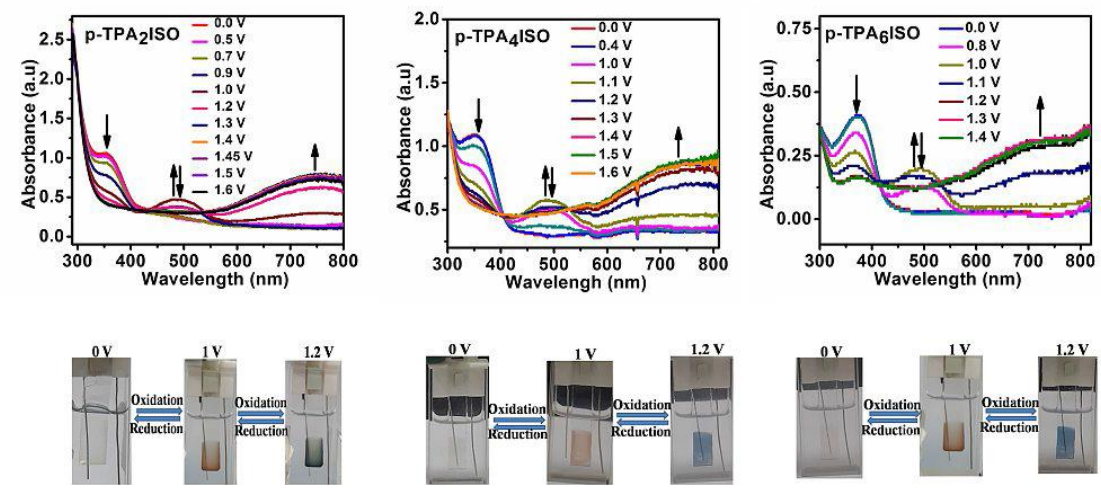

Fig. 3.07. Top panel: Change of absorption of the polymer films of **p-TPA$_2$ISO**, **p- TPA$_4$ISO** and **p-TPA$_6$ISO** on ITO-coated glass in 0.1 M TBAP/ACN solution. Bottom panel: change of colour of the same polymer film under applying potentials (0 V, 1 V and 1.2 V).

Further, the potential was enhanced to 1.2 V, the absorption intensities around 489, 491, 493 nm gradually diminished with the appearance of a new broad band at 737, 745 and

740 nm with the extended tail in the NIR region, indicating the formation of the TPB dication with the colour change brown to deep blue **[39].** On increasing potential more, no extra peak was observed. Color changes of the polymer films were reversible in nature upon oxidation and reduction and it was clearly perceived by naked eye. No special protection due to oxygen or humidity was required.

3.2.8. Electrochromic Switching of the Polymer Film

Electro-chromic switching studies were performed to determine the response time (coloration and bleaching time) by double step chronoampherometry method with the combination of UV-Vis technique and the change of transmittance at a particular wavelength with time using voltage ramping between 0 to 1.2 V for a pulse time 15 s in 0.1M TBAP/ACN solution. The coloration transmittance (the turn on state) obtained for **p-TPA$_2$ISO**, **p-TPA$_4$ISO**, **p-TPA$_6$ISO** were 19, 7.2 and 15% and the bleaching transmittance (the turn off state) were 70.4, 77 and 99.5% **(Fig. 3.08a)** respectively for the first potential switching step. In addition, the calculated optical contrasts were 51.4, 69.8 and 84.5% respectively for the three polymers, revealing that upon increasing TPA in polymer, optical contrast was enhanced to ~85%. Such a high value of optical contrast was scarcely seen for organic electrochromic material. Estimated times required for 95% full transmittance change for **p TPA$_2$ISO**, **p-TPA$_4$ISO**, **p-TPA$_6$ISO** were 1.28, 0.9 and 1.96 s for coloration step and 0.73, 0.57 and 0.51 s for bleaching step **(Fig. 3.08b).** Such a small time for coloration/bleaching was significantly excellent for organic materials. Coloration efficiency (η) was a useful parameter for determining the quality of an electrochromic material. The determination of the coloration efficiency was calculated according to the following Equation **[1, 2, 40, 41],**

$$\eta = \frac{\Delta OD}{Q_d} = \log \frac{T_b}{T_c} \Big/ Q_d$$

Where, ΔOD was the change of optical absorbance and Q_d (mC/cm^2) was the injected/ejected charge during the redox process which was calculated from chrono-amperometric plot. T_b and T_c were the percentage (%) of transmittance of the bleaching state and coloration state. Generally, the electrochromic material with high optical change and low value of ejected charge was expected for high coloration efficiency. Calculated coloration efficiency for all the three polymers were 203, 397 and 410 cm^2/C respectively at the wave length ~370 nm and all data were summarized in **Table 3.2.**

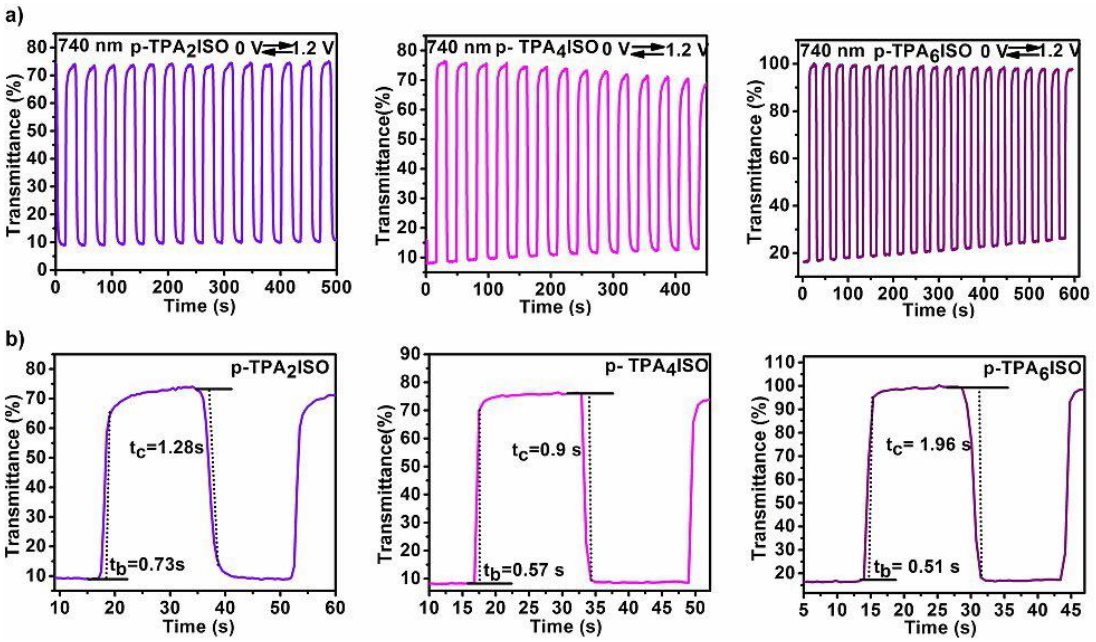

Fig. 3.08. a) Transmittance change during switching process of the polymers **p-TPA$_2$ISO**, **p-TPA$_4$ISO**, **p-TPA$_6$ISO** in switching time 15 s in 0.1 M TBAP/ CAN using ITO-coated glass as working electrode, Pt wire as counter electrode Ag/AgCl as reference electrode at 740 nm wavelength from 0 V to 1.2 V and b) represented their corresponding t_c, t_b values.

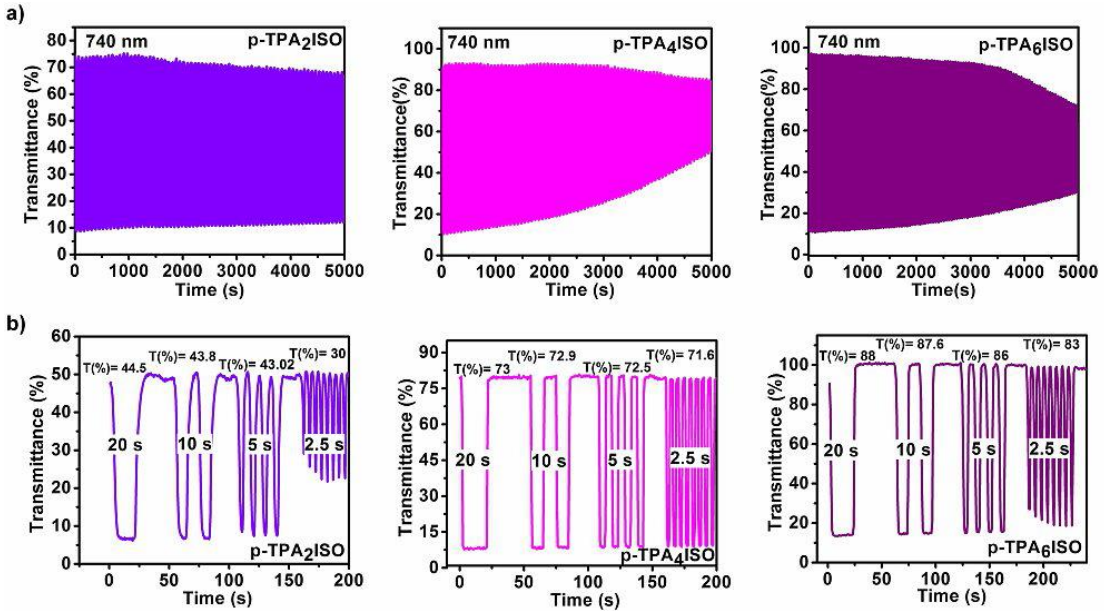

Fig. 3.09. a) Cyclic stability performance of the polymers **p-TPA$_2$ISO**, **p-TPA$_4$ISO**, **p-TPA$_6$ISO** in 0.1 M TBAP/ACN using ITO-coated glass as WE, Pt wire as CE, Ag wire as pseudo-RE at 740 nm wavelength from 0 V to 1.2 V. b) Transmittance change by varying switching time of the polymers **p-TPA$_2$ISO**, **p-TPA$_4$ISO**, **p-TPA$_6$ISO** in switching time in 0.1 M TBAP/ ACN using ITO-coated glass as WE, Pt wire as CE, Ag/AgCl as RE at 740 nm wavelength from 0 V to 1.2 V.

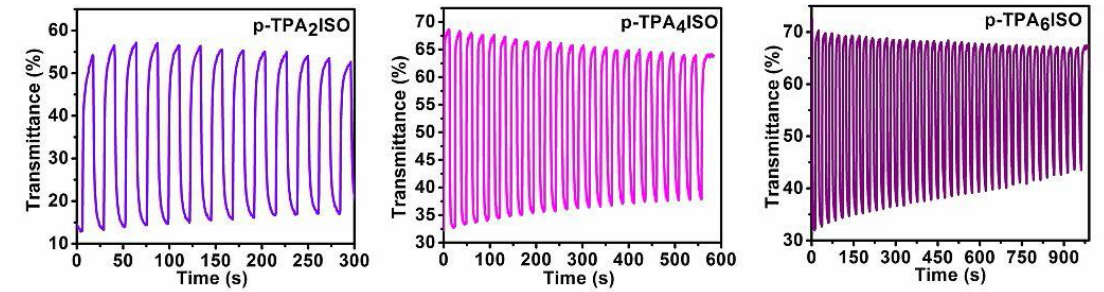

Fig. 3.10. Transmittance change during switching process of the solid state device obtained from **p-TPA$_2$ISO**, **p-TPA$_4$ISO**, **p-TPA$_6$ISO** in switching time 15 s at 740 nm wave length from 0 V to 2.5 V.

With increasing the number of TPA units in the polymer matrix, the value of coloration efficiency was increased and the highest value (410 cm^2/C) was observed for **p-TPA$_6$ISO**. Less than one second time required for bleaching/coloration process and the substantial value of coloration efficiency was extremely rare for the small organic based electrochromic derivatives **[35, 42]**. The cyclic stability of the electrochromic material was measured by potential step chronoampherometry with absorption studies. It was operated between 0 to 1.2 V at 740 nm for ~5000 s (or 500

cycles). It was observed that the activities loss were 10% after 3000s for **p-TPA$_2$ISO**, 3300s for **p-TPA$_4$ISO** and 3600s for **p-TPA$_6$ISO** respectively **(Fig.3.09a).** The switching potential between 0 and 1.2 V i.e. between neutral and fully oxidized state of the polymer films of **p-TPA$_2$ISO**, **p-TPA$_4$ISO**, **p-TPA$_6$ISO** were alternated by varying switching interval and monitoring the change of the transmittance. With decreasing the pulse width (20, 10, 5 and 2.5 s) the value of Δ%T was decreased as shown in **Fig.3.09b.** Whereas, values of Δ%T were more or less fixed for **p-TPA$_4$ISO**, **p-TPA$_6$ISO** films, though, it was tested for ~200 s.

Table 3.2. Electrochromic parameters of the polymers **p-TPA$_2$ISO**, **p-TPA$_4$ISO**, **p-TPA$_6$ISO**

Polymers	**Λ[a] max(nm)**	**ΔT%**	**Response Time[b]**		**ΔOD[c]**	**Q $_d$[d](mCcm^{-2})**	**CE[e] (cm^2/C)**
			t_c (s)	**t_b(s)**			
p-TPA$_2$ISO	362	51.4	1.28	0.73	0.57	2.8	203
p-TPA$_4$ISO	369	69.8	0.9	0.57	1.03	2.6	397
p- TPA$_6$ISO	370	84.5	1.96	0.51	0.82	2.0	**410**

[a] Wavelength of absorption maximum. [b] Time for 95 % of the full-transmittance change. [c] Optical density change (ΔOD) = Log [T $_{bleached}$ / T $_{colored}$], where T$_{colored}$ and T $_{bleached}$ were the maximum transmittance in the oxidized and neutral states respectively. [d] Q$_d$ was the ejected charge obtained from chronoampherometry measurement. [e] Coloration efficiency (CE) = ΔOD/Qd.

3.2.9. Solid State Device

To demonstrate the electrochromic phenomenon, a solid-state device was prepared utilizing the conducting gel electrolyte made of PMMA and $LiClO_4$ as plasticized with propylene carbonate. Firstly, the polymer was electrodeposited on ITO coated glass and dried properly. Gel electrolyte was spread on it and was cured. Two coated sides of ITO glass were sandwiched to make the device that was sealed by epoxy resin **[43, 44].** Upon the applying the potential, the devices exhibited brown color at the semi oxidized state and deep blue color at the fully oxidized state and the entire process was occurring reversibly **(Fig.3.11)** for several times. Upon increasing voltage from 0 to 1.5 V, the color changed from colorless to brown for **TPA** moieties, further increase of voltage to 2.5 V, color changed from brown to dark blue. Again, when the potential was subsequently set back at 0 V, the polymer film reverted to its initial color.

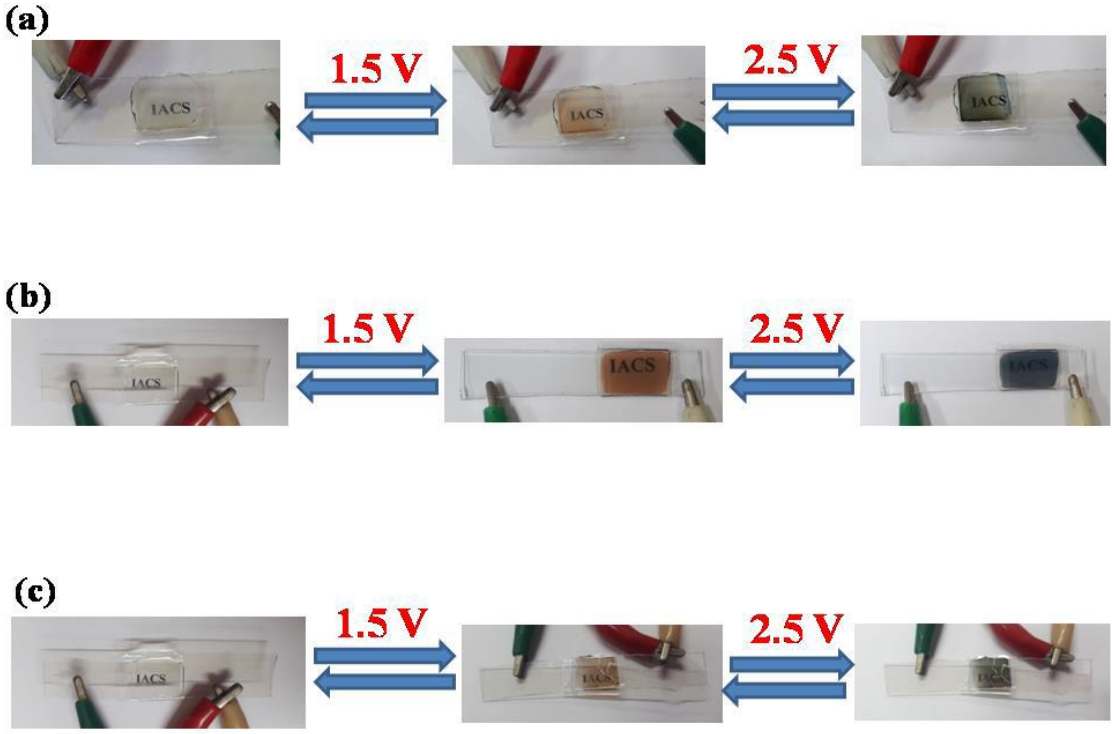

Fig. 3.11. Electrochromism of solid-state electrochromic device of (a) **p-TPA$_2$ISO**, (b) **p- TPA$_4$ISO**, (c) **p-TPA$_6$ISO**.

In the case of reverse potential, change of initial color was relatively faster than the oxidized color. Reversible color changes were perceived by naked eye for several times. Further, Cyclic stability studies of the devices were carried out at 740 nm from 0 to 2.5 V **(Fig. 3.10).** Stability studies were performed up to 300s for **TPA_2ISO**, 600s for **TPA_4ISO** and 980s for **TPA_6ISO**. In case of solid-state device, the relatively higher potential was required to drive electrochromism process, it was possibly owing to the lower ionic mobility of electrolyte in the semi-solid phase (gel phase). From the above results, it was overwhelmingly realized the potential utilization of all three polymers for the making electrochromic devices and optical display.

3.3. Conclusions

Three donor-acceptor-donor type monomers (**TPA_2ISO**, **TPA_4ISO**, **TPA_6ISO**) containing isonaphthalene diimide as acceptor core and electro-polymerizable triphenyl amine as the donor moiety were designed and successfully synthesized via imidization of isonaphthalene anhydride with corresponding triphenylamine derivatives to check the influence of multiple TPA units on the electrochromic behaviours. Energy optimized structure borne out by DFT calculation indicated that electron density of HOMO was centralized on the triphenyl amine unit only. Polymer films from three monomers were electrodeposited on ITO/glass electrodes and were characterized by CV studies. Three polymers revealed multi electrochromic properties in a reversible manner with the colour change from colourless to brown to blue at low working potential. The spectroelectrochemistry studies of the polymer films obtained from **p- TPA_2ISO**, **p-TPA_4ISO**, **p-TPA_6ISO** on ITO surface suggested the high optical contrast (51.4, 69.8 and 84.5% respectively) of the three polymers with the very fast bleaching (less than 1 s) and coloration time with relatively higher value of coloration efficiencies (~410 cm^2/C) that were tuned by inserting number of TPA unit in the monomer. The electro switching stability was performed and activity loss was only 10% after 3000 s. To demonstrate the potential of organic materials, a solid-state device was fabricated and it showed electrochromism in a very nice way without taking any precaution from air or moisture.

3.4 Experimental Section

3.4.1. Materials and instrumentations

Diphenylamine, triphenylamine (TPA), $Pd(PPh_3)_4$, bis (pinacolato) diboron, $Pd(dppf)Cl_2$, CuCN, calcium hydride, tetra-butyl ammonium perchlorate (Bu_4NClO_4, TBAP), lithium perchlorate ($LiClO_4$), polymethylmethacrylate (PMMA), silver chloride (AgCl) were purchased from Sigma Aldrich and used as received. 4-fluoro nitrobenzene, benzophenone, sodium hydride (NaH), sodium borohydride ($NaBH_4$), potassium acetate (KOAc), sodium carbonate (Na_2CO_3), potassium dichromate ($K_2Cr_2O_7$), sodium hydroxide (NaOH) were purchased from Merck chemicals. 2,6 dimethyl naphthalene was purchased from TCI Chemicals (India) Pvt. Ltd. N-bromo succinimide was purchased from Avra chemical which was used by recrystallization. The solvents like acetonitrile (ACN), dichloromethane (DCM), methanol (MeOH), dimethyl acetamide (DMAc), tetra-hydro furan (THF), dioxane, dimethyl formamide (DMF) and analytical grade reagents were used without further purification. DMF, acetonitrile, DCM and dioxane were dried by using calcium hydride and dry THF was obtained from the refluxing with sodium and benzophenone. The ^{1}H- and ^{13}C-NMR spectra were recorded on a Bruker 500 or 400 MHz spectrometer using chloroform- d ($CDCl_3$), dimethyl sulphoxide-d (DMSO-d_6) as solvent and tetramethylsilane (TMS) as an internal standard. MALDI-TOF (matrix assisted laser desorption ionization time-of-flight) mass spectrometry was carried out with Bruker Daltonics ultra-flextreme. Fourier transformed infrared (FT-IR) spectra were measured on a Horiba FT- 720 FT-IR spectrometer with KBr pellets. The UV-visible absorption spectrum was recorded on an Ocean Optics DH-mini UV-VIS-NIR light source and Ocean Optics flame Miniature Spectrometer. The electrochemical measurements were performed by using a CHI 6087E electrochemical workstation in a conventional three electrode cell containing 0.1M $LiClO_4$/ACN or DCM solution as the supporting electrolyte. Indium tin oxide (ITO) coated glass (MTI corporation Ltd., Rs,15 Ω–1) was used as working electrode, cleaned by double distilled water, ethanol and acetone successively with sonication. In general, electrochemical polymerization of the monomers was performed with the use of a three-electrode cell ITO coated glass slides as working electrode and Ag/AgCl, as reference electrode, Pt wire as counter

electrode using 1 mM monomer solution in 0.1M electrolytic solution of TBAP in distilled DCM via repetitive cycling with the potential barrier from 0 to 1.5 V at a scan rate 50 mVs^{-1} at room temperature. Ferrocene was used as an external reference for calibration (+0.44 V vs Ag/AgCl). The solid state device was prepared utilizing a transparent and conducting gel electrolyte having PMMA and $LiClO_4$ as plasticized with propylene carbonate. Firstly, the polymer was electrodeposited on ITO coated glass, rinsed with DCM and acetone to remove the monomers and oligomers and then dried properly. The gel electrolyte was spread on the polymer coated ITO surface and was kept on normal air for 30 minutes and after that it was kept on oven for 1 hour at 60°C. The conducting side of another ITO glass was sandwiched over it. Finally, the device was sealed by an epoxy resin.

3.4.2. Synthesis:

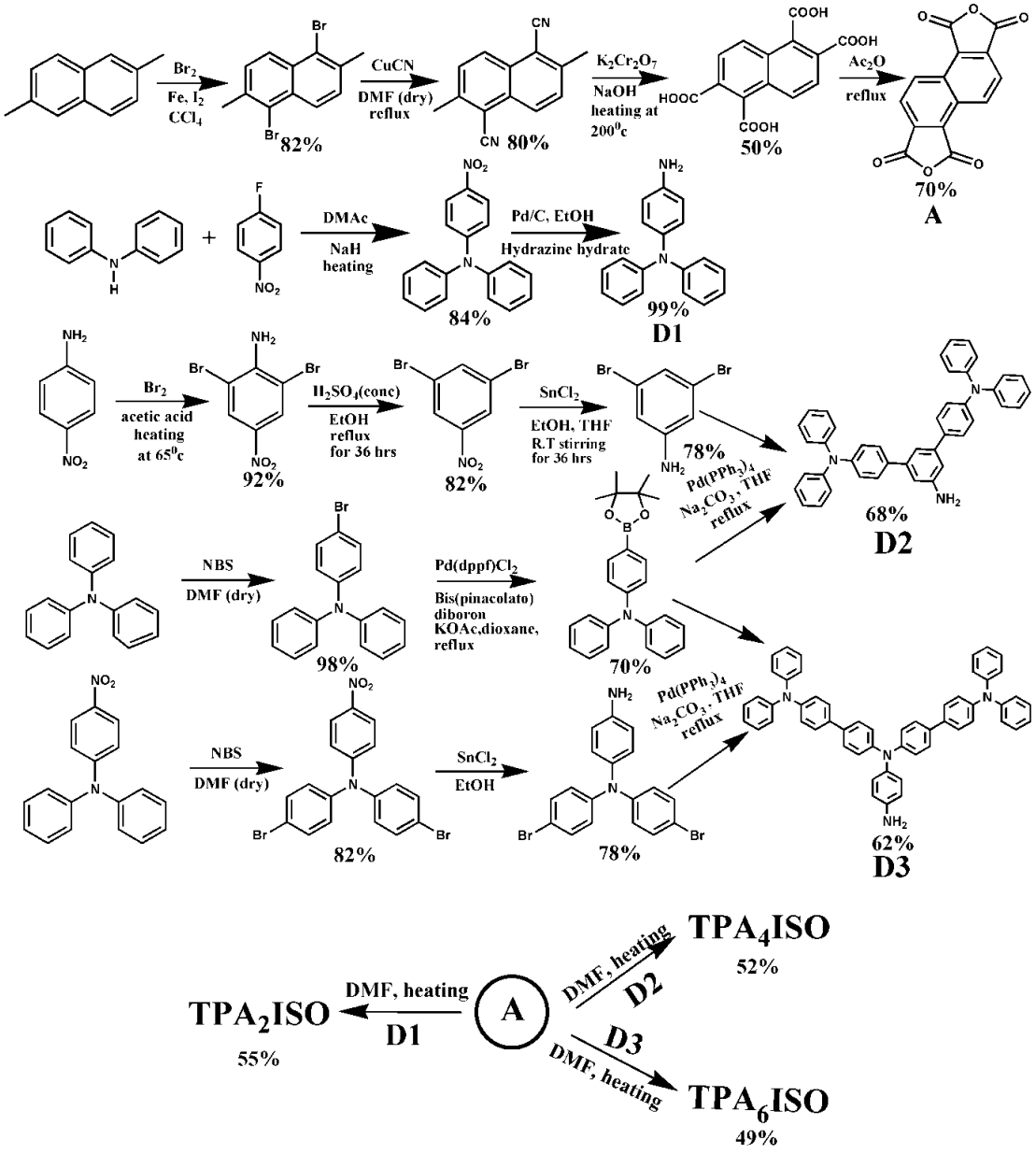

Fig. 3.12. Synthesis of **TPA$_2$ISO**, **TPA$_4$ISO**, **TPA$_6$ISO**.

Synthesis of 1, 5 dibromo 2, 6 dimethyl naphthalene : To a cold solution (-10^0C) of 2, 6 dimethyl naphthalene (730 mg, 4.67 mmol) in carbon tetrachloride (12 ml) catalytic amount iron powder (13 g, 0.23 mmol) and iodine (30 mg, 0.23 mmol) was added. Bromine solution (0.46 ml, 9.34 mmol) in carbon tetrachloride (8.4 ml) was added in a drop wise manner. After adding, the solution was allowed to stir at room temperature and stirred for 6 hrs. Aqueous solution of sodium hydrogen carbonate solution was added to the reaction mixture and extracted with $CHCl_3$, dried and concentrated the crude product. The pure product was obtained by recrystalized the crude product in chloroform with 82% yield (1.20 g).

^{1}H NMR: (400 MHz, $CDCl_3$, TMS) δ (ppm): 8.20 (2H, d), 7.427 (2H, d), 2.622 (6H, s),

^{13}C NMR: (100 MHz, $CDCl_3$, TMS) δ (ppm): 136.07, 132.14, 129.96, 126.53, 124.11.

Synthesis of 2,6-dimethylnapthalene-1,5-dicarbonitrile : To the solution of 1,5 dibromo-2,6- dimethylnaphthalene (560 mg, 1.78 mmol) in dry DMF (4 ml) copper cyanide (0.36 g, 4.10 mmol) was added. The solution was allowed to elevate to 160^0 C and stirred for 18 hrs. After cooled to room temperature, the solution was poured into water. Filtered the turbid, washed the filter cake with aq. ammonia (15 wt %) solution. The pure 1, 5-Dicyano-2, 6-dimethylnaphthalene was obtained after purifying the filter cake by column chromatography on silica gel with the yield of 80% (294 mg).

^{1}H NMR: (400 MHz, $CDCl_3$, TMS) δ (ppm): 8.322 (2H, d), 7.60 (2H, d), 2.80 (6H, s),

^{13}C NMR: (100 MHz, $CDCl_3$, TMS) δ (ppm): 143.87, 130.99, 130.49, 129.45, 116.38, 110.33.

Synthesis of 1,2,5,6-naphthalenetetracarboxylic acid : To a 20 ml Teflon liner autoclave 1,5- Dicyano-2,6-dimethylnaphthalene (330 mg, 1.60 mmol), potassium dichromate (1.88 g, 6.40 mmol), sodium hydroxide (121.44 mg, 3.17 mmol) and 6.3

ml water was taken. The mixture was stirred for 30 min at room temperature and was sealed in the stainless steel autoclave. Then it was elevated to 200^0C for 10 h. After cooled to room temperature, the mixture was filtered and the basic filtrate was washed with ether (4 ml). At last, the crude 1,2,5,6-naphthalenetetracarboxylic acid was obtained by reprecipitating the water layer with concentrated hydrochloric acid. The light yellow solid was collected by filtration with a yield of 50% (243 mg). The product was applied to the next reaction without further purification.

Synthesis of 1,2,5,6-naphthalenetetracarboxylic dianhydride (A) : The solution of 1,2,5,6- naphthalenetetracarboxylic acid (150 mg, 0.5 mmol) in acetic anhydride (15 ml) was refluxing for 4 hrs. After cooling the mixture at room temperature, the product was collected by filtration and the filter cake was washed with methanol several times. The light yellow solid was obtained after dried in vacuum oven with a yield of 70% (94 mg) and it was applied for the next reaction without further purification.

Mass (MALDI-TOF): m/z calculated 268.18, found 268.75.

Synthesis of 4- bromo N,N diphenyl aniline : Triphenylamine (3 g, 12 mmol) was dissolved in 30 ml distilled DMF, kept in low temperature bath at 0^0 C. 4 ml DMF solution of recrystallized NBS (2.13 g, 12 mmol) was added slowly to it. The reaction mixture was stirred at room temperature for 6 hrs. Distilled water was added to it in ice cold condition, a white ppt was obtained which was filtered, dried on oven, recrystallized in pet ether. A white shiny crystal was obtained with 98 % yield (3.81 g).

^{1}H NMR: (400 MHz, $CDCl_3$, TMS) δ (ppm): 7.35 (2H, d), 7.28 (4H, m), 7.08 (6H, m), 6.97 (2H, d),

^{13}C NMR: (100 MHz, $CDCl_3$, TMS) δ (ppm): 147.55, 147.20, 132.29, 129.51, 125.27, 124.57, 123.38, 114.92.

Synthesis of TPA - Borolane: In a two neck round bottomed flask, 4-bromo N,N diphenyl aniline (636 mg, 1.95 mmol), Bis (pinacolato) diboron (597 mg, 2.35 mmol),

$Pd(dppf)Cl_2$ (78.54 mg, 0.09 mmol), KOAc (1.15 g, 11.74 mmol) was taken and inerted properly in N_2 atm. 8 ml dry dioxane was added to it and refluxed for 24 hrs at 110^0C. After cooling the reaction mixture at room temperature, a dilute HCl solution was added and extracted with DCM and water. The crude product was purified by column chromatography using 1:1 (pet ether:ethyl acetate) with 70 % yield (506.8 mg).

^{1}H NMR: (400 MHz, DMSO-d_6, TMS) δ (ppm): 7.551 (2H, d), 7.32 (4H, t), 7.115 (2H, t), 7.05 (4H, d), 6.89 (2H, d), 1.29 (12H, s),

^{13}C NMR: (100 MHz, DMSO-d_6, TMS) δ (ppm): 150.10, 146.60, 135.68, 129.56, 124.84, 123.76, 120.61, 83.26, 24.56.

Synthesis of 2, 6-dibromo 4 –nitrobenzenamine: To a stirring solution of p-nitroaniline (2 g, 14.48 mmol) in 18 ml of glacial acetic acid, bromine (1.48 ml, 28.96 mmol) in glacial acetic (11 ml) acid was added portion wise upto 5 hrs. A heavy precipitate was formed after one third addition of bromine within one hour and the ppt was dissolved in hot water (4 ml) and then remaining bromine was added. After 2 hrs, remaining bromine was added. Again heavy precipitate was appeared; it was redissolved in hot water and stirred it for 1 hr. After completion of the reaction, the reaction mixture was poured into the slurry of water and ice. After washing with water and air drying, the compound was recrystallized from chloroform to give a niddle shaped yellow shiny crystals with 92 % yield (3.94 g).

^{1}H NMR: (400 MHz, $CDCl_3$, TMS) δ (ppm): 8.35 (2H, S), 5.27 (2H, S),

^{13}C NMR: (100 MHz, $CDCl_3$, TMS) δ (ppm): 159.55, 142.5, 126.30, 122.81.

Mass (MALDI-TOF): m/z calculated 295.92, found 295.80.

Synthesis of 1, 3-dibromo-5-nitrobenzene: To a stirred boiling mixture of 2, 6-dibromo-4-nitroaniline (1.7 g, 5.78 mmol) absolute ethanol (19 ml) and concentrated sulphuric acid (1.95 ml), sodium nitrite (1.28 g, 18.65 mmol) was added in portions as rapidly as foaming would permit. After refluxed at 90^0C for 36 hrs, the mixture was allowed to cool, poured into ice water and the solids were collected by filtration. The residue was thoroughly washed with water and the 3, 5 dibromo nitrobenzene was separated from remaining inorganic salts by dissolving it in boiling ethanol and

filtering in hot condition. It produced yellow solid product after drying in vacuum oven. The yellow solid product was purified by column chromatography using 10:1 (hexane:chloroform) as eluent. The desired product was obtained with 82 % yield (1.33 g).

^{1}H NMR: (400 MHz, $CDCl_3$, TMS) δ (ppm): 8.326 (2H, d), 7.99 (1H, t),

^{13}C NMR: (100 MHz, $CDCl_3$, TMS) δ (ppm): 152.78, 141.4, 126.1, 125.8.

Mass (MALDI-TOF): m/z calculated 280.9, found 281.

Synthesis of 3, 5-dibromoaniline : To a solution of 3, 5 dibromonitrobenzene (1.15 g, 4.09 mmol) in ethanol (10 ml) and THF (10 ml) stirred under air tin chloride dehydrate (4.57 g, 20.27 mmol) was added slowly in portion wise. The mixture was allowed to stir at room temperature for 20 hrs. The solvent was then evaporated in vacuum and an aq. NaOH solution was added to neutralize it. After stirring the mixture, it was extracted with diethyl ether. The combined organic phase was dried over sodium sulphate, filtered and dried. The product was purified by column chromatography in 5:2 (pet ether:DCM) with 78 % yield (800 mg).

^{1}H NMR: (400 MHz, $CDCl_3$, TMS) δ (ppm): 7.01 (1H, t), 6.74 (2H, d), 3.77 (2H, br),

^{13}C NMR: (100 MHz, $CDCl_3$, TMS) δ (ppm): 148.73, 123.44, 123.70, 116.66.

Mass (MALDI-TOF): m/z calculated 250.92, found 250.77.

Synthesis of N-(4-nitrophenyl)-n-phenylbenzenamine : In nitrogen atm., diphenyl amine (5.07 g, 30 mmol) was dissolved in 30 ml DMAc , to it NaH (1.12 g, 46.8 mmol) was added, stirred the solution at room temperature for 30 mins and then placed it at low temperature bath. 4-fluoro nitrobenzene (5.07 g, 36 mmol) in 30 ml DMAc was added dropwise to that mixture. It was then refluxed for overnight at 100^0 C. After cooling the reaction at room temperature, it was poured into ice cold HCl solution. The crude product was collected by filtration. It was purified by column chromatography using 6:4 (pet ether : chloroform) giving orange crystalline product with 84% yield (7.31 g).

^{1}H NMR: (400 MHz, DMSO-d6, TMS) δ (ppm): 8.07 (2H, d), 7.45 (t, ArH, 4H), 7.30-7.25 (m, ArH, 6H), 6.80 (d, ArH, 2H),

^{13}C NMR: (100 MHz, DMSO-d6, TMS) δ (ppm): 154.33, 146.20, 140.10, 130.66, 128.60, 126.30, 124.41, 118.56.

Synthesis of 4-bromo-N-(4-bromophenyl)-N-(4-nitrophenyl)benzenamine : N-(4-nitrophenyl)-n-phenyl benzenamine (3.5 g, 12.05 mmol) was dissolved in distilled DMF (30 ml) and kept it on low temperature bath. Recrystallized NBS (4.72 g, 26.53 mmol) was dissolved in DMF (22 ml). It was added drop wise to the reaction mixture. After complete addition of NBS the reaction mixture was stirred at room temperature for 48 hrs. The crude product was purified by column chromatography using Chloroform as eluent. The product was recrystallized in chloroform giving orange shinny crystal with 82 % yield (4.42 g).

^{1}H NMR: (400 MHz, $CDCl_3$, TMS) δ (ppm): 8.31 (d, 6H), 7.16 (d, 6H),

^{13}C NMR: (100 MHz, $CDCl_3$, TMS) δ (ppm): 152.69, 144.69, 141.34, 133.22, 127.74, 125.78, 119.37, 117.88.

Synthesis of N,N-(bis(4-bromophenyl) benzene-1,4-diamine : 4-bromo-N-(4-bromophenyl)-N-(4- nitrophenyl) benzenamine (2.54 g, 5.64 mmol) was dissolved in 86 ml of absolute EtOH, $SnCl_2$ (11 g, 33.85 mmol) was added to it. The reaction mixture was refluxed at 80^0C for 24 hrs. After completion of the reaction, it was filtered, washed with water, dried on vacuum oven, purified by column chromatography using 1:1 (pet ether : DCM) as eluent with 78 % yield (1.83 g).

^{1}H NMR: (400 MHz, $CDCl_3$, TMS) δ (ppm): 7.24 (4H, d), 6.88 (4H, d), 6.61 (4H, d),

^{13}C NMR: (100 MHz, $CDCl_3$, TMS) δ (ppm): 146.93, 143.84, 137.34, 132.06, 127.91, 126.58, 123.9, 120.88, 116.33, 114.21, 112.78.

Mass (MALDI-TOF): m/z calculated 418.59, found 418.62.

Synthesis of D1: To a 200 ml absolute ethanol solution of N-(4-nitrophenyl)-n phenyl benzenamine (2.16 g, 7.34 mmol), hydrazine hydrate (15.12 ml) was added. The reaction mixture was kept on an ice bath. 10% Pd/C (86.4 mg) catalyst was added to it slowly. It was refluxed for overnight at 100^0 C. The reaction mixture was filtered over

the celite powder bed to absorb Pd/C. After cooling the filtrate, distilled water was added to it. Upon keeping it for several hours, a yellow precipitate that was appeared was filtered, washed and dried in vacuum oven (1.9 g, 99% yield). The product was used for next step without further purification.

^{1}H NMR: (400 MHz, $CDCl_3$, TMS) δ (ppm): 7.24 (4H, d), 6.89 (8H, t), 6.61 (2H, t), 5.264 -NH, s);

^{13}C NMR: (100 MHz, CDCl3, TMS) δ (ppm): 146.93, 143.84, 137.34, 132.06, 127.91, 123.90, 120.88, 119.02, 116.10, 114.21, 112.78;

Mass (MALDI-TOF): m/z calculated 260.33, found 260.65.

Synthesis of D2: TPA-borolane (800 mg, 2.16 mmol), 3,5 dibromo aniline (208 mg, 0.83 mmol), $Pd(PPh_3)_4$ (144 mg, 0.10 mmol) was inerted properly with nitrogen gas for 30 minutes. Dry THF (20 ml) was added to it in stirring condition. Aqueous solution of K_2CO_3 (830 mg in 3 ml water) was dropwise added to the reaction mixture. It was refluxed for 48 hrs at 95°C. After the reaction completion, it was extracted with DCM and water. The product was purified by column chromatography using pet-ether: $CHCl_3$ (1:1) with 68% yield (326 mg).

^{1}H NMR: (400 MHz, DMSO-d6, TMS) δ (ppm): 7.52 (4H, d), 7.31 (8H, d), 7.04 (16 H, m), 6.77 (2H, s), 5.58 (NH, s), 5.30 (1H, s);

^{13}C NMR: (100 MHz, DMSO-d6, TMS) δ (ppm): 147.07, 140.83, 135.14, 129.46, 127.47, 123.40, 121.80, 110.65, 122.99;

Mass (MALDI-TOF): m/z calculated 579.73, found 579.48.

Synthesis of D3: TPA-borolane (582 mg, 1.567 mmol), N,N (bis(4- bromophenyl) benzene-1,4-diamine (252 mg, 0.60 mmol), $Pd(PPh_3)_4$ (105 mg, 0.1 mmol) was inerted properly with nitrogen gas for 30 minutes. Dry THF (15 ml) was added to it in stirring condition. Aqueous solution of K_2CO_3 (600 mg in 2 ml water) was added dropwise to the reaction mixture. It was refluxed for 48 hrs at 95°C. After the reaction completion, it was extracted with DCM and water. The product was purified by column chromatography using pet-ether: $CHCl_3$ (1:1) with 62% yield (279 mg).

^{1}H NMR: (400 MHz, DMSOd6, TMS) δ (ppm): 7.337 (16H, m), 7.07 (20H, m), 6.62 (4H, d), 5.160 (NH, s);
^{13}C NMR: (100 MHz, DMSO-d6, TMS) δ (ppm) 147.60, 136.26, 134.58, 132.85, 130.02, 129.79, 128.70, 127.38, 125.42, 124.39, 123.52, 122.17, 115.57;
Mass (MALDI-TOF): m/z calculated 746.94, found 746.33.

Synthesis of TPA$_2$ISO: In a 50 ml round bottom flask, **D1** (80 mg, 0.28 mmol) and 1,2,5,6-naphthalenetetracarboxylic dianhydride (30 mg, 0.11 mmol) were taken and inerted properly with nitrogen gas, dry DMF (2 ml) was added to it, heated for 24 hrs at 140 °C. After cooling the reaction mixture, MeOH was added to it, a yellow colored precipitate that was appeared at the bottom, was filtered and dried on oven. The precipitate was purified by column chromatography using mixture of pet-ether: DCM (1:1) with 55% yield (46 mg).
^{1}H NMR: (400 MHz, $CDCl_3$, TMS) δ (ppm): 9.49 (2H, d), 8.24 (2H, d), 7.31 (12 H, m), 7.19 (12 H, m), 7.08 (4H, m);
^{13}C NMR: (100 MHz, $CDCl_3$, TMS) δ (ppm): 147.49, 132.64, 129.60, 127.48, 125.20, 123.74, 123.09, 122.43;
Mass (MALDI-TOF): m/z calculated 753.20, found 753.33.

Synthesis of TPA$_4$ISO: In a 50 ml round bottom flask, **D2** (81.16 mg, 0.14 mmol), 1,2,5,6-naphthalenetetracarboxylic dianhydride (15 mg, 0.06 mmol) was taken and inerted properly with nitrogen, dry DMF (1.2 ml) was added to it, heated for 24 hrs at 140^0C. After cooling the reaction mixture, MeOH was added to it, a brown colored precipitate was appeared and it was filtered and dried in air and vacuum oven. The precipitate was purified by column chromatography using the mixture of pet-ether: ethylacetate (2:1) with 52% yield (41 mg).
^{1}H NMR: (400 MHz, $CDCl_3$, TMS) δ (ppm): 9.55 (2H, d), 8.26 (2H, d), 7.82 (2H, s), 7.62 (4H, s), 7.54 (8H, d), 7.30 (8H, m), 7.15 (24H, m), 7.04 (16 H, m);
Mass (MALDI-TOF): m/z calculated 1391.61, found 1391.05.

Synthesis of TPA$_6$ISO: In a 50 ml round bottom flask, **D3** (76.5 mg, 0.102 mmol), 1,2,5,6-naphthalenetetracarboxylic dianhydride (11 mg, 0.041 mmol) was taken and

inerted properly with nitrogen, dry DMF (1.2 ml) was added to it, heated for 24 hrs at 140°C. After cooling the reaction mixture, MeOH was added to it, a brown coloured precipitate that was appeared at the bottom of the flask, was filtered and dried in air and vacuum oven for the overnight. The precipitate was purified by column chromatography by $CHCl_3$ with 49% yield (35 mg).

^{1}H NMR: (400 MHz, $CDCl_3$, TMS) δ (ppm): 9.51 (2H, d), 8.27 (2H, d), 7.55 (24H, m), 7.49 (4H, s), 7.37 (24H, d), 7.30 (8H, m), 7.15 (20 H, m);

^{13}C NMR: (100 MHz, $CDCl_3$, TMS) δ (ppm): 168.18, 167.31, 147.12, 146.20, 136.01, 134.67, 132.64, 131.35, 129.34, 127.72, 127.42, 125.24, 125.54, 124.41, 124.33, 124.09, 123.09;

MS (MALDI-TOF): m/z calculated 1726.04, found 1726.06.

Mass data of 1,2,5,6-Naphthalenetetracarboxylic Dianhydride:

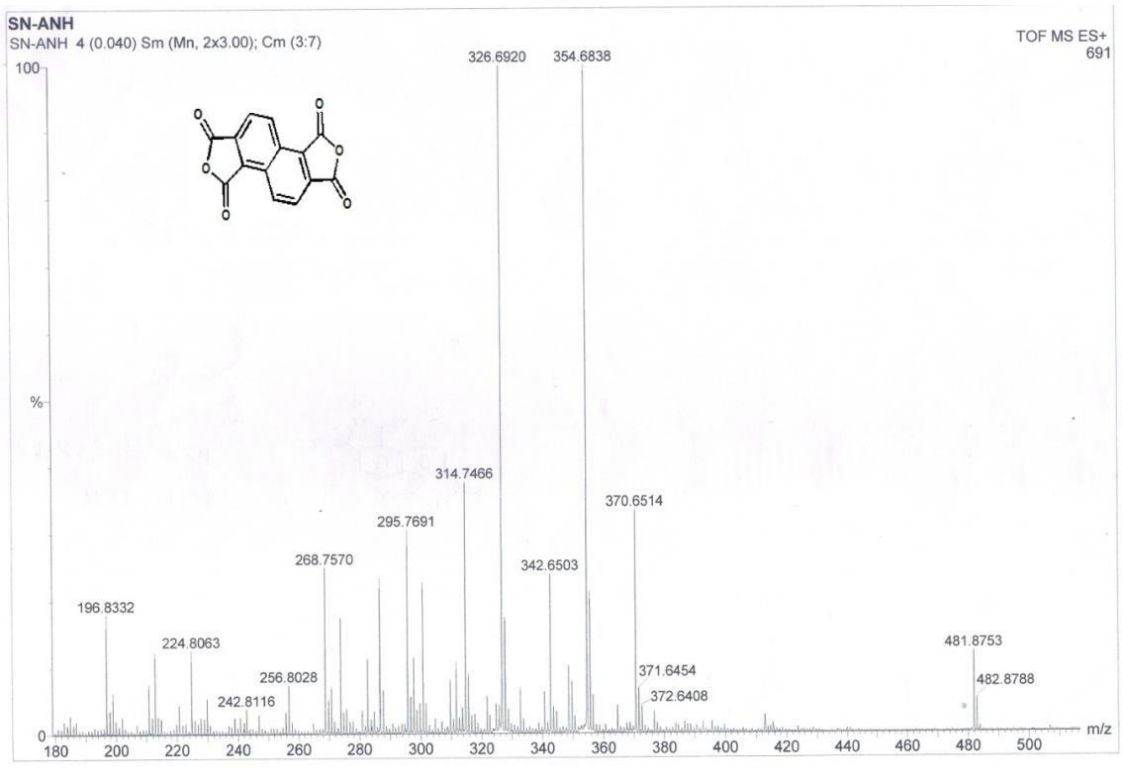

Fig. 3.13. HRMS mass spectra of 1,2,5,6-naphthalenetetracarboxylic dianhydride.

NMR and Mass data of TPA-borolane:

a)

b)

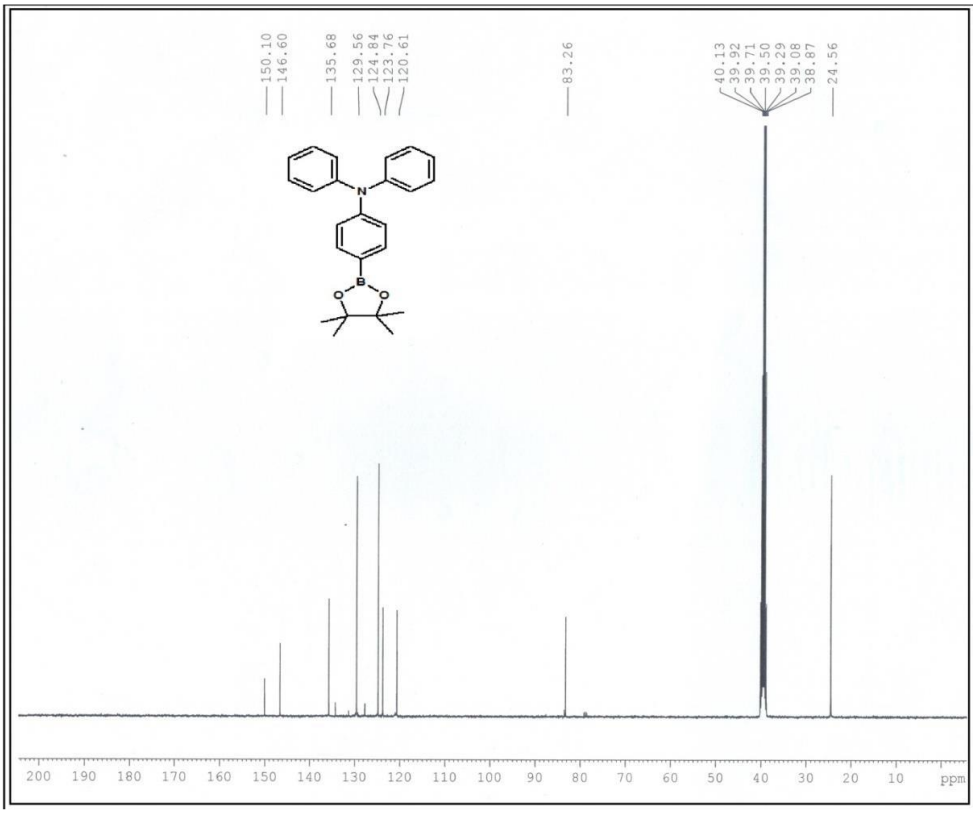

Fig. 3.14. a) **^{1}H NMR**, b) **^{13}C NMR** spectra of **TPA – Borolane** in DMSO-d6**.**

NMR and Mass data of D1

a)

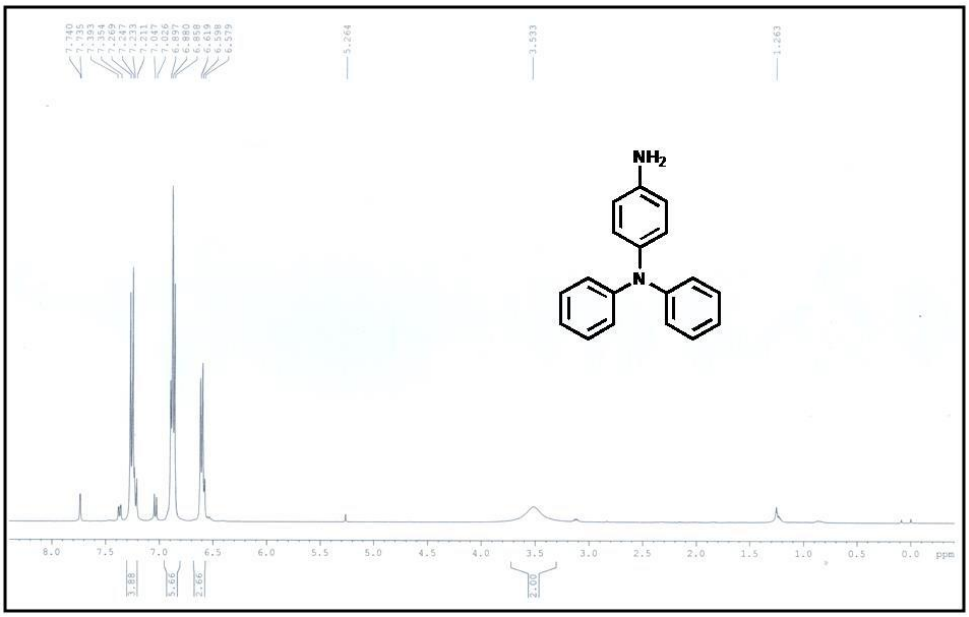

b)

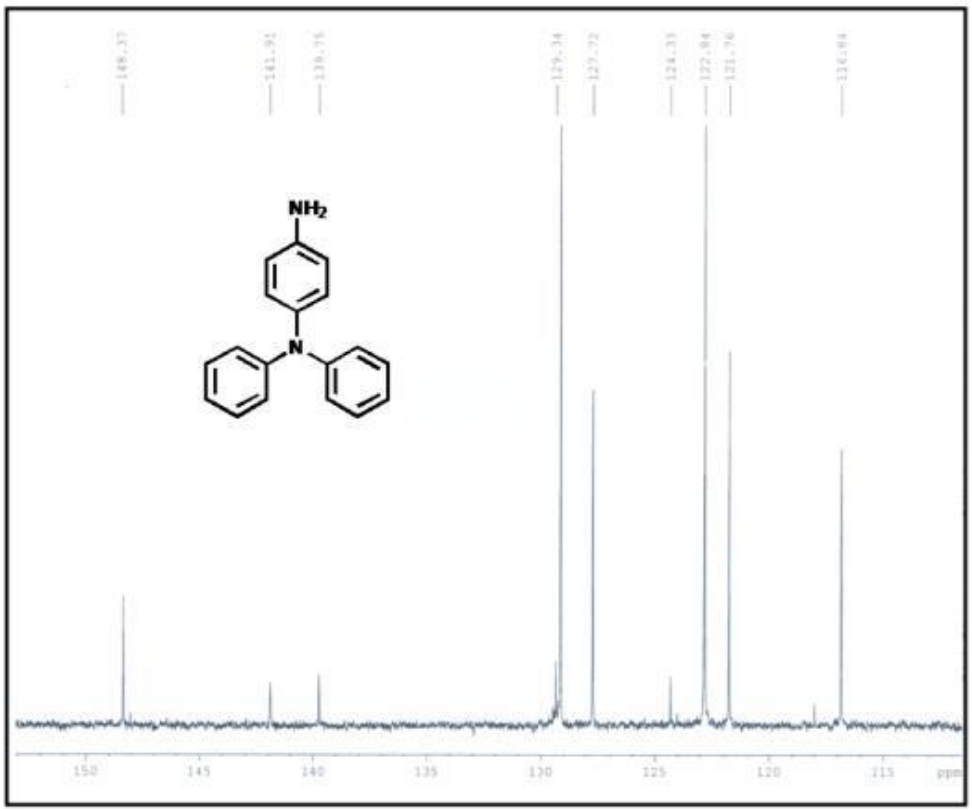

c)

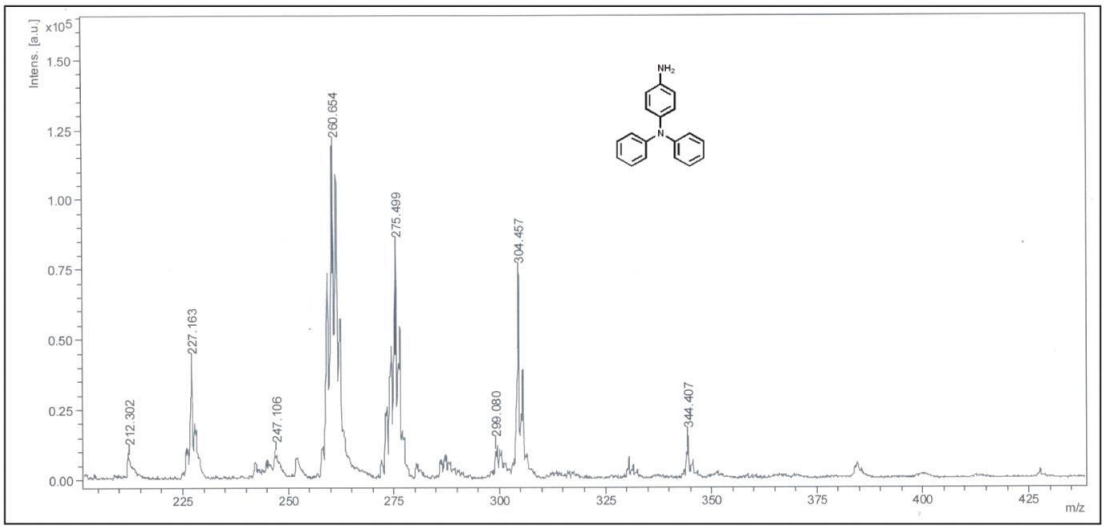

Fig. 3.15. a)**^{1}H NMR,** b)**^{13}C NMR in $CDCl_3$ and** c) **MALDI-TOF** spectra of **D1.**

NMR and Mass data of D2

a)

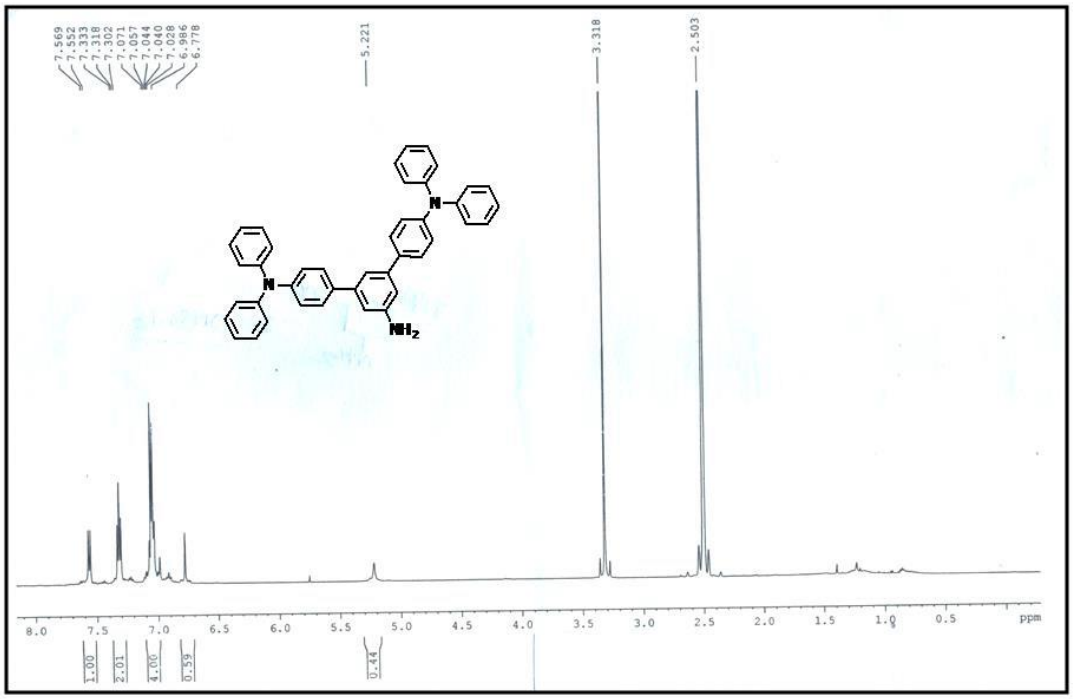

b)

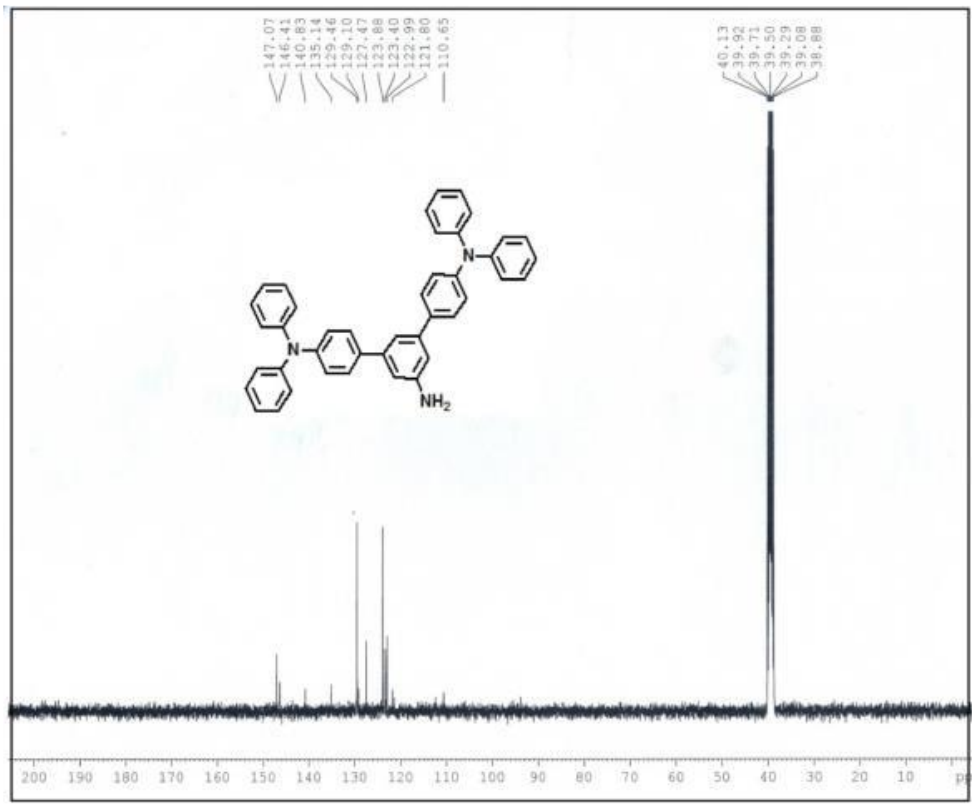

c)

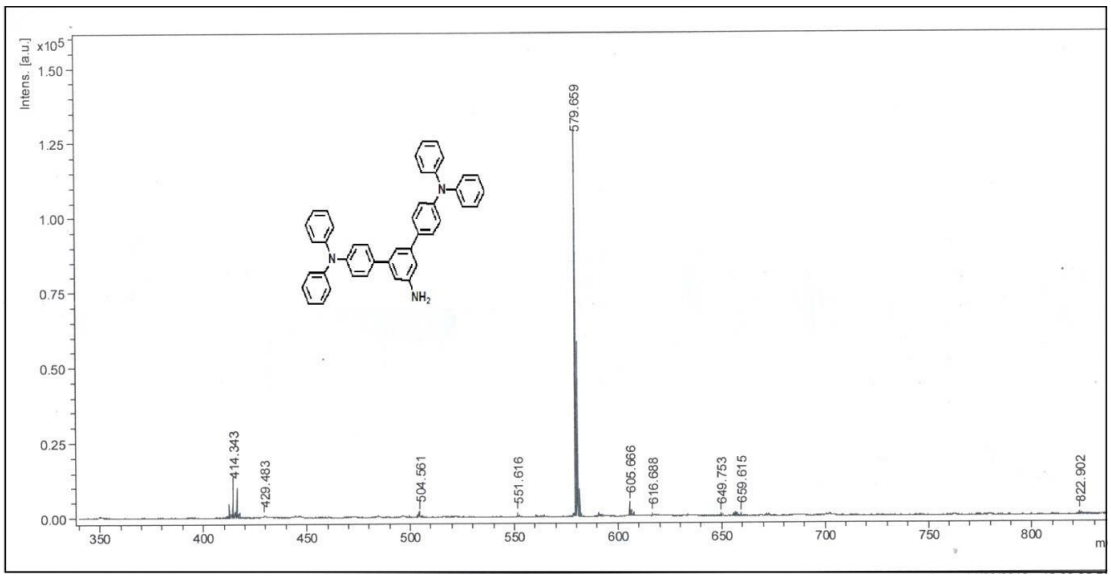

Fig. 3.16. a)**^{1}H NMR**, b) **^{13}C NMR** in DMSO-d6 and **MALDI-TOF** spectra of **D2.**

NMR and Mass data of D3

a)

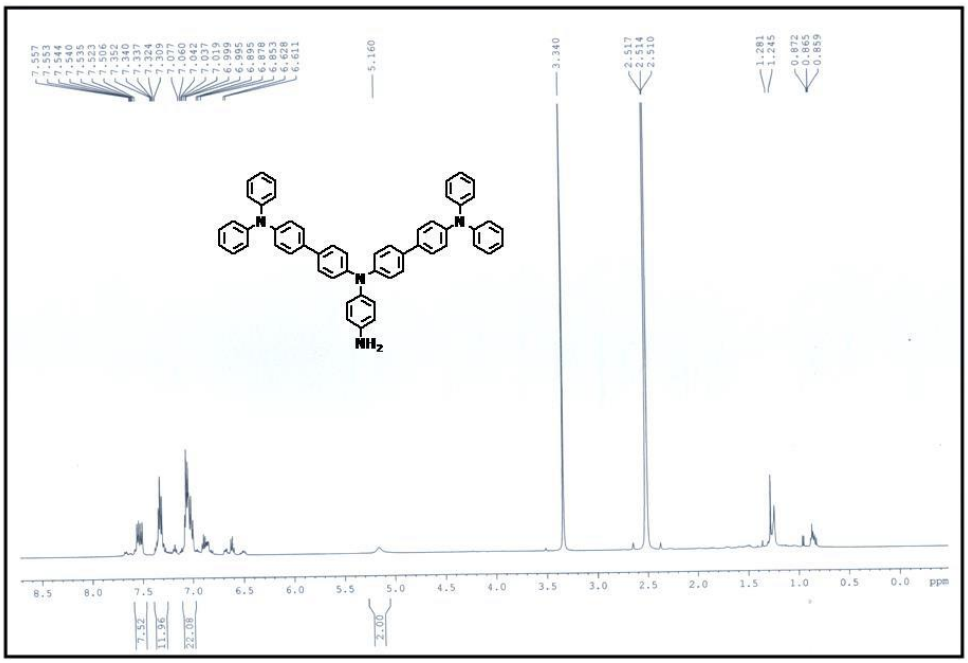

b)

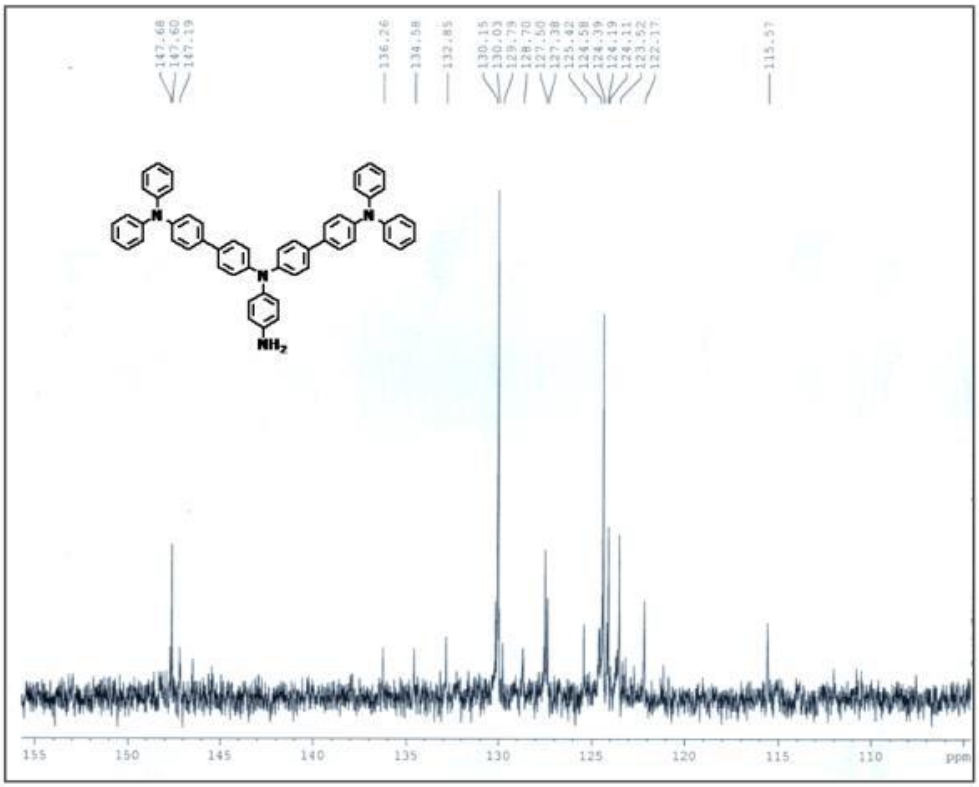

c)

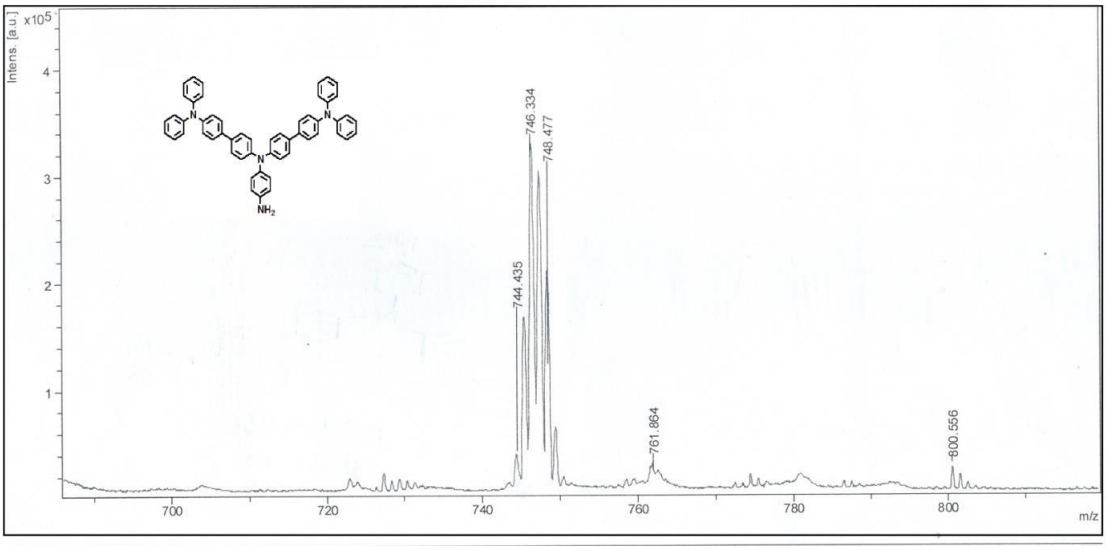

Fig. 3.17. a)**^{1}H NMR**, b)**^{13}C NMR** in DMSO-d6 and **MALDI-TOF** spectra of **D3.**

NMR and Mass data of TPA$_2$ISO

a)

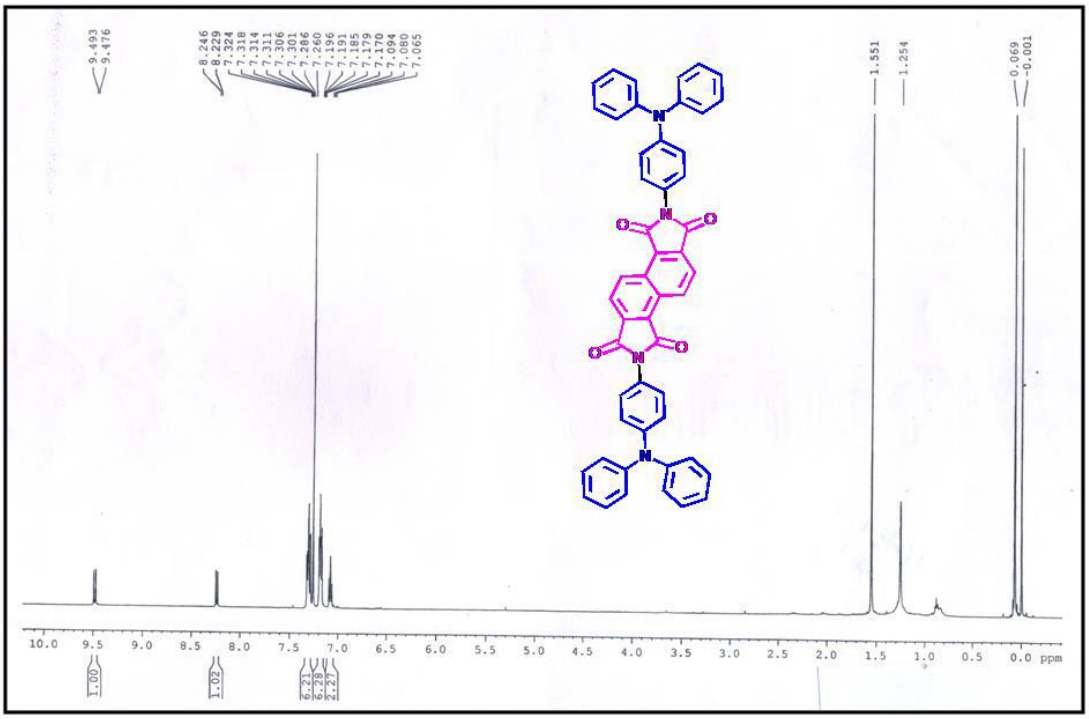

b)

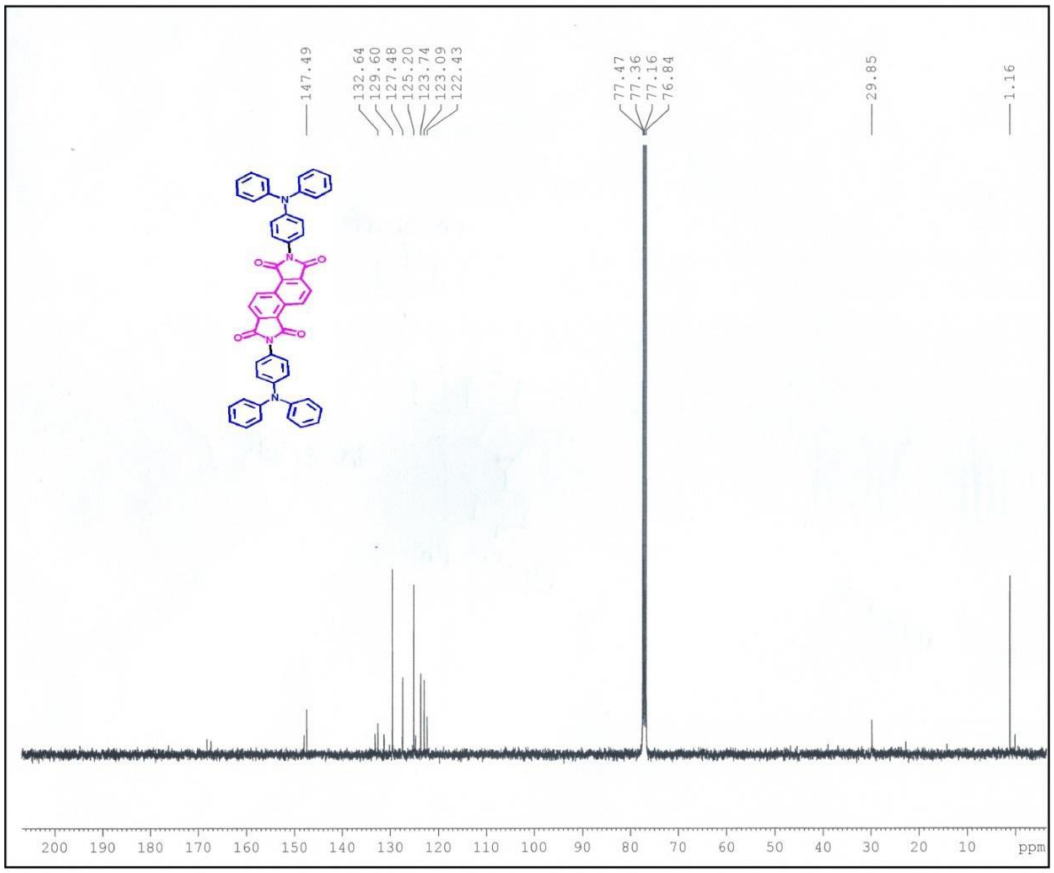

c)

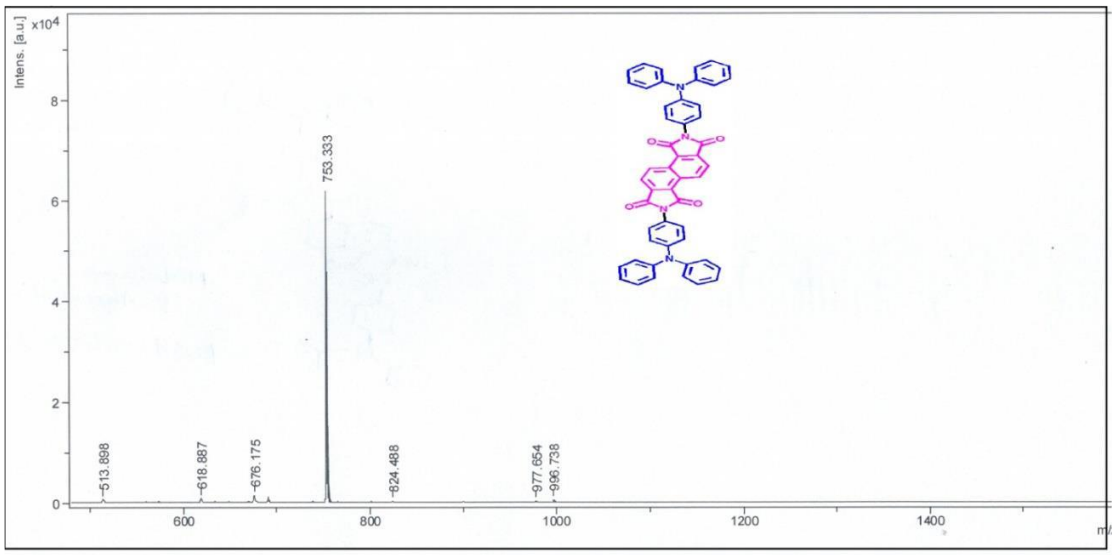

Fig. 3.18. a)**^{1}H NMR**, b)**^{13}C NMR** in $CDCl_3$ and **MALDI-TOF** spectra of **TPA_2ISO.**

NMR and Mass data of TPA_4ISO

a)

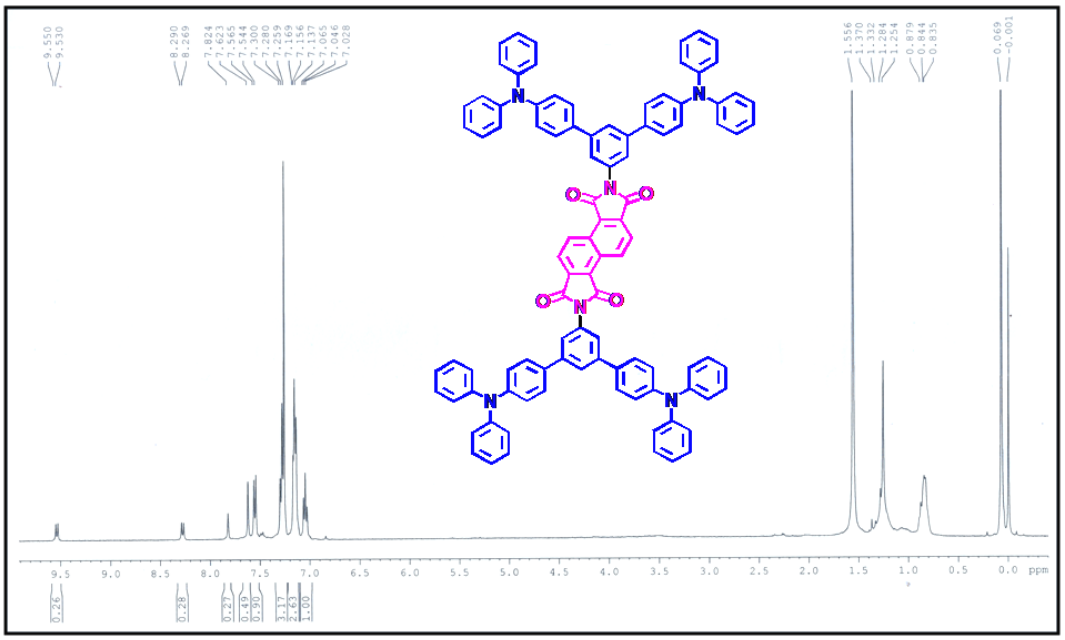

b)

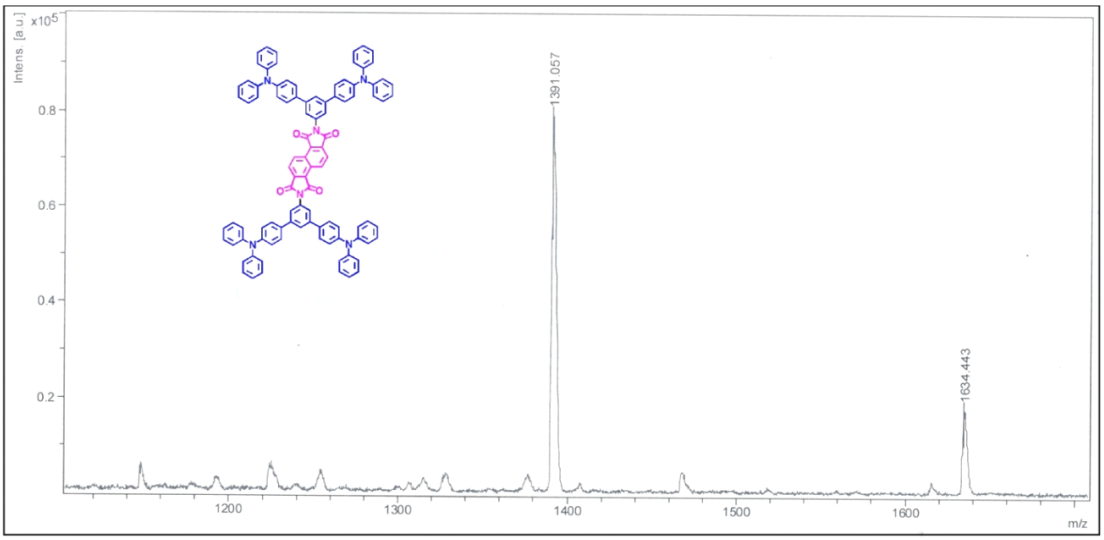

Fig. 3.19. a) **^{1}H NMR** in $CDCl_3$ and b) **MALDI-TOF** spectra of **TPA_4ISO.**

NMR and Mass data of TPA_6ISO

a)

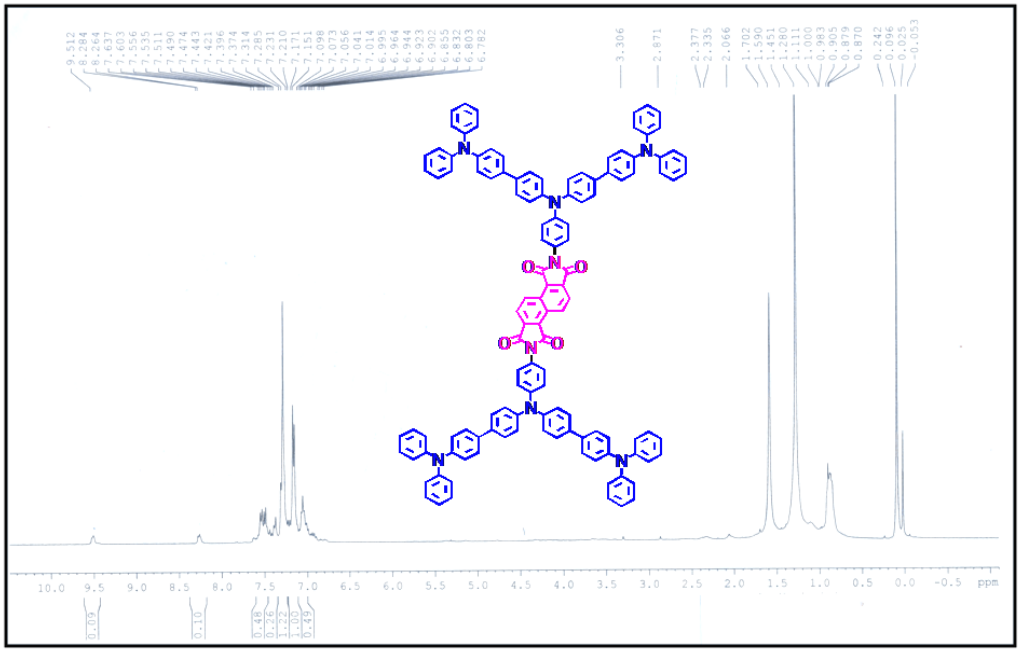

b)

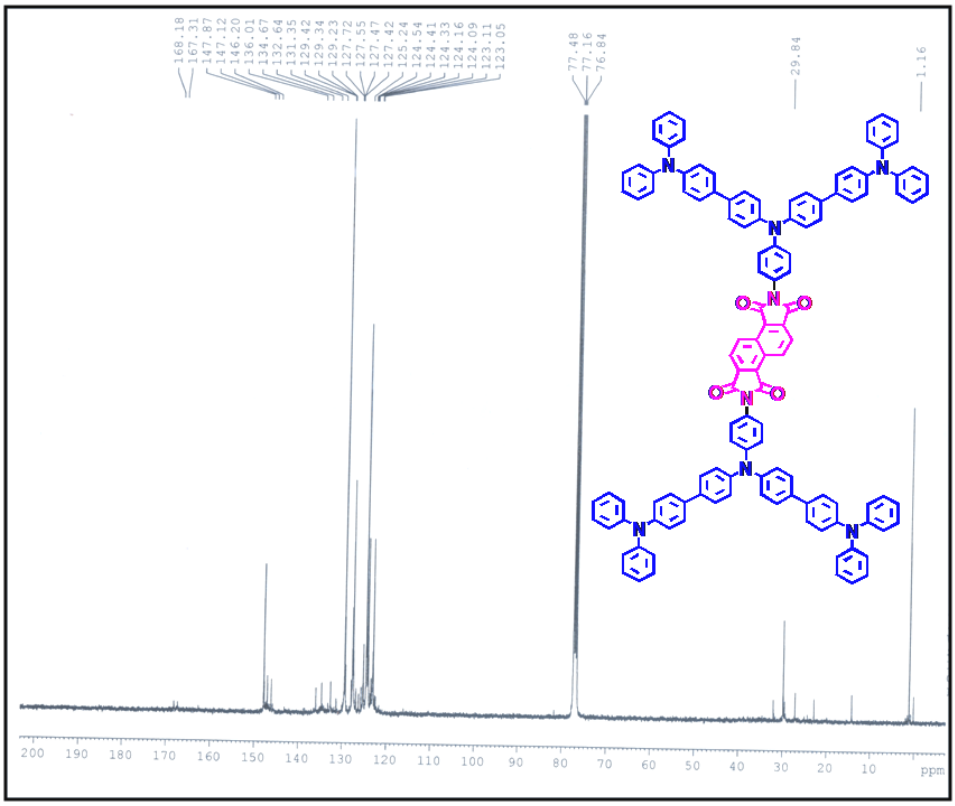

c)

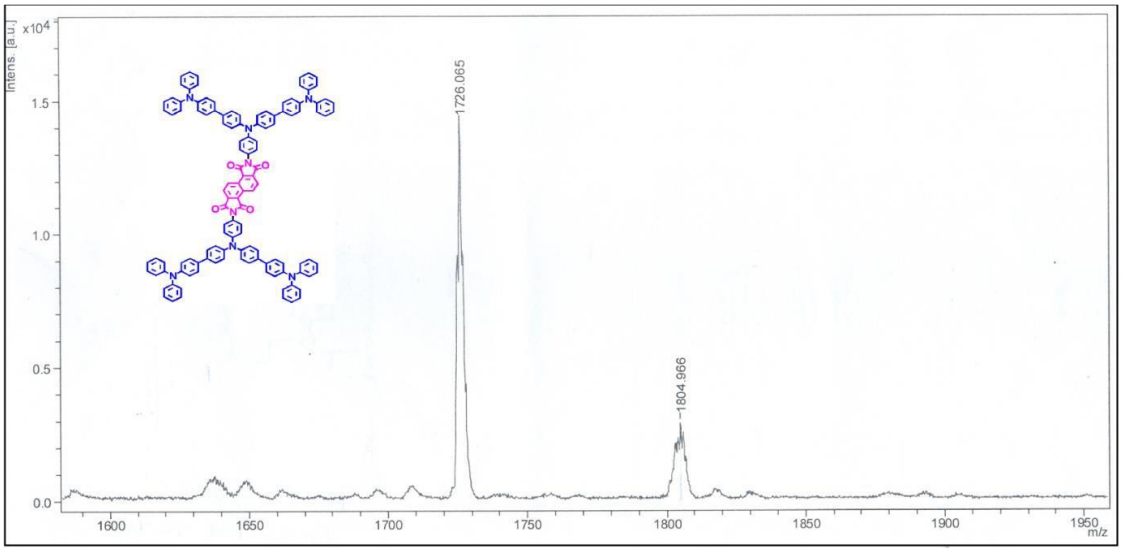

Fig. 3.20. a) **^{1}H NMR, ^{13}C NMR** in $CDCl_3$ and b) **MALDI-TOF** spectra of **TPA_6ISO.**

3.5. References

[1] P. M. S. Monk, R. J. Mortimer, D. R. Rosseinsky, Electrochromism fundamentals and applications, VCH, Weinheim, Germany, (1995) 4– 18;

[2] P. M. S. Monk, R. J. Mortimer, D. R. Rosseinsky, Electrochromism and Electrochromic Devices, Cambridge University Press, Cambridge, UK, (2007) 25–62.

[3] A. Michaelis, H. Berneth, D. Haarer, S. Kostromine, R. Neigl, R. Schmidt, Adv. Mater. 13 (2001) 1825–1828;

[4] H. W. Heuer, R. Wehrmann, S. Kirchmeyer, Adv. Funct. Mater. Chem. 12 (2002) 89–94;

[5] G. Sonmez, H. B. Sonmez, J. Mater. Chem. 16 (2006) 2473–2477;

[6] R. J. Mortimer, A. L. Dyer, J. R. Reynolds, Displays 27 (2006) 2–18;

[7] P. Anderson, R. Forchheimer, P. Tehrani, M. Berggren, Adv. Funct. Mater. 17 (2007) 3074– 3082;

[8] G. A. Niklasson, C. G. Granqvist, J. Mater. Chem. 17 *(*2007) 127–156;

[9] S. Beaupre, A. C. Breton, J. Dumas, M. Leclerc, Chem. Mater. 21 (2009) 1504–1513;

[10] R. Baetens, B. P. Jelle, A. Gustavsen, Sol. Energy Mater. Sol. Cells. 94 *(*2010) 87–105.

[11] S. H. Baeck, K. S. Choi, T. F. Jaramillo, G. D. Stucky, E. W. McFarland, Adv. Mater. 15 (2003) 1269–1273;

[12] S. H. Lee, R. Deshpande, P. A. Parilla, K. M. Jones, B. To, H. Mahan, A. C. Dillon, Adv. Mater. 18 (2006) 763–766.

[13] G. A. Niklasson, C. G. Granqvist, J. Mater. Chem. 17 (2007) 127–156.

[14] R. J. Mortimer, Chem. Soc. Rev. 26 (1997) 147–156.

[15] D. R. Rosseinsky, R. J. Mortimer, Adv. Mater. 13 (2001) 783–793.

[16] P. R. Somani, S. Radhakrishnan, Mater. Chem. Phys. 77 (2002) 117–133.

[17] N. Wu, L. Ma, S. Zhao, D. Xiao, Sol. Energy Mater. Sol. Cells 195 *(*2019) 114–121;

[18] S. Roy, C. Chakraborty, ACS Appl. Mater. Interfaces 12 (2020) 35181–35192.

[19] M. Li, O. A. Yassin, M. L. Baczkowshi, X. Zhang, R. Daniels, A. A. Deshmukh, Y. Zhu, M. T. Otley, G. A. Sotzing, Org. Electron. 84 (2020) 105748.

[20] D. T. Gillaspie, R. C. Tenent, A. C. Dillon, J. Mater. Chem. 20 (2010) 9585–9592.

[21] C. Lambert, G. Nöll, Synth. Met. 139 (2003) 57–62.

[22] Z. Fang, V. Chellappan, R. D. Webster, L. Ke, T. Zhang, B. Liu, Y.-H. Lai, J. Mater. Chem. 22 (2012) 15397–15404.

[23] M.Y. Chou, M.K. Leung, Y. O. Su, C. L. Chiang, C.C. Lin, J.H. Liu, C.K. Kuo, C.Y. Mou, Chem. Mater. 16 (2004) 654–661.

[24] K.Y. Chiu, T.X. Su, J.H. Li, T.H. Lin, G.S. Liou, S.H. Cheng, J. Electroanal. Chem. 575 *(*2005) 95–101.

[25] J. Natera, L. Otero, L. Sereno, F. Fungo, N.-S. Wang, Y.-M. Tsai, T.-Y. Hwu, K.-T. Wong, Macromolecules 40 (2007) 4456–4463.

[26] S.-H. Hsiao, H.-M. Wang, S.-H. Liao, Polym. Chem. 5 (2014) 2473–2483.

[27] C. Quinton, V. Alain-Rizzo, C. Dumas-Verdes, F. Miomandre, G. Clavier, P. Audebert, RSC Adv. 4 *(*2014) 34332–34342.

[28] D. Sek, B. Jarzabek, E. Grabiec, B. Kaczmarczyk, H. Janeczek, A. Sikora, A. Hreniak, M. Palewicz, M. Lapkowski, K. Karon, A. Iwan, Synth. Met. 160 (2010) 2065–2076.

[29] H.-J. Yen, G.-S. Liou, Polym. Chem. 3 (2012) 255–264.

[30] M. Oyama, K. Nozaki, S. Okazaki, Anal. Chem. 63 (1991) 1387–1392.

[31] E. T. Seo, R. F. Nelson, J. M. Fritsch, L. S. Marcoux, D. W. Leedy, R. N. Adams, J. Am. Chem. Soc. 88 (1966) 3498–3503.

[32] S. C. Creason, J. Wheeler, R. F. Nelson, J. Org. Chem. 37 *(*1972) 4440– 4446.

[33] T. Zhang, A. Brajter-Toth, Anal. Chem. 72 (2000) 2533–2540.

[34] M.-K. Leung, M.-Y. Chou, Y. O. Su, C. L. Chiang, H.-L. Chen, C. F. Yang, C.-C. Yang, C.-C. Lin, H.-T. Chen, Org. Lett. 5 (2003) 839–842.

[35] L. Otero, L. Sereno, F. Fungo, Y.-L. Liao, C.-Y. Lin, K.-T. Wong, Chem. Mater. 18 (2006) 3495–3502.

[36] H. Xia, J. He, P. Peng, Y. Zhou, Y. Li, W. Tian, Tetrahedron Lett. 48 (2007) 5877–5881.

[37] H.-J. Yen, H.-Y. Lin, G.-S. Liou, Chem. Mater. 23 (2011) 1874–1882.

[38] A. G. M. Ferrari, C. W. Foster, P. J. Kelly, D. A. C. Brownson, C. E. Banks, Biosensors 8 (2018) 53.

[39] D. C. Santra, S. Nad, S. Malik, J. Electroanal. Chem. 823 (2018) 203–212.

[40] G. Sonmez, H. Meng, F. Wudl, Chem. Mater. 16 (2004) 4.

[41] S. Mondal, Y. Ninomiya, T. Yoshida, T. Mori, M. K. Bera, K. Ariga, M. Higuchi, ACS Appl. Mater. Interfaces 12 (2020) 31896–31903.

[42] S. H. Hsiao, Y. Z. Chen, Dye and Pigments 144 *(*2017) 173–183.

[43] R. J. Mortimer, Annul. Rev. Mater. Sci. 41 (2011) 241–268.

[44] G. S. Liou, H. W. Lin, Polym. Chem. 7 (2016) 198–211.

Chapter-4

Fully organic electroactive monomers for electrochromic behaviors having high coloration efficiency and long cycle stability towards flexible Solid-State electrochromic device

The work reported in this chapter is published in Journal of Electroanalytical Chemistry 918 (2022) 116484

4.1. Introduction

Reversible and persistent colour changes happening by the materials in response to the external electric field through a redox mechanism are known as electrochromic material **[1].** Electrochromic materials have been visualized for the various applications, such as EC smart windows **[2],** auto-dimming rear view mirrors **[3],** energy storage devices **[4],** camouflage, and information storage **[5–9].** Specially, the EC materials in the near-infrared (NIR) region have potentially used in many civil and military areas **[10–11].** Apart from the usual colour switching behaviour of the EC materials, they keep their own places in smart technological device applications such as multi-usage in memory **[12],** supercapacitor **[13],** solar cell **[14].** Switchable electrochromic (EC) smart windows which allow the view of outsides, however, regulate glare, light and heat gains of insides, are the urgent need as these significantly help to reduce the energy use of the building as well as to maintain the impact of heating/cooling/ lighting demand for construction sectors **[15–17].** EC smart windows are visualized as potentially a good candidate for their abilities to adjust the dynamic modulation of the spectral properties within the visible and infrared ranges. It allows appropriate control of the penetration of solar radiation within the building **[18].** Up to date, there are many systems, such as transition metal oxides **[19–20],** conducting polymers **[21–22],** macromolecules, and their corresponding metal complexes **[23],** small molecules **[24–25]** have been investigated. As this phenomenon relies primarily on electron extraction/release process, inorganic counterparts are always enjoying superiority and WO_3/$LiClO_4$ pair is extensively utilized for electrochromic devices **[26].** Recent interest is switched towards fully organic based material due to the solution processibility, multichromic behaviour and faster switching operation **[27–30].** Moreover, organic materials are interested because they may be explicitly printed **[31],** sprayed **[32],** drop casted **[33]** or spin coated **[34]** onto patterned substrates and also structurally tuned at the level of monomer design, whereas, the conventional inorganic materials suffer from a) the limitation of colour shade upon potential change and b) the involvement of tedious fabrication costly processes. To have a superior EC material, it should have high optical contrast (the degree of relative transmittance change during the switching

process), low response time (required to change switching between the coloured state and bleached state), long term cycle stability (intact of optical contrast and charge density upon repetitive switching) and high colouration efficiency (optical change per unit charge density) **[35–36].** During the design of the novel electrochromic materials, colouration efficiency that is simply explained as the minimum charge required per unit area to occur redox reaction between coloured state and bleached state, is not generally considered as important parameter. Higher the value of colouration efficiency at the specific wavelength will lower the switching the states and the better will be the EC material.

Previously from our group, we have reported a series of novel redox-active TPA based isonaphthalene molecules and established that TPA_4ISO exhibits the enhanced long-term cycle stability as well as coloration efficiency with optimal (four) TPA units **[37].** Instead of keeping, single TPA unit as the electropolymerizable group, the incorporation of bulky, packing disruptive and two TPA units on each side of monomer may help to form polymer on conducting surface and may enhance thin-film-forming capability **[38–39].** Hence, from earlier studies it has been realized that right choice of TPA derivative (consisted of four TPA units) may enhance the long-term stability as well as coloration efficiency of electroactive polymers. The electro and photo-active behaviours of monomers have been studied intensively and it is shown that the resulting radical cations formed after oxidation are stable and exhibit a noticeable colour change during the oxidation redox process in the visible region **[40].** Motivated by these studies, three triphenylamine (TPA) based (consisted of four TPA units) organic donor–acceptor (D–A-D) based systems have been developed by varying the central arylimide acceptor cores (pyromellitic, naphthalene, perylene) to further improve the values of above mentioned parameters namely coloration efficiency and long-term stability towards the development of practically viable fully organic EC material **(Fig. 4.01).**

In the designed three D-A-D based systems, TPA is in non-conjugated from the central acceptor moiety to prevent the delocalization of the radical cation generated from the TPA oxidation process which is further confirmed by TD-DFT studies. All three monomers undergo oxidative electro-polymerization process by applying appropriate voltage to form polymers and electrochromic studies of prepared

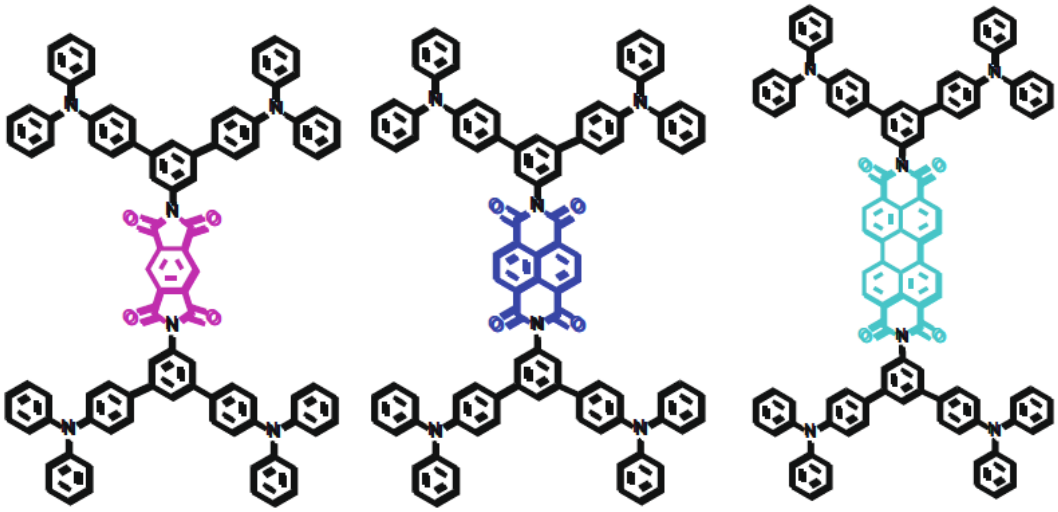

Fig. 4.01. Chemical structures of TPA_4PYRO, TPA_4NDI, TPA_4PERY.

polymers originating from both terminal TPA part via anodic oxidation process and also central acceptor part via cathodic reduction process have been explored. All polymers exhibit excellent optical modulation of >60% and long-life stability up to 10,000 cycles without any attenuation, multi-electrochromism with very high colouration efficiency (800 cm^2/C) for both cathodic and anodic response in a three-electrode configuration. Furthermore, successful fabrication of 5 × 5 cm^2 solid-state EC device for p-TPA_4NDI as well as solid state flexible device which is operated at a potential range from 0 to 2.5 V with reversible multiple EC colour change and the ΔT degraded only 9% after 4000 switching cycles, rest two solid-state ECDs have been assembled to show the potential of these derivatives as organic based multichromism.

4.2. Results and discussion

4.2.1. Synthesis of Monomers

The monomers **TPA$_4$PYRO**, **TPA$_4$NDI**, **TPA$_4$PERY** were synthesized by the condensation of pyromellitic dianhydride, naphthalenetetracarboxylic dianhydride, perylenetetracarboxylic dianhydride respectively with our designed TPA moiety (D) in dry DMF under heating condition with good yield and the scheme shown in **Fig.4.21.** The final products were characterized by NMR, MALDI - TOF mass and FT-IR results **(Figs. 4.02, 4.23–4.26).** The appearance of the peak at 1341.16, 1390.55 and 1515.81 **(Figs. 4.23, 4.24, 4.25)** for TPA$_4$PYRO, TPA$_4$NDI, TPA$_4$PERY respectively in MALDI TOF mass spectra, confirmed the formation of the product which further supported by the ^{1}H NMR and ^{13}C NMR signals. Due to limited solubility of TPA$_4$PERY, good quality of ^{13}C NMR was not achieved. The donor part (D) was synthesized by the cross coupling reaction from the borolane derivative of TPA and 3, 5 dibromo aniline which was synthesized from 4 amino nitrobenzene as precursor **(Fig. 4.22).** The formation of the product was confirmed by the appearance of the signal at 5.58 ppm which was due to the free NH_2 unit and disappearance of the proton signals at 1.29 ppm (12 protons) of the TPA-borolane unit in the ^{1}H NMR spectra. The TPA borolane was formed by the reaction of bis pinacolato diboron with 1 bromo TPA which was formed from the bromination of TPA. FTIR spectra also suggested the characteristic imide ring carbonyl stretching frequency **(Fig.4.02).** UV–Visible absorption spectra measured in DCM (5×10^{-4} M) solution revealed that all three monomers of TPA$_4$PYRO, TPA$_4$NDI, TPA$_4$PERY produced two absorption peaks at 310 and 338 nm from the donor part **(Fig. 4.04, panel 1).** The first absorption band was the characteristic peak of TPA and the second one was due to the absorption of the π-π* transition. The shoulder peak at 382 nm was due to the naphthalene moiety and 481 nm and 517 nm were originating from perylene moiety. The experimental band gap of the monomer was also estimated from the UV–Vis spectroscopy and the energy level of the HOMO has been calculated from the cyclic voltammetry using Ferrocene/Ferrocenium ion as external standard. The band gaps calculated from absorption edges as well as the HOMO and LUMO energy levels of TPA$_4$PYRO, TPA$_4$NDI, TPA$_4$PERY were provided in **Table 4.2.**

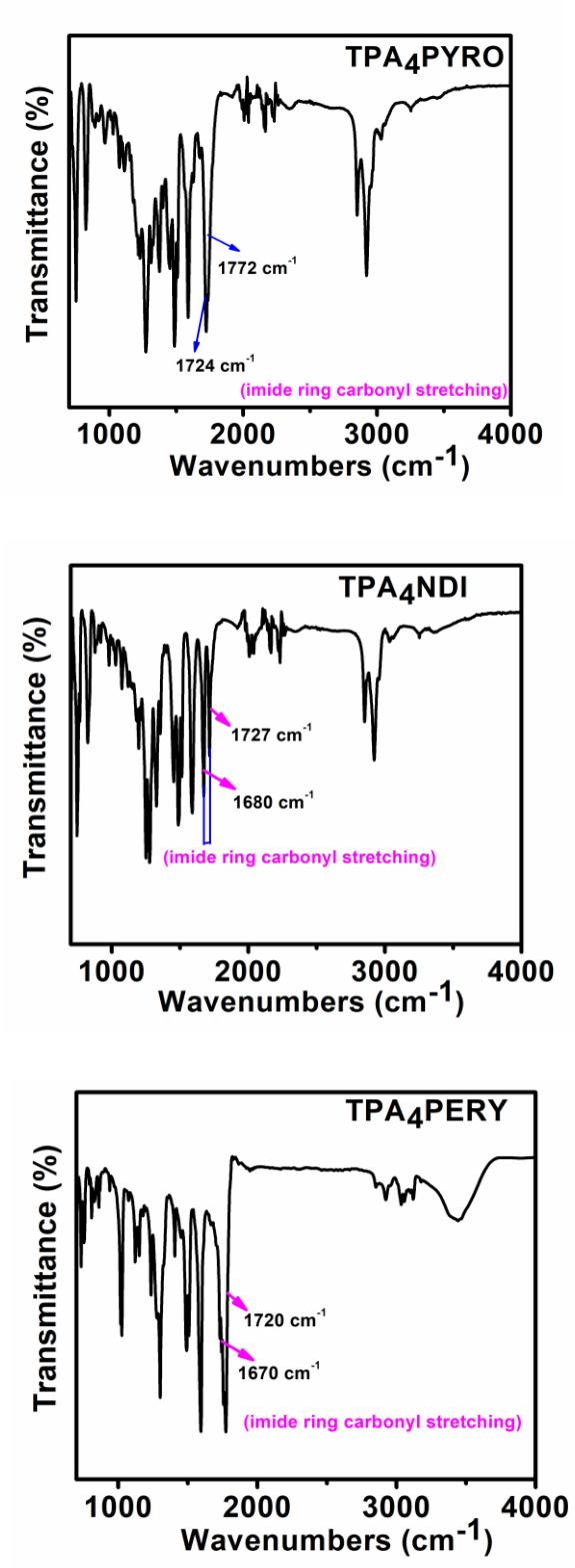

Fig. 4.02. FTIR spectra of **TPA_4PYRO, TPA_4NDI, TPA_4PERY** derivatives**.**

4.2.2. Optical study and electrochemistry of the polymer films

After electropolymerization on ITO coated glass, the polymer films were subsequently washed with DCM, ethanol and acetone to remove the unreacted monomer and oligomers. The film thickness was tuned by controlling the number of the CV scans. During the electropolymerization process, an oxidation was observed at near about 1.1 V in the first positive scan **(Fig. 4.04, panel 2)** due to the one electron oxidation of triphenyl amine unit. For the negative potential scan of the first cycle, two peaks appeared in CV were possibly due to the subsequent oxidation of tetraphenyl benzidine (TPB) unit formed by the rapid oxidative coupling between TPA units. Optical behaviours of the polymer films measured by UV–Vis spectroscopy revealed absorption peaks nearly 345 nm attributed due to the π-π* transition **[41, 42]** of TPA backbone **(Fig. 4.05)** and presence of shoulder at 385 and 505 nm was indicating the incorporation of naphthalene and perylene moiety into the respective monomer. Overall morphology and roughness of film were investigated by FESEM and AFM **(Fig. 4.03)**, the surface was coated with spherical shaped films and the roughness owing to the electropolymerization was relatively enhanced for all three polymers.

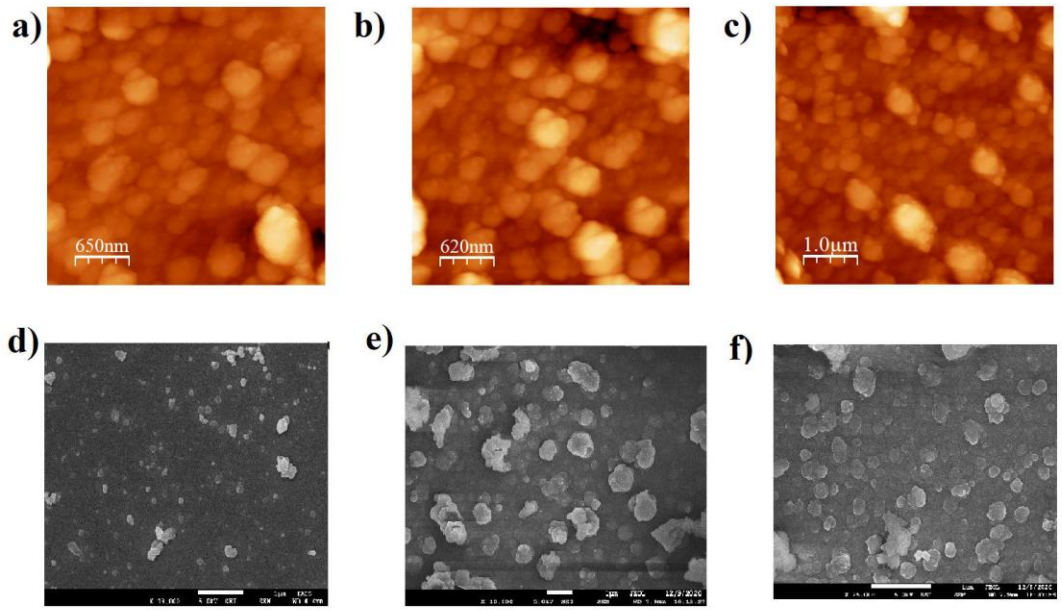

Fig. 4.03. Surface topology of a) **p-TPA4PYRO,** b) **p-TPA4NDI,** c) **p-TPA4PERY** on ITO coated glass and FESEM images of d) p-**TPA4PYRO,** e) **p-TPA4NDI** and d) **p-TPA4PERY**.

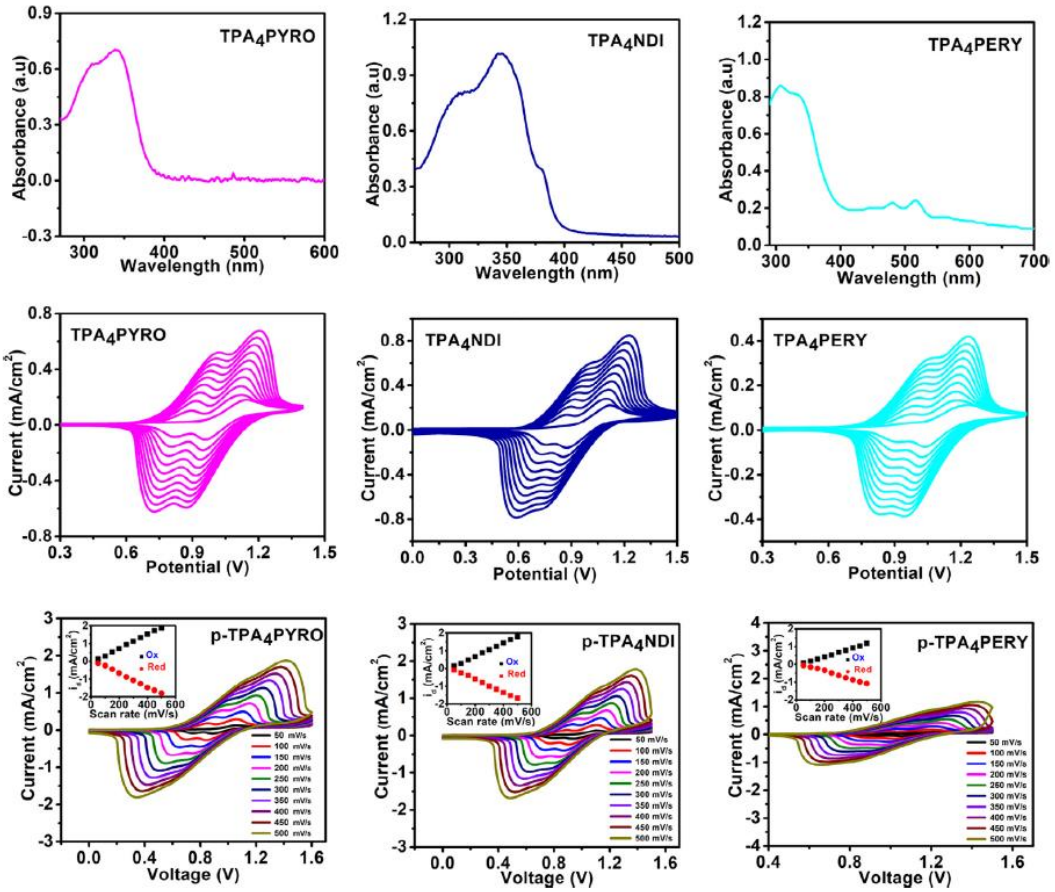

Fig. 4.04. Panel 1: Absorption spectra of the monomers, Panel 2: CV for 10 scan cycles using ITO as the working electrode, TBAP as supporting electrolytes at scan rate of 50 mV/s, Panel 3: Scan-rate-dependent (50–500 mV/s) CV spectra of a thin film deposited on ITO investigated in three-electrode systems with Inset: linear correlations between the peak current and the scan rate during oxidation (top) and reduction (bottom) processes ($R^2 > 0.98$ for fitting).

Electrochemical behaviours of the deposited films were investigated by cyclic voltametry in 0.1 M TBAP in ACN solution. The oxidation peaks were appeared at 1.45, 1.42, 1.53 V and reduction peaks were appeared at 0.68, 0.70, 0.53 V respectively for TPA4PYRO, TPA4NDI, TPA4PERY **(Fig. 4.05).** Scan rate dependent studies of the three polymer films have performed from 50 to 500 mV/s on ITO working electrode, Pt wire as counter and Ag/AgCl as reference electrode in 0.1 M TBAP/ACN solution **(Fig. 4.04, panel 3).** The peak current values are increased with increasing the scan rate. The reversible peak current intensity is linearly increased with the scan number for both positive and negative direction of all three polymers suggesting the reversible nature of the polymerisation process without any diffusion

limit [43]. The linear dependence plot upon plotting peak current vs scan rate is in inset of Fig. 4.04.

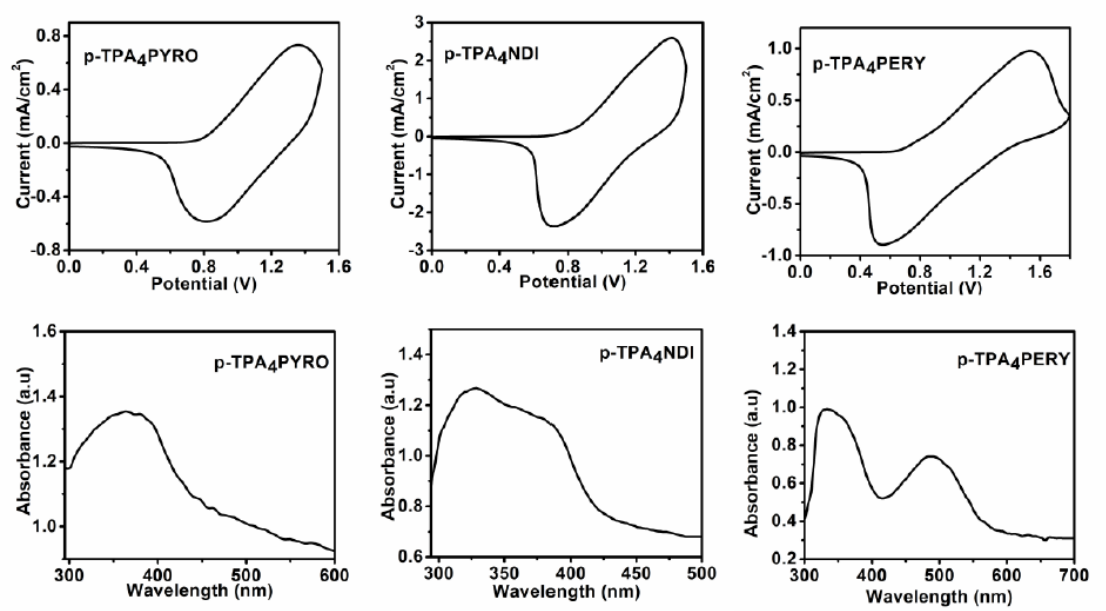

Fig. 4.05. CV of the cast film of individual polymer in 0.1 M TBAP/ACN solution (WE: Pt, CE: Pt wire, RE: Ag wire) at a scan rate 50 mV/s. UV-Vis spectra of the polymers.

Electrochromism of polymer films: The anodic electrochromic performances of the polymer films were evaluated using a three-electrode electrochemical cell where polymer-coated ITO glass was served as the working electrode, Ag/AgCl wire was used as the reference electrode and Pt wire was employed as the counter electrode in 0.1 M TBAP/ACN electrolyte solution. When no voltage was applied, the peak was appeared at 357 nm for p-TPA$_4$PYRO, 361 nm for p-TPA$_4$NDI and 333 and 486 nm for p-TPA$_4$PERY and those were for the π-π* transition peak of the TPA unit present in the respective polymer backbone **(Fig. 4.06).** With increasing the voltage, the intensity of this absorption band was gradually decreased. When the voltage was changing from 0 V to near about 1 V, a new absorption peak, that was appeared at approx 490 nm for the three polymer films, was the signature of the π − polaron transition for reversible redox of the TPA moiety (TPA ↔ TPA$^{\bullet+}$). The colour of the polymer film was consequently changed to brown for p-TPA$_4$PYRO and p-TPA$_4$NDI **(Fig. 4.07a, 4.08a).** However, for the p-TPA$_4$PERY **(Fig. 4.09a)** the brown colour

change of the polymer film was not clearly observed because of the red colour of the polymer film itself. Again, the potential was further enhanced to 1.2 V, the absorption band around 490 nm gradually diminished with the appearance of a new broad band at near about 750 nm with the extended tail in the NIR region, indicating the presence of TPB dication with the colour change from brown to deep blue. Further on increasing the voltage, no extra peak was observed. The above discussed EC behaviour in the anodic region was associated to the redox process in the TPA portion. The cathodic EC performance of the polymer films were evaluated also using a three-electrode electrochemical cell where polymer-coated ITO – PET served as the working electrode, Ag/AgCl used as the reference electrode and Pt wire used as the counter electrode in 0.1 M TBAP DMF electrolyte solution. At 0.0 V, an absorption peak was appeared to the same position of the anodic process for the three polymers. With increasing the bias from 0 V to −2 V, a deep pink colour **(Figs. 4.07a, 4.08a, 4.09a)** was developed due to the cathodic reduction of the central ring (pyromellitic, naphthalene, perylene ring) of the three polymers at the absorption band 545 nm. The new peak was appeared at −1.8 V and intensified at −2 V. The spectro-electrochemistry experiments were carried out at room temperature without taking any external precaution for avoiding moisture or air. To determine the optical

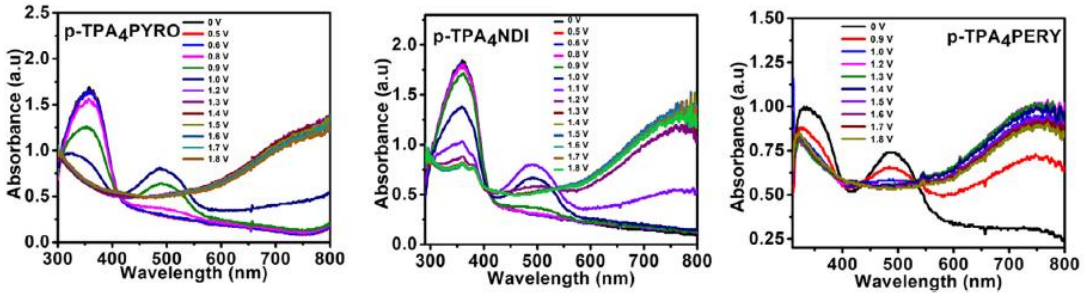

Fig. 4.06. Change of absorption of the polymer films on ITO-coated glass in 0.1 M TBAP/ACN solution with voltage change.

contrast, response time (coloration and bleaching time), colouration efficiencies and the behaviours of the polymer films upon applying positive (anodic) and negative (cathodic) voltage, EC switching studies were performed by CV method with the combination of UV–Vis spectroscopy and the change of transmittance at a fixed wavelength (740 nm) with time using voltage ramping between 0 and 1.2 V for a

pulse width 10 s in 0.1 M TBAP in ACN solution for the anodic process and 0 to−2 V with pulse time 10 s in 0.1 M TBAP in DMF solution for the cathodic process at 536 nm. A reversible colour changed from colourless to deep blue was observed for the polymer film in anodic process and colourless to deep pink in the cathodic process. The turn on state coloration transmittance obtained for p- TPA$_4$PYRO, p-TPA$_4$NDI, p-TPA$_4$PERY were 2.9%, 8.8% and 6.5% for anodic colouring **(Figs. 4.07b, 4.08b, 4.09b)** and 6.9%, 2.6%, 9.3% for cathodic colouring **(Fig. 4.12)** and the turn off state bleaching

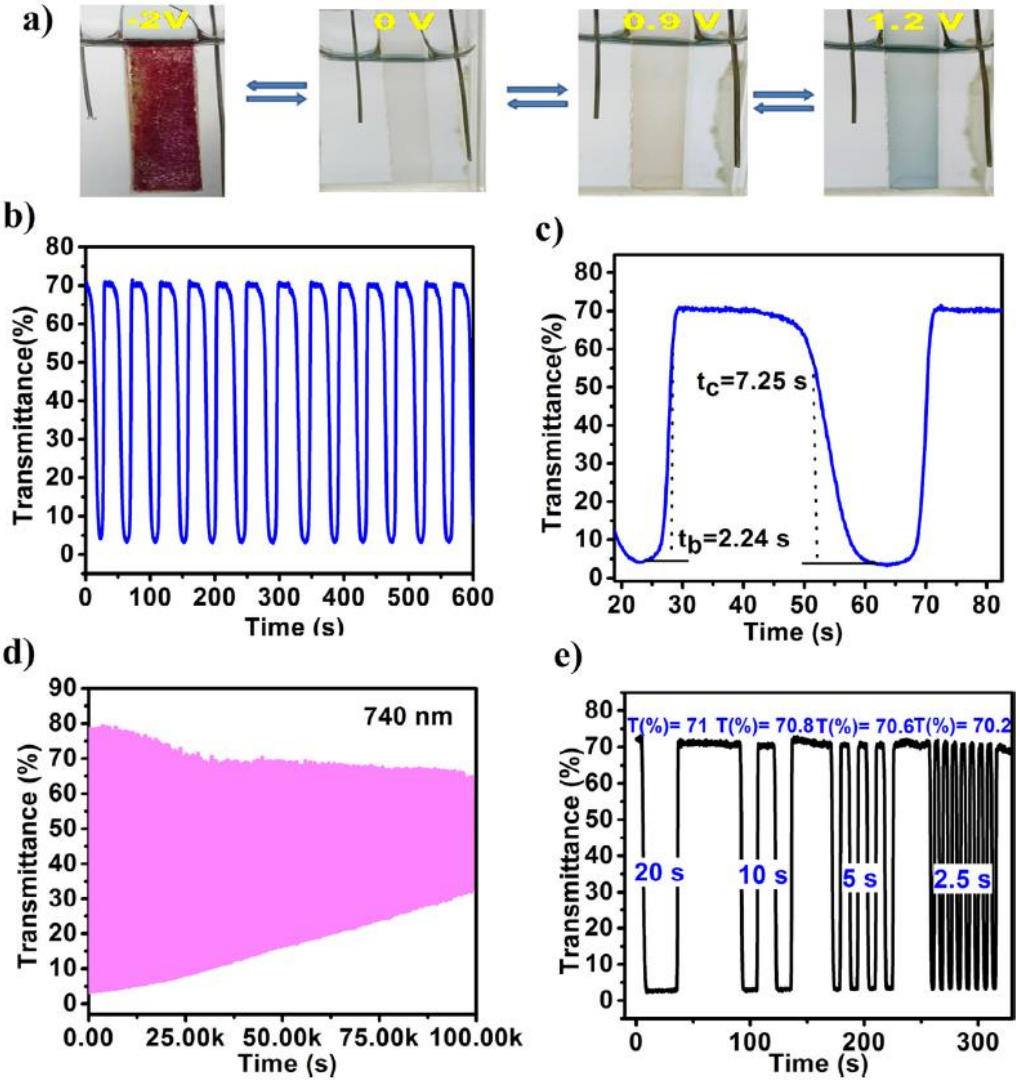

Fig. 4.07. p-TPA4PYRO system: (a) photographs of the film for both cathodic and anodic process, (b) transmittance spectra at 740 nm with pulse width of 10 s, (c) Response time colouration (tc) and bleaching (tb), In each case, the applied voltage was switched between 0 and 1.2 V. (d) Long term cyclic stability over 10,000 cycles upon applying voltages of 0/1.2 V with pulse width of 10 s, (e) Transmittance change (ΔT, %) at different pulse widths.

transmittance were 72%, 75% and 74% **(Figs. 4.07b, 4.08b, 4.09b)** respectively for anodic and 65%, 50%, 61% for the cathodic switching **(Fig. 4.10)** for the first potential switching step. The calculated values of optical contrast for the polymers were 69.1%, 66.2% and 67.5% respectively for anodic and 58.1%, 47.4%, 51.7% for cathodic switching. The coloration and bleaching times required for 95% full transmittance change for p- TPA$_4$PYRO, p-TPA$_4$NDI, p-TPA$_4$PERY were 7.25, 5.14 and 7.01 s and 2.24, 1.71 and 4.37 s **(Figs. 4.08c, 4.09c)** at 740 nm and 15, 3.64, 8.2 s and 6.91, 4.97, 9.0 s at 536 nm **(Fig. 4.10).** The coloration and bleaching times were relatively higher for those fully organic polymers as compared to inorganic metal oxides. An important EC parameter for knowing the quality of an EC material was coloration efficiency (η). The higher value of colouration efficiency better would be the EC material. This parameter could be determined by the following equation **[44].**

$$\eta = \frac{\Delta OD}{Q_d} = \log \frac{T_b}{T_c} \Big/ Q_d$$

where, T_b and T_c were the % of transmittance of the bleaching state and coloration state, ΔOD was the optical absorbance change and Q_d (mC/ cm^{-2}) was the ejected charge during the redox process and Q_d was calculated from chrono-ampherometric plot **(Fig. 4.11).** The obtained coloration efficiencies for the polymers were 771.06, 847.16 and 783 cm^2/C respectively for the colour changed from colourless to blue and 290, 558, 385 cm^2/C respectively for the colour change from colourless to pink. This excellent value of colouration efficiency was quite rare for purely organic based electrochromic materials. It predicted that those polymers could be commercialized as a good EC materials. All data were summarized in **Table 4.1.**

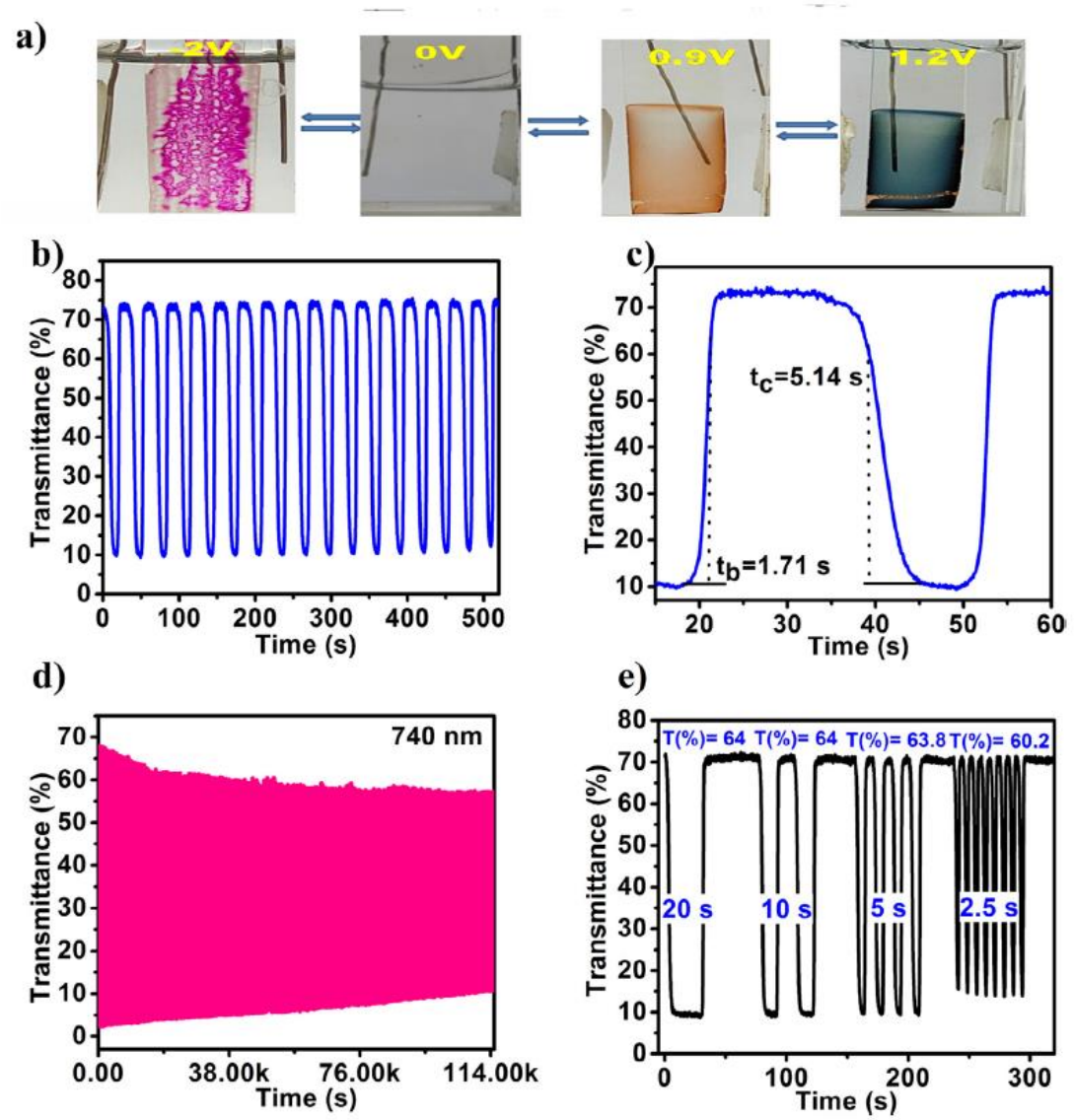

Fig. 4.08. p-TPA$_4$NDI system: (a) photographs of the film for both cathodic and anodic process, (b) transmittance spectra at 740 nm, (c) Response time colouration (t_c) and bleaching (t_b), In each case, the applied voltage was switched between 0 and 1.2 V. (d) Long term cyclic stability over 10,000 cycles upon applying voltages of 0/1.2 V with pulse width of 10 s, (e) Transmittance change (ΔT, %) at different pulse widths.

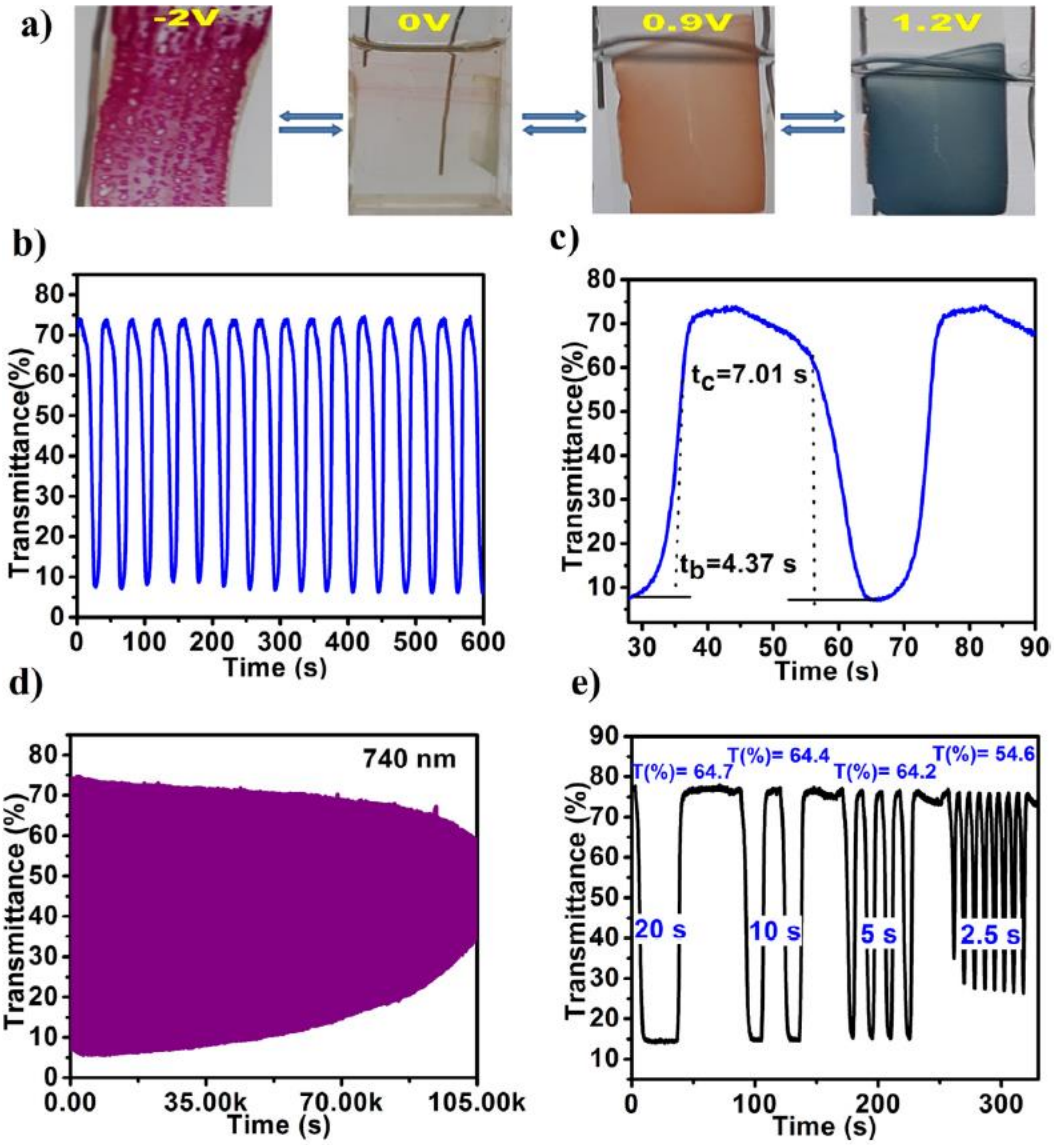

Fig. 4.09. p-TPA$_4$PERY system: (a) photographs of the film for both cathodic and anodic process, (b) transmittance spectra at 740 nm, (c) Response time colouration (t_c) and bleaching (t_b), In each case, the applied voltage was switched between 0 and 1.2 V. (d) Long term cyclic stability over 10,000 cycles upon applying voltages of 0/1.2 V with pulse width of 10 s, (e) transmittance change (ΔT, %) at different pulse widths.

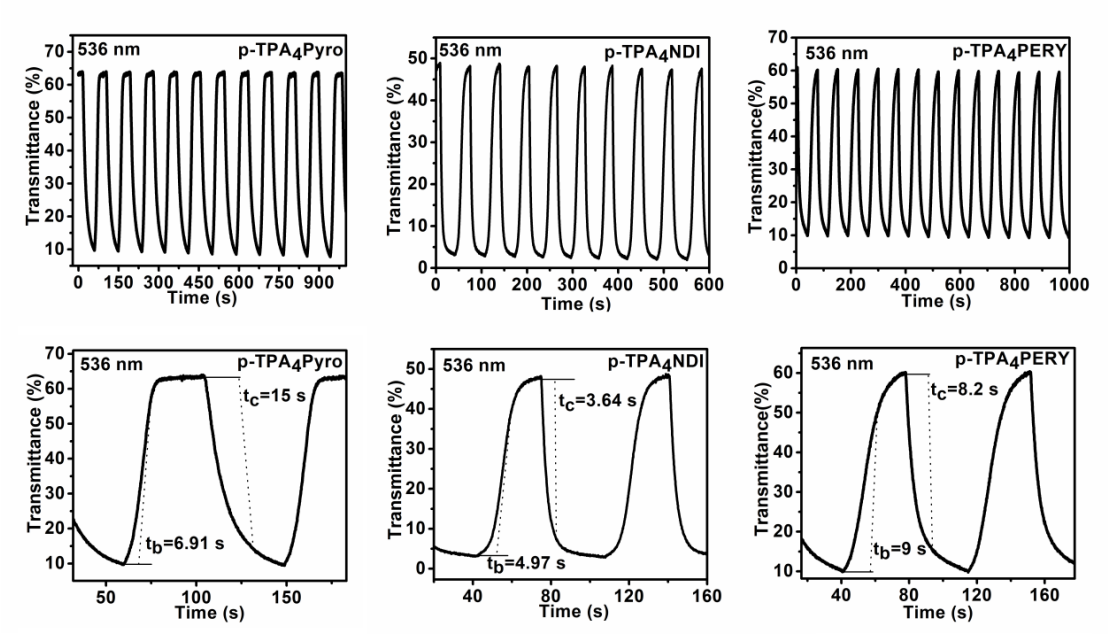

Fig. 4.10. Transmittance change during switching process of the polymers in pulse width of 10s, ITO-coated glass as working electrode, Pt wire as counter electrode Ag/AgCl as reference electrode at 536 nm wavelength and their corresponding t_c, t_b values.

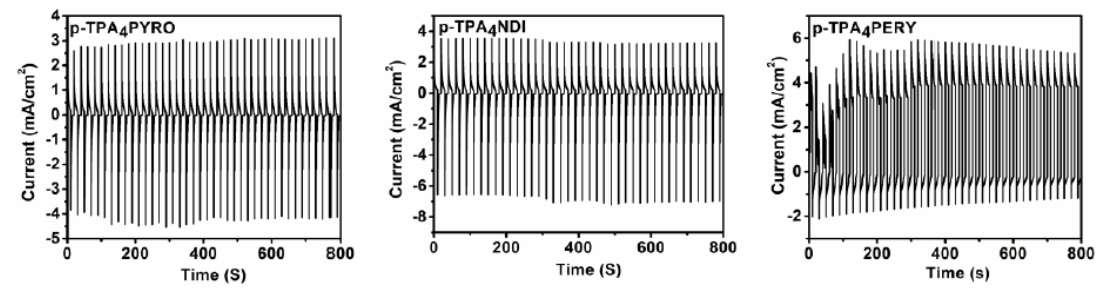

Fig. 4.11. Chrono-ampherometry studies of three polymer films.

The cycle stabilities of all those polymer films were tested for 10,000 switching cycles for the anodic colour change with a pulse width of 10 s at 740 nm between 0/1.2 V. The stability lost after 10,000 cycles was 42.57% for p-TPA$_4$PYRO, 18.3% for p-TPA$_4$NDI and 32% for p-TPA$_4$PERY **(Fig. 4.07d, 4.08d, 4.09d).** The stability of the polymer films also checked in the cathodic with a pulse width of 10 s at 536 nm for 300 cycles for TPA$_4$PYRO and p-TPA$_4$NDI and 600 cycles for p-TPA$_4$PERY

(Fig. 4.12) between the working potential 0 to −2 V. EC properties of our polymers were compared to some reported best performing EC materials **[45–54],** i.e., transition metal oxides, organic polymers, metal organic supramolecular polymers **(Table 4.5)** to show significant enhancement of coloration efficiency and switching performances.

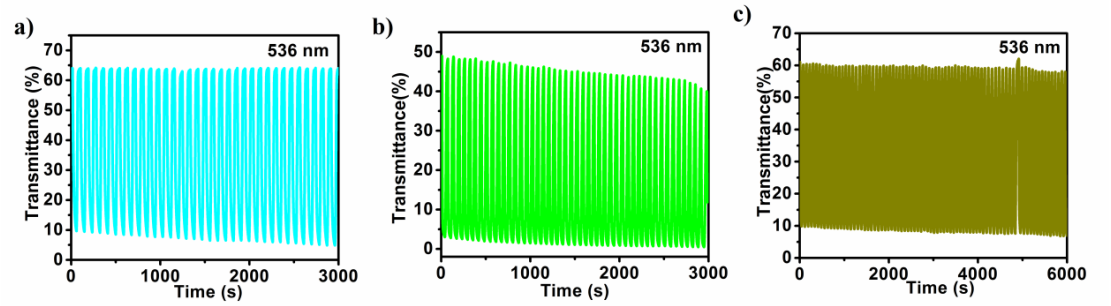

Fig. 4.12. Cathodic cyclic stability over 600 cycles upon applying voltages of 0/-2 V with a holding time of 10 s of a) **p-TPA4PYRO**, b) **p-TPA4NDI**, c) **p-TPA4PERY**.

Table 4.1. EC parameters of the polymers **p- TPA$_4$PYRO**, **p-TPA$_4$NDI, p-TPA$_4$PERY**

Polymers	**Λ[a] max(nm)**	**ΔT%**	**Response Time[b]**		**ΔOD[c]**	**Q $^{d}_{d}$ (mC/cm^2)**	**CE[e] (cm^2/C)**
			t_c (s)	**t_b (s)**			
p-TPA$_4$PYRO	740	69.1%	7.25	2.24	1.391	1.80	771
	545	58.1 %	15	6.91	0.880	3.06	290
p-TPA$_4$NDI	740	66.2%	5.14	1.71	0.898	1.06	847
	545	47.4 %	3.64	4.97	1.356	2.43	558
p- TPA$_4$PERY	740	67.5%	7.01	4.37	1.07	1.36	783
	545	51.7 %	8.2	9.0	0.816	2.12	385

Wavelength of absorption maximum. Time for 95 % of the full-transmittance change. Optical density change (ΔOD) = Log [$T_{bleached}$ / $T_{colored}$], where $T_{colored}$ and $T_{bleached}$ were the maximum transmittance in the oxidized and neutral states respectively. Q_d was the ejected charge obtained from chronoampherometry measurement. Coloration efficiency (CE) = ΔOD/Qd.

With decreasing the pulse width (20 s, 10 s, 5 s, 2.5 s), the value of Δ%T is decreased. The time varying switching potential was carried out between 0 and 1.2 V at 740

a)

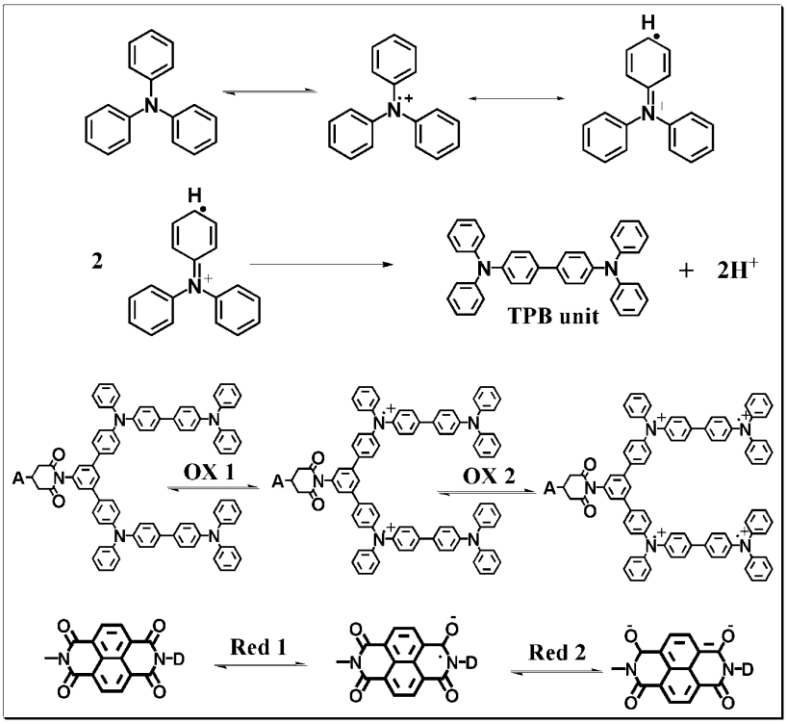

b)

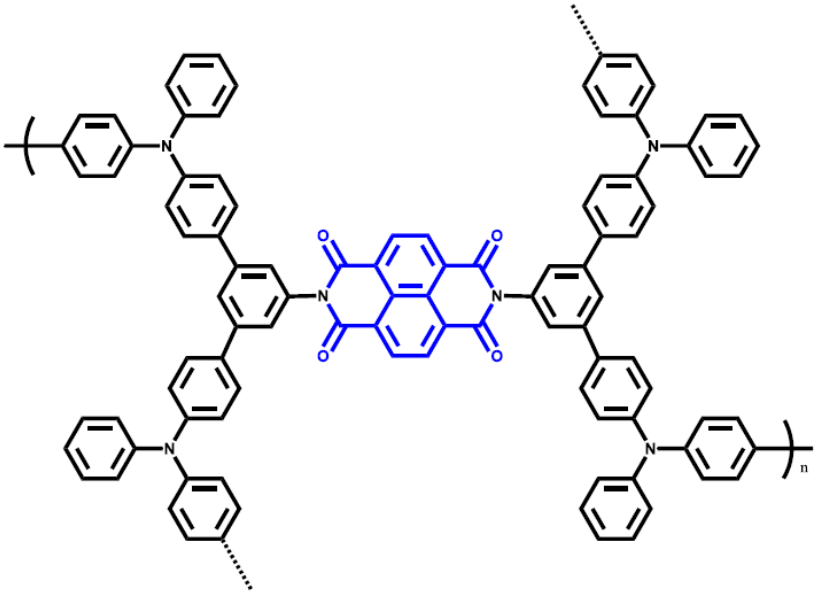

Fig. 4.13. a) Mechanism for anodic and cathodic colour change and **b)** Possible chemical structure of **p-TPA4NDI** (broken lines indicate another possibility for bond formation).

nm of the polymer films of p-TPA$_4$PYRO, p-TPA$_4$NDI, p-TPA$_4$PERY and monitoring the transmittance change **(Figs. 4.07e, 4.08e, 4.09e).** With decreasing the pulse width 2.5 s, the value of Δ%T was decreased. Retention of the ΔT was observed with the pulse width of 20 to 5 s for all the three polymers. The mechanism of anodic and cathodic colour change and the represented structure of the polymer formed were shown in **Fig. 4.13a** and **Fig. 4.13b**.

Computational details: All the DFT studies were performed using Gaussian 16 suite of programs **[55].** The geometry optimization of both the monomers and polymers was carried out employing hybrid DFT functional namely B3LYP **[56]** and 6-31G(d) basis set **[57].** Harmonic vibrational frequency analysis exhibited that all the minima structures had zero imaginary vibrational frequencies ensuring absence of any saddle point in the optimized structures. The optimized geometries were used for time-dependent DFT (TD-DFT) calculations to generate UV–Vis spectra. The TD-DFT calculations were performed using mPW1PBE/cc-PVDZ level of theory which was considered to be the benchmarking combination of functional and basis set for TD-DFT investigation of organic electrochromic materials **[58, 59].** Polymer films were modelled considering the polymerization of two triphenylamine (TPA) unit along one side of the core moieties while the other side was terminated with hydrogen as similar sort of polymerization would occur on the other side of core moieties. Based on earlier studies, it could be assumed that there would be minimum structural changes during oxidation and reduction of the polymer films and hence UV–Vis absorption data of radical cation and anion states were calculated using the optimized geometries of neutral polymers with inclusion of charge **[60, 61].** Semi-oxidized and fully-oxidized states were considered with inclusion of +2 and +4 charges in the modelled polymers while charges on radical anion and dianion species were −1 and −2 respectively as shown in **Fig. 4.16.**

Computational studies: To get a better understanding about the electro polymerization process of the monomeric species namely TPA_4PYRO, TPA_4NDI and TPA_4PERY, density functional theory (DFT) studies were performed to calculate the HOMO and LUMO distributions as well as HOMO-LUMO gaps (i.e. band gaps) of those monomers. As evident from **Fig. 4.14**, the HOMO orbitals were localized on the terminal TPA units of the monomers while LUMO was concentrated on the central acceptor moieties. The position of HOMO orbitals on TPA unit vividly indicated that the oxidation of TPA unit was more feasible through electron donation compared to the oxidation of central core moieties and hence polymerization propagated through the oxidation of TPA units of the monomers. The calculated energies of HOMO, LUMO energy levels and the corresponding HOMO LUMO gaps were shown in **Table 4.3** which nicely corroborated with the experimentally determined optical and electrochemical band gaps. The UV–Vis absorption spectra of the monomers were also simulated from TD-DFT calculations. As shown in **Fig. 4.15a,** the simulated absorption spectra of monomers exhibited peak maxima at 340, 344 nm respectively for TPA_4PYRO and TPA_4NDI while two absorption maxima were present at 340 and 505 nm for TPA_4PERY. Those simulated peak maxima were comparable to experimentally determined data. However, two key transitions with high oscillator strength were observed for TPA_4PYRO at around 310 and 340 nm. Peak at 310 nm with oscillator strength f=0.17 was due to HOMO-3 to LUMO+5 transition while that of 340 nm (f = 0.99) originated from two transitions HOMO to LUMO + 4 and HOMO-1 to LUMO + 3. On the contrary, peak maxima at 340 nm (f = 1.70) for TPA_4NDI was primarily formed by the HOMO-2 to LUMO + 4 excitation. In case of TPA_4PERY, the excited state at around 340 nm with f = 1.08 was found to contain HOMO-2 to LUMO + 5 transition while transition at 505 nm was from HOMO-4 to LUMO. For all the monomers, the most intense transition with high oscillator strength at around 340 nm assigned to π-π^* transition. To further elucidate the absorption behaviour of polymers namely p-TPA_4PYRO, p-TPA_4NDI and p-TPA_4PERY, TDDFT calculations were performed on the modelled polymers **(Fig. 4.16). Fig. 4.15** displayed the calculated UV–Vis absorption spectra of all the polymers in the neutral, semi-oxidized and fully-oxidized states. As evident form spectral data, there was a bathochromic or red shift of absorption spectra along with generation of new

transitions at higher wavelengths for all the oxidized polymers compared to their neutral analogues. Neutral p- TPA_4PYRO was found to have most intense and significant transition at around 360 nm with an oscillator strength of 2.15 while a red-shift of 8 nm was observed for its semi-oxidized state with f=1.22. Besides, a new weaker transition developed at 570 nm with f = 0.06. However, the fully oxidized state exhibited significantly higher red-shift of the spectrum in higher wavelength visible region or near IR region. This phenomenon was in line with previously reported studies. It was noteworthy to mention that transitions beyond visible region (>800 nm) was not discussed in the current study. Similar results were obtained for p-TPA_4NDI. On the contrary, for p-TPA_4PERY two significant transitions occured at around 367 (f = 0.87) and 505 nm (f = 0.80). Interestingly, the oscillator strengths for those two transitions were equivalent indicating dominance of higher wavelength transition compared to its neutral analogue where higher oscillator strength (f = 1.12) was observed for transition around 367 nm (f = 0.87 at 502 nm). To further elucidate the impact of oxidation on the change of colour of the polymers, the positions of HOMO, LUMO and their corresponding HOMO-LUMO energy gaps were determined for neutral as well as oxidized states. As shown in **Table 4.3,** significant lowering of HOMO and LUMO energies took place with progressive oxidation of the polymers from neutral to fully oxidized states. Additionally, HOMO and LUMO energy levels came closer with significant lowering of HOMO-LUMO energy gaps (following the order: neutral > semi-oxidized> fully-oxidized) upon oxidation of polymers justifying red shifts of the adsorption spectra. The observation was in accordance with earlier studies. Based on TD-DFT analysis on the modelled polymer structures, it was qualitatively concluded that significant lowering of HOMO and LUMO energy levels as well as HOMO-LUMO energy gaps upon oxidation caused high intensity electronic transitions at lower energy visible wavelength region resulting in different colours in the polymer.

Band gap calculation:

Table 4.2.: Estimation of HOMO and LUMO levels and band gap

Monomers	UV-vis wavelength (nm)		Oxidation potential (v)		Band gap (Exp) (ev)	HOMO (Exp) (ev)	LUMO (Exp) (ev)
	Λ_{max}	Λ_{onset}	E_{onset}	$E_{1/2ox1}$			
TPA_4PYRO	340	380	0.93	1.10	3.26	-5.49	-2.23
TPA_4NDI	344	382	0.96	1.11	3.24	-5.5	-2.26
TPA_4PERY	516	530	1.04	1.20	2.33	-5.59	-3.26

UV-vis absorption maximum and onset wavelengths for the monomers and polymer films. Read from the first CV scans, in acetonitrile at a scan rate of 50 mV/s (versus Ag/AgCl). Optical band gap was calculated from absorption edge.Eg = 1240/λonset . The HOMO and LUMO energy levels were calculated from Eox values of CV diagrams and were referenced to ferrocene (4.8 ev relative to vacuum energy level, Eonset = 0.37 V, $E_{1/2Fc}$= 0.41 V in acetonitrile. E_{HOMO} = -[(E1/2ox1 – 0.41)+4.8] (ev); E_{LUMO} = (E_{HOMO} + Band gap energy) (ev).

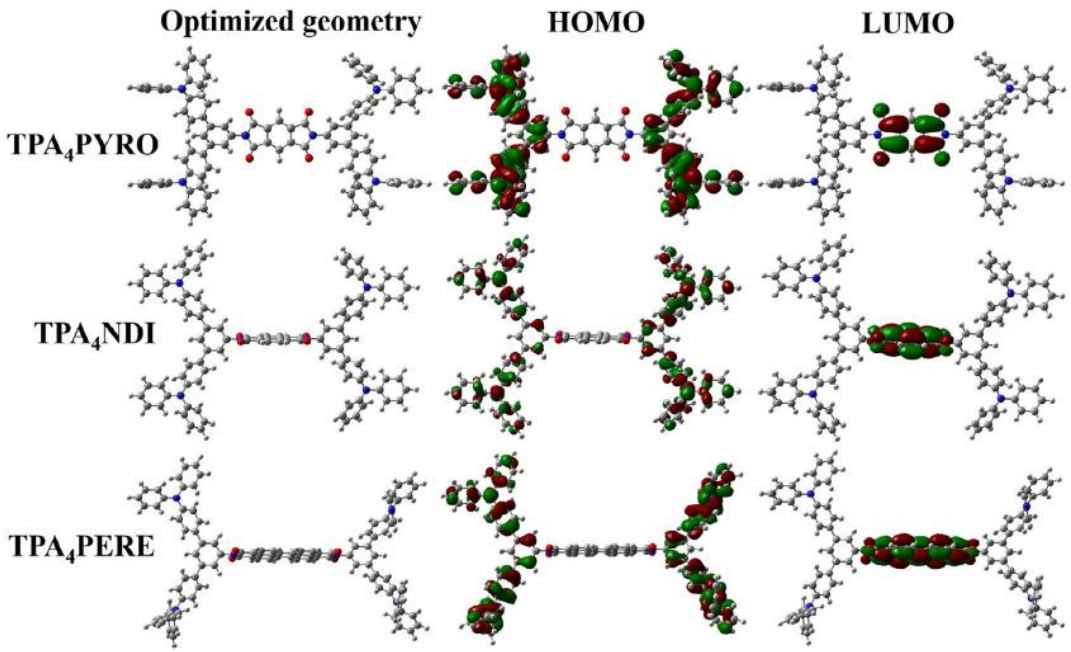

Fig. 4.14. DFT optimized geometries and HOMO-LUMO molecular orbital diagrams of the monomers.

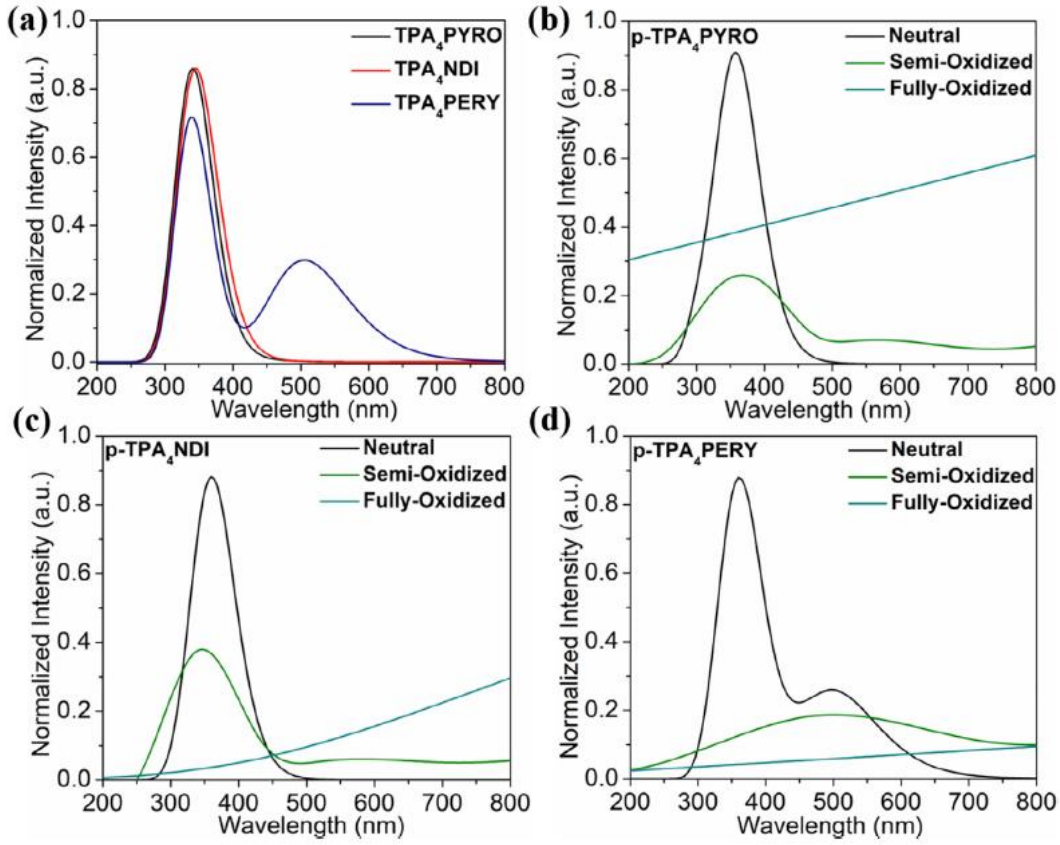

Fig. 4.15. Calculated UV–Vis absorption spectra of (a) monomers, (b-d) polymers at different oxidation states at mPW1PBE/cc-PVDZ level of theory.

Table 4.3. DFT determined HOMO and LUMO energy levels and calculated HOMO-LUMO gaps (band gaps) of monomers at mPW1PBE/cc-PVDZ level of theory.

Monomers	HOMO (eV)	LUMO (eV)	HOMO-LUMO gap (band gap) in eV
TPA_4PYRO	-5.36	-3.18	2.18
TPA_4NDI	-5.35	-3.38	1.97
TPA_4PERY	-5.31	-3.53	1.78

Table 4.4. DFT determined HOMO and LUMO energy levels and calculated HOMO-LUMO gaps (band gaps) of modelled polymers at different oxidation states at mPW1PBE/cc-PVDZ level of theory.

Polymers	States	HOMO	LUMO	HOMO-LUMO gap (band gap)
p-TPA$_4$PYRO	Neutral	-5.16	-3.22	1.94
	Semi-oxidized	-8.73	-8.44	0.29
	Fully-oxidized	-12.19	-11.97	0.22
p-TPA$_4$NDI	Neutral	-5.15	-3.48	1.67
	Semi-oxidized	-8.71	-8.43	0.28
	Fully-oxidized	-12.14	-11.85	0.27
p-TPA$_4$PERY	Neutral	-5.13	-3.61	1.52
	Semi-oxidized	-8.43	-8.20	0.23
	Fully-oxidized	-11.41	-11.19	0.22

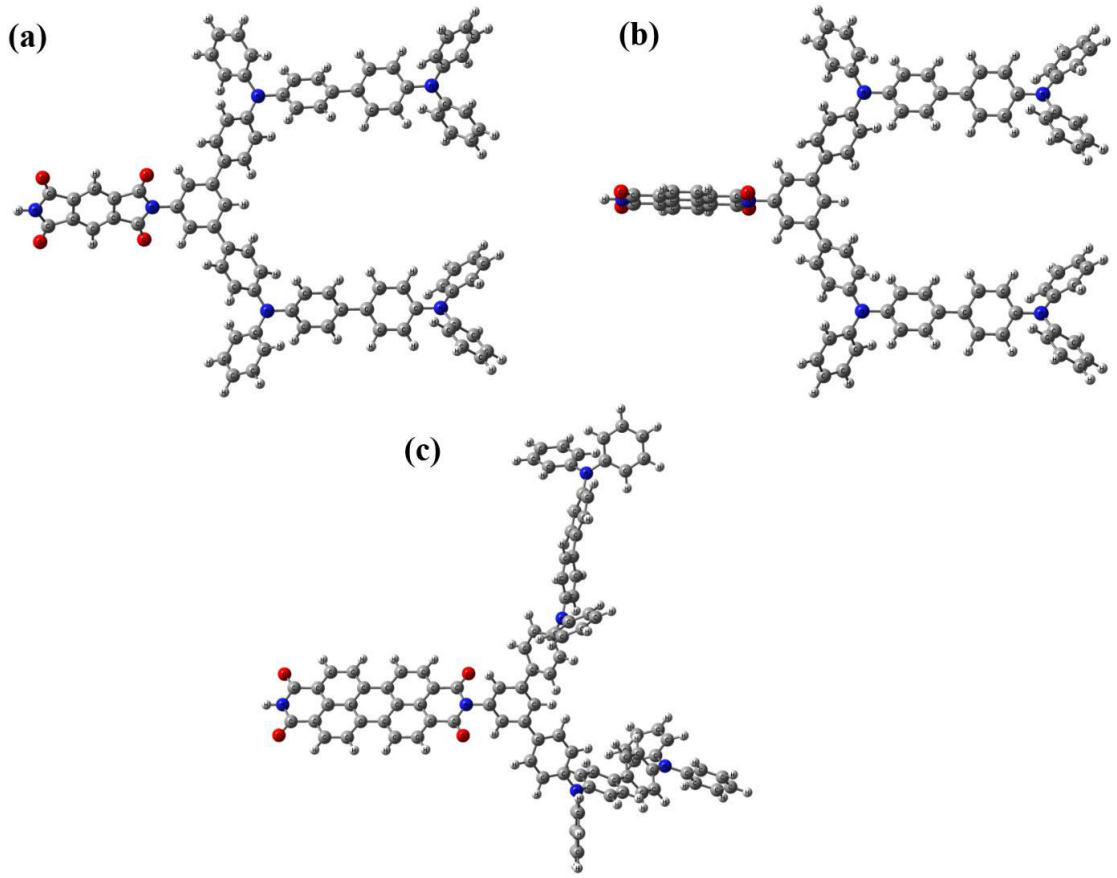

Fig. 4.16: DFT optimized geometries of different modelled polymers (a) **p-TPA$_4$PYRO**, (b) **p-TPA$_4$NDI**, (c) **p-TPA$_4$PERY**.

Solid-state ECD: For commercial utilization, it was very much important to fabricate ECDs exhibiting proper response with high ΔT. Therefore, besides the EC study in solution state, solid-state ECD was fabricated with gel electrolyte following the working principle of two electrode system. At the initial stage, the polymer was electrodeposited on ITO coated glass, rinsed with DCM and acetone to remove the monomers and oligomers and then dried properly. The transparent conducting gel electrolyte prepared from PMMA and $LiClO_4$ plasticized with propylene carbonate was spread on the polymer deposited side of ITO glass acted as working electrode, was sandwiched with ITO coated side of another ITO glass acted as counter electrode and was sealed by epoxy resin and kept on oven for 1 h at 60 °C.

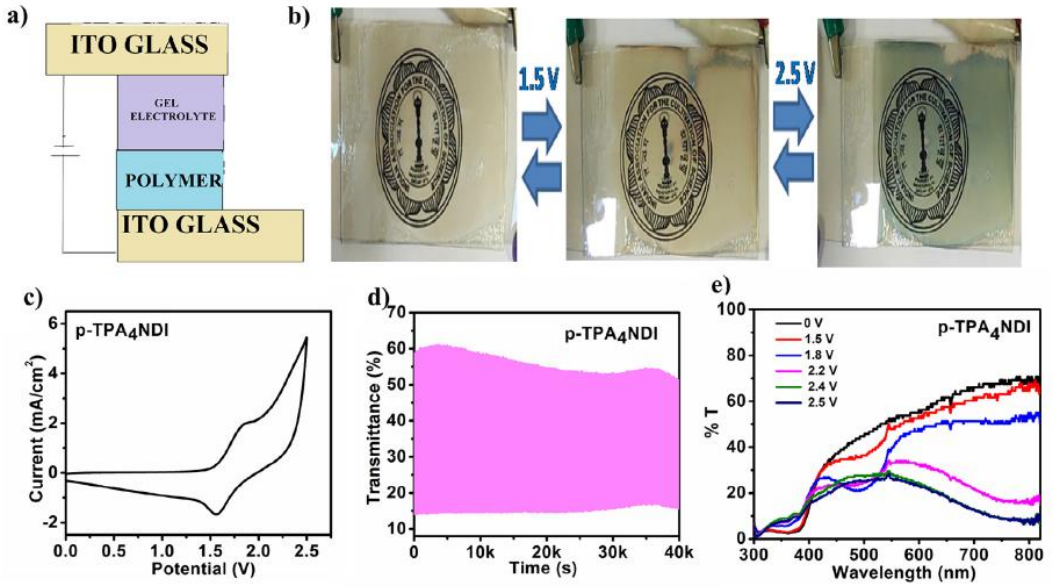

Fig. 4.17. For p-TPA$_4$NDI: (a) Schematic diagram of the device formation, (b) Device (5 × 5 cm^2) colour change with applying Voltage, (c) Represent CV of the device, (d) Cyclic stability over 4000 cycles upon applying voltages of 0/2.5 V with a holding time of 10 s. (e) Voltage dependent Transmittance changes.

The fabricated devices (5×5 cm^2) exhibited the EC change from colourless to brown by applying 1.5 V and colourless to deep blue by applying 2.5 V in a reversible way **(Fig.4.17b).** Cyclic voltametric studies of the three devices **(Fig. 4.17c, 4.19)** were performed at the potential windows from 0 to 2.5 V. The oxidation peaks appeared at 2.26, 1.85, 2.21 V respectively and reduction peak appeared at 2.05, 1.55, 1.72 V respectively for the three devices. Further, the device from p-TPA$_4$NDI (5 × 5 cm^2) showed an extremely high cyclic stability with an almost unchanged ΔT (9%) for 4000 cycles from 0 to 2.2 V at 740 nm wavelength. The ΔT value changed only 7% after 2000 cycles and 9% after 4000 cycles for ECD made of p-TPA$_4$NDI **(Fig. 4.17d).** The corresponding current flow between cathodes and anodes revealed a constant charge flow with time and it indicates a proper charge balance between two electrodes. Voltage dependent UV-Vis absorption studies also supported the colour changing to colourless brown and dark blue at 1.5 V and 2.5 V respectively with generation of the peaks at 500 and 740 nm **(Fig. 4.17e).**

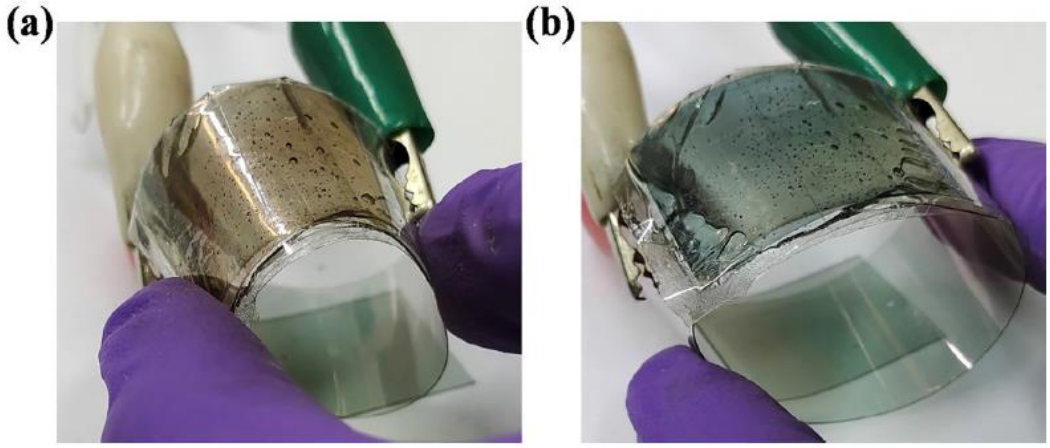

Fig. 4.18. The colour of the flexible device made of p-TPA4NDI on PET-ITO at applying voltage (a) 1.5 V and (b) 2.5 V, respectively.

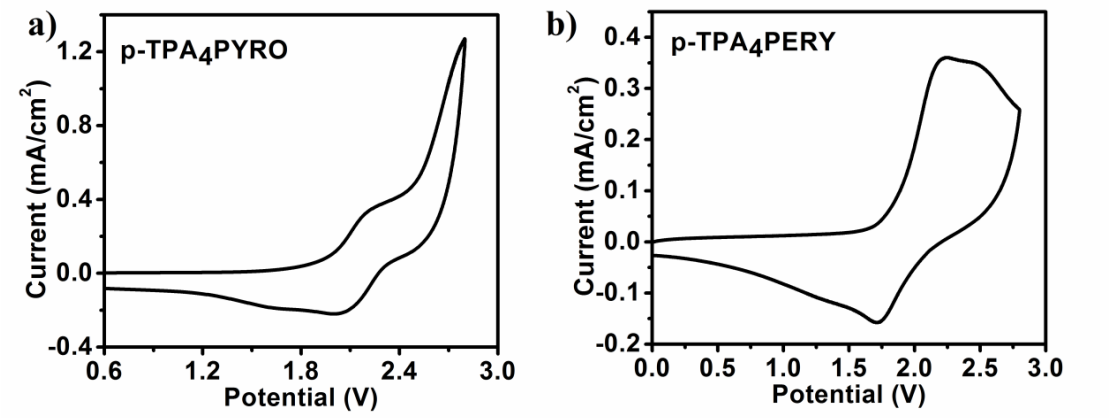

Fig. 4.19. a) b) CV studies from device of **p-TPA4PYRO** and **p-TPA4PERY.**

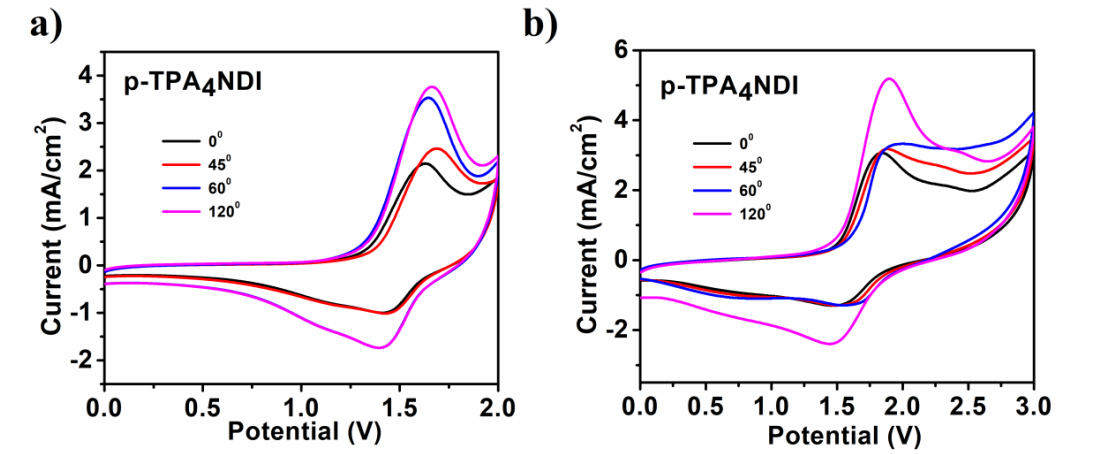

Fig. 4.20. CV from the flexible device of **p-TPA4NDI** at different bending angle with potential window a) **0-1.5 V** and b) **0-3.0 V**.

The solid-state device made of p-TPA$_4$NDI on PET-ITO (area = 4 cm × 2.5 cm, **Fig. 4.18**) was fabricated also to demonstrate the flexibility nature of device. It was observed from CV studies at various bending angles (45^0, 60^0, 120^0, 180°) that device made of p-TPA$_4$NDI reveal the same peak position in CV with different bending angles like at 1.5 V and 2.5 V **(Fig. 4.20)** and it suggested that there was no damage of the EC polymer film upon bending at different angles. Clearly, from the ECD study of p-TPA$_4$NDI exhibited a high optical contrast, rapid switching times, and long-life stability. The ECD device (p-TPA$_4$NDI) was comparable to various reported metal organic based ECDs showing high cycle stability but it was a rare example of pure organic based ECD showing high cycle stability with high coloration efficiency.

Comparative Studies based on literature surveys

Table 4.5. Electrochromic properties of our material in comparison with other ECMs.

Materials	**Polymer binding unit**	**Colouration efficiency**	**Device performance (operating voltage)**	**Device switching performance**	**References**
TPA$_4$NDI	**TPA**	**847**	**0/+2.5 V**	**4000 cycles**	**This work**
TPA$_6$ISO	TPA	410	0/+2.5 V	90 cycles	(37)
TPACNANT	TPA	371	0/+2.5 V	---	(38)
TPAANT	TPA	222	0/+1.6 V	---	(39)
CONASHs	TPA based terpyridine	123	-0.5/3.0V	---	(45)
π-Conjugated polymer	Dioxythiophene and Dioxypyrrole	---	-1/+1V	900 cycles	(46)
Small organic molecule	Viologen	274	0/1.2V	10,000 cycles	(47)
Metal oxide	WO_3	118	---	---	(48)
Metal-organic Molecular assemblies	Polypyridyl/ Fe, Ru and Os	474	−2.5 V to +3 V	75 cycles	(49)

Donor Acceptor conjugated polymer	Aromatic diimide	303	---	---	(50)
1,3,5-tris(4-pyridylium)bromides	Pyridine	327	---	---	(51)
NDI cored pyridinium salt	Pyridine	201	-1.4 V to 0 V	720 cycles	(61)
various substituent benzene	Viologen	---	-1.6 V to 0 V	---	(52)
PEB	Thiophene	1240	---	---	(53)

4.3. Conclusion

In summary, three donor - acceptor - donor (D-A-D) based moieties (TPA_4PYRO, TPA_4NDI, TPA_4PERY) were synthesized by the convenient condensation of pyromellitic dianhydride, naphthalenetetracarboxylic dianhydride, perylenetetracarboxylic dianhydride respectively with the designed TPA based donor moiety in dry DMF. All the synthesized molecules were characterized by and ^{1}H, ^{13}C NMR, MALDI - TOF mass and FTIR results. Electropolymerized films made of individual moiety on ITO glass surface were checked by absorption and spectro-electrochemistry techniques. To have energy minimized structure and to rationalize the mechanism of electropolymerization, DFT studies were performed. It revealed that HOMO was exclusively located on the TPA unit and it facilitated the electro-oxidation process to form polymer films. The electrochromic behaviours of the deposited polymers on ITO revealed reversible colour change of colourless to brown to deep blue in the anodic region by applying voltage 0 to 0.9 V to 1.2 V and also colourless to deep pink in the cathodic region with the voltage change of 0 to −2 V with high optical contrast (up to 67%), low switching times, and high coloration efficiencies (up to 847 cm^2/C). The reversibility of the electrochromic transition was shown for several switching cycles (l0,000 cycles for anodic and 600 cycles for cathodic process) for p-TPA_4NDI film. The fabrication of 5 × 5 cm^2 solid-state electrochromic device and solid state flexible device operated at a potential range of 0 to 2.5 V was successfully demonstrated by exhibiting a reversible electrochromic

colour change with the retention of 91% after 4000 switching cycles for p-TPA_4NDI. Interestingly, simulated absorption spectra from TDDFT calculations disclosed that bathochromic shifts of the absorption peak of the polymer upon oxidation was mainly responsible for the electrochromic behaviour. Moreover, substantial lowering of HOMO and LUMO energy levels as well as HOMO-LUMO gaps of the polymers in their oxidized states caused high intensity electronic transitions to occur in the visible wavelength region originating different colours. Overall, the present work introduced a series of fully organic based EC systems which showed excellent EC parameters. The highest electrochemical stability of the ECD made of p-TPA_4NDI might provide a hint that it might compete as potential EC materials for next-generation display applications along with the promising application in energy-saving buildings, smart windows, traffic signs, electronic paper, sunglasses, and so forth.

4.4. Experimental section

4.4.1. Materials required

Triphenylamine (TPA), $Pd(PPh_3)_4$, bis (pinacolato) diboron, $Pd(dppf)Cl_2$, calcium hydride, tetra-butyl ammonium perchlorate (TBAP), lithium perchlorate ($LiClO_4$), polymethylmethacrylate (PMMA), silver chloride (AgCl), propylene carbonate, pyromellitic dianhydride, naphthalenetetracarboxylic dianhydride, perylenetetracarboxylic dianhydride were purchased from Sigma Aldrich and used as received. Benzophenone, potassium acetate (KOAc), sodium carbonate (Na_2CO_3), sodium hydroxide (NaOH), sodium sulphate (Na_2SO_4), liquid bromine (Br_2), concentrated sulphuric acid (H_2SO_4), conc. HCl, acetic acid were purchased from Merck chemicals. N-bromo succinimide was purchased from Avra chemicals which was used after recrystallization. 4-Nitroaniline, $SnCl_2$ were purchased from Avra chemicals. Bulk solvents like acetonitrile (ACN), dichloromethane (DCM), chloroform ($CHCl_3$), methanol (MeOH), tetra-hydrofuran (THF), dioxane, dimethyl formamide (DMF), diethyl ether, pet ether and analytical grade reagents were used without further purification. DMF, acetonitrile, DCM and 1, 4-dioxane were dried by anhydrous calcium hydride and THF was drying by refluxing with sodium and benzophenone. Indium tin oxide (ITO) coated glass (MTI Corporation Ltd.) was used

as working electrode, cleaned by double distilled water, ethanol and acetone successively with sonication. ITO coated polyethylene terephthalate film (ITO-PET) was also used as working electrode purchased from Sigma Aldrich.

4.4.2. Measurements

The ^{1}H and ^{13}C NMR spectra were recorded on a Bruker 500 or 400 MHz spectrometer using chloroform-d ($CDCl_3$), dimethyl sulphoxide-d (DMSO d_6), N, N-dimethyl formamide (DMF-d_7) as solvent and tetramethylsilane (TMS) as an internal standard. MALDI-TOF (matrix assisted laser desorption ionization time-of-flight) mass spectrometry was carried out with Bruker Daltonics ultraflextreme. Fourier transformed infrared (FT-IR) spectra were measured on a Horiba FT- 720 FT-IR spectrometer with KBr pellets. The UV–visible absorption spectrum was recorded on an Ocean Optics DH-mini UV–VIS-NIR light source and Ocean Optics flame Miniature Spectrometer. The electrochemical measurements were performed by using a CHI6087E electrochemical workstation.

Preparation of polymer film on conductive surface: Polymer films were formed on transparent indium tin oxide (ITO)-coated glass (resistivity 8 Ω/ cm^2) by electropolymerisation process. Before film preparation, ITO glasses were cleaned with acetone, isopropanol, ethanol and doubled distilled water with sonication and dried on oven. The electrochemical workstation was first calibrated using Ferrocene as an external standard (+0.44 V vs Ag/AgCl). With the use of a three-electrode cell, ITO coated glass slides as working electrode and Ag/AgCl as reference electrode, Pt wire as counter electrode using 5×10^{-4} M monomer solution in 0.1 M electrolytic TBAP solution in dry DCM, the polymer was deposited on ITO glass via repetitive number of cycles with the potential barrier from 0 to 1.5 V at a scan rate 50 mV/s at room temperature with purging nitrogen gas. Using ITO–PET as working electrode, the electropolymerisation was performed at the identical condition method. With the increasing no of CV scans, peak current was also increased and the deposition of the polymer films on ITO surface was noticed.

A. **Synthesis:**

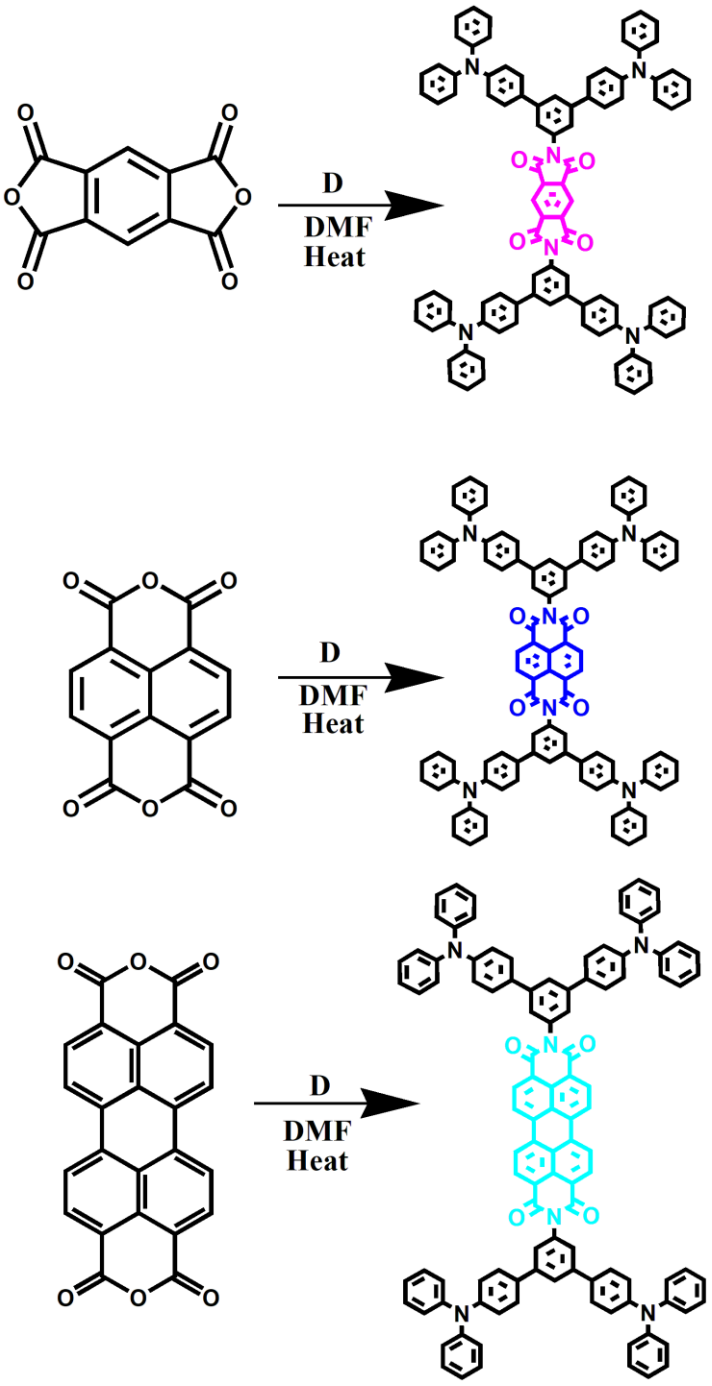

Fig. 4.21. Synthesis scheme of **TPA4PYRO**, **TPA4NDI** and **TPA4PERY.**

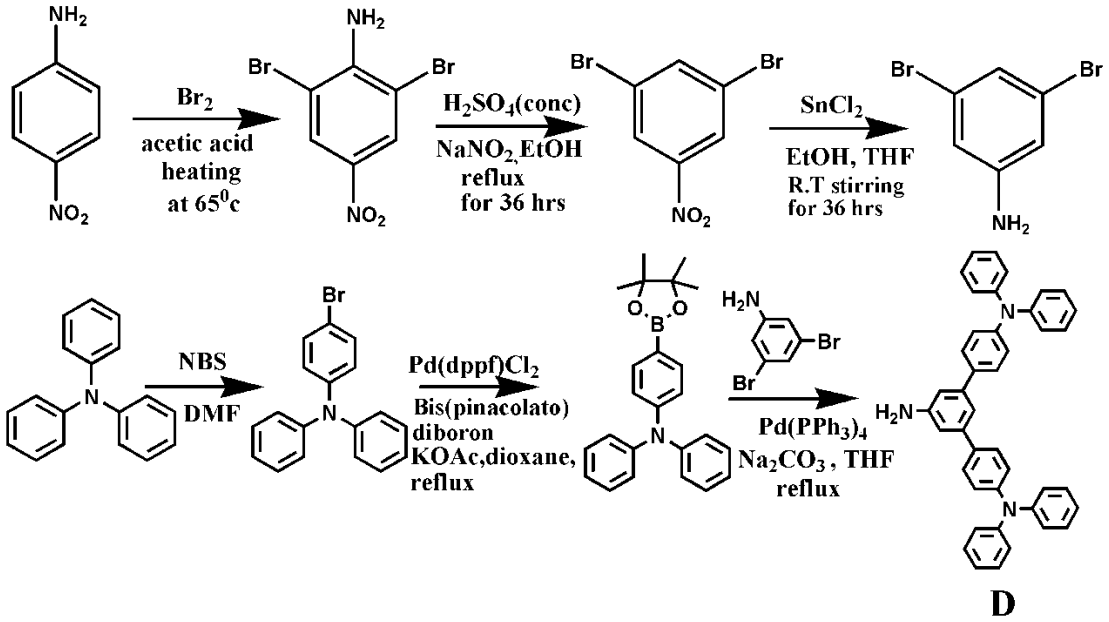

Fig. 4.22. Synthesis scheme of **D.**

4.4.3. Synthesis

Synthesis of TPA$_4$PYRO: In a two necked round bottom flask, D (65 mg, 0.112 mmol), pyromellitic dianhydride (10 mg, 0.045 mmol) were taken under nitrogen gas, dry DMF (2 ml) was added to it, heated for 18 hrs at 140 ℃. After cooling the reaction mixture, MeOH was added dropwise to it, a brown coloured precipitate was appeared, it was filtered and dried in vacuum oven. The precipitate was purified by column chromatography using the mixture of pet ether and DCM (2:1) with yield 55% (33 mg).

^{1}H NMR (400 MHz, CDCl$_3$, TMS) δ (ppm)): 8.46 (2H, s), 8.02 (2H, s), 7.32–7.27 (12H, d), 7.17–7.15 (32H, m), 7.10–7.06 (16H, m).

^{13}C NMR (100 MHz, CDCl$_3$, TMS) δ (ppm)): 163.23, 147.71, 129.49, 129.41, 128.16, 127.49, 124.96, 124.76, 124.69, 124.49, 123.81, 123.32, 123.23, 123.04.

Mass (MALDI-TOF, **diathranol matrix):** m/z calculated 1341.55, found 1341.16.

FTIR (cm^{-1}): 2917, 1772, 1724, 1597, 1499, 1333.

Synthesis of TPA$_4$NDI: In a two necked round bottom flask, D (27 mg, 0.046 mmol), naphthalenetetracarboxylic dianhydride (5 mg, 0.018 mmol) were taken under

nitrogen gas, dry DMF (2 ml) was added to it, heated for 24 hrs at 140 °C. After cooling the reaction mixture, MeOH was added to it, a blue coloured precipitate was appeared, it was filtered and dried in vacuum oven. The precipitate was purified by column chromatography using the mixture of pet ether and DCM (1:1) with yield 62% (40 mg).

^{1}H NMR: (400 MHz, $CDCl_3$, TMS) δ (ppm)): 8.89 (4H, s), 7.90 (2H, s), 7.56–7.54 (8H, m), 7.50 (6H, s), 7.35 (4H, d), 7.29–7.26 (6H, m), 7.15–7.14 (4H, m), 7.13–7.12 (20H, m), 7.04 (10 H, m).

^{13}C NMR: (100 MHz, $CDCl_3$, TMS) δ (ppm)): 163.23, 147.87–147.76, 142.93, 134.13, 131.67, 129.46, 128.19, 127.29, 125.22, 124.70, 123.88, 123.24.

Mass (MALDI-TOF, diathranol matrix): m/z calculated 1391.61, found 1390.55.

FTIR (cm^{-1}): 2930, 1727, 1680, 1576, 1484, 1330.

Synthesis of TPA_4PERY: In a round bottom flask, D (18 mg, 0.031 mmol), Perylenetetracarboxylic dianhydride (5 mg, 0.012 mmol) were inert properly with nitrogen, dry DMF (4 ml) was added to it, heated for 48 hrs at 155 °C. After cooling the reaction mixture, MeOH was added to it, a red coloured precipitate was appeared, it was filtered and dried in vacuum oven with yield 40% (19 mg).

^{1}H NMR: (400 MHz, $DMFd_7$, δ (ppm)): 8.49 (4H, s), 8.35 (4H, s), 7.83 (2H, d), 7.79 (8H, m), 7.68–7.65 (6H, t), 7.38–7.34 (4H, d), 7.34 (6H, m), 7.13 (4H, m), 7.10 (20H, m), 6.96 (10H, m).

Mass (MALDI-TOF, diathranol matrix): m/z calculated 1515.75, found 1515.81.

FTIR (cm^{-1}): 2925, 1720, 1670, 1590, 1484, 1302.

B. **NMR, MASS and IR spectra:**

i)

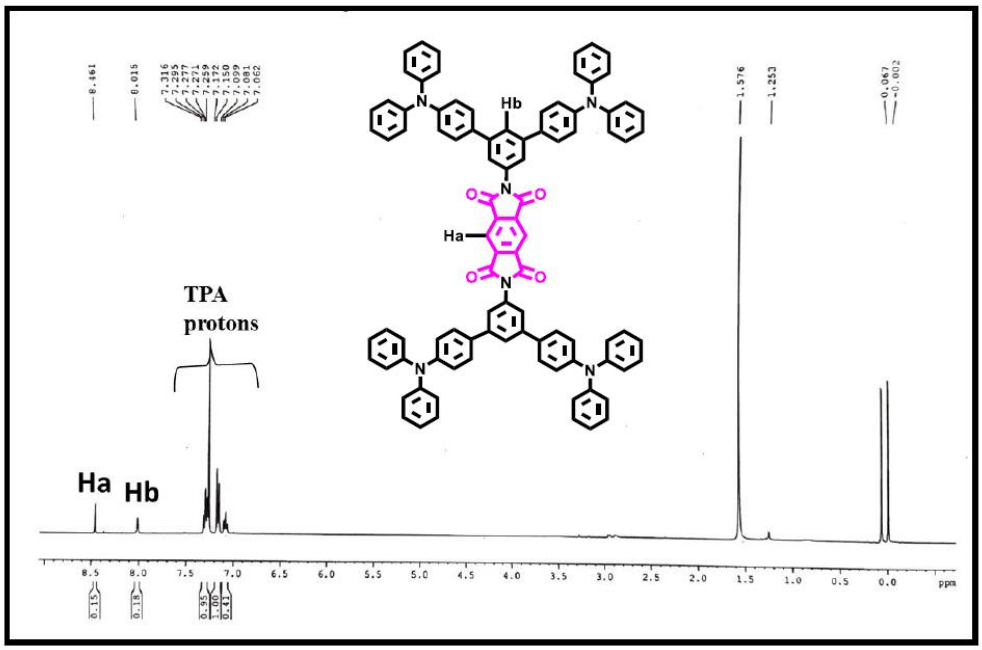

ii)

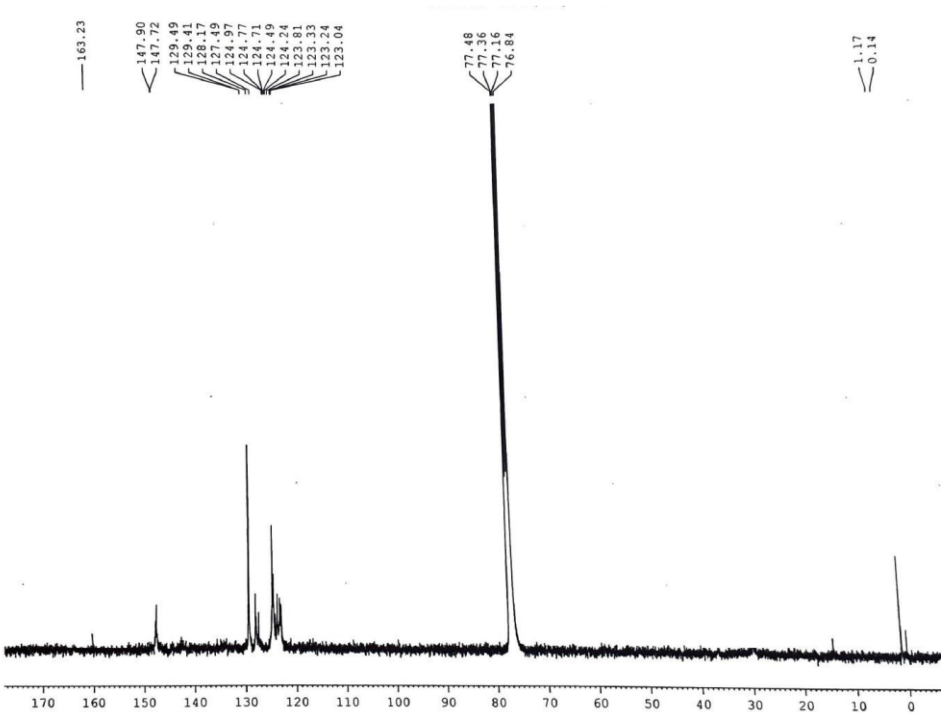

iii)

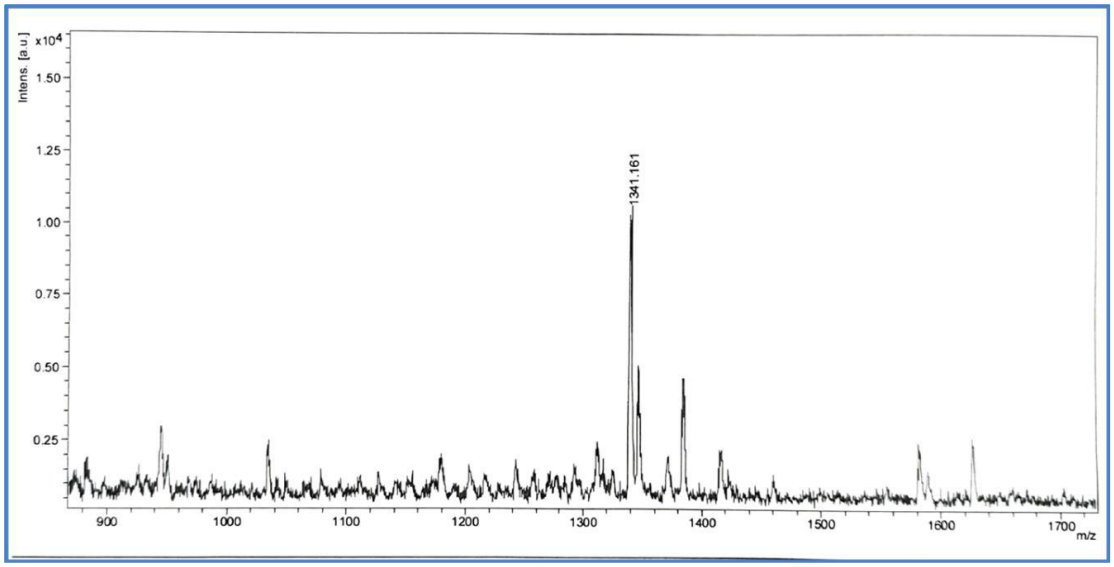

Fig. 4.23. i)^{1}H NMR ii)^{13}C NMR spectra in $CDCl_3$ iii)MALDI-TOF spectra of **TPA_4PYRO.**

i)

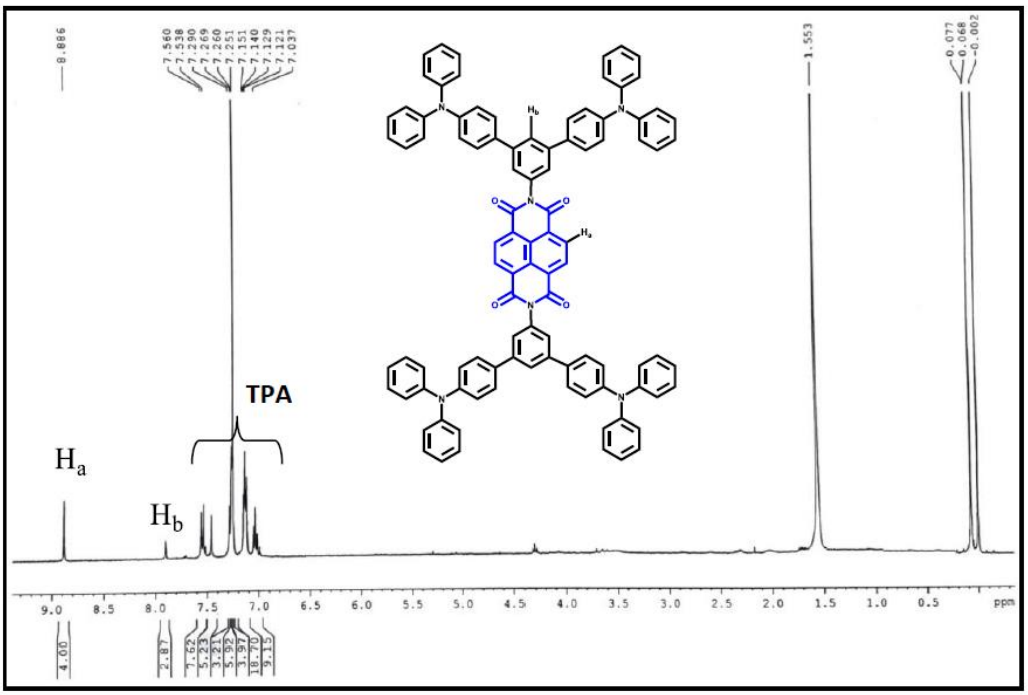

ii)

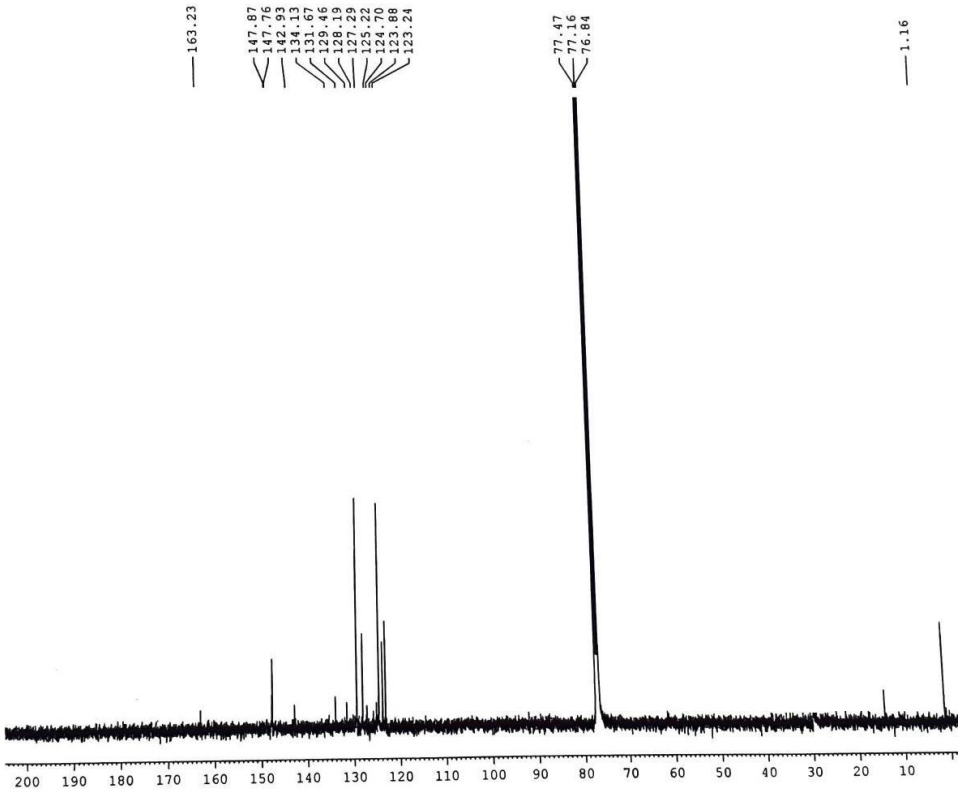

iii)

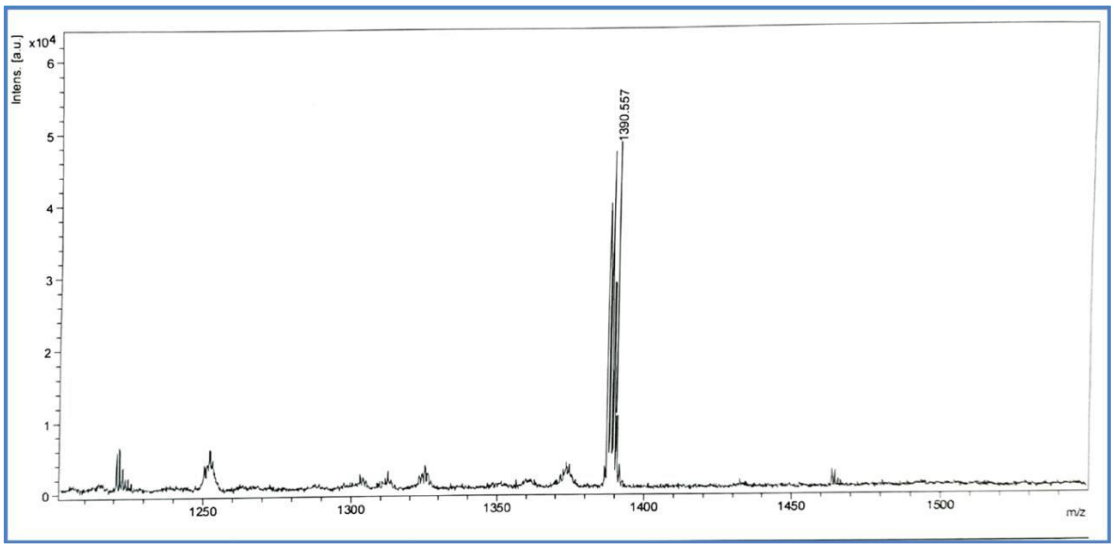

Fig. 4.24. i) ^{1}H NMR, ii) ^{13}C NMR spectra in CDCl3 and iii)MALDI-TOF spectra of **TPA$_4$NDI.**

i)

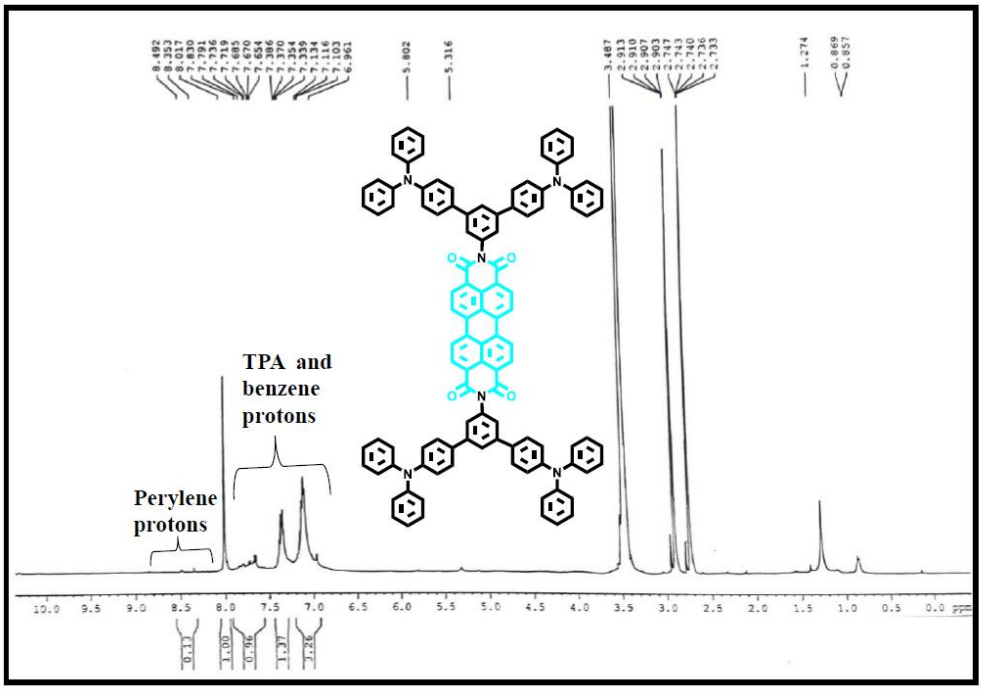

ii)

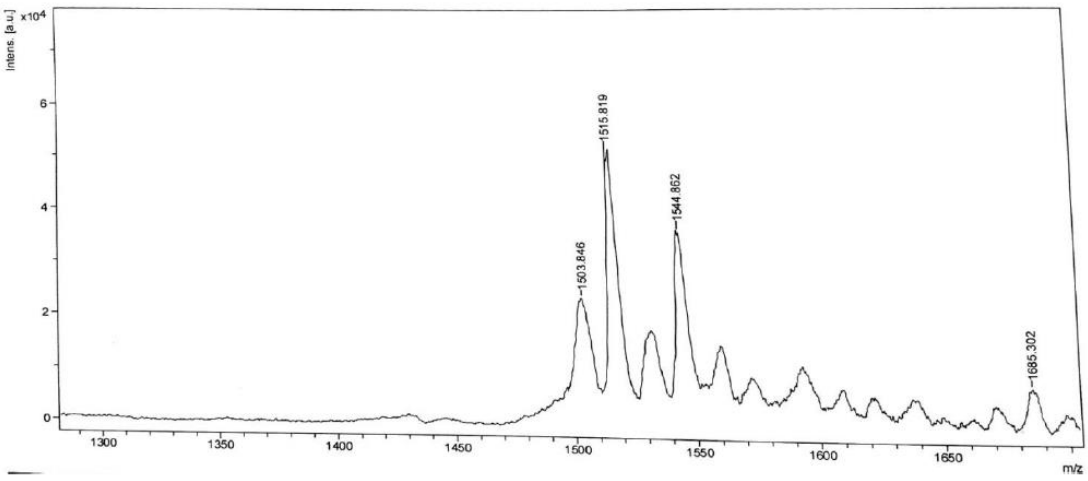

Fig. 4.25. i)^{1}H NMR in DMFd7 and ii) MALDI-TOF spectra of **TPA$_4$PERY.**

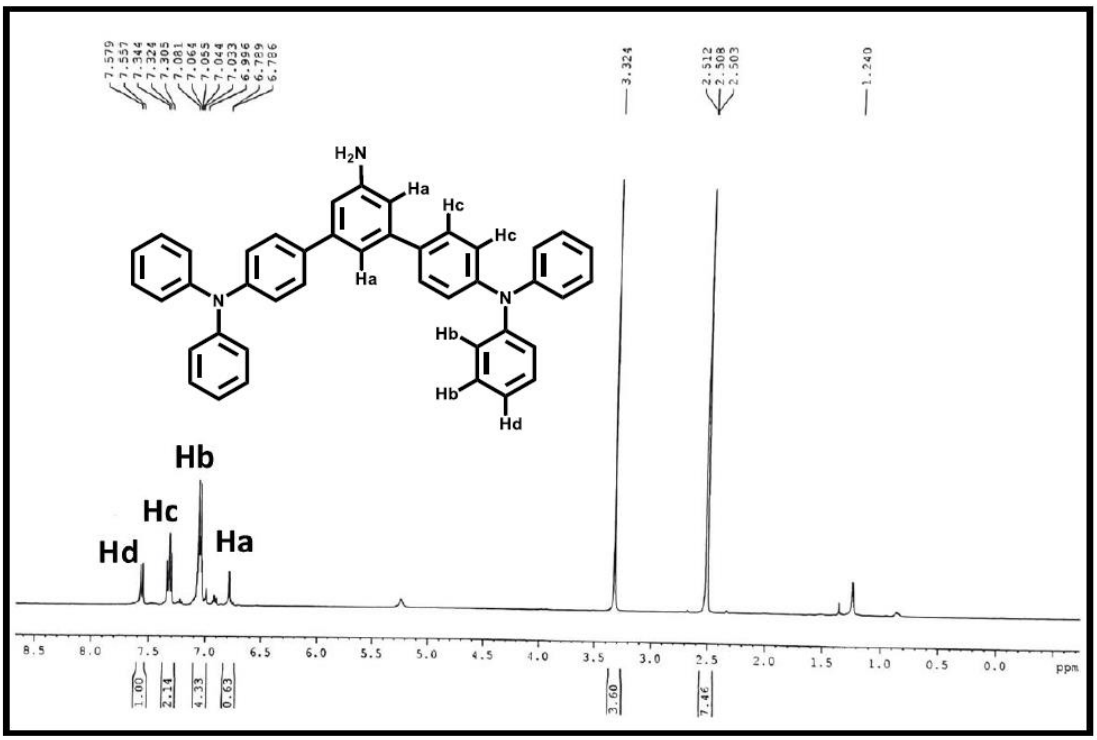

Fig. 4.26. i) ^{1}H NMR in CDCl3 of **D**

4.5. References

[1] R. J. Mortimer, Annu. Rev. Mater. Res. 41 (1) (2011) 241–268.

[2] C. G. Granqvist, Thin Solid Films. 564 (2014) 1–38.

[3] G. Sonmez, H. B. Sonmez, J. Mater. Chem. 16 (2006) 2473–2477.

[4] G. Cai, P. Darmawan, M. Cui, J. Wang, J. Chen, S. Magdassi, P. S. Lee, Adv. Energy Mater. 6 (2016) 1–8.

[5] R. J. Mortimer, Electrochim. Acta 44 (1999) 2971–2981.

[6] P. M. Beaujuge, J. R. Reynolds, Chem. Rev. 110 (2010) 268–320.

[7] F. A. Arroyave, J. R. Reynolds, Macromolecules 45 (2012) 5842–5849.

[8] E. P. Knott, M. R. Craig, D. Y. Liu, J. E. Babiarz, A. L. Dyer, J. R. Reynolds, J. Mater. Chem. 22 (2012) 4953–4962.

[9] M. Li, A. Patra, Y. Sheynin, M. Bendikov, Adv. Mater. 21 (2009) 1707–1711.

[10] E. N. Esmer, S. Tarkuc, Y. A. Udum, L. Toppare, Mater. Chem. Phys. 131 (2011) 519–524.

[11] F. Chen, J. Zhang, H. Jiang, X. Wan, Chem. - Asian J. 8 (2013) 1497–1503.

[12] R. Kumar, R. G. Pillai, N. Pekas, Y. Wu, R. L. McCreery, J. Am. Chem. Soc. 134 (2012) 14869–14876.

[13] D. A, G. Hegde, RSC Adv. 5 (2015) 88339–88352.

[14] S. K. Hau, H. L. Yip, A. Y. Jen, Polym. Rev. 50 (2010) 474–510.

[15] M. Wang, X. Xing, I. F. Perepichka, Y. Shi, D. Zhou, P. Wu, H. Meng, Adv. Energy Mater. 9 (2019) 1900433.

[16] G. Cai, J. Wang, P. S. Lee, Acc. Chem. Res. 49 (2016) 1469–1476.

[17] L. Wang, X. Zhang, X. Chen, X. Li, Y. Zhao, W. Li, J. Zhao, Z. Chen, Y. Li, J. Mater. Chem., C 9 (2021) 1641–1648.

[18] A. Cannavale, U. Ayr, F. Fiorito, Energies 13 (2020) 1–17.

[19] Y. Y. Song, Z. D. Gao, J. H. Wang, X. H. Xia, R. Lynch, Adv. Funct. Mater. 21 (2011) 1941–1946.

[20] Y. C. Nah, A. Ghicov, D. Kim, S. Berger, P. Schmuki, J. Am. Chem. Soc. 130 (2008) 16154–16155.

[21] P. M. Beaujuge, C. M. Amb, J. R. Reynolds, Adv. Mater. 22 (2010) 5383–5387.

[22] E. C. Rios, A. V. Rosario, A. Nogueira, L. Micaroni, Sol. Energy Mater. Sol. Cells 94 (2010) 1338–1345.

[23] P. J. Shi, M. Amb, E. P. Knott, E. J. Thompson, D. Y. Liu, J. G. Mei, A. L. Dyer, J. R. Reynolds, Adv. Mater. 22 (2010) 4949–4953.

[24] R. Li, K. Li, G. Wang, L. Li, Q. Zhang, J. Yan, Y. Chen, Q. Zhang, C. Hou, H. Wang, ACS Nano 12 (2018) 3759–3768.

[25] S. H. Hsiao, Y. Z. Chen, Dye. Pigment. 144 (2017) 173–183.

[26] S. K. Deb, Sol. Energy Mater. Sol. Cells 25 (1992) 327–338.

[27] C. K. Lo, D. E. Shen, J. R. Reynolds, Macromolecules 52 (2019) 6773–6779.

[28] D. T. Christiansen, J. R. Reynolds, Macromolecules 51 (2018) 9250–9258.

[29] M. Keersmaecker, J. R. Reynolds, ACS Appl. Mater. Interfaces 11 (2019) 47131–47142.

[30] A. Chaudhary, G. Siva Kumar, D. K. Pathak, M. Tanwar, R. Misra, R. J. Kumar, J. Mater. Chem. C 9 (2021) 3462–3469.

[31] P. Andersson, R. Forchheimer, P. Tehrani, M. Berggren, Adv. Funct. Mater. 17 (2007) 3074–3082.

[32] C. E. Patil, N. L. Tarwal, P. S. Shinde, H. P. Deshmukh, P. S. Patil, J. Phys. D: Appl. Phys. 42 (2008) 25404.

[33] A. Chaudhary, D. K. Pathak, S. Mishra, P. Yogi, P. R. Sagdeo, R. Kumar, Sol. Energy Mater. Sol. Cells 188 (2018) 249–254.

[34] E. Said, P. Andersson, I. Engquist, X. Crispin, M. Berggren, Org. Electron. 10 (2009) 1195–1199.

[35] G. Gunbas, L. Toppare, Chem Commun. 48 (2012) 1083–1101.

[36] X. Lv, W. Li, M. Ouyang, Y. Zhang, D. S. Wright, C. Zhang, J. Mater. Chem. C 5 (2017) 12–28.

[37] S. Nad, S. Malik, ChemElectroChem 7 (2020) 4144–4152.

[38] D. C. Santra, S. Nad, S. Malik, J. Electroanal. Chem. 823 (2018) 203–212.

[39] D. Chandra Santra, S. Mondal, S. Malik, RSC Adv. 6 (2016) 81597–81606.

[40] D. Sek, B. Jarzabek, E. Grabiec, B. Kaczmarczyk, H. Janeczek, A. Sikora, A. Hreniak, M. Palewicz, M. Lapkowski, K. Karon, A. Iwan, Synth. Met. 160 (2010) 2065–2076.

[41] H. Xia, J. He, P. Peng, Y. Zhou, Y. Li, W. Tian, Tetrahedron Lett. 48 (33) (2007) 5877–5881.

[42] H. J. Yen, H. Y. Lin, G. S. Liou, Chem. Mater. 23 (2011) 1874–1882.

[43] A. G. M. Ferrari, C. W. Foster, P. J. Kelly, D. A. C. Brownson, C. E. Banks, Biosens 8 (2018) 53.

[44] P. M. S. Monk, R. J. Mortimer, D. R. Rosseinsky, Electrochromism and Electrochromic Devices, Cambridge University Press, Cambridge, UK, 2007, pp. 25–62.

[45] Y. Liu, R. Sakamoto, C. L. Ho, H. Nishihara, W. Y. Wong, J. Mater. Chem., C 7 (2019) 9159–9166.

[46] S. L. Pittelli, D. E. Shen, A. M. Österholm, J. R. Reynolds, ACS Appl. Mater. Interfaces 10 (2018) 970–978.

[47] H. C. Lu, S. Y. Kao, H. F. Yu, T. H. Chang, C. W. Kung, K. C. Ho, ACS Appl. Mater. Interfaces 8 (2016) 30351–30361.

[48] G. Cai, M. Cui, V. Kumar, P. Darmawan, J. Wang, X. Wang, A. Lee-Sie Eh, K. Qian, P. S. Lee, Chem. Sci. 7 (2016) 1373–1382.

[49] N. Elool Dov, S. Shankar, D. Cohen, T. Bendikov, K. Rechav, L. J. W. Shimon, M. Lahav, M. E. van der Boom, J. Am. Chem. Soc. 139 (2017) 11471–11481.

[50] A. Drewniak, M. D. Tomczyk, K. Knop, K. Z. Walczak, P. Ledwon, Macromolecules 52 (2019) 8453–8465.

[51] L. Ma, S. Xiao, N. Wu, S. Zhao, D. Xiao, Dye. Pigment 168 (2019) 327–333.

[52] Y. Shi, G. Wang, Q. Chen, J. Zheng, C. Xu, Sol. Energy Mater. Sol. Cells 208 (2020) 110413.

[53] R. D. Rauh, F. Wang, J. R. Reynolds, D. L. Meeker, Electrochim. Acta 46 (2001) 2023–2029.

[54] W. Caia, Q. Lua, S. Wanga, T. Xiaoa, H. Niua, W. Wang, J. Electroanal. Chem. 801 (2017) 388–394.

[55] M. J. Frisch, G. W. Trucks, H. B. Schlegel, G. E. Scuseria, M. A. Robb, J. R. Cheeseman, G. Scalmani, V. Barone, G. A. Petersson, H. Nakatsuji, M. Caricato, A. V. Marenich, J. Bloino, B. G. Janesko, R. Gomperts, B. Mennucci, H. P. Hratchian, J. V. Ortiz, A. F. Izmaylov, J. L. Sonnenberg, D. Williams-Young, F. Ding, F. Lipparini, F. Egidi, J. Goings, B. Peng, A. Petrone, T. Henderson, D. Ranasinghe, V. G. Zakrzewski, J. Gao, N. Rega, G. Zheng, W. Liang, M. Hada, M. Ehara, K. Toyota, R. Fukuda, J. Hasegawa, M. Ishida, T. Nakajima, Y. Honda, O. Kitao, H. Nakai, T. Vreven, K. Throssell, J. A., Jr.Montgomery, J. E. Peralta, F. Ogliaro, F. M. J.

Bearpark, J. J. Heyd, E. N. Brothers, K. N. Kudin, V. N. Staroverov, T. A. Keith, R. Kobayashi, J. Normand, K. Raghavachari, A. P. Rendell, J. C. Burant, S. S. Iyengar, J.Tomasi, M. Cossi, J. M. Millam, M. Klene, C. Adamo, R. Cammi, J. W. Ochterski, R. L. Martin, K. Morokuma, O. Farkas, J. B. Foresman, D. J. Fox, Gaussian 16, Revision C.01, Gaussian, Inc., Wallingford CT, (2016).

[56] A. D. Becke, J. Chem. Phys. 98 (1993) 5648–5652.

[57] A. K. Rappe, C. J. Casewit, K. S. Colwell, W. A. Goddard, W. M. Skiff, J. Am. Chem. Soc. 114 (1992) 10024–10035.

[58] V. Barone, M. Cossi, J. Phys. Chem. A 102 (1998) 1995–2001.

[59] D. L. Wheeler, L. E. Rainwater, A. R. Green, A. L. Tomlinson, Phys. Chem. Chem. Phys 19 (2017) 20251–20258.

[60] T. M. McCormick, C. R. Bridges, E. I. Carrera, P. M. DiCarmine, G. L. Gibson, J. Hollinger, L. M. Kozycz, D. S. Seferos, Macromolecules 46 (2013) 3879–3886.

[61] F. Li, Z. J. Huang, Q. H. Zhou, M. Y. Pan, Q. Tang, C. B. Gong, J. Mater. Chem. C. 8 (2020) 10031–10038.

Chapter-5

Effect of Substituents of Naphthalene Diimide derivatives on Electrochromic behaviours observed in Proto-type devices

The work reported in this chapter is under revision in Journal of Electroanalytical Chemistry.

5.1. Indoduction

Recently, electrochromic materials (ECMs) which reversibly changed optical transmission with a small applied voltage, sparked the technology of switchable thin-film coating on glass or plastic as EC panels integrated few advantages such as i) modulation of the daylight, ii) reduction of energy use or electricals loads in climate adaptive buildings and iii) beautification together to generate "smart window" **[1], [2], [3], [4], [5], [6], [7], [8].** Similarly, EC also provided the boost to electrochromic displays, electronic paper, anti-glare glass. However, making thin-film coating on the wide area with tens or thousands switching cycles was a tremendous challenge for material scientists or technologists **[9], [10], [11], [12].** Initial efforts were made with inorganic metal oxides (mainly WO_3) or metal ligand complexes by taking the advantage of good optical switching, fast response time, low driving voltage **[13], [14], [15], [16], [17], [18].** The inorganic based ECMs suffered from the effect of multichromic behaviours as well as processability **[19].** As a result, organic based ECs which enjoyed the explicit advantage of spin coating, printing, spraying onto pre-patterned panels or substrates, were recently visualized as the next generation electrochromic materials having good optical switching **[20],** fast response time, flexibility, high coloration efficiency, low driving voltage, solution processability, easy molecular design and derivability **[21], [22], [23].** To address those issues, donor-acceptor based systems which were extensively applied in field-effect transistors (FETs), molecular electronic devices, liquid crystalline devices, colorimetric sensing **[24], [25], [26], [27].** Among different Π acceptor molecules, Naphthalene diimide (NDI) was a broad interest because of its high electron affinity, good charge-carrier mobility, and excellent thermal oxidative stability **[28], [29], [30], [31].** Through proper incorporation of electro-active unit excellent electrochromic properties could be achieved in the NDI derivatives. Generally, due to the electron deficiency of the NDI, substitution on the naphthalene core could effectively change the lowest unoccupied molecular orbitals (LUMOs) and ensuing optical and electrical performances **[32], [33].**

Recently, we reported a novel NDI and four triphenylamine based (TPA_4NDI) derivatives which exhibited extremely high cycle stability (10,000 cycles) with the excellent coloration efficiency (847cm^2/C). Recently, Zhiyong Guo and Hongbing Zhan group reported pyrrole core-substituted NDI group and unsubstituted NDI group and due to interaction with the counter ion with the pyrrole nitrogen atom after oxidation, extra stabilisation was achieved towards the EC behaviour than the unsubstituted NDI **[34].** Earlier studies indicated the alteration of HOMO-LUMO level with the replacement of alkoxy /alkyl amines that, the replacement of both alkoxy donors with alkyl amines in NDI might dramatically increase the HOMO and LUMO levels and endow them with redox reversibility **[35].**

In the present chapter, four core substituted NDI based derivatives (BRTPANDI, CNTPANDI, PHTPANDI, NPYTPANDI) were designed **[Fig.5.01],** prepared and investigated their electrochemical and electrochromic behaviour in combination with density functional theory (DFT) calculations. Incorporation of bulky, packing disruptive and two TPA units on each side of monomer might help to form polymer on conducting surface and might enhance thin-film-forming capability **[36].** TPA was in non-conjugated from the central acceptor to prevent the delocalization of the radical cation generated from the TPA oxidation process. A catalyst free, simple oxidative electro-polymerization technique was employed to polymerize all the monomers by applying appropriate voltage for a controllable film thickness. For an ECM, the switching-time performance and stability were the foundation of evaluating their quality which could be improved by decreasing the band gap energy for a donor acceptor system **[37].** DFT studies as well as experimental calculation suggested that substituted NDI derivatives by electron withdrawing group like -CN, -Br group decreased the band gap energy and electron donating group like –Ph, -Npy increase the same. Therefore, CNTPANDI showed good electrochemical and electrochromic properties with high coloration efficiency (560 cm^2/C) as well as prevented the degradation of optical contrast after long term switching (1200 cycles) in oxidation by creating electron deficiency in the acceptor core with proper alignment of the LUMO orbital along with decreasing the band gap energy tremendously by increasing the energy of the LUMO level. Besides, the device from p-CNTPANDI exhibited the EC

memory in open-circuit condition with 50% retention of its coloured state (blue colour) until 27 min. Therefore it might find a

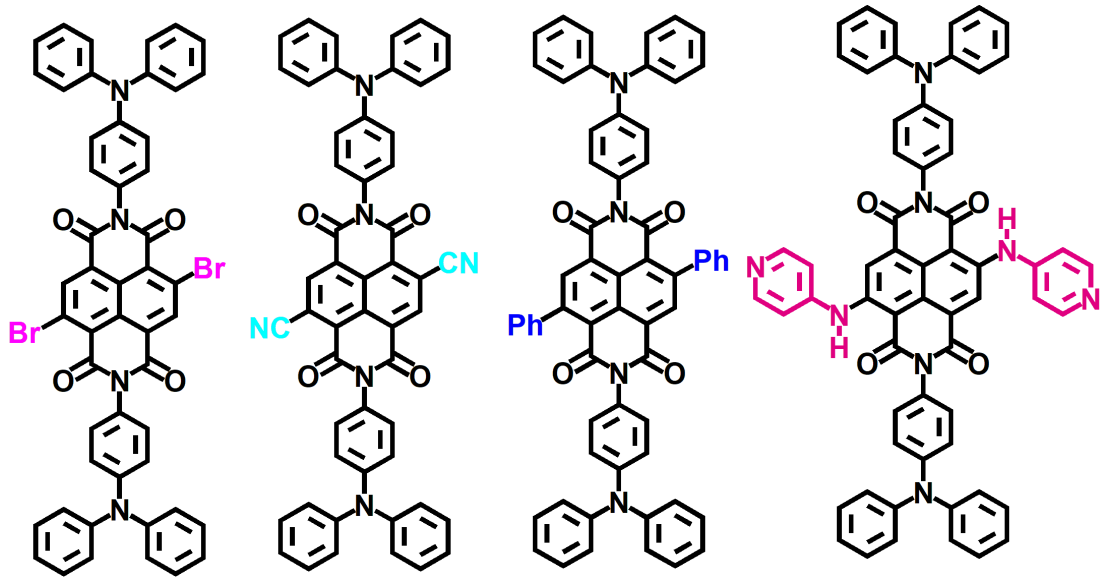

Fig. 5.01. Chemical structures of **BRTPANDI, CNTPANDI, PHTPANDI, NPYTPANDI**.

practical application in EC smart windows, auto-dimming rear view mirrors, sunglasses, traffic sign, military security equipment, energy storage devices, camouflage, and information storage systems **[38], [39], [40], [41], [42], [43].**

5.2. RESULTS AND DISCUSSION:

For the preparation of four electro-active monomer, first NDA was brominated with DBH to form 2,6-dibromo-1,4,5,8-naphthalene tetracarboxylic dianhydride, indicated by the appearance of the peak at 8.75 ppm in ^{1}H-NMR **[Fig. 5.15].** Again 4-amino TPA was formed from diphenyl amine according to the reported method **[35].** 4-amino TPA was condensed with NDA in dry DMF medium to form BRTPANDI (31% yield) and the formation was confirmed the presence of peaks at 7.30, 7.28, 7.16 and 7.08 ppm assigned to TPA moieties in NMR studies. Subsequently, the bromo group was substituted by cyano group by using CuCN to form CNTPANDI (86%

yield), indicated by the presence of cyanide stretching at 2260 cm^{-1} in FTIR. PHTPANDI was prepared by the substitution of the bromo group of BRTPANDI with phenyl group using phenyl boronic acid and the overwhelming presence of 7.49, 7.44, 7.30, 7.14, 7.09 ppm in ^{1}H-NMR revealed clearly its formation. Finally, NPYTPANDI was formed by the reaction of BRTPANDI with 4 amino pyridine. The resulting product was confirmed using ^{1}H and ^{13}C NMR **[Fig.5.16-5.19],** mass spectra and Fourier-transform infrared (FTIR) spectroscopy **[Fig.5.02].**

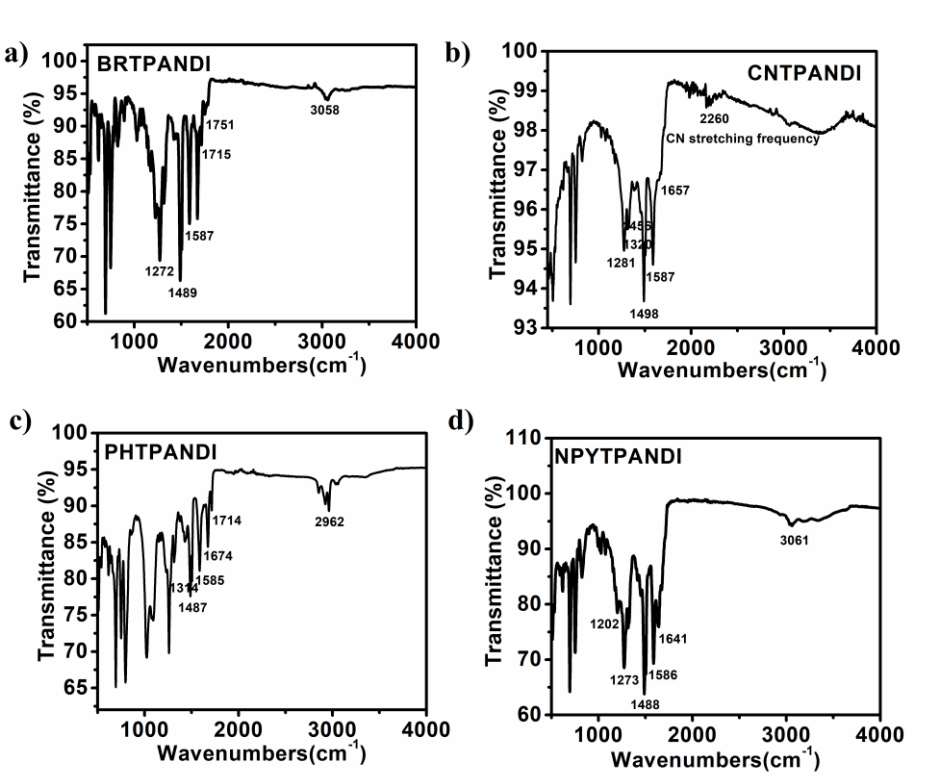

Fig. 5.02. FT-IR spectra of **(a) BRTPANDI, (b) CNTPANDI, (c) PHTPANDI and (d) NPYTPANDI.**

5.2.1. Theoretical studies:

DFT studies were conducted using Gaussian 16 suite of programs **[44].** The geometry optimization of all the monomers were carried out employing hybrid DFT functional namely B3LYP **[45]** and 6-31G(d) basis set **[46].** Harmonic vibrational frequency analysis exhibited that all the minima structures reached to zero imaginary vibrational frequencies ensuring absence of any saddle point in the optimized structures. DFT calculations suggested the optimized molecular structures of BRTPANDI, CNTPANDI, PHTPANDI, NPYTPANDI and subsequent the distribution of the frontier molecular orbitals **[Fig.5.03].** The HOMO levels were on the TPA portion with the energy of -5.45, -5.56, -5.37, -5.46 eV for BRTPANDI, CNTPANDI, PHTPANDI, NPYTPANDI. The electron cloud for the molecular orbital of LUMO was mainly distributed on the NDI core. Substitution of the NDI core with different electron donating as well as withdrawing group varied the LUMO energy level.

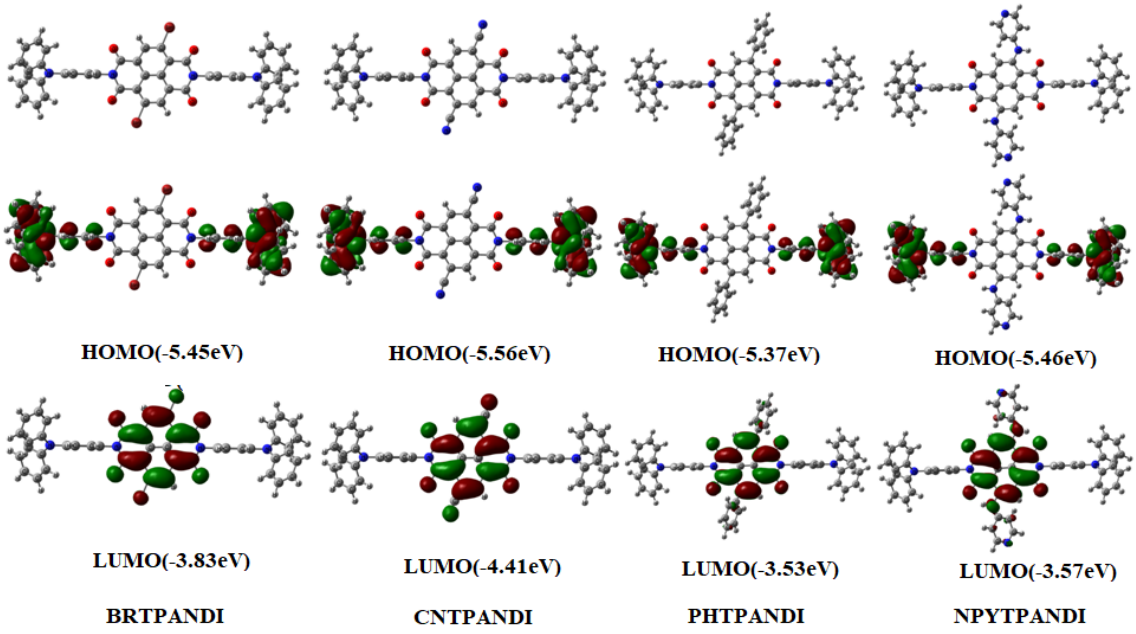

Fig.5.03. DFT optimized geometries and HOMO-LUMO molecular orbital diagrams of the monomers.

Among them, the substitution with cyano group tremendously decreased the LUMO energy level owing to the extensive conjugation with cyanide groups, however, phenyl and pyridyl were not coplanar with naphthalene core. The substituent orbitals occupied on the LUMO orbital and did not overlap with the HOMO energy level. The

calculated band gaps were found to be 1.62, 1.15, 1.84 and 1.89 eV for BRTPANDI, CNTPANDI, PHTPANDI, NPYTPANDI respectively.

5.2.2. Electrochemical polymerization

After getting significant information of the electron cloud distribution over the moieties from TD- DFT studies, a simple, less time taking, catalyst free polymerization technique was employed. Knowing about the oxidation potential of TPA, the electrochemical polymerization (EP) was carried out in a three-electrode cell (ITO coated glass as working electrode and Ag wire as reference electrode, Pt wire as counter electrode) keeping the monomer concentration of 5×10^{-4} molar in 0.1 (M) TBAP dry DCM solution within the voltage window of 0 to 1.5 V for 10 cycles. Prior to film preparation, ITO glasses were cleaned with acetone, isopropanol, ethanol and doubled distilled water and dried on oven. In the repetitive CV scans, gradual increase of the peak current with successive cycles indicated the linkage of the TPA units to form the polymer film on the conductive surface (ITO). In the first CV oxidation scan, only one peak was appeared, indicative of typical oxidation of TPA unit to form mono radical cation. In order to have successful electro-polymerization (EP) process, the radical cation should not be migrated towards the central acceptor core and it was prevented by the presence of one node at imide nitrogen atoms of NDI. In the remaining cycles, two oxidation waves which were appeared in the redox process,

were the successive oxidation of the benzidine group revealing the formation of the linear polymers. Due to the strong electron withdrawing effect of the CN and Br group present in the acceptor core, higher oxidation potentials were needed to the corresponding monomers of BRTPANDI, CNTPANDI than that of the remaining two electro-active monomers **[Fig.5.04].** The electro-polymerized film morphology was investigated by FESEM. **Fig.5.07b-5.07c** and **Fig.5.08b-5.08c** exhibited sphere-like protuberance for p-BRTPANDI, p-CNTPANDI while p-PHTPANDI showed sphere shaped smooth surface morphology **[Fig.5.09b, 5.09c]** and p-NPYTPANDI revealed a rough surface morphology **[Fig. 5.10b, 5.10c].** Those totally different surface morphologies illustrated the discrepancy in the EP process.

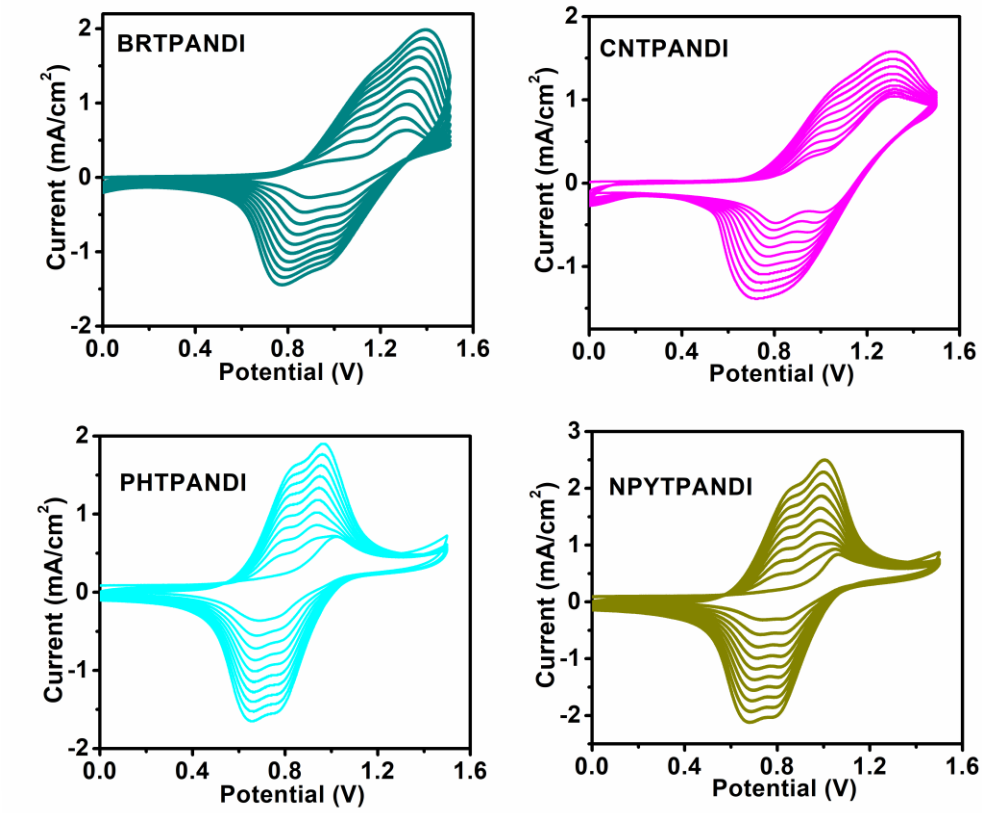

Fig.5.04. Electropolymerisation of the four monomers for making polymers with the voltage window 0 to 1.5 V.

5.2.3. Electro-optical properties of polymer films

Electrochemical behaviours of the polymer films were studied by the CV technique using three electrode system (ITO coated film as working electrode, Pt wire as counter and Ag/AgCl as reference electrode in TBAP/ACN solution and all the polymers revealed similar redox processes **[Fig.5.05].** One reversible oxidation peak at around 1.4 V, 1.60 V, 1.26 V, 1.23 V for p-BRTPANDI, p-CNTPANDI, p-PHTPANDI, p-NPYTPANDI might be ascribed as the formation of $[TPA]^{2+}$ radical cation **[47].** The polymer film made of the cyano substituted NDI derivative showed the higher oxidation potential owing to the strong electron withdrawing effect of the -CN group. The scan-rate dependence studies of the polymer films were carried out at various scan rate (50-250 mV/s) **[Fig.5.06].** With increasing the rate of scan, peak current density was increased or decreased during the oxidation / reduction process. A linear dependence of the peak current as a function of the scan rate for all the

polymers **[Fig.5.06]** indicated the reversibility nature of the electrochemical processes without any diffusion-limit **[48].**

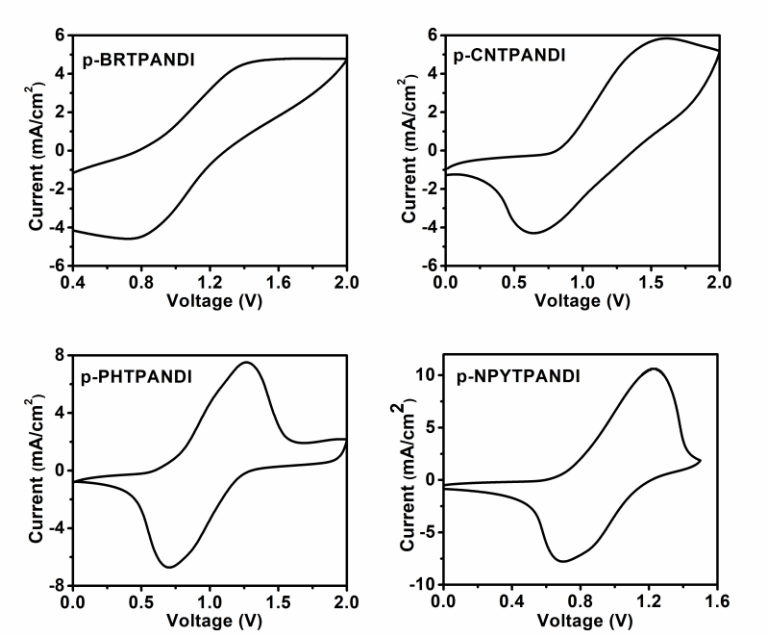

Fig.5.05. CV of the cast polymer films prepared by 10 cycles in 0.1 M TBAP/ACN solution.

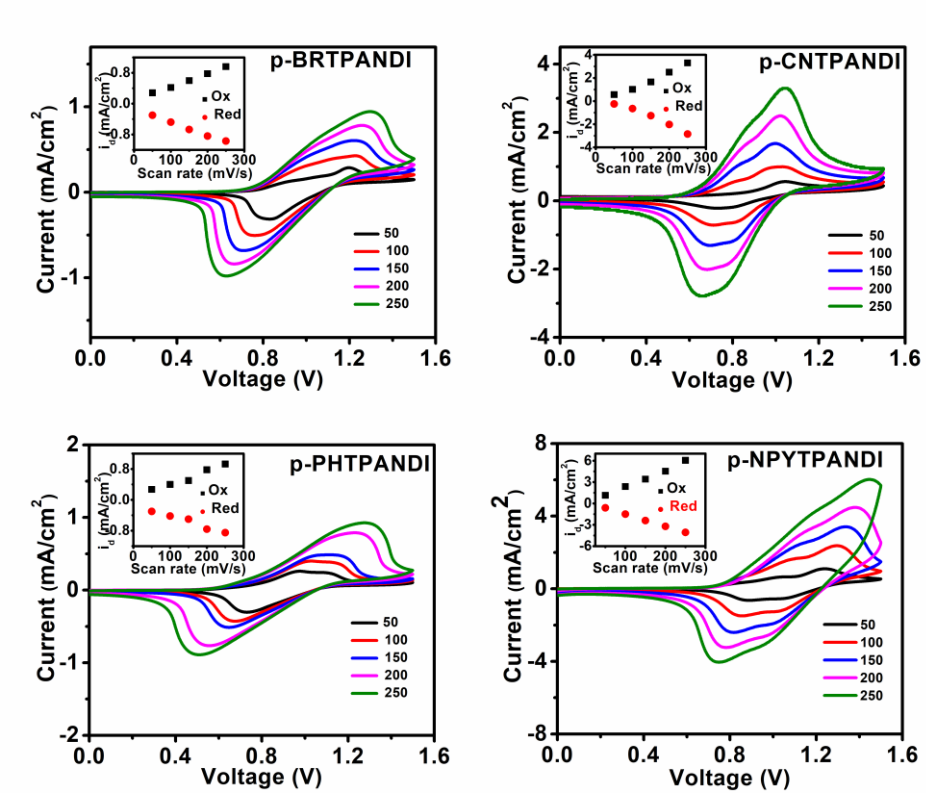

Fig. 5.06. Scan rate dependent plots for the four polymers with inset linear plot.

5.2.4. Spectro-electrochemistry

The in-situ absorption spectra of the four EC systems (polymer made from BRTPANDI, CNTPANDI, PHTPANDI, NPYTPANDI) were studied with a conventional three electrode configuration combined with absorption spectrometer to investigate the spectral changes upon applying voltage from 0.0 to 1.8 V **[Fig.5.07a, 5.08a, 5.09a, 5.10a].** When no voltage was applied i.e at 0 V, one absorption peak was centred at approximately 360 nm, assigned to the π- π* transition of the NDI core. The absorption band showed a red-shift compared to the peak of NDA at 335 nm which was possibly owing to the increase in the extent of conjugation. As the applied voltage was increased to 0.9 V, the position of absorption peak remained same with the reduction of the value of absorbance at 360 nm. Once, potential was increased around 1 V, a broad absorption band at 490 nm was appeared owing to the n - π* transition, and its intensity was also enhanced with the increasing applied potential. However, the colour change associated to this transition was not properly realized due to the greenish colour of the film itself. Further increasing the positive potential to 1.1 V for p-BRTPANDI, p-PHTPANDI, p-NPYTPANDI and 1.2 V for p-CNTPANDI, a new broad peak at around 710 nm was gradually developed with the colour change to intense blue indicating the formation of $[TPA]^{2+}$radical dication within the polymer matrix. At the cathodic potential at -1.8 V for NDA, a bright pink colour was observed due to the n-p* transition of NDI core and its intensity was increased with the decreasing applied potential and was reached to saturation near to applied potential at -2 V. It demonstrated that NDI core was the main electrochromic active unit during electrochemical reduction, the possible reason was considered to be the high electron mobility of the NDI unit **[49].**

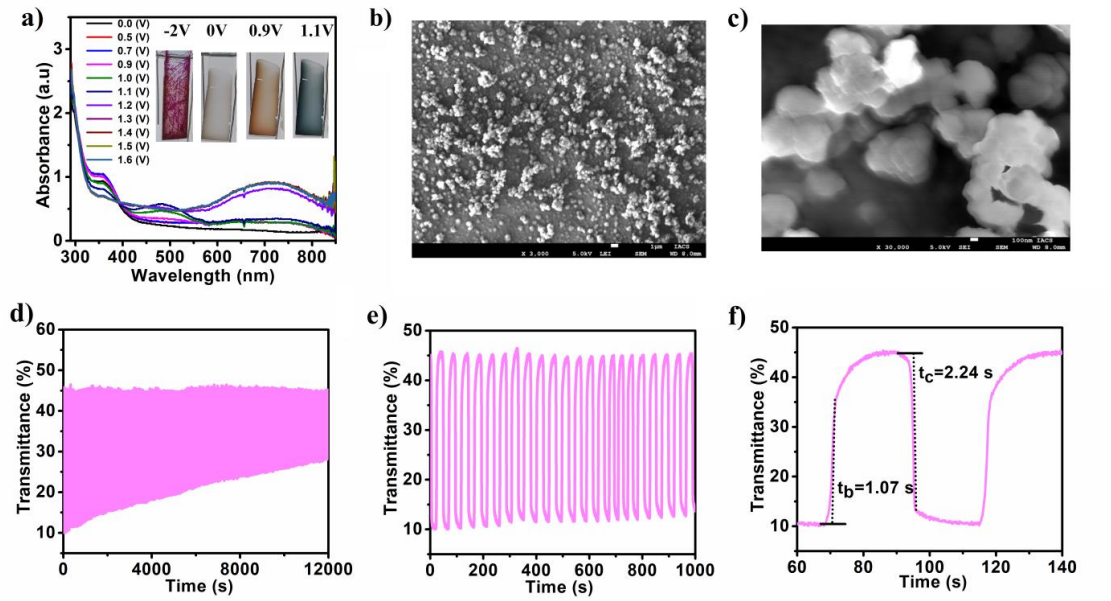

Fig. 5.07. For **p-BRTPANDI:** (a) Spectroelectrochemistry studies and inset is the photographs of the colour change of the film with voltage, (b) and (c) FESEM images, (d) Long term cyclic stability with a pulse width of 10 s, (e) Switching studies, (f) Response time colouration (t_c) and bleaching (t_b).

The optical contrast was investigated by applying square wave potential steps at appropriate specific wavelengths within a fixed voltage window. EC switching study were performed by double step chrono-ampherometry method with the combination of UV-Vis spectroscopy and the change of transmittance at a fixed wavelength (710 nm) was monitored with voltage ramping between 0 to 1.2 V for a pulse width 10 s in 0.1 M TBAP in ACN solution. The turn on state coloration transmittance obtained for p-BRTPANDI, p-CNTPANDI, p-PHTPANDI, p-NPYTPANDI were 9 %, 3 %, 17 %, 34 % and the turn off state bleaching transmittance were 47 %, 44 %, 60 %, 83 % **[Fig. 5.07e, 5.08e, 5.09e, 5.10e]** respectively for the first potential switching step. The calculated values of optical contrast for the polymers were 38 %, 41 %, 43%, 49 % respectively. The coloration time (t_c) / bleaching time (t_b) for p-BRTPANDI, p-CNTPANDI, p-PHTPANDI, p-NPYTPANDI films at 710 nm were found to be 2.24 s/1.07 s, 5.98 s/5.02 s, 1.98 s/0.44 s, 0.55 s/0.50s respectively **[Fig. 5.07f, 5.08f, 5.09f, 5.10f].** Due to strong electron withdrawing effect of the cyano group, p-CNTPANDI slowed down the oxidation resulting the higher value of bleaching and colouration times. While electron donating aryl substituent in p-PHTPANDI and the presence of

N donating centre in p-NPYTPANDI facilitated the electron transfer process, resulting the fast response time from p-PHTPANDI, p-NPYTPANDI polymers.

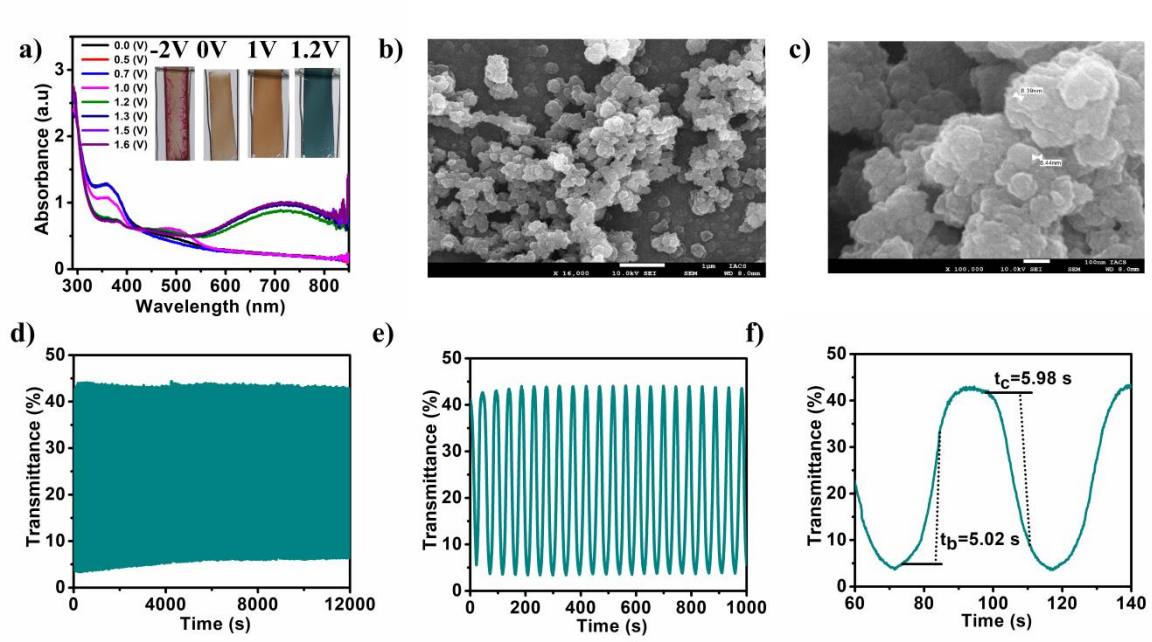

Fig. 5.08. For **p-CNTPANDI:** (a) Spectroelectrochemistry studies and inset is the photographs of the colour change of the film with voltage, (b) FESEM image, (c) Film thickness from FESEM, (d) Long term cyclic stability with a holding time of 10 s, (e) Switching studies, (f) Response time colouration (t_c) and bleaching (t_b).

The repeated electrochromic cycling of the polymers were tested with a pulse width 10 s at 710 nm for positive potential at 0 to 1.2 V. The stability was continued upto 1200 cycles for p-BRTPANDI and p-CNTPANDI, 800 cycles for p-PHTPANDI and 200 cycles for p-NPYTPANDI **[Fig. 5.07d, 5.08d, 5.09d, 5.10d].** The reduction of stability after 1200 cycles was only 2 % for p-CNTPANDI. The stability of the polymer film was tested between the working potential 0 to -2 V with a pulse width of 10 s at 536 nm, in the negative potential switching, it was performed upto 160 cycles for p-BRTPANDI and 100 cycles for p-CNTPANDI, 300 cycles for p-PHTPANDI and 400 cycles for p-NPYTPANDI **[Fig. 5.11].** The radical anion generated on the NDI core was inhibited to migrate to some extend towards the core by the strong electron withdrawing effect of cyano group. As a result, p-CNTPANDI showed the least cycle stability on electrochemical reduction.

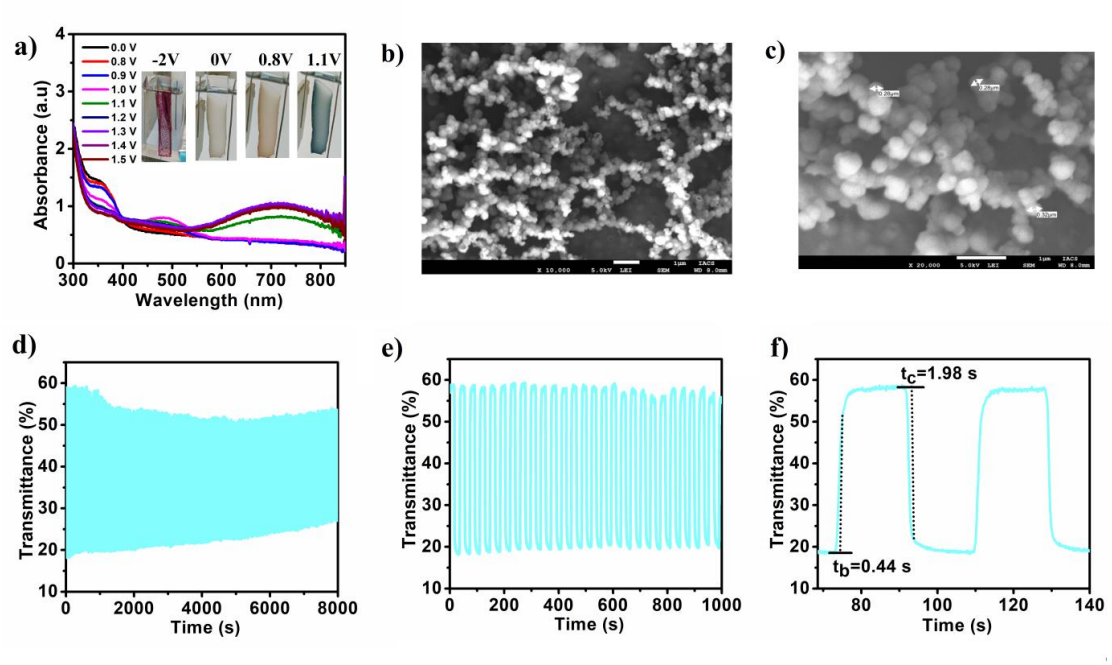

Fig. 5.09. For **p-PHTPANDI :** (a) Spectro electrochemistry studies and inset is the photographs of the colour change of the film with voltage, (b) FESEM image, (c) Film thickness from FESEM, (d) Long term cyclic stability with a holding time of 10 s, (e) Switching studies, (f) Response time colouration (t_c) and bleaching (t_b).

An important EC parameter, the coloration efficiency (η) was determined by the following equation **[50].** For a good EC material, it should have high colouration efficiency.

$$\eta = \frac{\Delta OD}{Q_d} = \log \frac{T_b}{T_c} \Big/ Q_d$$

Where, ΔOD was the optical absorbance change and Q_d (mC/ cm^{-2}) was the ejected charge during the redox process which was calculated from chrono-ampherometric plot **[Fig. 5.12]** and T_b and T_c was the % of transmittance of the bleaching state and coloration state. The calculated coloration efficiency for the polymers were 307, 560, 302, 232 cm^2/C respectively for p-BRTPANDI, p-CNTPANDI, p-PHTPANDI, p-NPYTPANDI and values of colouration efficiencies were more higher than the unsubstituted TPANDI based derivative reported by Zhiyong Guo and Hongbing Zhan group **[34].** All results were summarized in **Table 5.1** and EC performances of our material was compared with other reported TPA based works in **Table 5.2.**

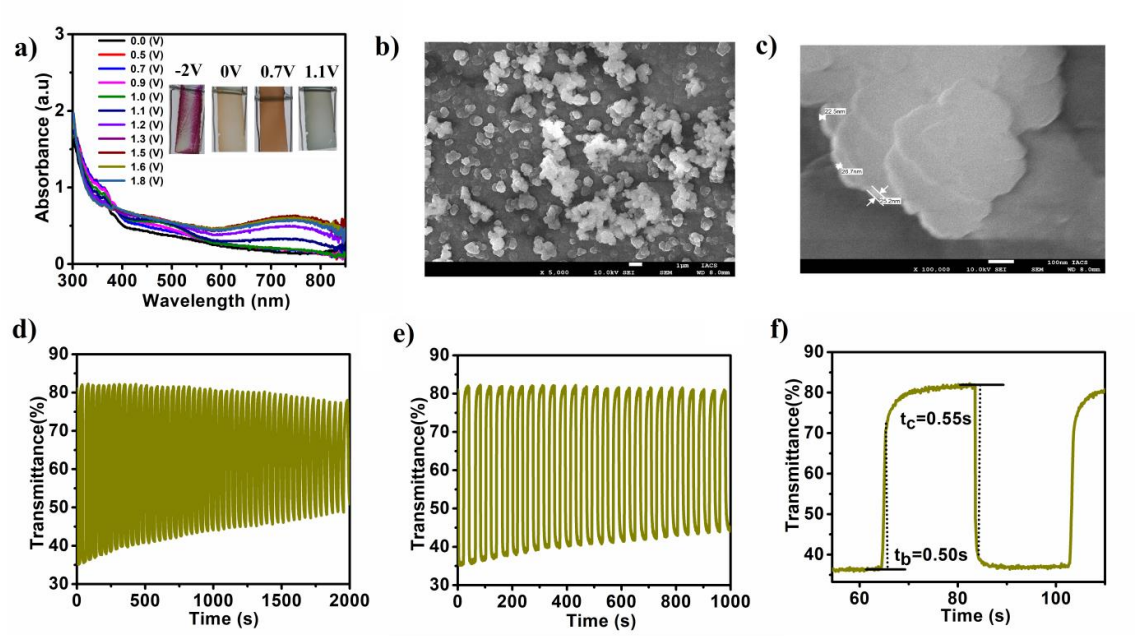

Fig. 5.10. For **p-NPYTPANDI :** (a) Spectro-electrochemistry studies and inset is the photographs of the colour change of the film with voltage, (b) FESEM image, (c) Film thickness from FESEM, (d) Long term cyclic stability with a holding time of 10 s, (e) Switching studies, (f) Response time colouration (t_c) and bleaching (t_b).

TABLE 5.1: EC parameters of the polymers

Polymers	**Λ_{max}(nm)**	**ΔT%**	**t_c(s)**	**t_b(s)**	**ΔOD**	**Q_d(mCcm^2)**	**CE(cm^2/C)**
p-BRTPANDI	710	38	2.24	1.07	0.67	2.18	307
p-CNTPANDI	710	41	5.98	5.02	1.23	2.20	560
p-PHTPANDI	710	43	1.98	0.44	0.55	1.8	302
p-NPYTPANDI	710	49	0.55	0.50	0.38	1.65	232

Wavelength of absorption maximum. Time for 95 % of the full-transmittance change. Optical density change (ΔOD) = Log [$T_{bleached}$ / $T_{colored}$], where $T_{colored}$ and $T_{bleached}$ were the maximum transmittance in the oxidized and neutral states respectively. Q_d was the ejected charge obtained from chronoampherometry measurement. Coloration efficiency (CE) = ΔOD/Qd.

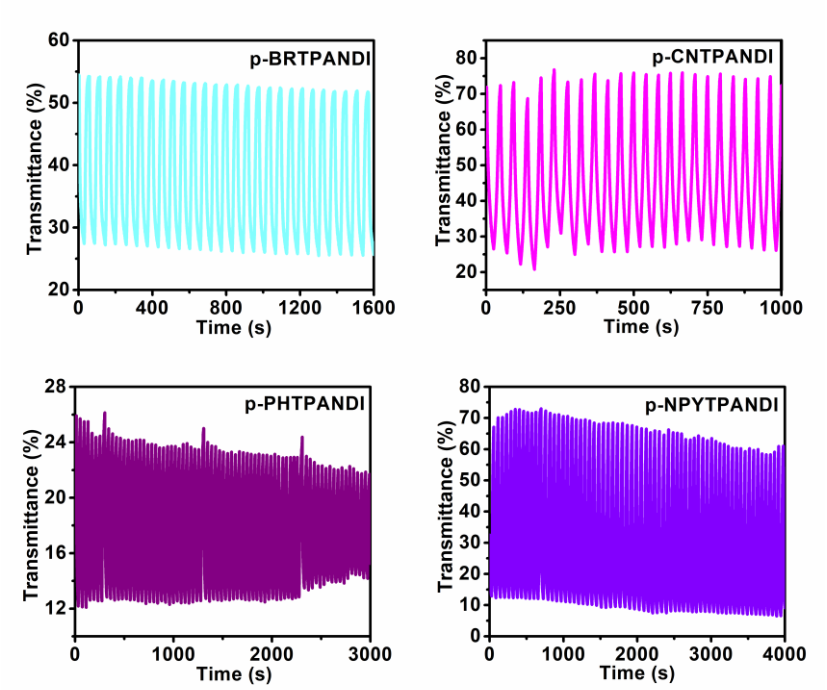

Fig. 5.11. Cathodic cyclic stability upon applying voltages of 0V to -2 V with a holding time of 10s.

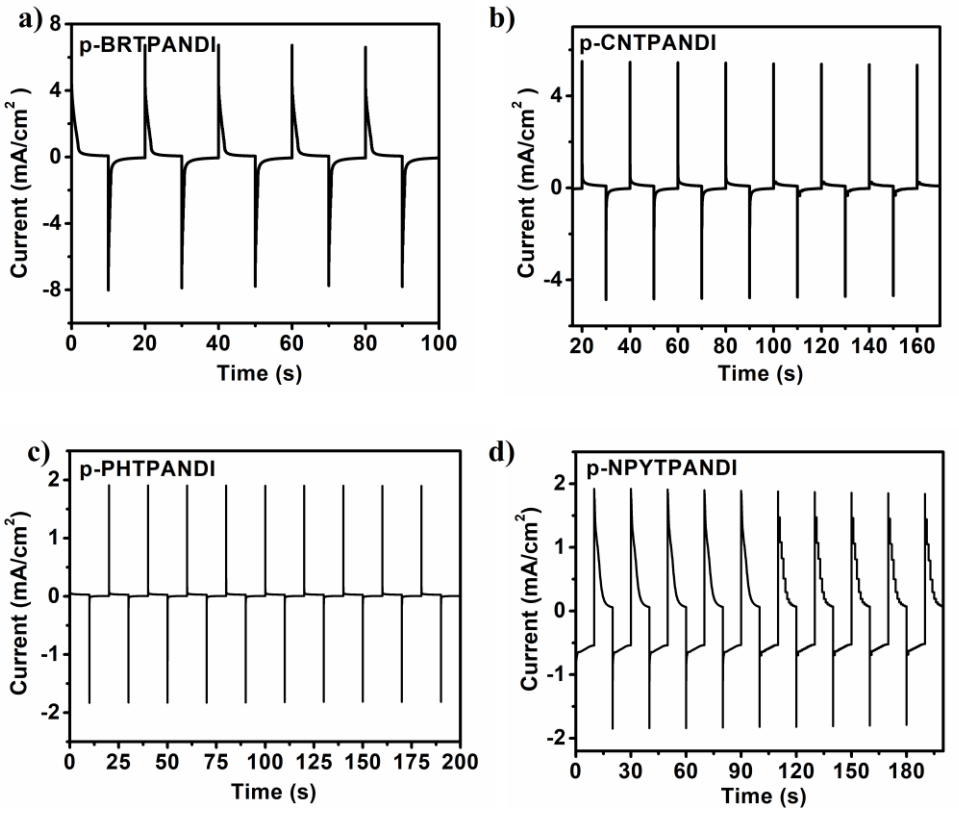

Fig.5.12. Chronoampherometric studies of four polymer films.

5.2.5. Solid-State ECD: Having a good colouration efficiency and maintain almost constant optical contrast value for long term switching process, p-CNTPANDI was considered to be commercialized by making solid state electrochromic device. Initially, the polymer was electrodeposited on ITO coated glass, rinsed with DCM and acetone to remove the monomer and oligomer and then dried properly. The transparent conducting gel electrolyte prepared from PMMA and $LiClO_4$ plasticized with propylene carbonate was spread on the polymer deposited side of ITO glass acted as working electrode, was sandwiched with ITO coated side of another ITO glass acted as counter electrode and was sealed by epoxy resin and kept on oven for 1 hr at 60°C. The colour change of the fabricated device with dimension 2*2 cm^2 **[Fig.5.13a]** was clearly visible nearly at 2.2 V and cyclic voltametric studies of the device were performed at the potential windows from 0 to 3 V. The small but significant oxidation peak was appeared at 2.20 V and reduction peak was at 1.63 V respectively **[Fig. 5.13b].**

5.2.6.Optical Memory of ECD: High optical memory for an ECD was an important parameter for the commercialization of a smart window. If an ECD, in a particular redox state having a colour or bleach state retained its originality in open-circuit condition (without applying voltage) for a long time, it might deliver a power-efficient or saving device. EC memory of p-CNTPANDI was considered for monitoring the absorbance change in open circuit condition after reaching the coloured state at 2.2 V. The absorbance change with time in open circuit condition started from the completely coloured state **[Fig.5.13c].** The gradual decrease of the absorbance peak and blue green colour with time were due to the self-reduction by the residual electrons from the electrode at open-circuit conditions **[51].** However, the ECD exhibited 50% retention of its colour till 27 min and returned its original state after 30 mins.

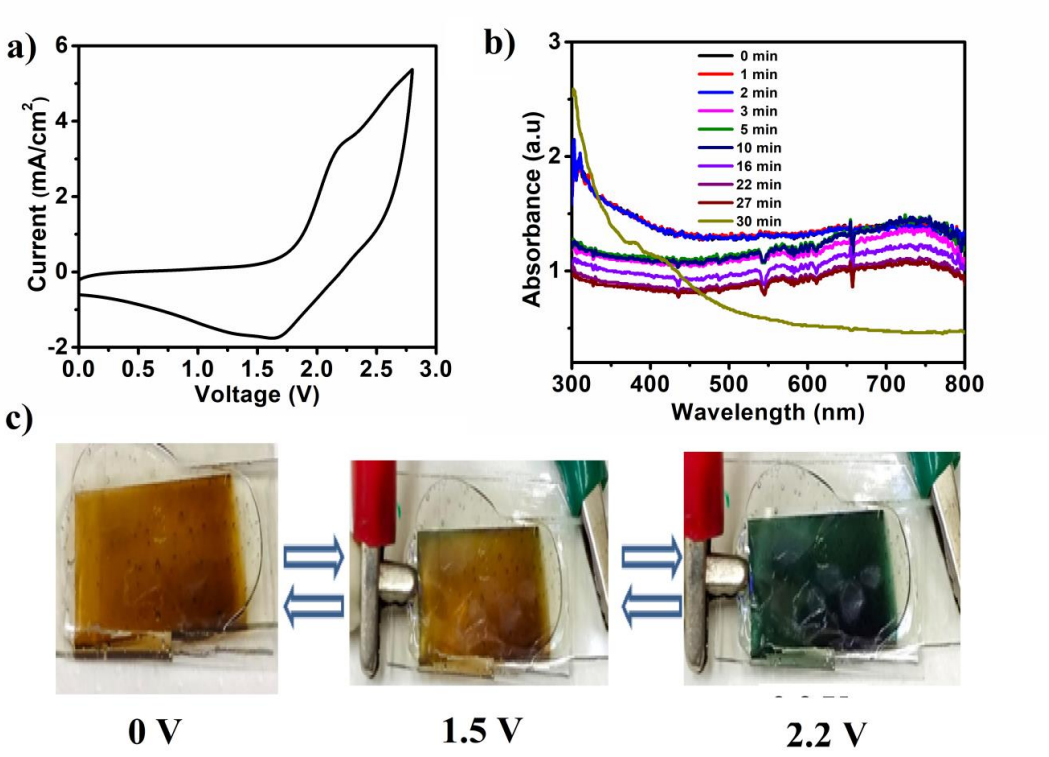

Fig. 5.13. For **p-CNTPANDI :** (a) CV spectra of the fabricated device, (b) Optical memory studies with time, (c) Device colour change with applying Voltage.

5.3. Conclusion:

Core substituted NDI-based monomers BRTPANDI, CNTPANDI, PHTPANDI, NPYTPANDI were electrodeposited on ITO surface to explore the effect of substitution on NDI core. By analyzing the electrochemical behaviour and theoretical calculation of the designed monomers, substitution with electron withdrawing group like Br and CN lowered the LUMO energy level and subsequently reduced the band gap energy as the LUMO was on the acceptor core and all substituents were not coplanar with naphthalene moiety. The reversible multiple colour change of brown to deep blue in the anodic region by applying voltage 0 to 1.1 V and also brown to deep pink in the cathodic region with the voltage change of 0 to -2 V were unambiguously explored with relatively good response times, optical contrast, switching stabilities, and coloration efficiencies. p-CNTPANDI could be switched upto 1200 cycles with the optimum colouration efficiency 560 cm^2/C in the anodic process and 300 cycles for the cathodic process in a three electrodes configuration. Prototype solid-state device made of p-CNTPANDI demonstrated the electrochromism operated at a

potential range of 0 to 2.2 V with multiple colour change and also it exhibited the EC memory in open-circuit condition with 50% retention of its coloured state until 27 min. The improvement of the EC properties by mainly electron withdrawing substitution of NDI core suggested a new class of fully organic based EC material for the next generation display device.

Table 5.2. Comparative studies based on literature surveys

Materials	**Binding unit**	**Colouration efficiency**	**Operating voltage (V)**	**2 electrode cycle stability**	**References**
CNTPANDI	**TPA**	**560**	**0/+2.2 V**	**---**	**This work**
TPA_6ISO	TPA	410	0/+2.5 V	90 cycles	(36)
TPACNANT	TPA	371	0/+2.5 V	---	(28)
TPAANT	TPA	222	0/+1.6 V	---	(52)
TPA_4NDI	TPA	847	0/+2.5 V	4000 cycles	(35)
DPyNDI-TPA	TPA	306	---	---	(34)
Small organic molecule	Viologen	274	0/1.2V	10,000 cycles	(53)
TPA-2Cz	TPA	59	---	---	(54)
Donor Acceptor conjugated polymer	Aromatic diimide	303	---	---	(55)
1,3,5-tris(4-pyridylium)bromides	Pyridine	327	---	---	(56)
NDI cored pyridinium	Pyridine	201	-1.4 V to 0 V	720 cycles	(57)

salt					
Various substituent benzene	Viologen	---	-1.6 V to 0 V	---	(58)

5.4. Experimental Section

5.4.1. Materials required

Naphthalene tetracarboxylic dianhydride (NDA), triphenylamine (TPA), $Pd(PPh_3)_4$, calcium hydride, tetrabutyl ammonium perchlorate (TBAP), lithium perchlorate ($LiClO_4$), polymethylmethacrylate (PMMA), propylene carbonate, phenyl boronic acid, 4 amino pyridine, Pd/C were purchased from Sigma Aldrich and used as received. Benzophenone, potassium carbonate (K_2CO_3), sodium hydroxide (NaOH), sodium sulphate (Na_2SO_4), concentrated sulphuric acid (H_2SO_4), acetic acid, CuCN, hydrazine hydrate were purchased from Merck chemicals. 4 fluoro nitrobenzene, NaH, 1,3-dibromo-5,5- dimethyl hydantoin (DBH) were purchased from Avra chemicals. Bulk solvents like acetonitrile (ACN), dichloromethane (DCM), chloroform ($CHCl_3$), methanol (MeOH), tetrahydrofuran (THF), dioxane, dimethyl formamide (DMF) and analytical grade reagents were used without further purification. DMF, ACN, DCM and 1, 4-dioxane were dried by anhydrous calcium hydride and THF was dried by refluxing with sodium and benzophenone. Indium tin oxide (ITO) coated glass (MTI Corporation Ltd.) was cleaned by double distilled water, ethanol and acetone.

5.4.2. Measurements

The ^{1}H and ^{13}C-NMR spectra were recorded on a Bruker 500 or 400 MHz spectrometer in chloroform-d ($CDCl_3$), dimethyl sulphoxide-d ($DMSO\text{-}d_6$) with tetra methylsilane (TMS) as an internal standard. MALDI-TOF (matrix assisted laser desorption ionization time-of-flight) mass spectrometry was carried out with Bruker Daltonics Ultra flextreme (laser intensity 80%). Fourier transformed infrared (FT-IR) spectra were measured on a Horiba FT-720 FT-IR spectrometer. The UV-visible absorption spectrum was recorded on an Ocean Optics DH-mini UV-VIS-NIR light source and Ocean Optics flame Miniature Spectrometer. The electrochemical

measurements were performed by using a CHI6087E electrochemical workstation in both 3 and 2 electrode system).

Scheme of synthesis:

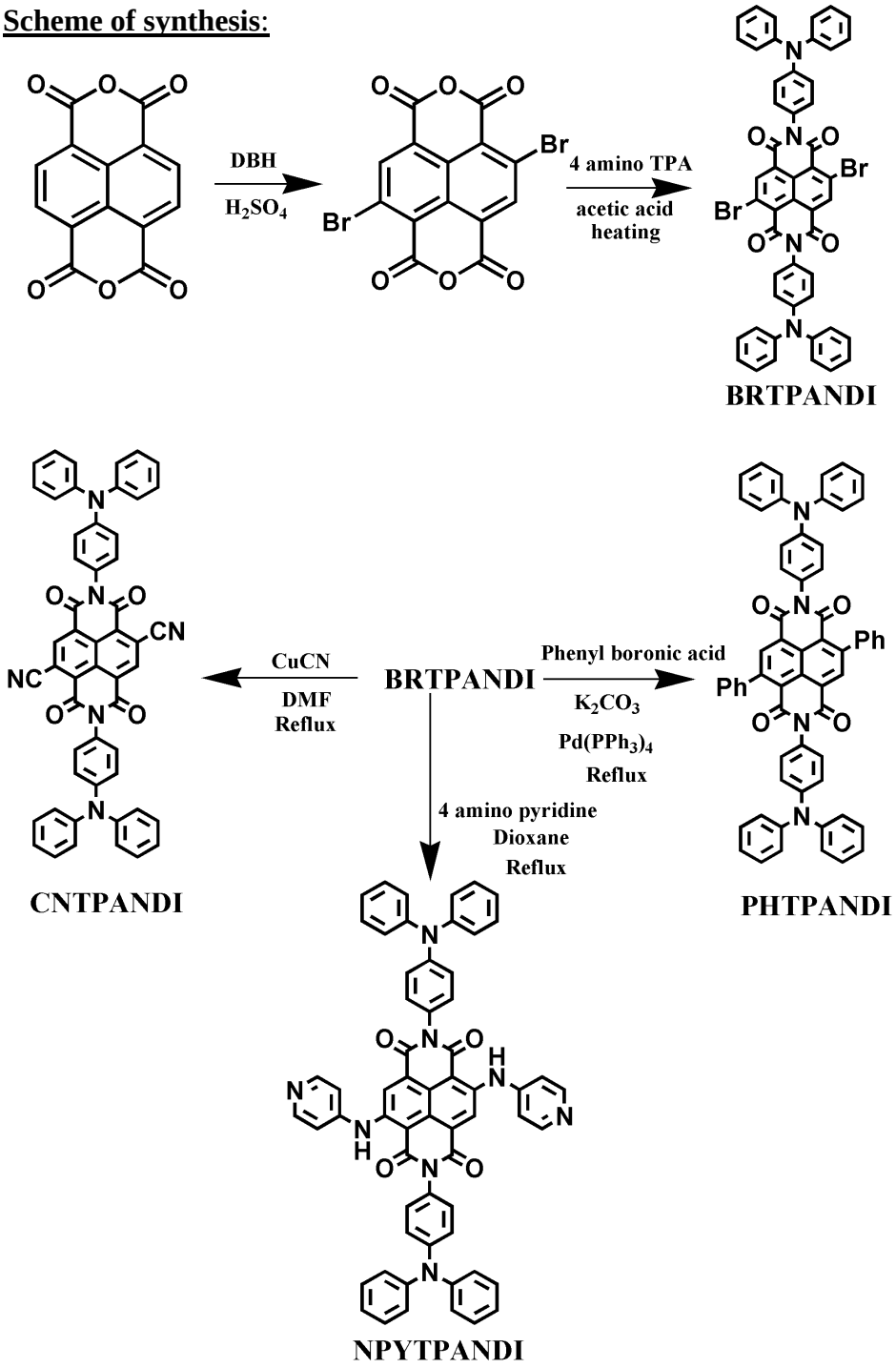

Fig. 5.14. Synthesis scheme of four electro active monomers**.**

5.4.3. Synthesis Procedure:

2,6-Dibromo-1,4,5,8-naphthalenetetracarboxylic Dianhydride:

In two necked RB flask, NDA (2.68 g, 10 mmol) was added to 25 ml concentrated sulfuric acid at room temperature, the mixture was stirred at room temperature for few minutes. DBH (3.57 g, 15 mmol) was added over a period of 1 h. The resulting yellow solution was stirred at 50^0C for 10 h. The mixture was poured into ice cold water to precipitate the solid. The precipitated solid was filtered, washed with water then with methanol, and finally dried in vacuum. The crude product was recrystalized in DMF. Finally obtained pure product is 3.55 g with yield 81%.

^{1}H NMR: (400 MHz, DMSOd_6, TMS) δ (ppm): 8.75 (s, 2H).

Synthesis of BRTPANDI: In a two necked round bottom flask, 2,6-Dibromo-1,4,5,8-naphthalenetetracarboxylic Dianhydride (50mg, 0.117 mmol), 4 amino TPA (78 mg, 0.3 mmol) were taken under nitrogen atmosphere, acetic acid (2 ml) was added to it, heated for 4 hrs at 120˚C. After cooling the reaction mixture, it was added to the ice cold water, a blue ppt was appeared and filtered. It was recrystalized in MeOH and dried in vacuum oven to have the title product of **BRTPANDI** with yield 31% (33 6mg).

^{1}H NMR: (400 MHz, $CDCl_3$, TMS) δ (ppm): 8.84 (2H, s), 7.30 (8H, m), 7.28 (6H, m), 7.16 (10H, m), 7.08 (4H, d).

^{13}C NMR (100 MHz, $CDCl_3$, TMS) δ (ppm): 163.23, 147.42, 131.57, 129.62, 129.07, 125.38, 125.26, 123.90, 123.12, 122.88, 121.35.

Mass (MALDI-TOF, diathranol matrix): m/z calculated 910.61, found 910.

IR (cm^{-1}): 3058, 1751, 1715, 1587, 1489, 1272.

Synthesis of CNTPANDI: In a two necked round bottom flask, BRTPANDI (40 mg, 0.043 mmol), CuCN (20 mg, 0.219 mmol) were taken under nitrogen gas, dry DMF (3 ml) was added to it, refluxed for 24 hrs at 160˚C. After completion of the reaction, aqueous ammonium hydroxide solution was added to the reaction mixture to remove the Cu^{+2} ion and it was filtered, a brown coloured product was obtained which was dried in vacuum oven. The obtained product was yield 86 % (30 mg).

^{1}H NMR: (400 MHz, $CDCl_3$, TMS) δ (ppm): 8.85 (2H, s), 7.52 (8H, m), 7.22 (4H, d), 7.15 (6H, m), 7.09 (10H, d).

^{13}C NMR: (100 MHz, $CDCl_3$, TMS) δ (ppm): 153.20, 144.65, 141.46, 140.86, 135.29, 128.69, 127.57, 126.10, 125.86, 123.70, 120.60, 119.71, 109.83.

Mass (MALDI-TOF, diathranol matrix): m/z calculated 802.83, found 803.

FTIR (cm^{-1}): 2260, 1657, 1587, 1498, 1456, 1281, 1320.

Synthesis of PHTPANDI: In a round bottom flask, BRTPANDI (50 mg, 0.054 mmol), Phenylboronic acid (30.11 mg, 0.247 mmol), $Pd(PPh_3)_4$ (2 mg) were inerted properly with nitrogen for 30 mins, dry 1,4 dioxane (5 ml) was added to it followed by addition of 22.38 mg (0.162 mmol) K_2CO_3 dissolved in 0.7 ml of water and heated for 24 hrs at 110°C. After cooling the reaction mixture, it was extracted with DCM and water and evaporated the DCM part. The crude product was purified by column chromatography with 1: 1 DCM and pet ether and the pure product was dried in vacuum oven with yield 39 % (19 mg).

^{1}H NMR: (400 MHz, $CDCl_3$, δ (ppm): 8.84 (2H, s), 7.49 (10H, m), 7.44 (6H, m), 7.30 (6H, m), 7.14 (6H, m), 7.09 (10H, d).

^{13}C NMR: (100 MHz, $CDCl_3$, TMS) δ (ppm): 163.23, 147.47, 132.38, 129.54, 129.25, 128.64, 127.98, 125.74, 125.44, 125.30, 123.81, 123.72, 122.79, 122.71.

Mass (MALDI-TOF, diathranol matrix): m/z calculated 905.01, found 905.

FTIR (cm^{-1}): 2962, 1714, 1674, 1585, 1487, 1314.

Synthesis of NPYTPANDI: In a two necked round bottom flask, BRTPANDI (50 mg, 0.054 mmol), 4 amino pyridine (130 mg, 1.373 mmol) were inerted properly with nitrogen, dry dioxane (2 ml) was added to it, refluxed for 12 hrs at 110°C. After cooling the reaction mixture, MeOH was added to it, a dark brown coloured precipitate was appeared, it was filtered, washed with MeOH and dried in vacuum oven with yield 60% (30 mg).

^{1}H NMR: (400 MHz, $CDCl_3$) δ (ppm): 8.84 (2H, s), 8.56 (4H, s), 7.36 (8H, m), 7.22 (4H, d), 7.11 (6H, m), 7.08 (10H, d), 6.50 (4H, s), 4.11 (2H, s).

^{13}C NMR: (100 MHz, $CDCl_3$, TMS) δ (ppm): 163.23, 151.43, 147.61, 147.46, 131.54, 131.01, 129.58, 129.14, 125.36, 125.11, 123.80, 122.91.

Mass (MALDI-TOF, diathranol matrix): m/z calculated 937.01, found 938.

FTIR (cm^{-1}): 3061, 1641, 1586, 1488, 1273, 1202.

NMR, MASS spectra:

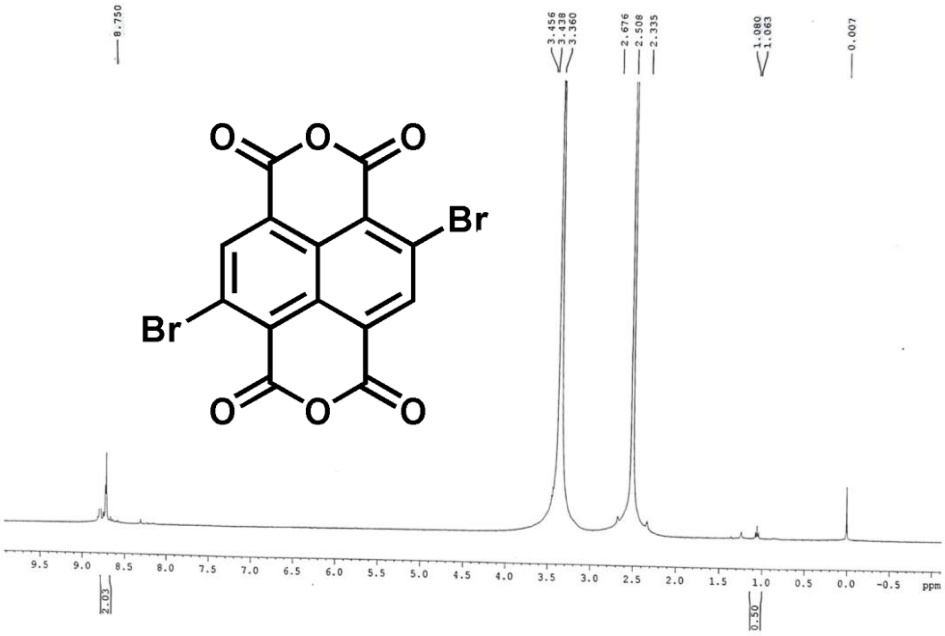

Fig. 5.15. i)^{1}H NMR spectra of 2,6-dibromo-1,4,5,8-naphthalene tetracarboxylic dianhydride**.**

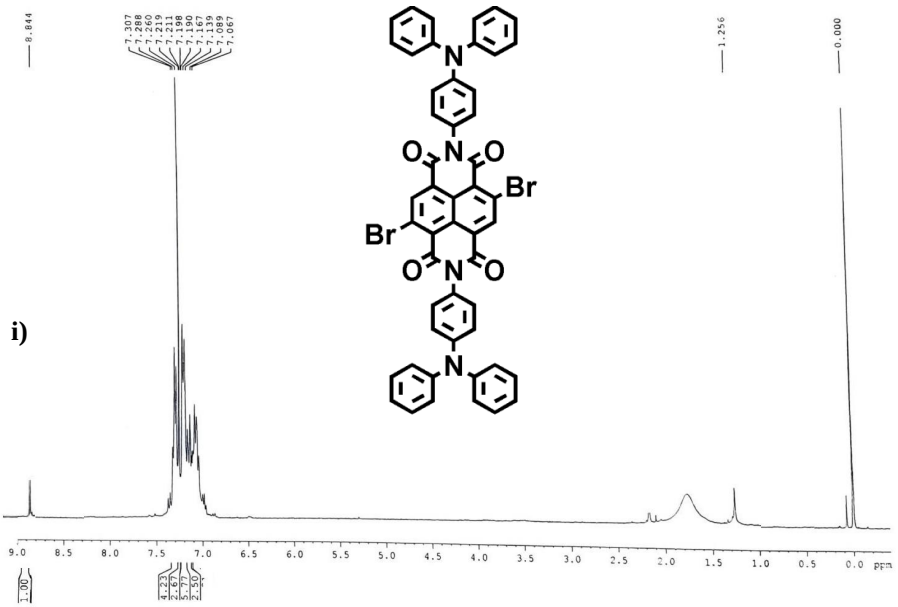

ii)

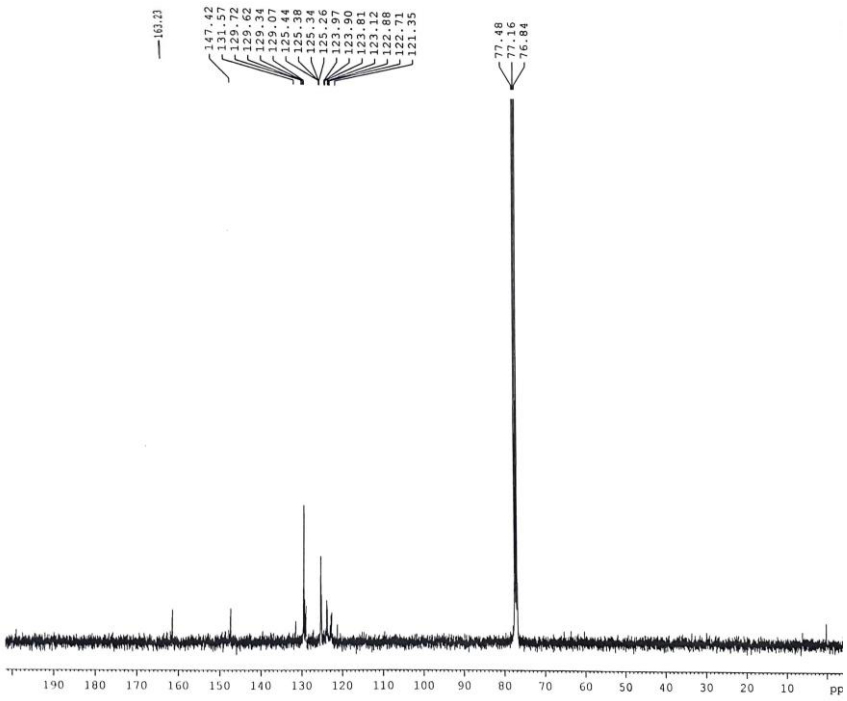

iii)

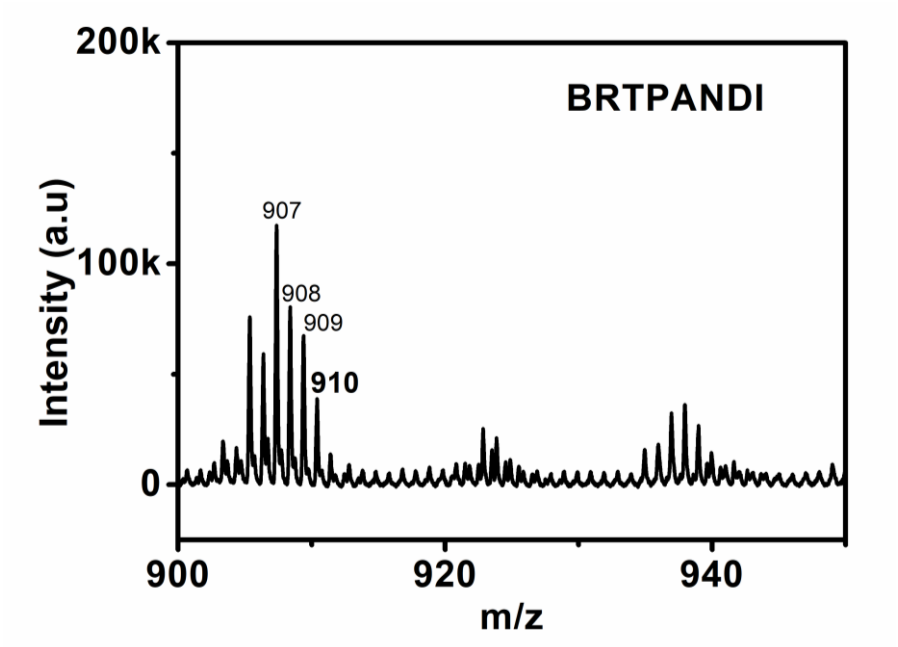

Fig. 5.16. i)^{1}H NMR ii)^{13}C NMR spectra in $CDCl_3$ iii) MALDI-TOF spectra of **BRTPANDI.**

i)

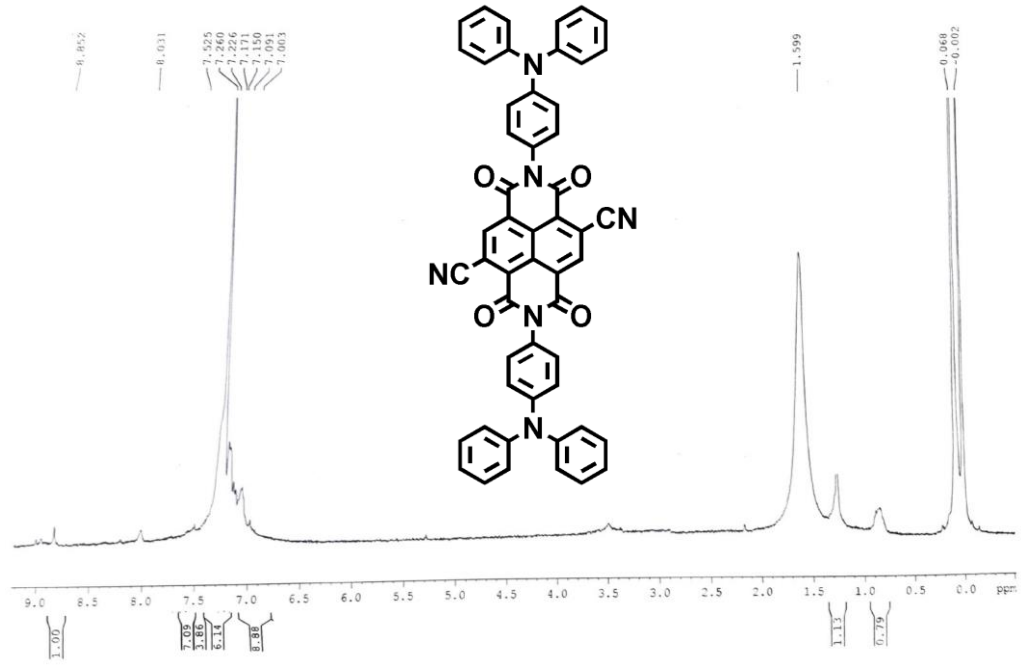
8.852
8.631
7.525
7.260
7.226
7.171
7.150
7.091
7.003
1.599
0.068
-0.002
CN
NC
O
N
9.0 8.5 8.0 7.5 7.0 6.5 6.0 5.5 5.0 4.5 4.0 3.5 3.0 2.5 2.0 1.5 1.0 0.5 0.0 ppm
1.00
7.09
3.86
6.14
8.88
1.13
6.79

ii)

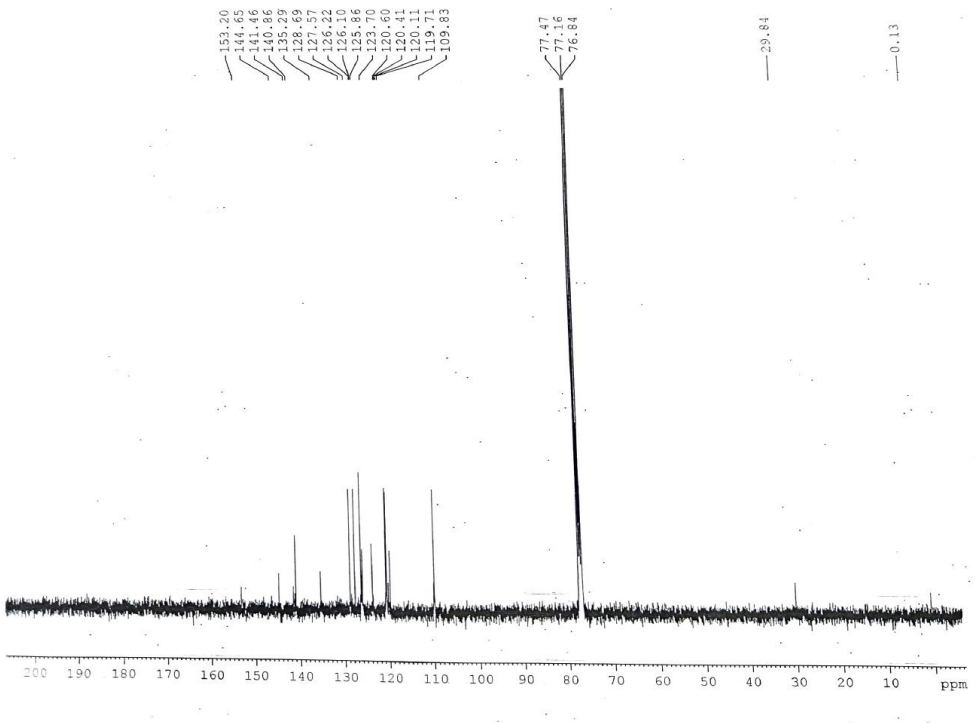
153.20
144.65
141.46
140.86
135.29
128.69
127.57
126.22
126.10
125.86
123.70
120.60
120.41
120.11
119.71
109.83
77.47
77.16
76.84
29.84
0.13
200 190 180 170 160 150 140 130 120 110 100 90 80 70 60 50 40 30 20 10 ppm

iii)

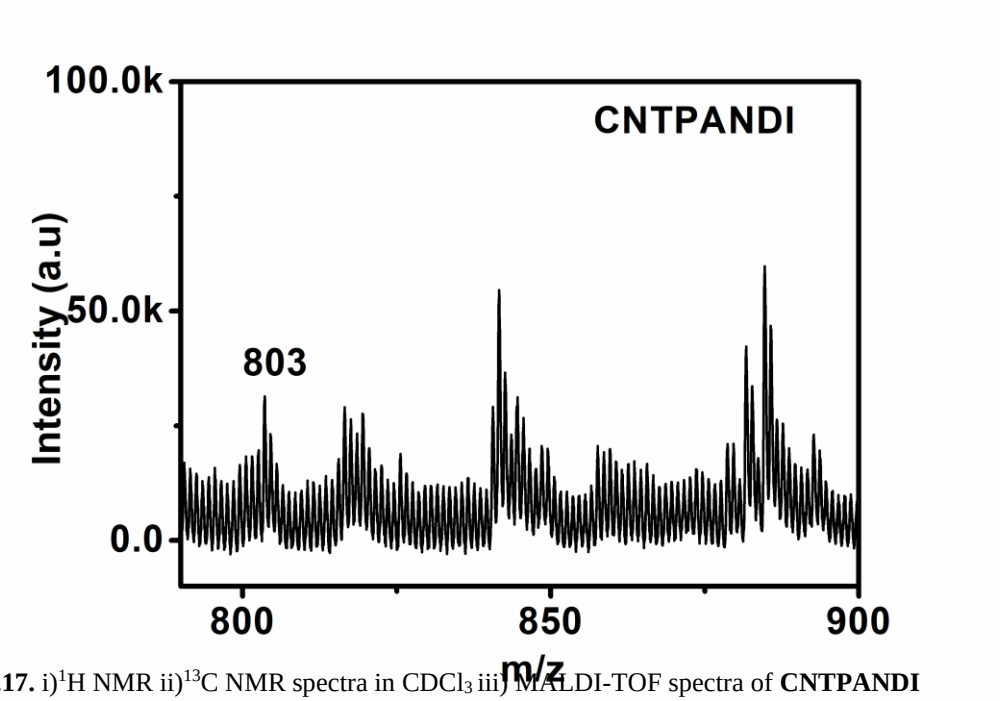

Fig. 5.17. i)^{1}H NMR ii)^{13}C NMR spectra in $CDCl_3$ iii) MALDI-TOF spectra of **CNTPANDI**

i)

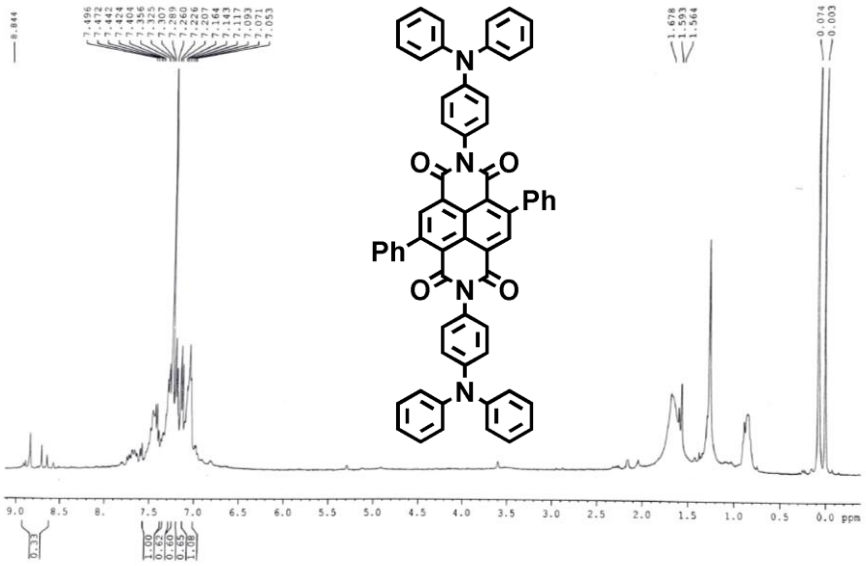

ii)

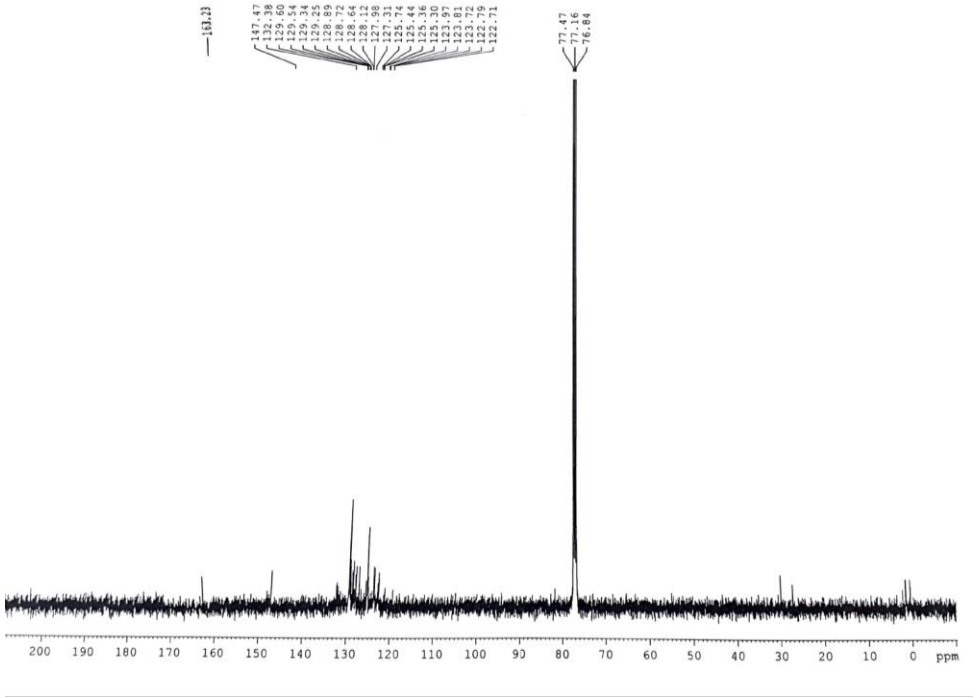

iii)

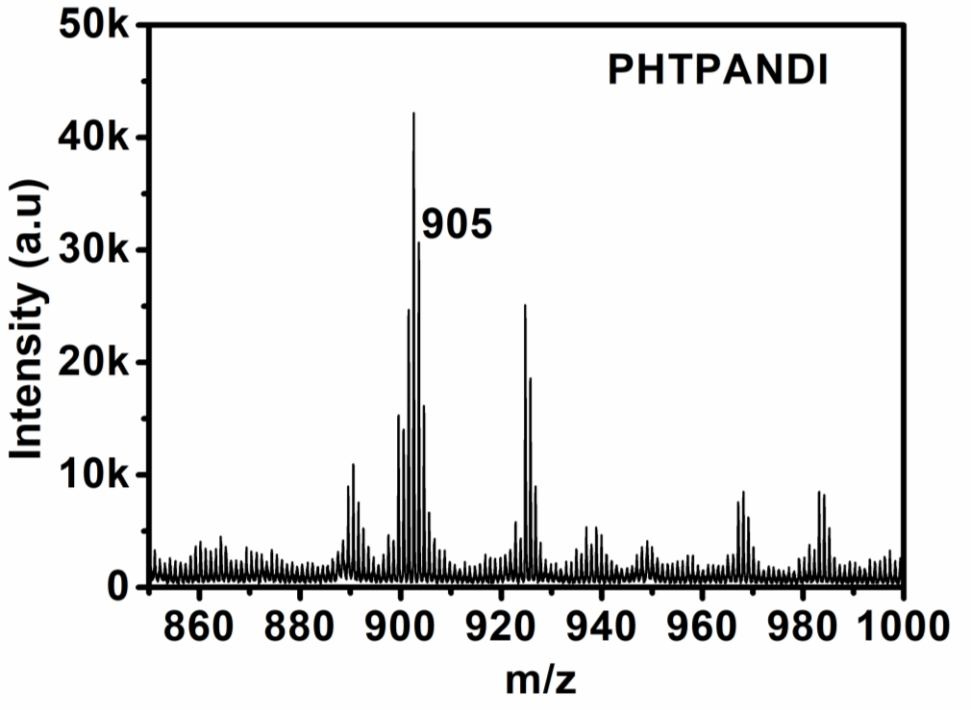

Fig. 5.18. i)^{1}H NMR, ii)^{13}C NMR spectra in $CDCl_3$ and iii) MALDI-TOF spectra of **PHTPANDI.**

i)

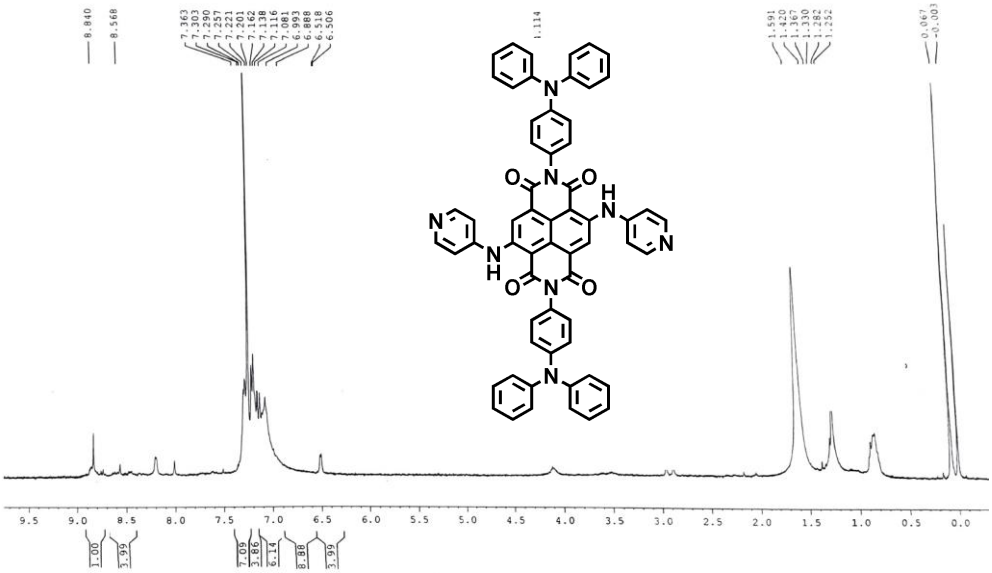
8.840
8.568
7.363
7.303
7.290
7.257
7.221
7.201
7.162
7.138
7.116
7.081
6.993
6.888
6.518
6.506
1.114
1.591
1.420
1.367
1.330
1.282
1.252
0.067
-0.003
9.5 9.0 8.5 8.0 7.5 7.0 6.5 6.0 5.5 5.0 4.5 4.0 3.5 3.0 2.5 2.0 1.5 1.0 0.5 0.0
1.00
3.99
7.09
3.86
6.14
6.88
3.99

ii)

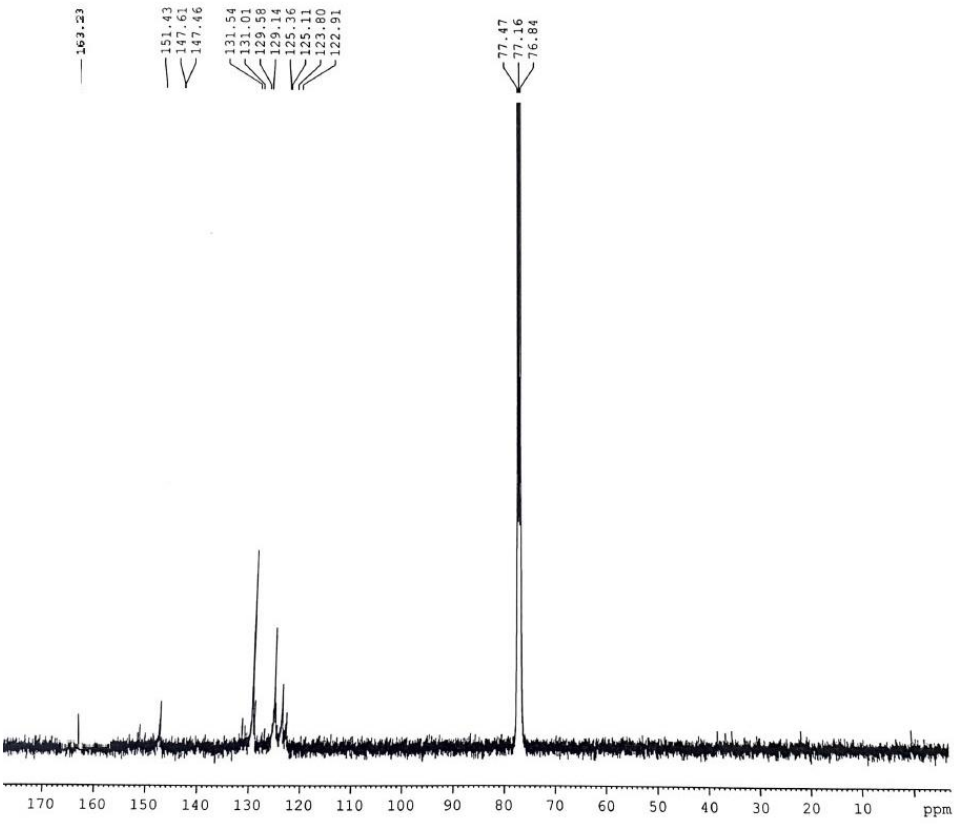
163.23
151.43
147.61
147.46
131.54
131.01
129.58
129.14
125.36
125.11
123.80
122.91
77.47
77.16
76.84
170 160 150 140 130 120 110 100 90 80 70 60 50 40 30 20 10 ppm

iii)

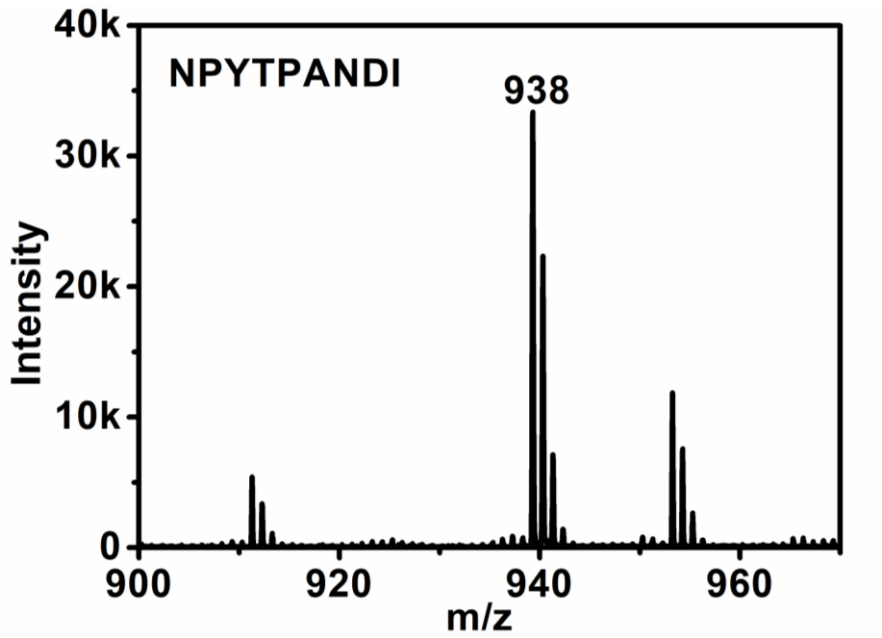

Fig. 5.19. i) ^{1}H NMR, ii) ^{13}C NMR spectra in $CDCl_3$ and iii) MALDI-TOF spectra of **NPYTPANDI.**

5.5. References:

[1] Q. Jiang, F. Liu, T. Li, T. Xu, J. Mater. Chem. C 2 (2014) 618–621.

[2] N. Kobayashi, S. Miura, M. Nishimura, H. Urano, Sol. Energy Mater. Sol. Cells 92 (2008) 136–139.

[3] A. Llordes, G. Garcia, J. Gazquez, D. J. Milliron, Nature 500 (2013) 323–326.

[4] H. F. Higginbotham, M. Czichy, B. K. Sharma, A. M. Shaikh, R. M. Kamble, P. Data, Electrochem. Acta 273 (2018) 264–272.

[5] A. L. Dyer, R. H. Bulloch, Y. H. Zhou, B. Kippelen, J. R. Reynolds, F. L. Zhang, Adv. Mater. 26 (2014) 4895–4900.

[6] R. J. Mortimer, A. L. Dyer, J. R. Reynolds, Displays 27 (2006) 2–18.

[7] T. Richardson, Solid State Ion. 165 (2003) 305–308.

[8] C. Ma, M. Taya, C. Y. Xu, Polym. Eng. Sci. 48 (2008) 2224–2228.

[9] A. M. Osterholm, D. E. Shen, J. A. Kerszulis, R. H. Bulloch, M. Kuepfert, A. L. Dyer, J. R. Reynolds, ACS Appl. Mater. Interfaces. 7 (2015) 1413–1421.

[10] S. Cong, F. Geng, Z. Zhao, Adv. Mater 28 (2016) 10518–10528.

[11] W. Wu, M. Wang, J. Ma, Y. Cao, Y. Deng, Adv. Electron. Mater. 4 (2018) 1800185.

[12] R. Argazzi, N. Y. Murakami, H. Zabri, F. Odobel, C. A. Bignozzi, Coord. Chem. Rev. 248 (2004) 1299–1316.

[13] D. Zhou, D. Xie, X. Xia, X. Wang, C. Gu, J. Tu, Sci. China Chem. 60 (2016) 3–12.

[14] C. G. Granqvist, Thin Solid Films 564 (2014) 1–38.

[15] J. Wang, J. Liu, M. Hu, J. Zeng, Y. Mu, Y. Guo, J. Yu, X. Ma, Y. Qiu, Y. Huang, J. Mater. Chem. A 6 (2018) 11113–11118.

[16] J. Zeng, Y. Wang, K. Rajan, Z. Xiao, R. U. Rehman Sagar, P. Liu, Sol. Energy Mater. Sol. Cells 226 (2021) 111070.

[17] S. Zhou, S. Wang, S. Zhou, H. Xu, J. Zhao, J. Wang, Y. Li, Nanoscale 12 (2020) 8934–8941.

[18] Y. Zhou, X. Liu, X. Jia, D. Chao, New. J. Chem. 43 (2019) 3829–3834.

[19] Y. Wang, X. Jia, M. Zhu, X. Liu, D. Chao, New. J. Chem. 44 (2020) 8138–8147.

[20] X. T. Wu, W. Wang, B. Li, Y. J. Hou, H. J. Niu, Y. H. Zhang, S. H. Wang, X. D. Bai, Spectrochim. Acta A 140 (2015) 398–406.

[21] L. H. He, G. M. Wang, Q. Tang, X. K. Fu, C. B. Gong, J. Mater. Chem. C 2 (2014) 8162–8169.

[22] S. Beaupre, J. Dumas, M. Leclerc, Chem. Mater. 18 (2006) 4011–4018.

[23] R. J. Mortimer, Annu. Rev. Mater. Res. 41 (2011) 241–268.

[24] S. K. Mohan Nalluri, J. Zhou, T. Cheng, Z. Liu, M. T. Nguyen, T. Chen, H. A. Patel, M. D. Krzyaniak, W. A. Goddard, M. R. Wasielewski, J. F. Stoddart, J. Am. Chem. Soc. 141 (2019) 1290–1303.

[25] B. A. Johnson, A. Bhunia, H. Fei, S. M. Cohen, S. Ott, J. Am. Chem. Soc. 140 (2018) 2985–2994.

[26] Z. Guo, D. K. Panda, M. A. Gordillo, A. Khatun, H. Wu, W. Zhou, S. Saha, ACS Appl. Mater. Interfaces 9 (2017) 32413–32417.

[27] H. Zhang, C. Gu, M. S. Yao, S. Kitagawa, Adv. Energy Mater. 33 (2021) 2100321.

[28] D. C. Santra, S. Nad, S. Malik, J. Electroanal. Chem. 823 (2018) 203–212.

[29] M. A. Kobaisi, S. V. Bhosale, K. Latham, A. M. Raynor, S. V. Bhosale, Chem. Rev. 116 (2016) 11685–11796.

[30] N. Sakai, J. Mareda, E. Vauthey, S. Matile, Chem. Commun. 46 (2010) 4225–4237.

[31] S. V. Bhosale, M. Al. Kobaisi, R. W. Jadhav, P. P. Morajkar, L. A. Jones, S. George, Chem. Soc. Rev. 50 (2021) 9845–9998.

[32] R. Bhosale, R. S. K. Kishore, V. Ravi kumar, O. Kel, E. Vauthey, N. Sakai, S. Matile, Chem. Sci. J. 1 (2010) 357–368.

[33] S. Chopin, F. Chaignon, E. Blart, F. Odobel, J. Mater. Chem. 17 (2007) 4139–4146.

[34] K. Wang, L. Zhu, X. Hu, M. Han, J. Lin, Z. Guo, H. Zhan, J. Mater. Chem. C. 9 (2021) 16959.

[35] S. Nad, R. Jana, A. Datta, S. Malik, J. Electroanal. Chem. 918 (2022) 116484.

[36] S. Nad, S. Malik, Chem. Electro. Chem. 7 (2020) 4144–4152.

[37] G. Sonmez, H. B. Sonmez, J. Mater. Chem. 16 (2006) 2473–2477.

[38] G. Cai, P. Darmawan, M. Cui, J. Wang, J. Chen, S. Magdassi, P S. Lee, Adv. Energy Mater. 6 (2016) 1–8.

[39] R. J. Mortimer, Electrochim. Acta 44 (1999) 2971–2981.

[40] P. M. Beaujuge, J. R. Reynolds, Chem. Rev. 110 (2010) 268–320.

[41] F. A. Arroyave, J. R. Reynolds, Macromolecules 45 (2012) 5842–5849.

[42] E. P. Knott, M. R. Craig, D. Y. Liu, J. E. Babiarz, A. L. Dyer, J. R. Reynolds, J. Mater. Chem. 22 (2012) 4953–4962.

[43] M. Li, A. Patra, Y. Sheynin, M. Bendikov, Adv. Mater. 21 (2009) 1707−1711.

[44] M. J. Frisch, G. W. Trucks, H. B. Schlegel, G. E. Scuseria, M. A. Robb, J. R. Cheeseman, G. Scalmani, V. Barone, G. A. Petersson, H. Nakatsuji, M. Caricato, A. V. Marenich, J. Bloino, B. G. Janesko, R. Gomperts, B. Mennucci, H. P. Hratchian, J. V. Ortiz, A. F. Izmaylov, J. L. Sonnenberg, C. Adamo, R . Cammi, J. W. Ochterski, R. L. Martin, K. Morokuma, O. Farkas, J. B. Foresman, D. J. Fox, Gaussian 16, Revision C.01, Gaussian, Inc., Wallingford CT (2016).

[45] A. D. Becke, J. Chem. Phys. 98 (1993) 5648-5652.

[46] A. K. Rappe, C. J. Casewit, K. S. Colwell, W. A. Goddard, W. M. Skiff, J. Am. Chem. Soc. 114 (1992) 10024−10035.

[47] E. N. Esmer, S. Tarkuc, Y. A. Udum, L. Toppare, Mater. Chem. Phys. 131 (2011) 519−524.

[48] P. M. S. Monk, R. J. Mortimer, D. R. Rosseinsky, Electrochromism and electrochromic devices, Cambridge University Press, Cambridge, UK. (2007) 25-62.

[49] M. Stolar, T. Baumgartner, Phys. Chem. Chem. Phys. 15 (2013) 9007–9024.

[50] A. G. M. Ferrari, C. W. Foster, P. J. Kelly, D. A. C. Brownson, C. E. Banks, Biosens 8 (2018) 53.

[51] S. Roy, C. Chakraborty**,** ACS Appl. Mater. Interfaces 12 (2020) 35181−35192.

[52] D. C. Santra, S. Mondal, S. Malik, RSC Adv. 6 (2016) 81597–81606.

[53] H. C. Lu, S. Y. Kao, H. F. Yu, T. H. Chang, C. W. Kung, K. C. Ho, ACS Appl. Mater. Interfaces 8 (2016) 30351–30361.

[54] S. H. Hsiao, J. C. Hsueh, J. Electroanal. Chem. 758 (2015) 100-110.

[55] A. Drewniak, M. D. Tomczyk, K. Knop, K. Z. Walczak, P. Ledwon, Macromolecules, 52 (2019) 8453–8465.

[56] L. Ma, S. Xiao, N. Wu, S. Zhao, D. Xiao, Dye. Pigment. 168 (2019) 327–333.

[57] F. Li, Z. Huang, M. Pan, Q. Tang, C. Gong, J. Mater. Chem. C., 8 (2020) 10031-10038.

[58] Y. Shi, G. Wang, Q. Chen, J. Zheng, C. Xu, Sol. Energy Mater. Sol. Cells, 208 (2020), 110413.

Chapter-6

Summary & Conclusions
Future Directions

Summary and Conclusions

Saving energy in automobile industry and building sectors mainly focus on maintaining comfortable and healthy indoor environment. Reversible modulation of the indoor environment is one of the suitable approaches to adjust it according to our daily needs. Now-a-days, it is possible to a greater extent with the integration of so-called chromogenic technologies into daily used items like automobiles, glazing in buildings, planes and various electronic displays as they can change their optical properties in a response to different external stimuli namely temperature (thermochromism), light (photochromism), external potential (electrochromism) and polymer dispersed liquid crystals. Among various chromogenic technologies, electrochromism has been considered to be superior compared to other technologies as electrochromic technology allows user friendly control of switching which is not directly possible by means of thermochromism or photochromism.

Chapter 3 describes the influence of number of electropolymerizable groups of the donor side on electrochromic behaviors, three donor-acceptor-donor type monomers containing isonaphthalene diimide as acceptor core and electro-polymerizable triphenyl amine (TPA) as the donor moiety have been designed and successfully synthesized via imidization of isonaphthalene anhydride with corresponding TPA derivatives. Three polymers show multi-electrochromic properties in a reversible manner with the colour change from colourless to brown to blue at low working potential. Spectro-electrochemistry studies of these films have revealed the high optical contrast (51.4%, 69.8 %, 84.5% respectively) of these polymers with the very fast bleaching (less than 1 s) and coloration (less than 2 s) time with very high coloration efficiencies. The electro switching stability has been performed up to 500 cycles and activity loses only 10% after 3000 s.

Chapter 4 presents the effect of different acceptor core like pyromellitic dianhydride, naphthalenetetracarboxylic dianhydride, perylenetetracarboxylic dianhydride and terminal triphenylamine based three DAD type monomers which are subsequently electropolymerized on conductive glass surface to have polymers which are explored by cyclic voltammetry studies. Density functional theory (DFT) studies disclose that HOMO is localized solely on triphenylamine unit which accounts for the electropolymerization process upon oxidation.

Besides, TD-DFT calculations unveil the responsible electronic transitions for electrochromism in the polymers. Three polymers exhibit the reversible multiple colour changes of colourless to brown to deep blue in the anodic region by applying voltage 0 to 1 to 1.2 V and also colourless to deep pink in the cathodic region (voltage window of 0 to -2 V) with attractive response times, optical contrast, switching stabilities, and coloration efficiencies. These polymers can be switched upto 10,000 cycles with the colouration efficiency 800 cm^2/C in the anodic process and 600 cycles for the cathodic process in a three electrodes configuration.

In **Chapter 5**, Several triphenylamine end capped to substituted central naphthalene tetracarboxylic diimide based four donor - acceptor - donor type electroactive monomers have been designed and developed to explore the effect of substituent on the formation of electro-polymers and subsequent the chromic effect of prepared films on the conductive surface. Initially, with the help of density functional theory (DFT) studies, it has observed that HOMO is located over triphenylamine unit, responsible electropolymerization process upon oxidation, LUMO is residing on the central naphthalene core, and all substituents are not coplanar with naphthalene moiety. Also, the band gap energy is gradually decreased with the effect of strong electron withdrawing substituents on NDI core. In three electrode configuration, reversible multiple colour changes of brown to deep blue by applying voltage 0 to 1.1 V and also brown to deep pink with the voltage change of 0 to -2 V are investigated with relatively good response times, optical contrast, switching stabilities, and coloration efficiencies.

Future Directions

As is well-known, the commercialization of EC displays has been explored for a long time. In the 1970s, Philips Research Laboratories reported the first simple monochrome protype EC digital display based on heptyl viologen. The display had a respectable high CR (20:1), short erasure times (ranging from 10 to 50 ms), and good reversibility (more than 105 cycles). The successful demonstration of this display product has greatly stimulated global interest in EC materials and boosted related R&D and commercialization. However, there are still problems that need to be solved. The first problem is that the self-aggregate and crystallize of viologen derivatives during their EC process, which seriously affects the cyclic life. The second problem is that related EC reaction is usually carried out in a solution or gel. Therefore, the active molecules easily diffuse away from the electrode. This blurs the displayed image and hinders it from being quickly erased by the current. At the same time, this problem also induces significant challenges and difficulties in manufacturing processes such as device sealing. The third problem is how to maintain the long term memory effect (bistability) of the displayed information. In response to the above technical problems, in 2003, NTera Ltd. developed a representative viologen-based EC display called NanoChromics. The displays demonstrated good cyclic life and durability. For example, the blue one could undergo 50,000 cycles at both room temperature and 50 °C; its contrast was maintained for more than 888 h under constant voltage, which indicated a good service life.

In 2006, Cambridge Research Laboratory of Epson, Seiko- Epson Corporation, and NTera Ltd. coreported a QVGA AMbased EC display with a high resolution of 200 dpi. The display was successfully driven with integrated driver electronics fabricated by low-temperature polysilicon thin-film transistor (LTPS-TFT) technology. The display also showed high contrast, high image quality, wide viewing angle, etc. In addition, a remarkable image retention time (bistability) was obtained: the displayed image could be partially read after 3 days without voltage treatment.

In 2008, Samsung Advanced Institute of Technology produced a 4.5-in. EC display driven by PM. The signal crosstalk problem was impressively solved by using the

isolated gel electrolytes. Next, RICOH Company developed a multilayer EC display (mECD) consisting of display units based on subtractive color mixing theory. In this work, researchers demonstrated the use of a 3.5-in. QVGA LTPS-TFT AM panel as the driving module. Each TFT-driven mECD unit was cleverly constructed from a shared counter electrode unit and three vertically stacked (cyan, magenta, and yellow) EC units (where each display unit is composed of a pair of EC substrates and a corresponding working electrode).

To date, the most widely known commercial ECDs are the antiglare rearview mirror and EC porthole on the Boeing 787 Dreamliner. These ECDs can automatically adjust the brightness, thereby eliminating dangerous glare from the rear vehicle headlights or improving the comfort level within the aircraft. Gentex has been extensively involved in the above two fields for many years and has been widely accepted in the marketplace. In addition, the rise of emerging companies (Heliotrope Technologies, Tynt Technologies, MiRuo China, Chromo- Genics, SageGlass, etc.) has also continuously added vitality into this field. In recent years, EC smart windows have been applied to the windows of cars and buildings. The grayscale ability of EC materials/devices makes it possible to control the transmittance of these “glasses” as needed. For example, Ambilight Inc. offers large-area (1.9 m^2) EC sunroofs for electrical vehicles created through roll-to-roll manufacturing processes. This successful product has laid an important foundation for further development of EC displays.

EC technologies have also begun to play an important role in portable consumer electronics such as mobile phones. In January 2020, the first smart concept phone equipped with EC technology was launched by OnePlus (as OnePlus Concept One). In this phone, the back camera module is hidden under an EC module and only appears when in use. This improves the overall look/feel of the device. Additionally, the color-switching speed is only 0.7 s, which does not affect the shooting process. At present, several mobile phone manufacturers are attempting to integrate EC technologies. For example, Ambilight Inc. teamed up with OPPO to successfully achieve mass production of an EC phone back cover with color-variable pictures (between silver and magenta).

In addition, existing commercialized EC display devices are mainly concentrated in electronic price tags, flexible electronic paper, etc. Ynvisible, Acero, and NTera Ltd., have made considerable effort and achieved great progress in developing these printing EC products. In summary, with the efforts of many related R&D teams, rapid progress has been made in the industrialization process of EC materials/devices. Although these products may not be displays or just low-end display components, they all represent the commercial development of electrochromics. This has paved the way for the realization of full-color EC displays in the future.

List of publications:

1. **Subhra Nad**, Sudip Malik*, Design, Synthesis, and Electrochromic Behaviors of Donor-Acceptor-Donor type Triphenylamine-iso-Naphthalenediimide Derivatives, **Chem Electro Chem 2020, 7, 4144–4152**.

2. **Subhra Nad**, Rajkumar Jana, Ayan Datta, Sudip Malik*, Fully organic electroactive monomers for electrochromic behaviors having high coloration efficiency and long cycle stability towards flexible Solid-State electrochromic device, **Journal of Electroanalytical Chemistry 918 (2022) 116484**.

3. Dines Chandra Santra, **Subhra Nad**, Sudip Malik*, Electrochemical polymerization of triphenylamine end-capped dendron, **Journal of Electroanalytical Chemistry 823 (2018) 203–212**.

4. **Subhra Nad**, Sudip Malik*, Effect of Substituents of Naphthalene Diimide on Electrochromic behaviours observed in Proto-type devices (manuscript under revision).

5. **Subhra Nad**, Sudip Malik*, Electrochromic films from diimide compounds with terminal triphenylamine and carbazole groups with oxidative polymerization (manuscript under preparation).

6. Apurba Maity, Amit Sil, **Subhra Nad**, Sanjib K. Patra*, A highly selective, sensitive and reusable BODIPY based 'OFF/ON' fluorescence chemosensor for the detection of Hg^{2+} Ions, **Sensors and Actuators B 255 (2018) 299–308**.

Curriculum Vitae

I was born on 05th September, 1992 at Paschim Medinipur, West Bengal, India. I completed my secondary (10th level) education in 2009 and higher secondary (12th level) education in 2011. After schooling, I started my bachelor degree (BSc.) study in Chemistry Honours from Midnapore College under the Vidyasagar University and received my BSc. degree with Honours in Chemistry in 2014. Later, I joined Indian Institute of Technology Kharagpur for my master study and obtained master degree in 2016. Later on, I joined **"Indian Association for the Cultivation of Science (IACS)"** as Junior Research Fellow (JRF) in the School of Applied and Interdisciplinary Sciences (SAIS) under the supervision of Prof. Sudip Malik in May, 2017 with DST-INSPIRE Fellowship and started my Ph. D carrier on the topic of **"Electro-polymerization of Organic Derivatives and their Electrochromic Effects"**. Besides research activities, I would like to sing and cook various items. I was also involved in different cultural programs in IACS.

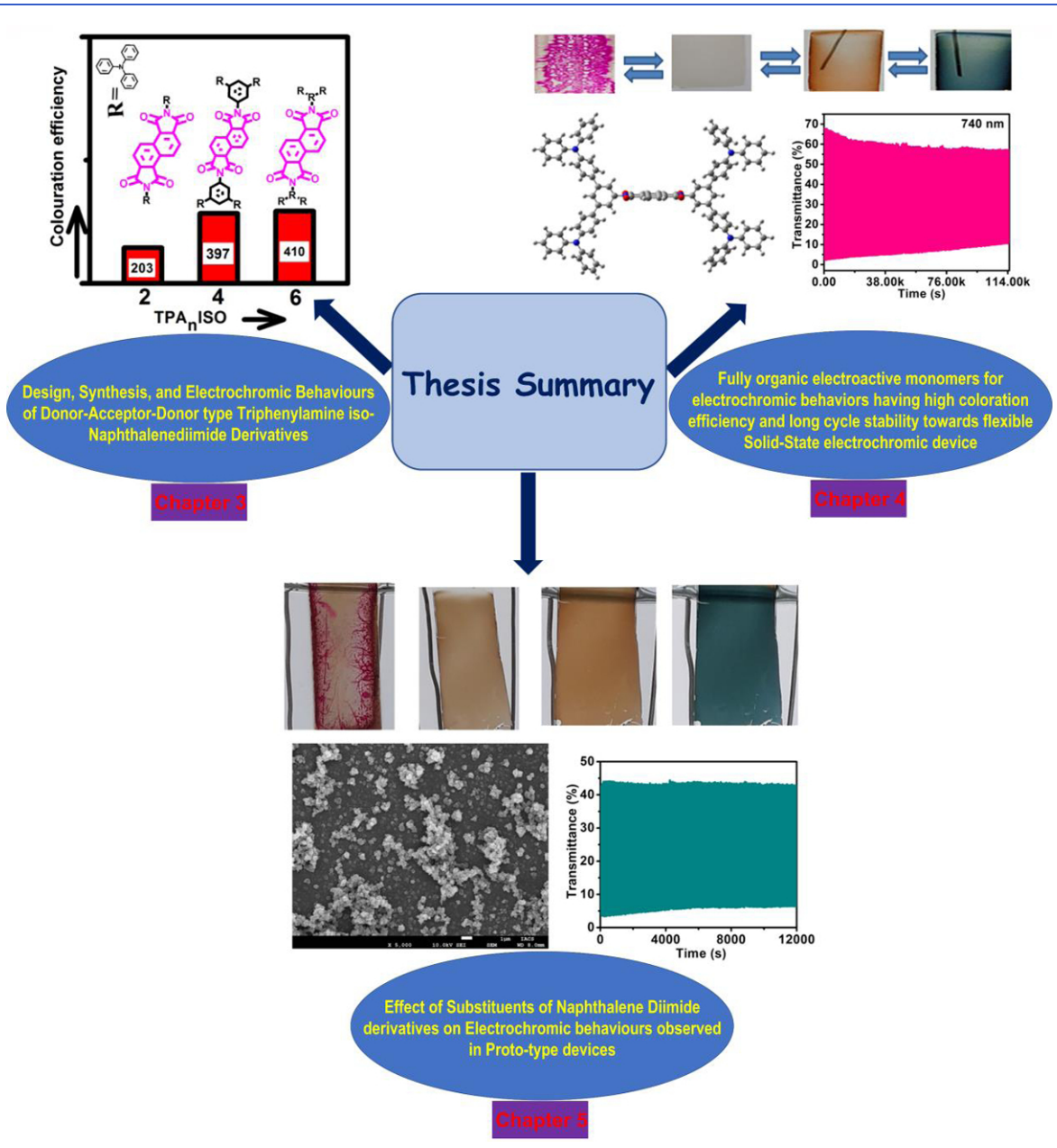
Colouration efficiency
R =
203
397
410
2
4
6
TPA$_n$ISO
740 nm
Transmittance (%)
Time (s)
Thesis Summary
Design, Synthesis, and Electrochromic Behaviours of Donor-Acceptor-Donor type Triphenylamine iso-Naphthalenediimide Derivatives
Chapter 3
Fully organic electroactive monomers for electrochromic behaviors having high coloration efficiency and long cycle stability towards flexible Solid-State electrochromic device
Chapter 4
Transmittance (%)
Time (s)
Effect of Substituents of Naphthalene Diimide derivatives on Electrochromic behaviours observed in Proto-type devices
Chapter 5